Aspects of Holographic Renormalization Group Flows on Curved Manifolds

Jewel Kumar Ghosh

Thèse de doctorat

de l'Université Sorbonne Paris Cité

Préparée à l'Université Paris Diderot

Ecole doctorale *Sciences de la Terre et de l'Environnement* et
Physique de l'Univers, Paris, ED 560
APC - AstroParticule et Cosmologie

Aspects of Holographic Renormalization Group Flows on Curved Manifolds

Par Jewel Kumar Ghosh

Thèse de doctorat de Physique

Dirigée par Elias KIRITSIS et Francesco NITTI

Présentée et soutenue publiquement à Paris le 19 June 2019

Président du jury : Dudas, Emilian, DR-CNRS , CPHT- Ecole Polytechnique.
Rapporteurs : Mateos Sole, David Julian, professeur à l' Universitat de Barcelona,
Parnachev, Andrei, professeur à l' Trinity College Dublin.
Examinateurs : Petrini, Michela, professeur à l'Sorbonne U,
Serreau, Julien, MCF à l'Université Paris Diderot, Laboratoire APC.
Directeur de thèse : Kiritsis, Elias Directeur de Recherche au CNRS/Laboratoire APC.
Co-directeur de thèse : Nitti, Francesco, Maître de Conférences à l'Université Paris Diderot/APC.

To,
Shitali Ghosh- who brought me to the light of world,
Samir Kumar Ghosh- who taught me how to walk in the light of world,
Chandita Urmi Ghosh- who brought colors to the light of my world.

Acknowledgments

During this thesis, I am indebted to many people for their help and support. It is my great opportunity to acknowledge their support.

I will start by thanking my supervisors Elias Kiritsis and Francesco Nitti for giving me the opportunity to work on this very interesting project. My skills flourished both scientifically and personally. I learned many facets of holography by working on this thesis under their supervision. I thank Francesco also for his kind support regarding administrative procedures which are intimidating sometimes.

I don't want to miss the opportunity to thank Lukas Witlowski, the person who helped me the most during my thesis. It was indeed a pleasure to collaborate with him. I thank him for helping me in all the places I got stumbled and providing me support when needed.

I also express my gratitude to Leandro Silva Pimenta for his friendship and providing me the necessary support. It was indeed a pleasure to share office with him and discussing many things.

I want to thank all the members of the jury board for their availability to attend my thesis defense. I also thank them for reading my thesis.

I am greatly indebted to my peers and colleagues from APC, from other institutions of Paris and also from other universities in different places across the globe. I express my gratitude to Pierre Auclair, Makarim Bouyahiaoui, Gabriel Moreau, Calum Murray and Theodoros Papanikolaou for helping me many times.

Thank you Alessandra Tonazzo and Yannick Giraud-Héraud for providing me with instructions. Thanks goes to Béatrice Silva and Francois Carré for assisting in managing my travel to attend conferences. I also thank all the staffs of APC whose works made my stay comfortable.

Last but not the least, I am forever grateful to my parents Samir Kumar Ghosh and Shitali Ghosh for their unconditional love and giving me everything they have. I also thank Chandita Urmi Ghosh for her love and support in my hard times and also for her loving care.

PhD is challenging, I could not accomplish this hard journey without the kind help and support from many people I know and I don't know, thanks everyone.

Résumé

La correspondance CFT (Anti-De Sitter) (AdS) / Théorie des champs conformes (CFT), également connue sous le nom de dualité holographique, constitue un lien remarquable entre la théorie des cordes (qui inclut la gravité) et les théories de jauge. Elle relie une CFT dans un espace-temps d-dimensionnel à une théorie de la gravité dans un espace-temps dimension supérieur, également appelé bloc. Ce dernier a une limite dans laquelle réside la théorie du champ conforme.

Dans cette thèse, le sujet d'étude est la description holographique des flux de groupes de renormalisation (RG) des théories (de champ) sur les espaces-temps à symétrie maximale. Le cadre théorique que j'ai utilisé est la théorie d'Einstein-scalaire. L'inclusion du champ scalaire dynamique correspond à la rupture de l'invariance conforme aux limites. Dans ce travail, les limites et les tranches du bloc sont choisies pour âtre des espaces-temps à symétrie maximale et l'évolution des champs en bloc est étudiée. Il décrit les écoulements RG holographiques sur des variétés courbes. De plus, deux applications sont présentées dans cette thèse. La première application s'inscrit dans le contexte des théorèmes F et la seconde concerne un defaut incurvé dans les flux RG holographiques en masse.

Les théorèmes F pour les théories de champs quantiques (QFT) définies dans des espaces-temps tridimensionnels exigent l'existence de fonctions dites F. Ce sont des fonctions décroissantes de façon monotone le long du flux RG. Dans ce travail, de nouvelles fonctions F pour les théories holographiques ont été découvertes. Elles sont construites à partir de l'action sur la paroie d'une solution de flux holographique RG sur une sphère à 3-sphères. Ils permettent une interprétation entropique, fournissant ainsi un lien direct entre la formulation entropique du théorème F et sa définition en termes d'é nergie libre.

La deuxiéme application des flux RG holographiques explorée dans cette thèse se situe dans le contexte de modèles affichant un mécanisme d'autoajustement en tant que résolution proposée du probléme de la constante cosmologique (CC). Dans ces modèles, notre univers à 4-dimensions est réalisé comme une brane intégrée dans un volume à 5-dimensions. Ce cadre permet des solutions où la géométrie de la brane est plate malgré la présence d'une énergie de vide non triviale sur son worldvolume. Ceci est appelé réglage automatique. De chaque côté de la brane, les solutions sont des flux RG holographiques. Le nouvel aspect introduit dans cette thèse consiste à utiliser les flux RG holographiques sur des variétés courbes, ce qui permet à son tour d'étudier des solutions à réglage automatique dans lesquelles la brane est également courbe.

Mots-clés : Holographie, dualité Gauge/Gravité, AdS/CFT, flux RG, transition de phase, courbure, monde de Barne.

Abstract

The Anti-de Sitter (AdS)/Conformal Field Theory (CFT) correspondence, also known as holographic duality, is a remarkable connection between string theory (which includes gravity) and gauge theories. It relates a CFT in a d-dimensional space-time to a gravity theory in higher dimensional space-time which is also referred to as the bulk. The latter has a boundary on which the conformal field theory may be thought to reside.

In this thesis, the subject of study is the holographic description of Renormalization Group (RG) flows of (field) theories on maximally symmetric space-times. The theoretical framework I used is Einstein-scalar theory. Inclusion of the dynamical scalar field corresponds to breaking boundary conformal invariance. In this work, both the boundary and bulk slices are chosen to be maximally symmetric space-times and the evolution of bulk fields is studied. It describes holographic RG flows on curved manifolds. Furthermore, two applications are presented in this thesis. The first application is in the context of F-theorems and the second is regarding a curved defect in the bulk holographic RG flows.

F-theorems for Quantum Field Theories (QFT) defined on 3-dimensional space-times demand the existence of so-called F-functions. These are monotonically decreasing functions along the RG flow. In this work, new F-functions for holographic theories have been found which are constructed from the on-shell action of a holographic RG flow solution on a 3-sphere. They allow an entropic interpretation, therefore providing a direct connection between the entropic formulation of the F-theorem and its definition in terms of free energy.

The second application of holographic RG flows explored in this thesis is in the context of models displaying a self-tuning mechanism as a proposed resolution of the cosmological constant (CC) problem. In these models, our 4-dimensional universe is realized as a brane embedded in a 5-dimensional bulk. This framework allows solutions where the brane geometry is flat despite of the presence of non-trivial vacuum energy on its worldvolume. This is referred to as self-tuning. On each side of the brane, the solutions are holographic RG flows. The new aspect introduced in this thesis is to use the holographic RG flows on curved manifolds, which in turn allows the study of self-tuning solutions where the brane is also curved.

Keywords: Holography, Gauge/Gravity duality, AdS/CFT, RG flows, phase transition, curvature, barne-world.

Contents

Chapter 1

Introduction

1.1 Motivation

Two of the most successful physical theories for describing our universe are the standard model of particle physics and the general theory of relativity. The standard model is a quantum field theory which describes phenomena at the subatomic scale. On the other hand, general relativity describes gravity at large scales.

One revolution of modern physics came through Einstein's theory of relativity. In the special theory of relativity, the idea of absolute time was abandoned, space and time were unified into space-time. According to this theory, the physical laws are invariant under Lorentz transformations instead of Gallilean transformations and the velocity of light is a fundamental constant of nature. It has passed many checks by experiments and the relativistic effects have become indispensable in modern particle physics experiments.

General Relativity (GR) includes gravity in relativity theory. In GR, gravity is a geometric property of space-time. The presence of matter acts as a source that curves the geometry, which is determined by Einstein's equation

$$R_{ab} - \frac{1}{2}Rg_{ab} + \Lambda g_{ab} = 8\pi G_N T_{ab}, \tag{1.1.1}$$

where g_{ab} is the metric of the space-time, R_{ab} is the Ricci tensor, R is the scalar curvature, Λ is known as the cosmological constant and T_{ab} is the stress-energy tensor. Test particles follow the geodesic motion under the influence of gravity.

Quantum field theory, on the other hand is based on quantum mechanics. The advent of quantum mechanics revolutionized physics. The classical deterministic view was replaced by the quantum probabilistic view. In quantum mechanics, objects can display both wave and particle properties.

Uncertainty is an inevitable phenomenon in the microscopic world. Therefore quantum mechanics has changed the way of looking at physics departing from a classical point of view.

Quantum Field Theory (QFT) combines special relativity, quantum mechanics and classical field theory. In QFT particles are excited states of quantum fields. The most successful QFT is the standard model of particle physics which is a gauge theory, i.e. the Lagrangian is invariant under a certain local group of transformations. One simple example of a gauge theory is electromagnetism described by

$$\mathcal{L} = -\frac{1}{4g^2} F_{\mu\nu} F^{\mu\nu} \tag{1.1.2}$$

where g is a coupling constant and

$$F_{\mu\nu} = \partial_\mu A_\nu - \partial_\nu A_\mu \tag{1.1.3}$$

is known as the field strength tensor. The latter is invariant under

$$A_\mu \to A_\mu + \partial_\mu \lambda(x) \tag{1.1.4}$$

where $\lambda(x)$ is a scalar function. Eq. (1.1.4) can also be written as

$$A_\mu \to G A_\mu G^{-1} - i(\partial_\mu G) G^{-1} \ , \tag{1.1.5}$$

where $G(x) = e^{i\lambda(x)}$. In group theoretical language, $G(x)$ are elements of a group referred to as $U(1)$. The Lagrangian (1.1.2) is invariant under the transformation (1.1.5) . Therefore, electromagnetism is a gauge theory under the gauge group $U(1)$.

The above example is an Abelian gauge theory where different elements of the gauge group commute. When they do not commute, QFT invariant under the gauge group is known as a non-Abelian gauge theory. An example is Yang-Mills theory

$$\mathcal{L} = -\frac{1}{4g_{YM}^2} \operatorname{Tr}\left(F_{\mu\nu} F^{\mu\nu}\right) \tag{1.1.6}$$

with gauge group $U(N)$ and coupling g_{YM}. The field strength tensor is in the adjoint representation of the group: $F_{\mu\nu} = F^a_{\mu\nu} T^a$ where T^as are the generators of the group and $a = 1, 2, \cdots \dim(G)$ is group index. The trace in Eq. (1.1.6) is taken with respect to the group index. For $U \in U(N)$, the field strength tensor transforms as

$$F_{\mu\nu} \to U F_{\mu\nu} U^\dagger \ . \tag{1.1.7}$$

The Yang-Mills Lagrangian (1.1.6) is invariant under this transformation and N is called the rank of the gauge group.

The gauge/gravity duality is a connection between gauge theories and gravitational theories in higher dimensions. The latter are string theories or an appropriate limit thereof (e.g. supergravity). This is an explicit realization of the holographic principle [1][2] as the gauge theory may be thought to be defined on the boundary of the space-time. The idea of the holographic principle emerged from the fact that black holes have an entropy [3] which is proportional to the area of the horizon [4]. In section 1.2, I will review the black hole thermodynamics.

The original idea of the AdS/CFT correspondence emerged from considering a collection of N $D3$ branes in IIB string theory and considering the physics from two different points of view. In one picture, the $D3$ branes act as sources for various fields of IIB string theory. The low energy limit of the metric is a product geometry $AdS_5 \times S^5$. In another picture, the $D3$ branes describe $\mathcal{N} = 4$ super Yang-Mills theory with gauge group $U(N)$. Combining these two views leads to the duality between $\mathcal{N} = 4$ super Yang-Mills theory with gauge group $U(N)$ and IIB string theory in $AdS_5 \times S^5$. When the rank of the gauge group N and the coupling are large, the string theory can be well described by supergravity and the duality is between supergravity in $AdS_5 \times S^5$ and $\mathcal{N} = 4$, $U(N)$ super Yang-Mills theory. I will present various aspects of the AdS/CFT in section 1.3.

The AdS/CFT correspondence provides us with a novel way of finding different quantities in the QFTs by computing proper objects on the gravity side. One of the important concepts of QFT is running of coupling constants as a function of energy scale. The evolution is encoded into a first order differential equation which is referred to as renormalization group (RG) equation. Holography provides a tool to describe RG flows from the gravity dual. I will review holographic RG flows in section 1.4.

Holographic RG flows are most often studied when the background space-time of the field theory is flat. However, we can also study the holographic RG flows when the field theory is defined on a curved background. In this thesis, I have studied the holographic RG flow solutions on curved manifolds. To describe these flows, we need to foliate the bulk by curved slices. The boundary metric inherits the curvature from the slicing. In this thesis, I have considered both the boundary and bulk slices to be maximally symmetric space-times. These can be either flat, de Sitter (dS) or AdS in the Lorentzian signature and flat, sphere or hyperbolic space in the Euclidean signature. The holographic RG flows can be described from the evolution of the bulk fields. In the simplest case, these solutions are monotonic between the fixed points. However, there exist solutions which seem exotic from the view of

QFT perturbation theory. These are flows which can reverse the directions in the coupling constant space, previously referred to as bounces in the flat case [5] and flows those skip the nearest possible endpoints. For the latter, there can be multiple flows representing the vacua of the dual field theory defined on a curved background. In this case, we observe a phase transition driven by the boundary curvature.

Beside the general analysis, in this thesis I have studied two applications of holographic RG flows on curved manifolds. The first application is the study of free energies of QFTs defined on 3-spheres in the context of the F-theorem. The subject of F-theorems is the existence of "F-functions", monotonic along RG flows, which interpolate between the UV and IR values of the corresponding CFT central charges. In this work, new F-functions for holographic theories have been found, which are constructed from the on-shell action of a holographic RG flow solution on the 3-sphere. By the holographic dictionary, the Euclidean on-shell action of the gravity dual corresponds to the free energy of the boundary QFT. The F-functions also allow an interpretation as an entanglement entropy, thus providing a direct link between the entropic formulation of the F-theorem and its definition in terms of the free energy. I confirmed monotonicity of these functions in several holographic examples and also for free field theories.

The second application is in the context of braneworlds. One of the central ideas of braneworlds is the realization of our universe as a 4-dimensional defect, also referred to as the brane, embedded in a 5-dimensional bulk. As observed in [6, 7], such bulk-brane setups may offer a resolution of the cosmological constant problem which is the discrepancy between the observed value of the cosmological constant and the vacuum energy predicted by the standard model. In particular, braneworlds allow solutions where the brane is flat despite of the presence of a non-vanishing brane vacuum energy. This is known as the self-tuning mechanism (in the context of braneworlds). In the self-tuning models constructed in [7], the bulk space-time is AdS or asymptotically AdS. The bulk geometry on both sides of the brane is the same as the one encountered in holographic RG flows. The new aspect introduced in this thesis is the generalization of these solutions to holographic RG flows on curved space-times including a defect. This in turn allows the study of self-tuning solutions in which the brane is also curved. We show in several examples that the main feature of self-tuning persists in that the brane curvature is dynamically selected and not just determined by the brane vacuum energy, and the brane position is dynamically stabilized.

The thesis is organized as follows. In the rest of this chapter, I will review the AdS/CFT correspondence focusing on the aspects which will be essential for the following chapters. In chapter 2, I will present the holographic renor-

malization group flows on curved space-times. In chapter 3, I will discuss four proposals of F-functions. In chapter 4, I will present a curvature driven quantum phase transition. I will discuss a self-stabilization mechanism of a curved brane in chapter 5.

The works presented in this thesis have been published in 3 seperate papers. Chapters 2 and 4 are based on [8], chapter 3 is based on [9] and chapter 5 is based on [10].

1.2 Black hole entropy and the holographic principle

In the 70s, works of several scientists revealed more and more information about black holes. From the works of Bardeen, Carter and Hawking [11], it emerged that the laws of black holes are similar to the laws of thermodynamics.

To state the first law of black hole mechanics, consider a black hole of mass M, horizon area A and angular momentum J. Also consider that the black hole metric is static. This implies that there is a Killing vector associated with time translation vector $\xi = \partial_t$. Surface gravity of the black hole κ is defined by

$$\kappa\xi^\mu = \xi^\nu \nabla_\nu \xi^\mu \tag{1.2.1}$$

where μ, ν are the space-time indices and ∇ denotes the covariant derivative with respect to the metric. Consider a process where the static black hole is transformed into another static black hole of mass $M + \delta M$, horizon area $A + \delta A$ and angular momentum $J + \delta J$. The first law of black hole mechanics relates all these quantities by

$$\delta M = \frac{\kappa}{8\pi}\delta A + \Omega_H \delta J, \tag{1.2.2}$$

where Ω_H is the angular velocity of the black hole.

The second law of black hole mechanics states that under weak energy condition, the area of the horizon is a non-decreasing function of time. The weak energy condition demands that for any observer in space-time, energy density of a matter distribution is non-negative. Suppose v^μ is a four-velocity vector of an observer in space-time and $T_{\mu\nu}$ is the stress-energy tensor of a system. Weak energy condition implies that

$$T_{\mu\nu} v^\mu v^\nu \geq 0. \tag{1.2.3}$$

Under this assumption, the second law of black hole mechanics can be written as

$$\frac{dA}{dt} \geq 0. \tag{1.2.4}$$

Now consider a thermal system at equilibrium temperature T. The first law of thermodynamics states that

$$dE = TdS + dW \tag{1.2.5}$$

where dE is the change in internal energy, dS is the change in entropy and dW is the work done on the system by exterior agents. When the system is rotating with an angular velocity Ω and angular momentum J, the work done on the system is

$$dW = \Omega dJ \tag{1.2.6}$$

and the first law of thermodynamics (1.2.5) becomes

$$dE = TdS + \Omega dJ \ . \tag{1.2.7}$$

Note that this equation is similar to the first law of black hole mechanics (1.2.2). The second law of thermodynamics states that the entropy of a closed system is non-decreasing. This is also similar to the second law of black hole mechanics (1.2.4). Therefore there is a striking resemblance between thermodynamics and black hole mechanics where κ has the similar role as temperature and A is similar to entropy. Later, the calculation of Hawking showed that entropy corresponding to a black hole is

$$S_{BH} = \frac{A}{4\pi G_N} \ . \tag{1.2.8}$$

Entropy in ordinary field theory is an extensive quantity. For example, consider a volume V and assume for simplicity that the space is discretized with lattice size ℓ_P. Also, consider a binary spin system with one spin at each site. Then the total number of configurations this system can have is

$$N = 2^n = 2^{V/\ell_P^3} \ . \tag{1.2.9}$$

The entropy is given by Boltzmann's relation

$$S_V = k_B \ln \left(2^{V/\ell_P^3}\right) \sim V \ . \tag{1.2.10}$$

Therefore we observe that the entropy is proportional to the volume of the space. This holds in general for local QFTs.

However, the black hole entropy is proportional to the area of the horizon. Bekenstein argued that black hole possesses the maximum amount of entropy in a bounded volume V. The argument is the following. Suppose there exists a system which occupies the volume V with smaller energy but with higher entropy than a black hole. By throwing matter inside, a black hole can be formed which will have smaller entropy. This violates the second law of thermodynamics. Bekenstein therefore concluded that the maximum entropy is carried by the black hole that would fit in that volume.

An interpretation of the black hole entropy was given by 't Hooft [2]. He suggested that it should be possible to describe the physics inside a volume V by the physics on the boundary enclosing the region. This is the idea that quantum gravity is holographic where the physics inside can be equivalently described by the physics on the boundary. This is the essence of the holographic principle.

1.3 The AdS/CFT correspondence

The AdS/CFT correspondence is an explicit realization of the holographic principle. It connects a gravitational theory to a non-gravitational theory. Before embarking on the details of the correspondence, we will define the necessary ingredients.

1.3.1 Anti-de Sitter space-time

AdS stands for Anti-de Sitter space-time. It is the maximally symmetric space-time with constant negative curvature. It is also the solution of Einstein's equation

$$R_{\mu\nu} - \frac{1}{2}Rg_{\mu\nu} + \Lambda g_{\mu\nu} = 0 \ , \tag{1.3.1}$$

with negative cosmological constant Λ. For a $(d+1)$-dimensional AdS space-time the value is

$$\Lambda = -\frac{d(d-1)}{2\ell^2} \tag{1.3.2}$$

where ℓ is called the AdS length and it is related to Ricci curvature by

$$R = -\frac{d(d+1)}{\ell^2} \tag{1.3.3}$$

which can be obtained by contracting Eq. (1.3.1) with the metric.

A $(d+1)$-dimensional AdS of length ℓ can be described as embedded in flat $\mathbb{R}^{2,d}$ by the equation

$$-X_1^2 - X_2^2 + \sum_{i=3}^{d+2} X_i^2 = -\ell^2 \tag{1.3.4}$$

where $X_1, X_2, \cdots, X_{d+2}$ are the coordinates of $\mathbb{R}^{2,d}$. Different parametrizations of these coordinates will describe AdS in different coordinates. Two of these are described below.

Global coordinates

In global coordinates, the embedding can be written as

$$X_1 = \sqrt{r^2+\ell^2}\cos(t/\ell) \ , \tag{1.3.5}$$
$$X_2 = \sqrt{r^2+\ell^2}\sin(t/\ell) \ , \tag{1.3.6}$$
$$X_3 = r\hat{x_3} \ , \tag{1.3.7}$$
$$\cdots \tag{1.3.8}$$
$$X_{d+2} = r\hat{x}_{d+2} \ . \tag{1.3.9}$$

where $\hat{x_3}, \cdots, \hat{x}_{d+2}$ satisfy $\hat{x}_3^2 + \cdots + \hat{x}_{d+2}^2 = 1$ and parametrize a unit $(d-1)$-dimensional sphere, S^{d-1}. In these coordinates, AdS metric is

$$ds^2 = -\left(1+\frac{r^2}{\ell^2}\right)dt^2 + \left(1+\frac{r^2}{\ell^2}\right)^{-1} dr^2 + r^2 d\Omega_{d-1}^2 \tag{1.3.10}$$

where $d\Omega_{d-1}^2$ is the line element of unit S^{d-1}. The spatial boundary is located at $r=\infty$ where the volume element diverges. For a lightlike geodesic it takes $t = \dfrac{\pi\ell}{2}$ to reach the boundary from the origin.

The topology of the boundary in global coordinates is $\mathbb{R}\times S^{d-1}$. In some cases, it will be desirable to describe AdS in coordinates with a d-dimensional flat boundary. This is achieved in the Poincaré patch coordinates.

Poincaré patch coordinates

For Poincaré patch coordinates $(z, t, \vec{x})$, the following transformations are used

$$X_1 = \frac{z}{2}\left(1 + \frac{\ell^2 + \vec{x}^2 - t^2}{z^2}\right) , \tag{1.3.11}$$

$$X_2 = \ell\frac{t}{z} , \tag{1.3.12}$$

$$X_i = \ell\frac{x_i}{z} \quad \text{where } i = 3, 4, \cdots, d+1 , \tag{1.3.13}$$

$$X_{d+2} = \frac{z}{2}\left(1 - \frac{\ell^2 + \vec{x}^2 - t^2}{z^2}\right) . \tag{1.3.14}$$

In the Poincaré patch coordinates, the metric of a $(d+1)$-dimensional AdS space-time becomes

$$ds^2 = \frac{\ell^2}{z^2}\left(dz^2 - dt^2 + \vec{x}^2\right) . \tag{1.3.15}$$

The AdS metric in the Poincaré patch coordinates is conformal to the flat space-time. The boundary is located at $z = 0$ with the topology of $\mathbb{R}^{1,d-1}$ and this parametrization is useful to describe QFTs in flat space-time.

1.3.2 Conformal Field Theory

CFT stands for conformal field theory. CFTs are invariant under coordinate transformations called the conformal transformations. Under these transformations, $x^\mu \to x'^\mu$, the metric changes as the local rescaling

$$g_{\mu\nu} \to \omega^2(x) g_{\mu\nu}, \tag{1.3.16}$$

where $\omega(x)$ is known as the conformal factor. These transformations form a group referred to as the conformal group. For the flat space-time, this group consists of four types of generators.

- Translations $P_\mu = -i\partial_\mu$: The metric is invariant when the space-time is translated. As a consequence, the conformal factor is 1.
- Lorentz generators $M_{\mu\nu} = i(x_\mu\partial_\nu - x_\nu\partial_\mu)$: These are isometries of Minkowski spacetime. In this case the conformal factor is 1 as the metric is invariant.
- Scaling $D = -ix_\mu\partial^\mu$: This generates scaling of the coordinates $x^\mu \to \lambda x^\mu$. The conformal factor for this case is $\omega = \frac{1}{\lambda}$.

- Special conformal transformations $K_\mu = i(x^2\partial_\mu - 2x_\mu x_\nu \partial^\nu)$: These transformations are composed of an inversion followed by a translation and inversion. Under these transformations the coordinates transform as

$$\frac{x'^\mu}{x'^2} = \frac{x^\mu}{x^2} - b^\mu \tag{1.3.17}$$

where b^μ is a constant vector. The conformal factor for this case is

$$\omega(x) = (1 - 2b^\mu x_\mu + b^\mu b_\mu x^\nu x_\nu) \ . \tag{1.3.18}$$

Fields of a CFT can be classified by their scaling dimension Δ. Under the scaling $x^\mu \to \lambda x^\mu$, a field of dimension Δ transforms as

$$\mathcal{O}(x) \to \lambda^{-\Delta}\mathcal{O}(\lambda^{-1}x) \ . \tag{1.3.19}$$

For a unitary CFT, the dimensions of the fields are bounded from below and for a scalar field the bound is $\Delta \geq \frac{d-2}{2}$.

As CFTs have more symmetries than generic QFTs, correlation functions of a CFT are more constrained as they should transform accordingly under the conformal transformations. In particular, the two point function of fields $\mathcal{O}_i$ and $\mathcal{O}_j$ with scaling dimensions Δ_i and Δ_j is entirely determined by conformal symmetry

$$\langle \mathcal{O}_i(x_1)\mathcal{O}_j(x_2)\rangle = \frac{\delta_{i,j}}{|x_1 - x_2|^{2\Delta_i}} \ . \tag{1.3.20}$$

Higher point correlation functions are not fully determined by the conformal symmetry but they must transform accordingly under the full conformal group.

Conformal invariant field theories appear at the second order phase transitions of statistical systems. Another example of a CFT is $\mathcal{N} = 4$ Super Yang-Mills (SYM) which is an important ingredient in the AdS/CFT correspondence [12].

1.3.3 The AdS/CFT correspondence and its limits

The argument leading to the AdS/CFT correspondence came by considering N coincident $D3$ branes in type IIB superstring theory in 10-dimensions [13], [14]. Dp branes are $(p+1)$-dimensional hypersurfaces where open strings can end. The $D3$ brane has 3 spatial coordinates and 1 time coordinate. String theory with $D3$ branes contains two kind of perturbative excitations: closed strings and open strings. Closed strings describe the excitations of

empty space whereas open strings describe excitations of the D-branes. At low energies, the closed string massless states are gravity supermultiplets and the effective action is type IIB supergravity. In the low energy limit, open string massless states are $\mathcal{N} = 4$ vector supermultiplet and the low energy effective description is $\mathcal{N} = 4$, $U(N)$ SYM in $3 + 1$ dimensions. The Yang-Mills coupling g_{YM} is related to the string coupling g_s by $g_{YM}^2 = 4\pi g_s$. In this limit, the systems decouple and the effective descriptions are bulk supergravity and $\mathcal{N} = 4$, $U(N)$ SYM with no interaction between them.

From a different point of view, the $D3$ branes act as sources for various supergravity fields (closed string sector). The $D3$ branes can couple to gravity and also a 4-form potential with a 5-form field strength. The $D3$ brane solution of the low energy effective action of type IIB supergravity is

$$ds^2 = \frac{1}{\sqrt{f}}\left(-dt^2 + dx_1^2 + dx_2^2 + dx_3^2\right) + \sqrt{f}\left(dr^2 + r^2 d\Omega_5^2\right), \tag{1.3.21}$$

$$F_5 = (1 + \star) dt dx_1 dx_2 dx_3 df^{-1}, \tag{1.3.22}$$

$$f = 1 + \frac{\ell^4}{r^4}, \quad \ell^4 = 4\pi g_s \alpha'^2 N, \tag{1.3.23}$$

where t, x_1, x_2, x_3 are the coordinates on the D3 brane, r is the radial distance from the brane and $d\Omega_5^2$ is the metric of a unit S^5. Here $\star$ denotes the Hodge star with respect to the 10-dimensional metric.

There are two important limits of the metric (1.3.21). For an observer at $r = \infty$, the metric becomes flat

$$ds^2 = \left(-dt^2 + dx_1^2 + dx_2^2 + dx_3^2\right) + \left(dr^2 + r^2 d\Omega_5^2\right) \ . \tag{1.3.24}$$

The other limit is referred to as the near horizon or the throat limit where $r \ll \ell$. In this limit we can write

$$f \sim \frac{\ell^4}{r^4} \ , \tag{1.3.25}$$

and the 10-dimensional metric becomes

$$ds^2 = \frac{r^2}{\ell^2}\left(-dt^2 + dx_1^2 + dx_2^2 + dx_3^2\right) + \frac{\ell^2}{r^2}\left(dr^2 + r^2 d\Omega_5^2\right) \ . \tag{1.3.26}$$

A coordinate transformation

$$u = \frac{\ell^2}{r} \tag{1.3.27}$$

transforms the metric to

$$ds^2 = \frac{\ell^2}{u^2}\left(du^2 - dt^2 + dx_1^2 + dx_2^2 + dx_3^2\right) + \ell^2 d\Omega_5^2 \ . \tag{1.3.28}$$

The first part of the metric above is a 5-dimensional AdS metric with length ℓ written in Poincaré patch coordinates. Therefore the near horizon limit is a product geometry $AdS_5 \times S^5$ where both AdS_5 and S^5 have the same radius of curvature, ℓ.

The time component of the metric (1.3.21) depends on the observer's location. Therefore there will be a gravitational redshift in the energy measured by two observers located at different positions. If the energy of an object measured by an observer located at r is $\tilde{E}$ and the energy measured by an observer located at infinity is E, these two quantities are related by

$$E = f^{-1/4}\tilde{E} \ . \tag{1.3.29}$$

When the object is close to the horizon, this relation becomes

$$E \approx \frac{r}{\ell}\tilde{E} \ . \tag{1.3.30}$$

This implies that the energy of a localised object near the throat becomes lower and lower as measured by an observer at infinity.

From the point of view of an observer at infinity, there are two kinds of low energy excitations. The first kind are the massless long wavelength excitations in the asymptotically flat region. The second kind of excitations approach to the near horizon region, $r \to 0$. In the low energy limit these two types of excitations decouple from each other [13].

We observe that the system of N D3 branes can be described in two different ways in the low energy limit. In one picture, it is described by decoupled bulk supergravity and $\mathcal{N} = 4$ SYM and in the other picture it is described by decoupled supergravity and near horizon geometry $AdS_5 \times S^5$. Combining these two views led to the statement of the AdS/CFT correspondence: $\mathcal{N} = 4$ Super Yang-Mills (SYM) theory with gauge group $U(N)$ in $3+1$ dimensions is equivalent to type IIB superstring theory on $AdS_5 \times S^5$.

On the field theory side, there are two parameters: the Yang-Mills coupling g_{YM} and the rank of the gauge group N. These two parameters combine into the 't Hooft parameter $\lambda = g_{YM}^2 N$. On the string theory side there are three basic scales: the string length ℓ_s, the AdS length ℓ and the 10-dimensional Newton's constant G_{10}. From these, two independent ratios can be formed. The AdS/CFT correspondence relates these as:

$$\frac{\ell^4}{\ell_s^4} = 4\pi g_s N = g_{YM}^2 N = \lambda, \quad \frac{16\pi G_{10}}{\ell_s^8} = (2\pi)^7 g_s^2 = \frac{8\pi^5 \lambda^2}{N^2}. \tag{1.3.31}$$

There are two important limits when the gauge theory parameters are large.

The first limit is when N is large. From the relation (1.3.31), we observe that, at fixed λ,

$$G_{10} \sim \frac{1}{N^2}. \tag{1.3.32}$$

This implies that the quantum gravitational effects are suppressed when $N \gg 1$. The 10-dimensional Newton's constant sets the Planck length $G_{10} \sim \ell_P^8$. From (1.3.31), we find

$$\left(\frac{\ell}{\ell_P}\right)^8 \sim N^2. \tag{1.3.33}$$

Therefore, the large N limit also implies that the AdS length scale ℓ is large compared to the Planck length, ℓ_P. Therefore the geometry is classical in this limit. On the field theory side, large N implies that the correlators receives leading contribution form planar diagrams.

Once the large N limit has been taken, other free parameter is λ. On the field theory side, perturbation theory is valid when this parameter λ is small. On the dual side, it is useful to take the opposite limit namely the large coupling limit. As we can write

$$\frac{\ell^4}{\ell_s^4} \sim \lambda \ , \tag{1.3.34}$$

the large coupling constant implies that the AdS radius is larger than the string length. In this limit the stringy corrections are suppressed and supergravity can be used as valid approximation. Therefore we conclude that when both N and λ are large, the gauge theory can be well described by classical IIB supergravity on $AdS_5 \times S^5$. This form of the duality is the most convenient for practical calculation. It also provides a framework to perform non-perturbative calculation of the gauge theory quantities.

1.3.4 CFT correlators from gravity

The AdS/CFT correspondence relates gravity theories to CFTs in large N and large 't Hooft coupling limit. The space-time of the gravity theory has a boundary on which the gauge theory may be thought to reside. A prescription to compute the gauge theory quantities from the gravity dual was given by Gubser-Klebanov-Polyakov-Witten (GKPW) [15],[16] which relates partition functions of both sides of the duality.

Consider an Euclidean CFT and a local operator $\mathcal{O}(x)$. The observables are vacuum correlation functions

$$\langle \mathcal{O}(x_1)\mathcal{O}(x_2)\cdots\mathcal{O}(x_n)\rangle \tag{1.3.35}$$

which are defined as the vacuum expectation values of product of the operators. The generating functional of the correlation functions is defined as

$$Z[J] = \left\langle e^{-\int d^d x J(x)\mathcal{O}(x)} \right\rangle_{CFT} \tag{1.3.36}$$

where $J(x)$ is the source for $\mathcal{O}(x)$. The correlation functions are obtained by taking functional derivatives with respect to the source and setting it to zero:

$$\langle \mathcal{O}(x_1)\mathcal{O}(x_2)\cdots\mathcal{O}(x_n)\rangle = (-1)^n \frac{1}{Z[0]}\frac{\delta}{\delta J(x_1)}\frac{\delta}{\delta J(x_2)}\cdots\frac{\delta}{\delta J(x_n)} Z[J]\Big|_{J=0} . \tag{1.3.37}$$

The GKPW rule relates the generating functional of the CFT to the partition function of gravity in the supergravity limit

$$Z[J] = \left\langle e^{-\int d^d x J(x)\mathcal{O}(x)} \right\rangle_{CFT} = \int D[\varphi_i] e^{-S_{grav}[\varphi_i]} \tag{1.3.38}$$

where φ_i denote the bulk supergravity fields. These are dual to the boundary operators. For simplicity, we consider a bulk scalar field which is dual to the boundary operator $\mathcal{O}(x)$. The boundary condition of φ is set by the source $\varphi|_{boundary} \sim J$. I will discuss the boundary condition precisely below for an example of a saclar field. In the large N and large coupling limit, the partition function of gravity is determined semiclassically and it is dominated by the classical saddle points. In this case, Eq. (1.3.38) can be written as

$$Z[J] = e^{-S_{grav,on-shell}[\varphi]} . \tag{1.3.39}$$

The right hand side is the gravity action evaluated such that the equations of motion are satisfied with prescribed boundary conditions set by the J which I will discuss next in the case of a scalar field.

The bulk fields are dual to some local operators on the field theory side. As an example, consider a massive scalar field in $(d+1)$-dimensional AdS space-time written in Poincaré patch coordinates

$$ds^2 = \ell^2 \frac{dz^2 + dx^\mu dx_\mu}{z^2} \tag{1.3.40}$$

and assume for simplicity that the field is constant on the compact space. Here we denote the bulk coordinates as $x^A = (x^\mu, z)$ where $A = 0, 1, \cdots, d$ and $\mu = 0, 1, \cdots, d-1$. The boundary is located at $z = 0$. The action for a massive scalar field is

$$S = -\frac{1}{2\ell^{d-1}} \int d^{d+1}x \sqrt{g} \left(g^{AB}\partial_A\varphi\partial_B\varphi + m^2\varphi^2 \right) \tag{1.3.41}$$

where g^{AB} is the inverse metric of (1.3.40) . Stationarity of the action under a small variation of the field gives the equation of motion. We must consider the boundary contribution as AdS has a boundary. Integrating (1.3.41) by parts once and keeping the boundary contribution we obtain

$$S = -\frac{1}{2\ell^{d-1}} \int_{\partial AdS} d^d x \sqrt{g} g^{zA} \varphi \partial_A \varphi + \frac{1}{2\ell^{d-1}} \int d^{d+1} x \sqrt{g} \varphi \left(\nabla^2 - m^2\right) \varphi \ . \tag{1.3.42}$$

where the Laplacian is defined as $\nabla^2 = \frac{1}{\sqrt{g}} \partial_A \left(\sqrt{g} g^{AB} \partial_B\right)$. The first term is the boundary contribution and the second term yields the bulk equation of motion

$$\left(\nabla^2 - m^2\right) \varphi = 0 \ . \tag{1.3.43}$$

Therefore we observe that the on-shell action of a massive scalar field receives contribution only from the boundary term.

To solve the equation of motion we can Fourier decompose the field. This is possible because the action (1.3.41) is invariant under $x^\mu \to x^\mu + a^\mu$ as this is an isometry of the AdS metric (1.3.40). We write

$$\varphi(x, z) = \frac{1}{(2\pi)^d} \int d^d k e^{i k_\mu x^\mu} f_k(z) \tag{1.3.44}$$

where k^μ is the momentum vector in d-dimensions and $f_k(z)$ are Fourier modes. These modes satisfy the following equation

$$\left(z^2 k^2 - z^{d+1} \partial_z (z^{-d+1} \partial_z) + m^2 \ell^2\right) f_k(z) = 0 \ . \tag{1.3.45}$$

Solutions of this equation are the Bessel functions. Near the boundary $z = \epsilon$ we use the ansatz $f_k(z) \sim z^\Delta$. Inserting this into (1.3.45) we obtain

$$\left(k^2 z^2 + \Delta(d - \Delta) + m^2 \ell^2\right) z^\Delta = 0 \ . \tag{1.3.46}$$

Near the boundary $z \to 0$, this requires

$$\Delta(d - \Delta) = -m^2 \ell^2 \ . \tag{1.3.47}$$

This equation has two solutions

$$\Delta_\pm = \frac{d}{2} \pm \frac{d}{2} \sqrt{1 + \frac{4 m^2 \ell^2}{d^2}} \ . \tag{1.3.48}$$

The Δ_- solution is always smaller than the Δ_+ solution. In fact, we observe that $\Delta_- < d/2$ and $\Delta_+ > d/2$ and they satisfy

$$\Delta_- + \Delta_+ = d \ . \tag{1.3.49}$$

Near the AdS boundary, the scalar field behaves as

$$\varphi(z,x) = z^{\Delta_-}\varphi_-(x)\left(1+\mathcal{O}(z^2)\right) + z^{\Delta_+}\varphi_+(x)\left(1+\mathcal{O}(z^2)\right) \ , \qquad (1.3.50)$$

where $\varphi_-(x)$ and $\varphi_+(x)$ are two a priori arbitrary functions in the near boundary expansion. However, regularity in the interior fixes the function φ_+ in terms of φ_-. I will present this in the next section.

In AdS/CFT, φ is dual to the operator $\mathcal{O}$ of the boundary field theory. When the dimension of the operator $\mathcal{O}$ is Δ then the dimension of the source J is $d-\Delta$. As φ is dimensionless, dimensional analysis shows that the dimensions of φ_- and φ_+ are Δ_- and Δ_+ respectively. In the standard AdS/CFT dictionary, the scaling dimension of the field is identified with Δ_+, i.e. $\Delta_+ = \Delta$, φ_- is identified with the source at the boundary $J(x)$ and $\varphi_+(x)$ is related to the vacuum expectation value (vev) of the local operator $\mathcal{O}$ by the following relation [17]

$$\langle \mathcal{O}(x) \rangle = (2\Delta_+ - d)\varphi_+(x) \ . \qquad (1.3.51)$$

With this identification, correlation functions are obtained from the on-shell gravity action (1.3.39). Reality of the scaling dimension requires that

$$-\frac{d^2}{4\ell^2} \leq m^2 \qquad (1.3.52)$$

which is known as the Breitenlohner and Freedman (BF) bound.

From (1.3.48), we observe that $\Delta_+ \geq d/2$ and in the standard dictionary it is identified with the scaling dimension, Δ, of the dual operator. On the other hand, when the operator has a scaling dimension $\Delta < d/2$, the interpretations of φ_- and φ_+ are interchanged, i.e. φ_+ is interpreted as the source and φ_- determines the vev. In this case, the on-shell action is identified with the quantum effective action of the boundary field theory.

1.4 Holographic RG flows in flat space-time

In the previous section, we have discussed the holographic prescription to obtain CFT correlators from the dual gravity in AdS space-time. CFT is a scale invariant theory. As a consequence, coupling parameters are independent of the energy scale. Conformal invariance can be broken by adding a deformation. In this way, we can get a QFT by adding an extra term to the CFT action

$$S_{QFT} = S_{CFT} + \int d^d x J(x)\mathcal{O}(x) \ , \qquad (1.4.1)$$

where $\mathcal{O}(x)$ is an operator of dimension Δ by which we break the conformal invariance and $J(x)$ is the source. As a consequence of breaking conformal invariance, coupling parameters of the theory will be energy dependent. The evolution is governed by first order differential equations known as the Renormalization Group (RG) equations.

On the dual gravity side, the breaking of boundary conformal symmetry means that the bulk space-time is no longer AdS everywhere. In this context, the holographic dimension serves as an effective RG scale in the dual QFT, thus geometrizing the notion of RG flow. In essence, RG flows can be understood as bulk evolution in the holographic dimensions [18, 19, 20, 21, 22, 23, 24, 25, 26, 27, 28, 29, 30, 31, 32, 33, 34, 5, 35]. In the bulk, the simplest holographic RG flows are described by Einstein-scalar theory with a minimally coupled scalar field [21],[5],[36], [37]. It is described by the following action

$$S[g,\varphi] = M^{d-1}\int du\, d^dx\, \sqrt{|g|}\left(R^{(g)} - \frac{1}{2}\partial_a\varphi\partial^a\varphi - V(\varphi)\right) + S_{GHY}\,, \quad (1.4.2)$$

where the Gibbons-Hawking-York boundary term, S_{GHY}, is added to make the variational problem well defined. Here M is the Planck mass. The holographic RG flow solutions can be described by the domain wall ansatz

$$\varphi = \varphi(u)\,, \qquad ds^2 = du^2 + e^{2A(u)}\eta_{\mu\nu}dx^\mu dx^\nu\,. \quad (1.4.3)$$

This ansatz is the most general homogeneous metric (up to diffeomorphisms) preserving the boundary Poincaŕe invariance. To see this, suppose we use a seemingly more general ansatz preserving the boundary Poincaŕe invariance

$$ds^2 = e^{2X(w)}dw^2 + e^{2Y(w)}\eta_{\mu\nu}dx^\mu dx^\nu\ . \quad (1.4.4)$$

However, the coordinate transformation defined by

$$e^{X(w)}dw = du \quad (1.4.5)$$

will transform the metric (1.4.4) into (1.4.3).

The equations of motions are

$$2(d-1)\ddot{A} + \dot{\varphi}^2 = 0\,, \quad (1.4.6)$$

$$d(d-1)\dot{A}^2 - \frac{1}{2}\dot{\varphi}^2 + V = 0\,, \quad (1.4.7)$$

$$\ddot{\varphi} + d\dot{A}\dot{\varphi} - V' = 0\,. \quad (1.4.8)$$

where the following notation is used

$$\dot{} = \frac{d}{du}, \quad {}' = \frac{d}{d\varphi}\ . \quad (1.4.9)$$

The first two equations (1.4.6)-(1.4.7) are obtained from the Einstein's equations and (1.4.8) is the Klein-Gordon equation for the scalar field. These three equations are not independent. For example, (1.4.8) can be obtained from Eqs. (1.4.6)-(1.4.7).

The equations of motion are second order differential equations. To make contact with the RG flows we first introduce the superpotential $W(\varphi)$ such that

$$W(\varphi(u)) = -2(d-1)\dot{A}(u) \ . \tag{1.4.10}$$

W in terms of φ can be defined piecewise in any interval where the scalar field is monotonic. In terms of this function, Eq. (1.4.6) can be written as

$$\dot{\varphi}(u) = W'(\varphi(u)) \tag{1.4.11}$$

which describes the evolution of the scalar field. Equation (1.4.7) becomes the following superpotential equation

$$\frac{d}{4(d-1)}W^2 - \frac{1}{2}W'^2 + V = 0 \ . \tag{1.4.12}$$

Therefore, introduction of the superpotential $W(\varphi)$ has turned the second order equations of motion into first order ordinary differential equations.

One of the properties of $W(\varphi)$ is that for a negative definite potential, V, it lies above a critical curve defined by

$$B(\varphi) = \sqrt{-\frac{4(d-1)}{d}V(\varphi)} \ . \tag{1.4.13}$$

This property can be seen from (1.4.12):

$$|W| = \sqrt{\frac{4(d-1)}{d}\left(\frac{1}{2}W'^2 - V\right)} \geq \sqrt{-\frac{4(d-1)}{d}V(\varphi)} \tag{1.4.14}$$

for a potential, V, which is always negative. This implies that when W is positive, it will stay positive as the critical curve is positive definite.

In holography, we identify $\varphi(u)$ with the running coupling corresponding to the perturbing operator. The energy scale of the renormalization group flow is identified with

$$\mu = \mu_0 e^{A(u)} \ , \tag{1.4.15}$$

where μ_0 is a reference scale. This identification gives the correct trace identity [34, 38]. Holographic beta function corresponding to the running of the coupling parameter can be written as

$$\beta(\varphi) = \mu\frac{d\varphi}{d\mu} = \frac{d\varphi}{d\ln(\mu/\mu_0)} = -2(d-1)\frac{W'(\varphi)}{W(\varphi)} \ . \tag{1.4.16}$$

Thus the beta function can be obtained from $W(\varphi)$. For simple flows, $\beta(\varphi) = 0$ will correspond to a fixed point.

In a simple holographic RG flow, we consider a potential with a maximum and a minimum. The ultraviolet (UV) and the infrared (IR) fixed points are identified with the maximum and the minimum of the potential respectively. Without a loss of generality, assume that the UV fixed point is at $\varphi = 0$. The value of the potential sets the negative cosmological constant. The bulk geometry in the UV is approximately AdS and this is dual to a CFT. In the u-coordinate, we choose the UV is at $u = -\infty$. Near the AdS boundary, the bulk metric can be written as

$$ds^2 \approx du^2 + e^{-\frac{2u}{\ell}} \eta_{\mu\nu} dx^\mu dx^\nu \ . \tag{1.4.17}$$

This can be obtained by solving (1.4.7) near $\varphi = 0$ to find $A(u) \approx \frac{-u}{\ell} + c$. The constant can be set to zero which is equivalent to a boundary coordinate transformation. The scale factor diverges and consequently the energy scale $\mu = \mu_0 e^{A(u)}$ diverges. From the RG point of view, this corresponds to the UV.

When the scalar field is a non-trivial function, the bulk geometry is no longer AdS everywhere. From the dual quantum field theory point of view, this corresponds to breaking the conformal invariance of the UV CFT by an operator with dimension Δ. In general, the potential near the UV ($\varphi = 0$) is

$$V(\varphi) = -\frac{d(d-1)}{\ell^2} - \frac{m^2}{2}\varphi^2 + \mathcal{O}(\varphi^3) \ , \tag{1.4.18}$$

where ℓ is the UV AdS length and $m^2 > 0$ (for maximum) is the mass parameter which is related to the dimension of the perturbing operator Δ by

$$\Delta(d - \Delta) = m^2 \ell^2 \ . \tag{1.4.19}$$

Solutions of this equation are

$$\Delta_\pm = \frac{d}{2} \pm \frac{d}{2}\sqrt{1 - \frac{4m^2\ell^2}{d^2}} \ . \tag{1.4.20}$$

As discussed in the previous section, in the standard dictionary ($\Delta > d/2$) we identify $\Delta_+ = \Delta$.

From the near UV potential (1.4.18), we can solve Eq. (1.4.12) in a series of φ. There are two types of solutions, given by [5]

$$W_-(\varphi) = \frac{1}{\ell}\left[2(d-1) + \frac{\Delta_-}{2}\varphi^2 + \mathcal{O}(\varphi^3)\right] + \frac{C}{\ell}\,|\varphi|^{\frac{d}{\Delta_-}}\,\left[1 + \mathcal{O}(\varphi) + \mathcal{O}(C)\right], \tag{1.4.21}$$

$$W_+(\varphi) = \frac{1}{\ell}\left[2(d-1) + \frac{\Delta_+}{2}\varphi^2 + \mathcal{O}(\varphi^3)\right] \ . \tag{1.4.22}$$

where C is an integration constant. The W_- solution is a continuous family of solutions parametrized by C whereas W_+ is an isolated solution. We can now use Eq. (1.4.11) to obtain the scalar field. We find,

$$\dot{\varphi} = W'_- \Rightarrow \varphi(u) = \varphi_- \ell^{\Delta_-} e^{\Delta_- u/\ell} + \frac{Cd\,|\varphi_-|^{\Delta_+/\Delta_-}}{\Delta_-(d-2\Delta_-)}\,\ell^{\Delta_+} e^{\Delta_+ u/\ell} + \dots\,, \tag{1.4.23}$$

$$\dot{\varphi} = W'_+ \Rightarrow \varphi(u) = \varphi_+ \ell^{\Delta_+} e^{\Delta_+ u/\ell} + \cdots\,. \tag{1.4.24}$$

As discussed in the previous section, for the $(-)$ solution we identify φ_- with the source J. In this case, the vacuum expectation value (vev) of the perturbing operator is

$$\langle \mathcal{O} \rangle_- = \frac{Cd}{\Delta_-} |\varphi_-|^{\Delta_+/\Delta_-} (M\ell)^{d-1}. \tag{1.4.25}$$

For the $(+)$ solution, source is zero and the vev is given by

$$\langle \mathcal{O} \rangle_+ = (2\Delta_+ - d)\varphi_+ (M\ell)^{d-1}\,. \tag{1.4.26}$$

In this case the flow is purely driven by the vev.

Near the minimum, the potential takes the same form as (1.4.18) but $m^2 < 0$. In this case, from Eq. (1.4.20) we see that $\Delta_- < 0$ and $\Delta_+ > d$. Similar to what we have done in the UV, we can solve Eq. (1.4.12) to find [5] :

$$W_\pm(\varphi) = \frac{1}{\ell}\left[2(d-1) + \frac{\Delta_\pm}{2}\varphi^2 + \mathcal{O}(\varphi^3)\right]\,. \tag{1.4.27}$$

Note that, in this case there is no integration constant C. As $\Delta_- < 0$ for a minimum, term like $|\varphi|^{d/\Delta_-}$ will diverge when $\varphi \to 0$. Hence in the minimum we need to set $C = 0$. Using Eqs. (1.4.11) and (1.4.10) we find

$$\dot{\varphi} = W'_- \Rightarrow \varphi(u) = \varphi_- \ell^{\Delta_-} e^{\Delta_- u/\ell} + \cdots \tag{1.4.28}$$

$$\dot{\varphi} = W'_+ \Rightarrow \varphi(u) = \varphi_+ \ell^{\Delta_+} e^{\Delta_+ u/\ell} + \cdots \tag{1.4.29}$$

$$A_\pm(u) = -\frac{u - u_\star}{\ell} - \frac{1}{8(d-1)}\varphi_\pm^2 e^{2\Delta_\pm u/\ell} + \cdots \tag{1.4.30}$$

where φ_-, φ_+ and $u_\star$ are integration constants. Eqs. (1.4.28) and (1.4.29) are valid when φ is small. As $\Delta_- < 0$, (1.4.28) requires $u \to \infty$. Consequently, $\mu = \mu_0 e^{A(u)}$ goes to 0. Therefore, the W_- solution corresponds to the flow that arrives to the IR. On the other hand, as $\Delta_+ > 0$, vanishing φ in Eq.

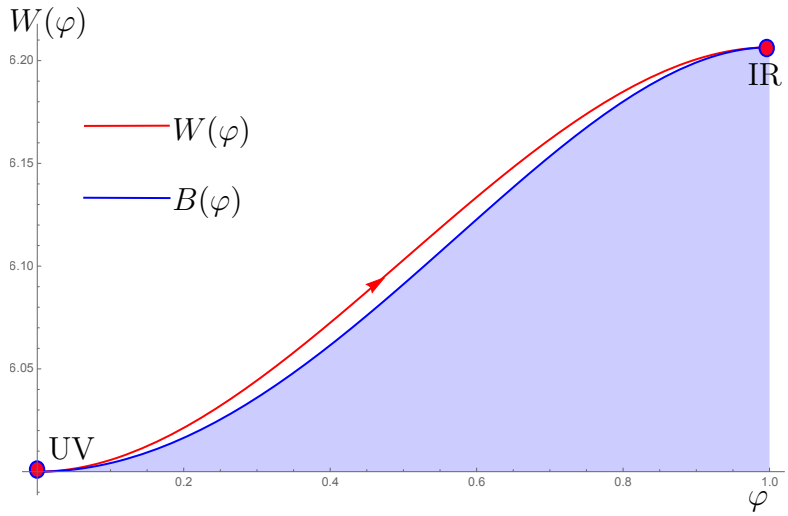

Figure 1.1: $W(\varphi)$ corresponding to $V(\varphi)$ in Eq. (1.4.31). We use $\lambda = m^2/4$ such the the minimum is at $\varphi_{\rm min} = 1$. This superpotential describes the holographic RG flow from the UV fixed point at $\varphi = 0$ to the IR fixed point at $\varphi = 1$. The blue shaded region is the forbidden region of $W(\varphi)$.

(1.4.29) requires $u \to -\infty$. In this case, the energy $\mu = \mu_0 e^{A(u)}$ goes to ∞. Therefore, the W_+ solution corresponds to a vev driven flow leaving from a UV fixed point.

After discussing the behavior of $W(\varphi)$ near the maximum and the minimum, we now return to the full solution interpolating between them. In the UV, W_- solution has a continuous parameter C. Only one flow leaving from the UV fixed point reaches the IR fixed point as the W_- solution in the IR is unique. Therefore, the W_- solution corresponds to a regular flow leaving a UV fixed point and reaching a IR fixed point. For this particular solution, the integration constant C and consequently the vev are fixed.

To present an example of a regular flow, we choose a potential

$$V(\varphi) = -\frac{d(d-1)}{\ell^2} - \frac{m^2}{2}\varphi^2 + \lambda\varphi^4 \,. \tag{1.4.31}$$

Local maximum of this potential is located at $\varphi = 0$. There are two minima and for convenience we choose $\lambda = m^2/4$ such that the minima are at $\varphi_{\rm min} = \pm 1$. A plot of the superpotential $W(\varphi)$ is shown in Fig. 1.1 which has been obtained by solving Eq.(1.4.12) for a potential as in (1.4.31) with $\ell = 1$ and $m^2\ell^2 = 3.36$.

From the superpotential $W(\varphi)$, we can use the equation

$$\dot{\varphi}(u) = W'(\varphi(u)) \tag{1.4.32}$$

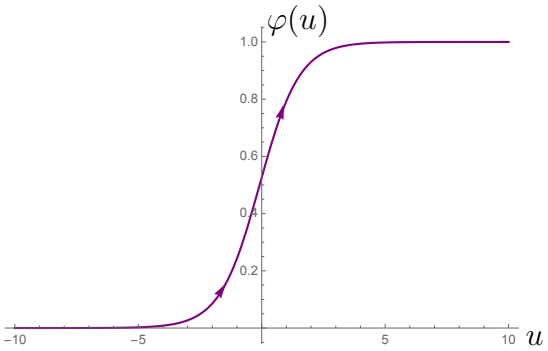

Figure 1.2: Scalar field φ as a function of u. The scalar field interpolates from the UV to the IR value. The arrow denotes the RG flow direction.

to find the scalar field as a function of u. A plot of this is shown in Fig. 1.2 which has been obtained by integrating (1.4.32) with $\varphi_- = 1$ as the source.

From the superpotential $W(\varphi)$, we can also compute the beta function from Eq. (1.4.16). A plot of this beta function is shown in Fig. 1.3. Note

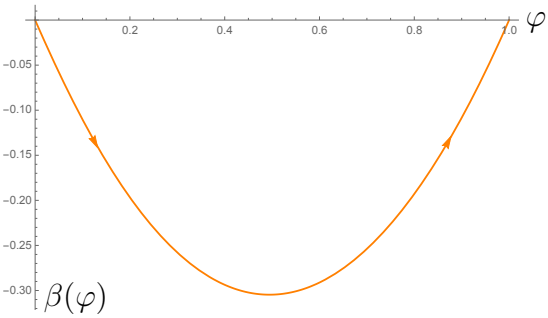

Figure 1.3: $\beta(\varphi)$ as a function of φ. The arrow denotes the RG flow direction.

that the beta function vanishes at $\varphi = 0$ and $\varphi = 1$ which are the maximum and the minimum of the potential (1.4.31). Vanishing beta function corresponds to fixed points in a simple holographic RG flow. As $\beta(\varphi) < 0$, this corresponds to a holographic RG flow from the UV CFT to the IR CFT on flat space-time.

To describe the RG flows on curved space-times, we need to modify the form of near-boundary metric. We can write the bulk metric in Fafferman-Graham coordinates

$$ds^2 = \frac{\ell^2}{z^2}\left(dz^2 + \omega_{\mu\nu}(z,x)dx^\mu dx^\nu\right) \tag{1.4.33}$$

where the boundary is located at $z = 0$ and $\omega_{\mu\nu}(z,x)$ has the following expansion

$$\omega_{\mu\nu} = \omega^{(0)}_{\mu\nu} + \omega^{(2)}_{\mu\nu} z^2 + \cdots + \omega^{(d)}_{\mu\nu} z^d + h^{(d)}_{\mu\nu} z^d \log\left(z^2\right) + \mathcal{O}(z^{d+1}) \ . \tag{1.4.34}$$

The log term appears when d is even and for odd d the series goes into even powers up to order z^{d-1}. In holography, the QFT metric $\zeta_{\mu\nu}$ is identified with [39], [40]

$$\zeta_{\mu\nu} = \omega^{(0)}_{\mu\nu} \ . \tag{1.4.35}$$

The boundary is curved when the curvature associated with the boundary metric is non-zero.

In this thesis, I have considered the boundary space-time to be maximally symmetric which in the Lorentzian signature can be flat, de Sitter or Anti-de Sitter. To describe the RG flows in Eulcidean signature we consider the boundary either flat, sphere or the hyperbolic space. The RG flows on maximally symmetric space-times are the subject of the next chapter.

Chapter 2

Holographic RG flows on curved manifolds

2.1 Introduction

Renormalization group (RG) flows in Quantum Field Theory (QFT) are usually studied in flat space. There are many reasons to consider QFTs on curved manifolds and study the associated RG flows.

One reason is that curved manifolds are considered in order to render QFTs well defined or well controlled in the IR, by taming IR divergences. There are many facets of this idea, going back to [41], and to [42] for a similar approach of regulating IR divergences in string theory. On the holographic side of QFTs, this is the role played by global AdS space. There, the QFT lives on $R \times S^d$, where the spatial part is a sphere.

One object of interest is the partition function on curved manifolds. In particular, the partition function on spheres was argued to serve as an analogue of the c-functions in odd dimensions. The case of three dimensions is well known, [43, 44] but from holographic arguments the case can be made also for other dimensions, [35, 45]. The dynamics of QFTs on curved manifolds may have interesting and different structure from that on flat manifolds, especially in the case of QFTs on AdS manifolds, [46].

Cosmology is another important context where quantum field theories on curved space-times may be considered. There is a vast body of work in this context. In connection to the renormalization group flow aspect, for example, the non-perturbative RG group on de Sitter backgrounds was studied for large-N scalar field theories in [47, 48, 49, 50, 51, 52, 53, 54, 55].

There is a folk theorem which says that RG flows of QFTs on curved manifolds are very similar to those on flat manifolds. The argument for this

is that β-functions are determined by UV/short-distance divergences and the short distance structure of a given QFT is independent of its curvature. Although the leading intuition of such statements is basically correct, the folk theorem fails on several grounds. Indeed, the leading UV divergences are independent of curvature. However, subleading ones do depend on curvature. We will see this clearly and in a controlled fashion in this chapter, although it is known [39, 56, 57]. A further observation is that already for CFTs, curvature is a source of breaking of scale invariance via the conformal anomaly, [58]. For general QFTs driven by relevant couplings, the β functions do in general depend on curvature, [38]. The same is true for the vacuum expectation values of operators. More generally, one may expect that curvature becomes very important in the IR and this expectation is, in general, correct.

In this chapter we will discuss the RG behavior of QFTs on maximally symmetric curved space-times using the framework of holography. The holographic correspondence, [12, 15, 16], provides a map between QFT and gravity/string-theories in higher dimensions, at least in the limit of large N.

We study an Einstein-scalar theory in $(d+1)$-dimensions described by (1.4.2). To study the holographic RG flows, we can employ domain wall coordinates and choose the following ansatz for φ and the $(d+1)$-dimensional metric (for both Euclidean and Lorentzian signatures):

$$\varphi = \varphi(u)\,, \qquad ds^2 = du^2 + e^{2A(u)}\zeta_{\mu\nu}dx^\mu dx^\nu\,. \tag{2.1.1}$$

Here, $A(u)$ is a scale factor that depends on the coordinate u only, while $\zeta_{\mu\nu}$ is a metric describing a d-dimensional maximally symmetric space-time. As a consequence of maximal symmetry we have[1]

$$R^{(\zeta)}_{\mu\nu} = \kappa\zeta_{\mu\nu}\,, \quad R^{(\zeta)} = d\kappa\,, \quad \text{with} \quad \kappa = \begin{cases} \frac{(d-1)}{\alpha^2} & \mathrm{dS}_d \ \text{ or } \ S^d \\ 0 & \mathcal{M}_d \\ -\frac{(d-1)}{\alpha^2} & \mathrm{AdS}_d \end{cases}, \tag{2.1.2}$$

where α is the curvature length scale of $\zeta_{\mu\nu}$ and $\mathcal{M}_d$ denotes d-dimensional Minkowski space. We also define the induced metric $\gamma_{\mu\nu}$ on a d-dimensional slice at constant u

$$\gamma_{\mu\nu} \equiv e^{2A(u)}\zeta_{\mu\nu}\,. \tag{2.1.3}$$

[1] In the case of a foliation with positive curvature slices, these can be given by d-dimensional de Sitter space or a d-sphere. In the rest of the chapter we will mainly refer to the case of the sphere, keeping in mind that the results will also hold for de Sitter.

In the following, we will also adhere to the following shorthand notation. Derivatives with respect to u will be denoted by a dot while derivatives with respect to φ will be denoted by a prime, i.e.:

$$\dot{f}(u) \equiv \frac{df(u)}{du}\,, \qquad g'(\varphi) \equiv \frac{dg(\varphi)}{d\varphi}\,. \tag{2.1.4}$$

Varying the action (1.4.2) with respect to the metric and the scalar φ gives rise to the equations of motion:

$$2(d-1)\ddot{A} + \dot{\varphi}^2 + \frac{2}{d}e^{-2A}R^{(\zeta)} = 0\,, \tag{2.1.5}$$

$$d(d-1)\dot{A}^2 - \frac{1}{2}\dot{\varphi}^2 + V - e^{-2A}R^{(\zeta)} = 0\,, \tag{2.1.6}$$

$$\ddot{\varphi} + d\dot{A}\dot{\varphi} - V' = 0\,. \tag{2.1.7}$$

These equations are the same for both Lorentzian and Euclidean signatures, so all our results will hold for both cases (unless stated explicitly).

2.2 The first order formalism

As in chapter 1, it will be convenient to rewrite the second-order Einstein equations as a set of first-order equations, which will allow an interpretation as gradient RG flows. This is locally always possible, except at special points where $\dot{\varphi} = 0$, which we will later refer to as bounces, as previously observed in [5]. Given a solution, as long as $\dot{\varphi}(u) \neq 0$, we can invert the relation between u and $\varphi(u)$ and define the following *scalar* functions of φ:

$$W(\varphi) \equiv -2(d-1)\dot{A}\,, \tag{2.2.1}$$

$$S(\varphi) \equiv \dot{\varphi}\,, \tag{2.2.2}$$

$$T(\varphi) \equiv e^{-2A}R^{(\zeta)} = R^{(\gamma)}\,. \tag{2.2.3}$$

where the expressions on the right hand side are evaluated at $u = u(\varphi)$.

In terms of the functions defined above, the equations of motion (2.1.5) –(2.1.7) become

$$S^2 - SW' + \frac{2}{d}T = 0\,, \tag{2.2.4}$$

$$\frac{d}{2(d-1)}W^2 - S^2 - 2T + 2V = 0\,, \tag{2.2.5}$$

$$SS' - \frac{d}{2(d-1)}SW - V' = 0\,, \tag{2.2.6}$$

which are coordinate independent, first-order non-linear differential equations in field space. In the flat case $T = 0$ and we recover the usual superpotential equation (1.4.12) for W by setting $S = W'$. Thus, the difference between S and W' is a measure of the curvature of the boundary.

Note that equations (2.2.4-2.2.6) are algebraic in T. We can hence partially solve this system by eliminating T so that we are left with the following two equations

$$\frac{d}{2(d-1)}W^2 + (d-1)S^2 - dSW' + 2V = 0\,, \tag{2.2.7}$$

$$SS' - \frac{d}{2(d-1)}SW - V' = 0\,. \tag{2.2.8}$$

Next, we can solve the second equation (2.2.8) for W algebraically. Substituting into the first equation (2.2.7) we obtain

$$dS^3S'' - \frac{d}{2}S^4 - S^2(S')^2 - \frac{d}{d-1}S^2V + (d+2)SS'V' - dS^2V'' - (V')^2 = 0 \tag{2.2.9}$$

This is a second order equation in S and its integration requires two integration constants. As we will see in the next section, one integration constant will be related to the vev of the perturbing operator, while the other integration constant will be related to the UV curvature.

In the following we will work both with the full set of equations (2.2.4)–(2.2.6), with the two equations (2.2.7)–(2.2.8) or with (2.2.9) choosing whichever is more convenient.

A few important properties of the functions W, S and T are discussed below (see appendix B for more details):

1. At a generic point in field space, there exist two branches of solutions, with opposite signs of S and W'. In each branch, S and W' have the same sign.

2. The critical curve $B(\varphi)$ was defined in (1.4.13). In the flat case, $W(\varphi)$ has to satisfy $|W(\varphi)| \geq B(\varphi)$, and equality can be reached only where $W' = 0$. For positive non-zero curvature, the bound is stricter, and the critical curve cannot be reached, except in the UV where $T \to 0$. On the other hand, for negative curvature W can cross the critical curve.

3. As shown in appendix A, curvature invariants are finite as long as $S(\varphi)$ and $V(\varphi)$ are both finite. On the other hand a divergent $W(\varphi)$ does not necessarily imply that the solution is singular.

4. Points where $S \to 0$ (i.e. $\varphi(u)$ has an extremum) correspond to points of enhanced symmetry: In fact, around these points the metric is approximately maximally symmetric, i.e.

$$S(\varphi_*) = 0 \quad \Rightarrow \quad R_{ab} = \frac{V(\varphi_*)}{d-1} g_{ab}. \tag{2.2.10}$$

This has to be confronted with generic points, where $R^{(g)}_{\mu\nu} = k g_{\mu\nu}$, $R^{(g)}_{uu} = k' g_{uu}$, with $k' - k = S^2/2$ as shown in (B.2.2) and (B.2.3) .

Holographic RG flows are in one-to-one correspondence with regular solutions to the equations of motion (2.1.5)–(2.1.7). Assuming the scale factor plays the same role of energy scale as in the flat case, the holographic β-function can be expressed in terms of $W(\varphi)$ and $S(\varphi)$:

$$\beta(\varphi) \equiv \frac{d\varphi}{dA} = -2(d-1)\frac{S(\varphi)}{W(\varphi)}\,. \tag{2.2.11}$$

The space of regular solutions for $W(\varphi)$ and $S(\varphi)$ coincides with the space of possible RG flows up to a choice of two initial conditions: (1) The value of the deformation parameter in the UV, φ_-, which is called the source and it corresponds to the UV coupling constant of the relevant operator dual to the scalar. (2) The UV value of the scalar curvature $R^{\rm uv}$ of the manifold on which the field theory is defined. Therefore, by classifying all solutions $W(\varphi)$, $S(\varphi)$ to the equations (2.2.7) and (2.2.8) for a given potential $V(\varphi)$, we can characterize all possible RG flows corresponding to a given bulk theory. Hence, in the following we will be interested in solutions to these equations for various choices of the potential $V(\varphi)$.

To be specific, we will assume that $V(\varphi)$ has at least one maximum, where V takes a negative value. This ensures that there exists a conformal fixed point, and a family of asymptotically AdS solutions which correspond to deforming the theory away from the fixed point by a relevant operator.

In addition, $V(\varphi)$ may have other maxima and/or minima representing distinct UV or IR fixed points for the dual CFT. The aim of the next section is to study the solutions *at* the fixed points in the presence of curvature, but with the relevant deformation set to zero.

2.3 Conformal fixed points

A conformal fixed point corresponds to a solution of (2.1.5)–(2.1.7) with $\varphi = \text{const.}$, i.e. $\dot\varphi = 0 = \ddot\varphi$. Such solutions are associated with extrema $\varphi_{\rm ext}$ of the potential, at which $V'(\varphi_{\rm ext}) = 0$.

In this case, the solution (2.1.1) is always the space-time AdS_{d+1}, written in different coordinate systems, regardless of the curvature of the d-dimensional slices with metric $\zeta_{\mu\nu}$. Indeed, AdS_{d+1} admits d-dimensional de Sitter (or sphere, in the Euclidean version), Minkowski or AdS slicings of the form (2.1.1), with (see e.g. [59]):

$$e^{A(u)} = \begin{cases} \dfrac{\ell}{\alpha}\sinh\left(-\dfrac{u+c}{\ell}\right), & -\infty < u \leq -c, \qquad \mathrm{dS}_d \text{ or } S^d \\ \exp\left(-\dfrac{u+c}{\ell}\right), & -\infty < u < +\infty, \qquad \mathcal{M}_d \\ \dfrac{\ell}{\alpha}\cosh\left(\dfrac{u+c}{\ell}\right), & -\infty < u < +\infty, \qquad \mathrm{AdS}_d \end{cases} . \tag{2.3.1}$$

Here ℓ is the AdS_{d+1} length ℓ defined via $V(\varphi_{\mathrm{ext}}) = -\frac{d(d-1)}{\ell^2}$, while the length scale α was introduced in (2.1.2). We also chose the boundary of AdS_{d+1} to be located at $u \to -\infty$. The parameter c is an integration constant.

Although the bulk space-time is the same, the asymptotic boundary is different in the three cases. This leads to inequivalent boundary theories. As the d-dimensional boundaries of the space-times (2.3.1) are all conformally equivalent, at the fixed point the effect of curvature is completely encoded in the conformal anomaly. This will change when we consider RG-flows and introduce an explicit breaking of conformal invariance.

In the case of Minkowski slices, c can be removed by a conformal rescaling of the boundary metric and we can set $c = 0$. However, for dS and AdS slices the constant c contains physical information and cannot be removed. In particular, c determines the curvature of the d-dimensional slices. To see this, first note that the length scale α is unphysical and can be chosen freely. It is an artifact of splitting the induced metric $\gamma_{\mu\nu}$ on the d-dimensional slices into a scale factor $e^{A(u)}$ and $\zeta_{\mu\nu}$. This can be seen e.g. by evaluating $R^{(\gamma)}$, i.e. the scalar curvature associated with the induced metric $\gamma_{\mu\nu}$ on the d-dimensional slices, which is given by

$$R^{(\gamma)} = e^{-2A(u)} R^{(\zeta)} . \tag{2.3.2}$$

For a conformal fixed point we hence find

$$R^{(\gamma)} = \begin{cases} \dfrac{d(d-1)}{\ell^2}\sinh^{-2}\dfrac{u+c}{\ell} & \mathrm{dS}_d \text{ or } S^d \\ -\dfrac{d(d-1)}{\ell^2}\cosh^{-2}\dfrac{u+c}{\ell} & \mathrm{AdS}_d \end{cases} , \tag{2.3.3}$$

i.e. the parameter α has dropped out from the expressions. Instead, it is the parameter c which contains information about the curvature.

An important quantity will be the scalar curvature $R^{\rm uv}$, which we define as the scalar curvature associated with the UV limit of the (rescaled) induced metric $\gamma^{\rm uv}_{\mu\nu} \equiv \lim_{u\to-\infty} e^{2u/\ell}\gamma_{\mu\nu}$. Indeed, the metric $\gamma^{\rm uv}_{\mu\nu}$ is the leading boundary data appearing in the Fefferman-Graham expansion near the boundary, and in holography it is interpreted as the metric of the dual field theory, as discussed in chapter 1. The associated curvature $R^{\rm uv}$ is given by:

$$R^{\rm uv} = \lim_{u\to-\infty} e^{-2u/\ell} R^{(\gamma)}\,, \tag{2.3.4}$$

For the case of a conformal fixed point we find

$$R^{\rm uv} = \pm\frac{4d(d-1)}{\ell^2}\, e^{2c/\ell}\,, \tag{2.3.5}$$

where the positive (negative) sign is appropriate for dS (AdS) curvature.

For later use, it will be convenient to expand the scale factor (2.3.1) in the vicinity of the boundary $u \to -\infty$. Restricting attention to the cases of S^d/AdS_d slicings we obtain

$$\begin{aligned} A(u) &= \ln\Big(\frac{\ell}{2\alpha}\Big) - \frac{u+c}{\ell} \mp e^{2(u+c)/\ell} + \mathcal{O}(e^{4u/\ell}) \\ &= -\frac{u}{\ell} + \frac{1}{2}\ln\Big(\frac{R^{(\zeta)}}{R^{\rm uv}}\Big) - \frac{\ell^2 R^{\rm uv}}{4d(d-1)}\, e^{2u/\ell} + \mathcal{O}(e^{4u/\ell}) \end{aligned} \tag{2.3.6}$$

where the last line is valid for both S^d/AdS_d slicings.

For most practical purposes it will be convenient to set $R^{(\zeta)} = R^{\rm uv}$, which we can always achieve by choosing $\alpha = \frac{\ell}{2}\, e^{-c/\ell}$ for the arbitrary parameter α. This is the convention that we will adopt throughout this thesis. Note that in this case the constant term in (2.3.6) vanishes. This also holds for space-times which only asymptote to AdS_{d+1} near the boundary: We can always ensure that $R^{(\zeta)} = R^{\rm uv}$ for an asymptotically AdS space-time by setting the constant term in the near-boundary expansion of $A(u)$ to zero.

2.4 Perturbative analysis near extrema of the potential

We will now examine solutions of our system in the vicinity of extremal points of V. We then proceed to determining the near-boundary geometry.

Without loss of generality we take the extremum to be at $\varphi = 0$. It will then be sufficient to consider the potential

$$V = -\frac{d(d-1)}{\ell^2} - \frac{m^2}{2}\varphi^2 + \mathcal{O}(\varphi^3)\,, \tag{2.4.1}$$

where we will choose $m^2 > 0$ for maxima and $m^2 < 0$ for minima. In the following we will solve equations (2.2.4)–(2.2.6) for $W(\varphi)$, $S(\varphi)$ and $T(\varphi)$ near $\varphi = 0$. The relevant calculations are performed in appendix C. Here we present and discuss the results.

2.4.1 Expansion near maxima of the potential

We work in an expansion in φ about the maximum at $\varphi = 0$. Like in the case of zero boundary curvature discussed in e.g. [5], there are two branches of solutions to equations (2.2.4)–(2.2.6), and we will distinguish them by the subscripts $(+)$ and $(-)$. The $(-)$ solutions are:

$$\begin{aligned} W_-(\varphi) = \frac{1}{\ell}\left[2(d-1) + \frac{\Delta_-}{2}\varphi^2 + \mathcal{O}(\varphi^3)\right] + \frac{\mathcal{R}}{d\ell}\,|\varphi|^{\frac{2}{\Delta_-}}\,\left[1 + \mathcal{O}(\varphi) + \mathcal{O}(\mathcal{R})\right] \\ + \frac{C}{\ell}\,|\varphi|^{\frac{d}{\Delta_-}}\,\left[1 + \mathcal{O}(\varphi) + \mathcal{O}(C) + \mathcal{O}(\mathcal{R})\right], \end{aligned} \tag{2.4.2}$$

$$\begin{aligned} S_-(\varphi) = \frac{\Delta_-}{\ell}\varphi\,\left[1 + \mathcal{O}(\varphi)\right] + \frac{Cd}{\Delta_-\ell}\,|\varphi|^{\frac{d}{\Delta_-}-1}\,\left[1 + \mathcal{O}(\varphi) + \mathcal{O}(C)\right], \\ + \frac{1}{\ell}\mathcal{O}\left(\mathcal{R}|\varphi|^{\frac{2}{\Delta_-}+1}\right) + \frac{1}{\ell}\mathcal{O}\left(\mathcal{R}C|\varphi|^{\frac{2+d}{\Delta_-}-1}\right) \end{aligned} \tag{2.4.3}$$

$$T_-(\varphi) = \ell^{-2}\,\mathcal{R}\,|\varphi|^{\frac{2}{\Delta_-}}[1 + \mathcal{O}(\varphi) + \mathcal{O}(C) + \mathcal{O}(\mathcal{R})]\,, \tag{2.4.4}$$

where C and $\mathcal{R}$ are integration constants, and we have defined:

$$\Delta_\pm = \frac{1}{2}\left(d \pm \sqrt{d^2 - 4m^2\ell^2}\right) \qquad \text{with} \quad 0 < m^2 < \frac{d^2}{4\ell^2} \tag{2.4.5}$$

The (+) solution is given by:

$$W_+(\varphi) = \frac{1}{\ell}\left[2(d-1) + \frac{\Delta_+}{2}\varphi^2 + \mathcal{O}(\varphi^3)\right] + \frac{\mathcal{R}}{d\ell}\,|\varphi|^{\frac{2}{\Delta_+}}\,\left[1 + \mathcal{O}(\varphi) + \mathcal{O}(\mathcal{R})\right], \tag{2.4.6}$$

$$S_+(\varphi) = \frac{\Delta_+}{\ell}\varphi\,\left[1 + \mathcal{O}(\varphi)\right] + \mathcal{O}\left(\mathcal{R}|\varphi_-|^{\frac{2}{\Delta_+}+1}\right), \tag{2.4.7}$$

$$T_+(\varphi) = \ell^{-2}\,\mathcal{R}\,|\varphi|^{\frac{2}{\Delta_+}}[1 + \mathcal{O}(\varphi) + \mathcal{O}(\mathcal{R})]\,. \tag{2.4.8}$$

The above expressions describe two continuous families of solutions, whose structure is a *universal* analytic expansion in integer powers of φ, plus a series of non-analytic, subleading terms which, in principle, depend on two (dimensionless) integration constants C and $\mathcal{R}$. Note that the $(-)$-branch of solutions depends on two integration constants C and $\mathcal{R}$, while only the integration constant $\mathcal{R}$ appears in the solutions of the $(+)$-branch. The notation $\mathcal{O}(C)$ and $\mathcal{O}(\mathcal{R})$ does not imply that C or $\mathcal{R}$ have to be small. Rather, this is shorthand to indicate that these terms will be accompanied by higher powers of φ thus justifying their omission.[2]

The solutions (2.4.2)–(2.4.4) generalize the near-extremum superpotential solutions that arise in the flat case (1.4.21), where only the integration constant C was present. Indeed, setting $\mathcal{R} = 0$ we recover the flat result for $W(\varphi)$ and we also find $S = W'$ and $T = 0$. This indicates that $\mathcal{R} = 0$ is strictly related to the curvature of the d-dimensional metric, a fact that will be confirmed explicitly below.

Given our results for W, S and T, we are now in a position to solve for $\varphi(u)$ and $A(u)$. For the $(-)$-branch we solve (2.2.2) and (2.2.1) subject to

[2]For example, the solution for W on the $(-)$-branch can be written schematically as the following triple expansion:

$$W_-(\varphi) = \frac{1}{\ell}\sum_{l=0}^{\infty}\sum_{m=0}^{\infty}\sum_{n=0}^{\infty} A_{l,m,n}\left(C\,|\varphi|^{d/\Delta_-}\right)^l\left(\mathcal{R}\,|\varphi|^{2/\Delta_-}\right)^m\varphi^n \tag{2.4.9}$$

(2.4.3) and (2.4.2) to obtain

$$\varphi(u) = \varphi_- \ell^{\Delta_-} e^{\Delta_- u/\ell} \left[1 + \mathcal{O}\left(\mathcal{R}|\varphi_-|^{2/\Delta_-} e^{2u/\ell}\right) + \ldots\right] \tag{2.4.10}$$
$$+ \frac{Cd\,|\varphi_-|^{\Delta_+/\Delta_-}}{\Delta_-(d-2\Delta_-)}\,\ell^{\Delta_+} e^{\Delta_+ u\ell}\left[1 + \mathcal{O}\left(\mathcal{R}|\varphi_-|^{2/\Delta_-} e^{2u/\ell}\right) + \ldots\right] + \ldots\,,$$

$$A(u) = \bar{A}_- - \frac{u}{\ell} - \frac{\varphi_-^2\,\ell^{2\Delta_-}}{8(d-1)} e^{2\Delta_- u/\ell} - \frac{\mathcal{R}|\varphi_-|^{2/\Delta_-}\,\ell^2}{4d(d-1)} e^{2u/\ell} \tag{2.4.11}$$
$$- \frac{\Delta_+ C|\varphi_-|^{d/\Delta_-}\,\ell^d}{d(d-1)(d-2\Delta_-)} e^{du/\ell} + \ldots\,.$$

Here, we introduced the integration constants φ_- and $\bar{A}_-$. We can repeat the analysis for the (+)-branch of solutions by solving (2.2.2) and (2.2.1) subject to (2.4.7) and (2.4.6). We find:

$$\varphi(u) = \varphi_+ \ell^{\Delta_+} e^{\Delta_+ u/\ell}\left[1 + \mathcal{O}\left(\mathcal{R}|\varphi_+|^{2/\Delta_+} e^{2u/\ell}\right) + \ldots\right] + \ldots\,, \tag{2.4.12}$$

$$A(u) = \bar{A}_+ - \frac{u}{\ell} - \frac{\varphi_+^2\,\ell^{2\Delta_+}}{8(d-1)} e^{2\Delta_+ u/\ell} - \frac{\mathcal{R}|\varphi_+|^{2/\Delta_+}\,\ell^2}{4d(d-1)} e^{2u/\ell} + \ldots\,, \tag{2.4.13}$$

where we introduced the integration constants φ_+ and $\bar{A}_+$. A few comments are in order.

- As our solutions for W, S and T are only valid for small φ, the above results are the leading terms in $\varphi(u)$ and $A(u)$ for $u \to -\infty$.

- For both the (+) and (−)-branch, the result for $A(u)$ exhibits the behavior expected for a scale factor in the near-boundary region of an AdS_{d+1} space-time with length scale ℓ, as can be seen by comparing with (2.3.6). As explained in section 2.3, for asymptotically AdS space-times we can always choose a metric ansatz such that $R^{(\zeta)} = R^{\mathrm{uv}}$. This amounts to setting $\bar{A}_\pm = 0$.

- For the (−)-branch of solutions, we identify φ_- as the source for the scalar operator $\mathcal{O}$ in the boundary field theory associated with φ. The vacuum expectation value of $\mathcal{O}$ depends on C and is given by

$$\langle\mathcal{O}\rangle_- = \frac{Cd}{\Delta_-}\,|\varphi_-|^{\Delta_+/\Delta_-}(M_P\ell)^{d-1}\,. \tag{2.4.14}$$

  Thus the (−)-branch of solutions is a source flow.

- For the (+)-branch of solutions, the bulk field φ is also associated with a scalar operator $\mathcal{O}$ in the boundary field theory. However, in this case the source is identically zero, yet there is a non-zero vev given by

$$\langle\mathcal{O}\rangle_+ = (2\Delta_+ - d)\,\varphi_+(M_P\ell)^{d-1}\,. \tag{2.4.15}$$

Therefore, the (+) solution is a vev deformation. There is also an associated moduli space of vevs, as φ_+ is arbitrary, being an integration constant of the first order flow equation.

- We can learn even more by comparing the two expressions for $A(u)$ in (2.4.11) and (2.3.6). Matching the coefficients of $e^{2u/\ell}$ implies

$$\mathcal{R} \equiv \begin{cases} R^{\rm uv}|\varphi_-|^{-2/\Delta_-} & (-)\text{-branch} \\ R^{\rm uv}|\varphi_+|^{-2/\Delta_+} & (+)\text{-branch} \end{cases} . \tag{2.4.16}$$

  Thus, the integration constant $\mathcal{R}$ is related to the curvature, $R^{\rm uv}$ in units of the source/vev of the manifold on which the UV QFT is defined.

- Interestingly, the $(-)$ and $(+)$-branches of solutions are not completely unrelated. One can check that given a solution of the $(-)$-branch, we can arrive at a solution on the $(+)$-branch by performing the following rescaling:

$$\varphi_- \to 0\,, \quad C \to +\infty\,, \quad C|\varphi_-|^{\frac{\Delta_+}{\Delta_-}} = \text{const.}\,, \qquad \mathcal{R}|\varphi_-|^{\frac{2}{\Delta_-}} = \text{const.} \tag{2.4.17}$$

  To be specific, under this rescaling the solutions in (2.4.10) and (2.4.11) can be brought into the form of (2.4.12) and (2.4.13). This gives rise to another interpretation of the $(+)$-branch of solutions. In particular, for fixed $R^{\rm uv}$ a W_+ solution is the upper envelope of the family of W_- solutions parameterized by C. This is similar to the flat case [25, 5].

Overall, the above findings imply that, as in the flat case, *maxima of the potential are associated with UV fixed points*. The bulk space-time asymptotes to AdS_{d+1} and reaching the maximum of the potential is equivalent to reaching the boundary. Moving away from the boundary corresponds to a flow leaving the UV. Flows corresponding to solutions on the $(-)$-branch are driven by the existence of a non-zero source φ_- for the perturbing operator $\mathcal{O}$. Flows corresponding to solutions on the $(+)$-branch are driven purely by a non-zero vev for $\mathcal{O}$, as the source vanishes identically.

Finally, notice that as expected near a UV fixed point, the curvature terms proportional to $\mathcal{R}$ only enter as subleading corrections in W, S and the bulk solution (2.4.10)–(2.4.13).

2.4.2 Expansion near minima of the potential

In this section, we will display solutions for $W(\varphi)$, $S(\varphi)$ and $T(\varphi)$ corresponding to flows that either leave or arrive at minima of the potential. We

will again consider the potential (2.4.1), but now we have $m^2 < 0$. In the following, we present the results, while detailed calculations can be found in appendix C. Again, we find that there exist (+) and (−)-branches in the space of solutions, which we will discuss in turn.

(+)-branch

For the (+)-branch the expansions around a minimum of V take the same form as in the vicinity of a maximum. Therefore, we obtain:

$$W_+(\varphi) = \frac{1}{\ell}\left[2(d-1) + \frac{\Delta_+}{2}\varphi^2 + \mathcal{O}(\varphi^3)\right] + \frac{\mathcal{R}}{d\ell}\,|\varphi|^{\frac{2}{\Delta_+}}\,\left[1 + \mathcal{O}(\varphi) + \mathcal{O}(\mathcal{R})\right], \tag{2.4.18}$$

$$S_+(\varphi) = \frac{\Delta_+}{\ell}\varphi\,\left[1 + \mathcal{O}(\varphi)\right] + \frac{1}{\ell}\mathcal{O}\left(\mathcal{R}|\varphi|^{\frac{2}{\Delta_+}+1}\right), \tag{2.4.19}$$

$$T_+(\varphi) = \ell^{-2}\,\mathcal{R}\,|\varphi|^{\frac{2}{\Delta_+}}\left[1 + \mathcal{O}(\varphi) + \mathcal{O}(\mathcal{R})\right], \tag{2.4.20}$$

with Δ_+ defined as before in (2.4.5), but now we have that $m^2 < 0$. The integration constant $\mathcal{R}$ is continuous and gives rise to a family of solutions. As before, we can integrate to obtain:

$$\varphi(u) = \varphi_+ \ell^{\Delta_+} e^{\Delta_+ u/\ell}\left[1 + \mathcal{O}\left(\mathcal{R}|\varphi_+|^{2/\Delta_+} e^{2u/\ell}\right) + \ldots\right] + \ldots, \tag{2.4.21}$$

$$A(u) = \bar{A}_+ - \frac{u}{\ell} - \frac{\varphi_+^2\,\ell^{2\Delta_+}}{8(d-1)} e^{2\Delta_+ u/\ell} - \frac{\mathcal{R}|\varphi_+|^{2/\Delta_+}\,\ell^2}{4d(d-1)} e^{2u/\ell} + \ldots, \tag{2.4.22}$$

This solution has the following interpretation:

- Recall that the expansions of W, S and T are valid only for small φ. As $\Delta_+ > d$ at a minimum, it follows from (2.4.21) that small φ requires $u \to -\infty$. Using (2.4.22), this in turn implies that $e^{A(u)} \to \infty$ when approaching the minimum of the potential. This is the behavior expected when approaching a UV fixed point.

- In the boundary QFT, the bulk field φ will be associated with an operator $\mathcal{O}$. However, the absence of a term $\sim e^{\Delta_- u/\ell}$ in (2.4.21) implies that the source of this operator vanishes. On the other hand, there is a non-zero vev given by

  $$\langle\mathcal{O}\rangle_+ = (2\Delta_+ - d)\varphi_+ (M_P \ell)^{d-1}\,. \tag{2.4.23}$$

  The solution (2.4.21) is to be interpreted as a flow purely driven by a vev.

- Matching the expression (2.4.22) with the near-boundary expansion (2.3.6) we again find that $\mathcal{R}$ is related to the curvature $R^{\rm uv}$ of the background manifold of the UV QFT:

$$\mathcal{R} = R^{\rm uv}|\varphi_+|^{-2/\Delta_+} \,. \tag{2.4.24}$$

To summarize, as in the flat case, for solutions of the (+)-branch *minima of the potential correspond to UV fixed points*. Flows from such UV fixed points are not driven by a source for the perturbing operator $\mathcal{O}$, but rather by its vev $\langle\mathcal{O}\rangle_+$. This corresponds to a spontaneous breaking of conformal invariance.

As in the flat case, these solutions are generically singular in the IR, because unlike the (−)-branch solutions departing from a UV *maximum*, they have no continuous adjustable parameter (beside the UV data $R^{\rm uv}$) which one may vary to select a solution with regular interior geometry. In the (−)-branch on the other hand, this role is played by the extra integration constant C. Nevertheless, one can construct specific examples where regular solutions of the (+) type exist [5].

(−)-branch

Interestingly, we will need to distinguish between the two cases where the boundary field theory is defined on a curved manifold ($R^{\rm uv} \neq 0$) and a flat manifold ($R^{\rm uv} = 0$). A key result is that for $R^{\rm uv} \neq 0$ the (−)-branch of solutions does not exist. A proof (at the level of the functions $\varphi(u)$ and $A(u)$) can be found in appendix D. More specifically, there are no solutions in the (−)-branch corresponding to flows that either leave or arrive at a minimum of V for $R^{\rm uv} \neq 0$. Such a solution only exists if $R^{\rm uv} = 0$ and we recover the result from [5], where RG flows for QFTs on flat manifolds were studied.

For $R^{\rm uv} = 0$ we have that $T_-(\varphi) = 0$ identically. In addition, (2.1.5) implies that $S(\varphi) = W'(\varphi)$ and the solution is completely specified by $W(\varphi)$. Our findings can be summarized as follows:

$$R^{\rm uv} \neq 0 : \qquad \text{No solution.} \tag{2.4.25}$$

$$R^{\rm uv} = 0 : \qquad W_-(\varphi) = \frac{1}{\ell}\left[2(d-1) + \frac{\Delta_-}{2}\varphi^2 + \mathcal{O}(\varphi^3)\right] \,. \tag{2.4.26}$$

For the case $R^{\rm uv} = 0$ we can determine $\varphi(u)$ and $A(u)$ by integrating (2.2.1),

(2.2.2) subject to (2.4.26) and $S = W'$. One obtains

$$\varphi(u) = \varphi_- \, \ell^{\Delta_-} \, e^{\Delta_- u/\ell} + \dots \,, \tag{2.4.27}$$

$$A(u) = \bar{A} - \frac{u}{\ell} - \frac{\varphi_-^2}{8(d-1)} \, \ell^{2\Delta_-} \, e^{2\Delta_- u/\ell} + \dots \,, \tag{2.4.28}$$

with $\bar{A}$ and φ_- integration constants. We recover the result from chapter 1 that for $R^{\rm uv} = 0$ *minima of the potential correspond to IR fixed points*, as φ small now requires $u \to +\infty$ (as $\Delta_- < 0$ at a minimum) which in turn implies $e^{A(u)} \to 0$. On the other hand, no such IR limit exist in the presence of curvature, unlike around a UV fixed point, where curvature only added subleading corrections. One is then led to wonder what is the fate of curved RG flows in the interior where curvature becomes the dominant driving parameter. This is the subject of the next section.

2.5 The geometry in the interior

After having analyzed the behavior close to the UV boundary, in this section we analyze the geometry in the interior. In particular, we will be interested in the way the space-time can "end" in a regular way, i.e. where the scale factor shrinks to zero but the bulk curvature invariants are finite. These are the curved analogs of flat IR fixed points.

Unlike what happens close to the AdS boundary, where curvature leads only to subleading corrections to the near-boundary asymptotics, in the interior curvature can drastically change the geometry with respect to the flat case. As we will see, for positive curvature, the RG flow reaches an end before the (would-be) IR fixed point of the flat theory; for negative curvature, on the other hand, both the scalar field and the scale factor turn around and the flow reaches the boundary on both sides. Non-zero curvature can also deform the geometry near *bounces* (points where the scalar field inverts its flow direction [5] but the scale factor is still monotonically decreasing).

In this analysis, a key role is played by the critical points in the 1st order equations. These are points where $\dot{\phi} = 0$. Before discussing the non-zero curvature case, we briefly review the analysis of critical points for zero curvature.

2.5.1 Review of flat case

In the flat case critical points correspond to points along the flow with vanishing W'. Extrema of W in the interior of the geometry belong to two classes: regular IR fixed points, and bounces [5].

- **Flat IR fixed points.** A regular IR endpoint of the geometry is attained, in the flat case, when the flow asymptotes to a minimum (which we denote by φ_{IR}) of the scalar potential. In this case, $\dot{\varphi} \to 0$ and the geometry in the interior is asymptotically AdS_{d+1}, with

$$e^A(u) \simeq e^{-u/\ell_{IR}}, \qquad \varphi(u) \to \varphi_{IR}, \qquad u \to +\infty \tag{2.5.1}$$

  In the language of the superpotential, as $\varphi \to \varphi_{IR}$, $W \to 2(d-1)/\ell_{IR}$ and $W' \to 0$, and the (flat) holographic β-function vanishes:

$$\beta(\varphi) = -2(d-1)\frac{W'}{W} \to 0\,, \qquad \varphi \to \varphi_{IR}. \tag{2.5.2}$$

  The condition $W'(\varphi_{IR}) = 0$ by itself does not imply that the flow has reached a fixed point: for that, we also need $W''(\varphi)$ to be finite, and this only happens when $V'(\varphi_{IR}) = 0$, i.e. φ_{IR} is also a minimum of the bulk potential as we have assumed above. If the latter condition is not met, then the geometry features a bounce, as discussed below.

- **Flat Bounces.** A generic extremum of W, i.e. a point φ_B in field space such that $W'(\varphi_B) = 0$ but $V'(\varphi_B) \neq 0$, corresponds to a *bounce*, i.e. a point where the flow inverts its direction [5]. The superpotential becomes singular because φ is not a good coordinate around such points. The flow however can be continued by gluing to another branch, where $\dot{\varphi}$ has the opposite sign. Close to a bounce, the superpotential behaves as:

$$W(\varphi) \simeq W_b \pm c(\varphi_B - \varphi)^{3/2} + O\Big((\varphi_B - \varphi)^2\Big), \tag{2.5.3}$$

  where c is a constant and we have supposed that the flow reaches the bounce from below ($\varphi < \varphi_B$). The two signs correspond to the two branches of the superpotential along the RG flow before and after the bounce, which can be glued at $\varphi = \varphi_B$ giving rise to a regular solution $\varphi(u), A(u)$, in which all curvature invariants are finite. The holographic β function still vanishes at φ_B, but it becomes multivalued:

$$\beta(\varphi) \simeq \mp\frac{3(d-1)}{W_b}\sqrt{\varphi_B - \varphi} + O\Big((\varphi_B - \varphi)\Big)\,. \tag{2.5.4}$$

2.5.2 Positive curvature flows: IR endpoints

It is natural to ask what happens to IR fixed points and bounces when the boundary theory lives on a curved space-time. In the maximally symmetric case analyzed in this chapter, the condition $\dot{\varphi} = 0$ is now the vanishing of

the function $S(\varphi)$, which in the flat case coincides with W'. The analysis of the possible ways in which S can vanish is presented in Appendix E. As it is shown there, the asymptotic behavior of the functions W, S and T always takes the general form of an expansion in half-integer powers of $x \equiv (\varphi_0 - \varphi)$ (which we assume to be positive, for simplicity):

$$S(x) = \sqrt{x}\left(S_0 + S_1\sqrt{x} + S_2 x + \cdots\right) \ , \tag{2.5.5}$$

$$W(x) = \frac{1}{\sqrt{x}}\left(W_0 + W_1\sqrt{x} + W_2 x + \cdots\right) \ , \tag{2.5.6}$$

$$T(x) = \frac{1}{x}\left(T_0 + T_1\sqrt{x} + T_2 x + \cdots\right) \ , \tag{2.5.7}$$

On the other hand, we have assumed that the potential has a regular expansion around φ_0:

$$V(x) = V_0 + V_1 x + V_2 x^2 + \cdots \ . \tag{2.5.8}$$

Depending on the sign of the curvature and on the values of the the coefficients in (2.5.5-2.5.7), the solution around $\varphi = \varphi_0$ can be of be three possible types:

1. Fixed points (positive curvature only)
2. Reflection points (negative curvature only)
3. Bounces (both signs of the curvature)

In this section we will discuss the IR endpoints for positively curved case.

Let us suppose that φ_0 is such that $S(\varphi_0) = 0$, and the leading coefficients S_0, W_0 and T_0 are all non-vanishing (this corresponds to case (b) in Appendix E). Then, $T = R^{(\zeta)}e^{-2A}$ diverges at φ_0, implying that the scale factor e^A shrinks to zero size. However, this does not imply a singularity but as we will see below, it represents a coordinate horizon (or a regular end of space in the Euclidean signature).

To leading order in $\varphi_0 - \varphi$, we have:

$$S(\varphi) \simeq S_0(\varphi_0 - \varphi)^{1/2}, \qquad W(\varphi) \simeq \frac{W_0}{(\varphi_0 - \varphi)^{1/2}}, \tag{2.5.9}$$

$$T \simeq \frac{T_0}{(\varphi_0 - \varphi)}, \tag{2.5.10}$$

where the coefficients are fixed by the equations of motion to be:

$$S_0^2 = \frac{2V_1}{d+1}, \qquad W_0 = (d-1)S_0, \qquad T_0 = \frac{d(d-1)}{4(d+1)}\,S_0^2 \ . \tag{2.5.11}$$

We see that this solution, obtained assuming $\varphi < \varphi_0$, makes sense only for $V_1 > 0$, i.e. $V'(\varphi_0) < 0$ (cfr. equation (2.5.8)). Similarly, it is easy to show that, for $V'(\varphi_0) > 0$ we have to reach φ_0 from above. In both cases, equation (2.5.10) implies $T > 0$. From the definition (2.2.3), this in turn implies that such behavior can occur only for *positive curvature*.

With expressions (2.5.9-2.5.10) for W, S and T, we can integrate equations (2.2.1-2.2.2) order by order in $(\varphi_0 - \varphi)$ to find the expressions for the scale factor $A(u)$ and the scalar field $\varphi(u)$. We define the "end of space" point u_0 where

$$\varphi(u_0) = \varphi_0, \qquad e^{A(u_0)} = 0, \tag{2.5.12}$$

To lowest order, one finds:

$$\varphi = \varphi_0 - \frac{S_0^2}{4}(u-u_0)^2 + O((u-u_0)^3)\,, \qquad A(u) = \ln(u-u_0) + A_0 + O(u-u_0). \tag{2.5.13}$$

The parameter A_0 is an integration constant for equation (2.2.1), but it is determined algebraically by the asymptotic form of the function $T(\varphi)$ close to φ_0:

$$T \equiv R^{(\zeta)} e^{-2A(u)} \simeq \frac{T_0}{\varphi_0 - \varphi} \tag{2.5.14}$$

Inserting the expansions (2.5.13), and using the relations (2.5.11) and the fact that $R^{(\zeta)} = d(d-1)/\alpha^2$, one easily finds:

$$A_0 = -\log \alpha \tag{2.5.15}$$

Interestingly, it is precisely (and only) for this value of A_0 that there is no singularity at u_0. Recall that the metric is given by:

$$ds^2 = du^2 + e^{2A(u)} ds^2_{\mathrm{dS}_\alpha} = du^2 + \alpha^2 e^{2A(u)} ds^2_{\mathrm{dS}_{\alpha=1}}\,, \tag{2.5.16}$$

where $ds^2_{\mathrm{dS}_\alpha}$ is the de Sitter metric with radius α. Near $u \to u_0$, this becomes,

$$ds^2 \simeq du^2 + \alpha^2 e^{2A_0} (u-u_0)^2 ds^2_{\mathrm{dS}_{\alpha=1}}. \tag{2.5.17}$$

For $A_0 = -\log\alpha$, the d-dimensional part of the metric vanishes exactly like it does at the "end of space" in the dS slicing of AdS_{d+1}, as can be seen from equation (2.3.1) by expanding the scale factor around the point $u = -c$. Equivalently, if we go to Euclidean signature, unit-curvature dS_d becomes the unit sphere S_d, and for $A_0 = -\log\alpha$ the metric close to u_0 is approximately:

$$ds^2_E = d\rho^2 + \rho^2 dS^2_d, \qquad \rho \equiv |u - u_0| \tag{2.5.18}$$

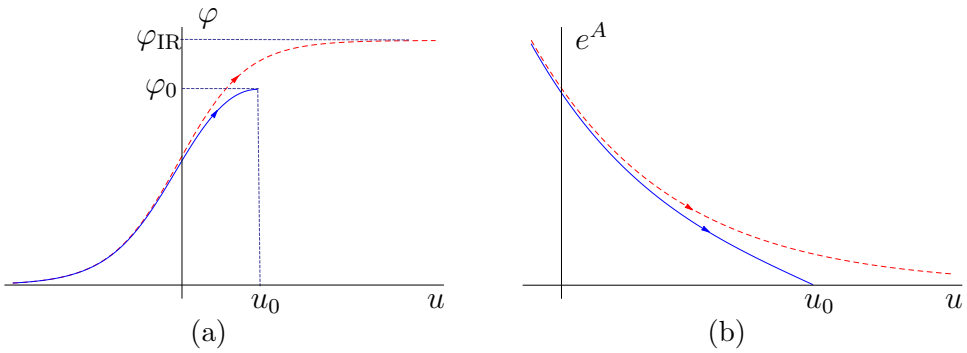

Figure 2.1: The solid lines show the scalar field (left) and scale factor (right) profiles of a positive curvature RG flow geometry, from the UV ($u \to -\infty$, $\varphi \to 0$) to the IR endpoint ($u = u_0$, $\varphi = \varphi_0$). The dashed lines represent the solutions with zero curvature, extending all the way to $u \to +\infty$ and to the IR fixed point at $\varphi = \varphi_{\rm IR}$.

i.e. the metric around the origin of Euclidean $d+1$-space in spherical coordinates.

Notice that the qualitative behavior of the solution is different, and the IR endpoint discussed here does not exist, if $V'(\varphi_0) = 0$: indeed, in this case $T_0 = 0$. Thus, solutions with positive slice curvature cannot reach a would-be flat IR fixed point φ_{IR}, which corresponds to a minimum of the scalar potential. This is in agreement with the result found in Appendix D, that curved RG flows cannot end at minima of the potential.

From the above analysis we can infer the general structure of a positive curvature RG flow in a model with a bulk potential having several maxima and minima. Consider a *flat* RG flow connecting a UV maximum at $\varphi = \varphi_{UV}$ to an IR minimum at $\varphi = \varphi_{IR}$. In the region $\varphi_{UV} < \varphi < \varphi_{IR}$, we have $V'(\varphi) < 0$ by construction. Thus, adding positive curvature forces the flow to stop at an intermediate point $\varphi_{UV} < \varphi_0 < \varphi_{IR}$. This behavior is illustrated in Figure 2.1.

The position of the endpoint in field space is determined by equations (2.5.11) and by the value of the UV data, i.e. the source term φ_- in the scalar field UV asymptotics, and the boundary curvature $R^{\rm uv}$. This can be seen as follows: from the IR equations, choosing the endpoint φ_0 determines all the expansion coefficients in the functions, (2.5.11), through the values of $V(\varphi)$ and its derivatives at φ_0. On the other hand, the integration constant A_0 in the scale factor is fixed by the curvature parameter by equation (2.5.15). Since all the integration constants are fixed, if we integrate the equations towards the UV we will find a given value of the UV source and vev parameters, φ_- and φ_+. Turning it around, for a given set of UV data φ_-

and $R^{\rm uv}$, there exist a single regular solution with a specific vev $\varphi_+(\varphi_-, R^{\rm uv})$ and a specific endpoint $\varphi_0(\varphi_-, R^{\rm uv})$.

As we will see in the next section, and as expected on general grounds, the position of the endpoint actually depends only on the dimensionless combination $\mathcal{R} \equiv R^{\rm uv}(\varphi_-)^{-2/\Delta_-}$. Indeed, from the UV expansions (2.4.2-2.4.4) it is clear that the functions know only about the integration constant $\mathcal{R}$, and do not depend separately on the source φ_-. Thus it is the combination $\mathcal{R}$ which determines the endpoint. As $\mathcal{R}$ ranges from zero to infinity, the endpoint moves from φ_{IR} to φ_{UV}.

Finally, the IR endpoint discussed in this section, constitutes a special case of the general result we present as property 5 of functions $S(\varphi), T(\varphi), W(\varphi)$ in Appendix B, namely that around a point where $S = 0$, the bulk metric is approximately maximally symmetric. In other words, the IR fixed point is a point of enhanced symmetry. This is similar to the flat case, where at an IR fixed point, Poincaré symmetry is upgraded to conformal invariance.

2.5.3 Negative curvature flows: AdS throat

The endpoint behavior presented in the previous section requires positive curvature slices. If the curvature is negative, then we must consider (a) in Appendix E. This generically corresponds to a bounce (which will be discussed in the next section) *except* in the special case $W_0 = W_1 = 0$ (referred to as case (c) in Appendix E):

$$S_0^2 = 2V_1, \quad W_0 = W_1 = 0, \quad T_0 = T_1 = 0 \tag{2.5.19}$$

$$W_2 = \frac{4V_0}{dS_0}, \qquad T_2 = V_0. \tag{2.5.20}$$

At leading order the functions $S(\varphi), T(\varphi), W(\varphi)$ are (assuming $\varphi < \varphi_0$):

$$S \simeq S_0(\varphi_0 - \varphi)^{1/2} + \dots, \quad W \simeq W_2(\varphi_0 - \varphi)^{1/2} + \dots, \quad T \simeq T_2 + \dots \tag{2.5.21}$$

This solution is possible only for negative slice curvature, since $T = e^{-2A}R^{(\zeta)}$ has the same sign as the potential $V(\varphi_0)$, which we assumed to be negative definite. Notice that now W vanishes at φ_0, and $T = e^{-2A}R^{(\zeta)}$ remains finite. This implies that $\dot{A} = 0$ and A is finite at φ_0, i.e. the scale factor has a turning point.

By integrating the first order flow equations, one can show that this solution corresponds to the following geometry for $u \to u_0$:

$$\varphi(u) \simeq \varphi_0 - \frac{S_0^2}{4}(u - u_0)^2, \tag{2.5.22}$$

$$ds^2 \simeq du^2 + e^{2A_0}\left(1 + \frac{(u-u_0)^2}{\ell_{IR}^2}\right) ds^2_{{\rm AdS}_{d,\alpha}}, \tag{2.5.23}$$

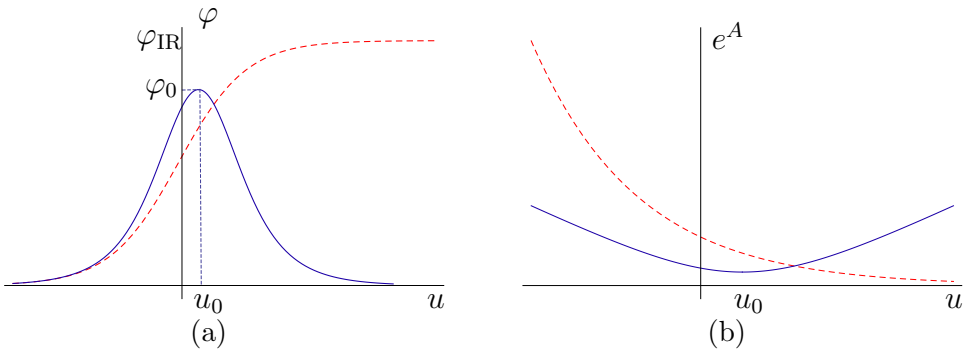

Figure 2.2: The solid lines show the scalar field (left) and scale factor (right) profiles of a negative curvature RG flow geometry, from the left boundary ($u \to -\infty$, $\varphi \to 0$) to the turning point ($u = u_0$, $\varphi = \varphi_0$), to the right boundary ($u \to +\infty$, $\varphi \to 0$). The solution is symmetric around u_0. The dashed lines represent the zero-curvature solution interpolating from the UV boundary to the IR fixed point at $\varphi = \varphi_{IR}$, and featuring a monotonic scale factor.

where A_0 is an integration constant, $ds^2_{\mathrm{AdS}_d,\alpha}$ is a metric on AdS_d with length scale α and $\ell^2_{IR} = d(d-1)/|V(\varphi_0)|$. The behavior around u_0 matches that of space AdS_{d+1}, with length scale ℓ_{IR}, sliced with AdS_d hypersurfaces, as seen in (2.3.1).

The conditions $\dot{A}(u_0) = \dot{\varphi}(u_0) = 0$ imply that we can continue the geometry for $u > u_0$ by gluing its reflected image around u_0. The resulting geometry is regular since the metric and scalar field, as well as their derivatives, are all continuous across u_0. If the solution starts at a UV fixed point reached as $u \to -\infty$, the resulting doubled geometry will reach a "second" UV boundary again as $u \to +\infty$, connected by a throat where the scale factor reaches a minimum, as shown in figure 2.2.

This geometry does not really have two disconnected boundaries: rather, the two boundaries at $u = \pm\infty$ are connected through the boundary of the lower-dimensional AdS_d slices. This was discussed in [60] in the case of the AdS_{d+1} geometry written in AdS_d slices.

As was the case for the endpoint in the positive curvature case, the turning point φ_0 is completely determined by the UV data φ_- and $R^{\rm uv}$.

2.5.4 Bounces

The generic situation of such a point φ_B with vanishing S and finite W corresponds to $W_0 = 0$ but $W_1 \neq 0$ (case (a) in Appendix E). To leading

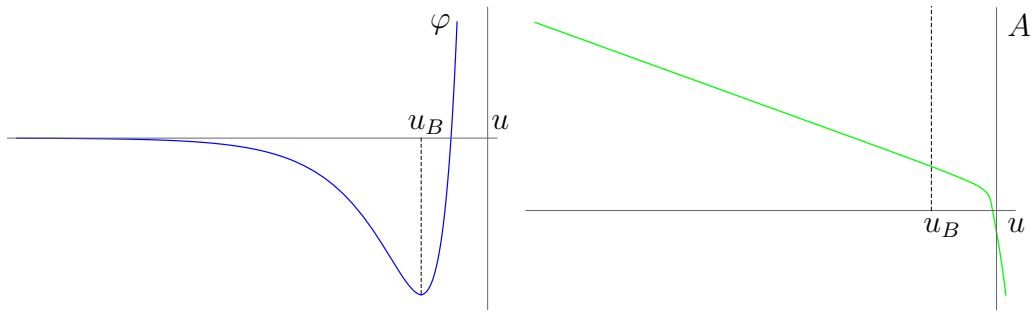

(a) (b)

Figure 2.3: φ and A vs. u for an example exhibiting a bounce at $u = u_B$.

order, the functions $S(\varphi), T(\varphi), W(\varphi)$ behave as (assuming $(\varphi < \varphi_B)$:

$$S \simeq S_0(\varphi_B - \varphi)^{1/2} + \ldots, \quad W \simeq W_1 + W_2(\varphi_B - \varphi)^{1/2} + \ldots, \quad T \simeq T_2 + \ldots \tag{2.5.24}$$

where

$$S_0^2 = 2V_1, \quad T_2 = V_0 + \frac{dW_1^2}{4(d-1)}, \tag{2.5.25}$$

and W_1 is arbitrary ($W_1 = 0$ corresponds to the special case of the AdS throat analyzed in the previous subsection). In this case, the scalar field has a turning point, but the scale factor has a non-vanishing derivative. Since $V_0 < 0$, T_2 does not have a definite sign and therefore this solution is allowed for both positive and negative curvature.

The solution (2.5.25) actually describes two branches, with $S_0 = \pm\sqrt{V_1}$, corresponding to the two branches of the functions $S(\varphi), T(\varphi), W(\varphi)$ discussed in section 2.2: at a bounce, these two branches can be glued, giving rise to a regular geometry, exactly as in the flat case [5]. Integrating the first order equations we find the bulk solution close to φ_B in terms of the u coordinate (where $u = u_B$ is the bounce point):

$$\varphi(u) \simeq \varphi_B - \frac{S_0^2}{4}(u - u_B)^2 + \ldots \quad A(u) = A_B - \frac{W_1}{2(d-1)}(u - u_B) + \ldots \tag{2.5.26}$$

This solution is regular both for $u < u_B$ ($S(\varphi) > 0$) and $u > u_B$ ($S(\varphi > 0)$. The functions $S(\varphi), W(\varphi)$ is singular because at φ_B because φ ceases to be a good coordinate at φ_B, but the geometry (2.5.26) is smooth. The typical scalar field profile is illustrated in Fig. 2.3a. Like in the flat case, we refer to this as a bouncing flow.

The fact that the geometry is regular at the bounce can be also be seen from the fact that all the curvature invariants can be written in terms of

the potential $V(\varphi)$ and the function $S(\varphi)$ only. As the behavior of $S(\varphi)$ is regular near the bounce, all the curvature invariants are finite, as one can see from the expressions in Appendix A.

We can relate the value of the scale factor at the bounce by evaluating the relation $T = R^{(\zeta)}e^{-2A}$ at $u = u_B$, using equations (2.5.24) and (2.5.26):

$$T_2 = R^{(\zeta)}e^{-2A_B}. \tag{2.5.27}$$

Using the expression of T_2 from Eq. (2.5.25), we find a relation between A_B, W_1 and $V(\varphi_B)$:

$$A_B = -\ln(\alpha) - \frac{1}{2}\ln\left|\left(\frac{W_1}{2(d-1)}\right)^2 - \frac{1}{\ell_B^2}\right| \tag{2.5.28}$$

where we have defined

$$V(\varphi_B) = -\frac{d(d-1)}{\ell_B^2}\ . \tag{2.5.29}$$

As $S = 0$ at the bounce, the bulk geometry is approximately maximally symmetric, as shown in Appendix B.

2.6 Examples of complete RG flows

In this section, we will display solutions corresponding to full RG flows for different choices of potentials. The examples are chosen to illustrate various properties of RG flows of theories on curved manifolds described in the previous sections. The flows will originate from a UV fixed point at a maximum of the potential, which we choose to locate at $\varphi = 0$ for convenience, and will end at an IR point φ_0, which does not need to be an extremum of the potential. We will distinguish between flows where φ changes monotonically between the UV and IR points and situations where the flow in φ changes direction, an effect referred to as a bounce. In addition, we will describe how the flows are deformed by changes to UV data such as the dimensionless curvature $\mathcal{R}$.

2.6.1 Generic flows

We will refer to flows as generic if they exhibit the following two properties: they originate at a maximum of the potential and end in the region between this maximum and the nearest minimum. In addition, φ changes monotonically along the flow from UV to IR. We call such solutions 'generic' as they

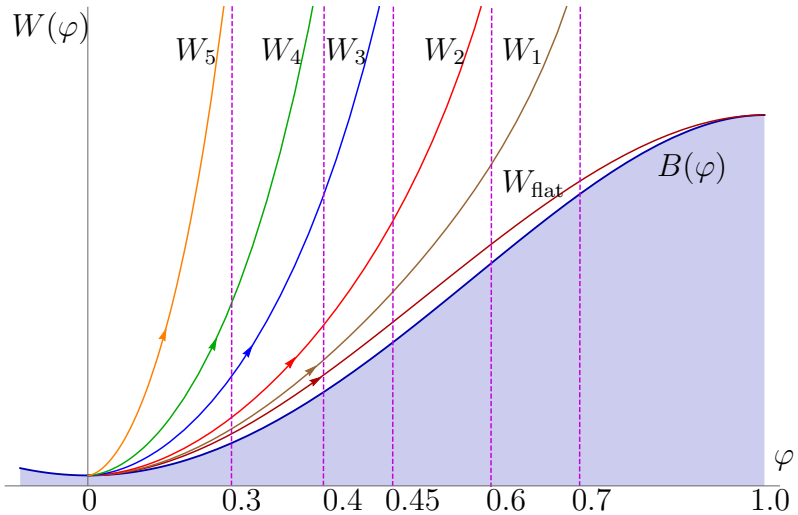

Figure 2.4: Solutions for $W(\varphi)$ with $\mathcal{R} \geq 0$ and for the potential (2.6.1) with $\Delta_- = 1.2$. The five solutions $W_i(\varphi)$ with $i = 1, \ldots, 5$ differ in the value of their IR endpoint φ_0. The critical curve is defined as $B(\varphi) = \sqrt{-3V(\varphi)}$. In the case of zero and positive curvature, the function $W(\varphi)$ cannot enter into the region below the critical curve, which is depicted as the shaded region.

arise for generic potentials as long as they possess at least one maximum and one minimum.

To illustrate generic flows, a potential exhibiting a maximum and at least one minimum will be sufficient.[3] For this purpose we consider the following quadratic-quartic potential:

$$V(\varphi) = -\frac{d(d-1)}{\ell^2} - \frac{m^2}{2}\varphi^2 + \lambda\varphi^4 \,. \tag{2.6.1}$$

This potential has one maximum at $\varphi_{\text{max}} = 0$. We will also find it convenient to choose $\lambda = m^2/4$ such that the minima occur at $\varphi_{\text{min}} = \pm 1$. We then proceed to studying RG flows by solving (2.2.7)–(2.2.8) numerically for $W(\varphi)$ and $S(\varphi)$. In practice, it is easiest to specify boundary conditions for W and S at or close to the IR end point φ_0. The relevant boundary conditions for RG flows are described in sections 2.5.2 and 2.5.3 for the two cases of a QFT on a sphere or AdS. Given the symmetry of the setup, we restrict our attention to flows that end in the region $\varphi_0 \in [0, 1]$.

[3] In fact, the existence of a minimum at a finite value of φ is not strictly necessary, but will be useful for illustrating further properties of these flows. Similar conclusions apply also to potentials that extend to infinity in field space, which in the flat case were also discussed in [5].

QFT on S^d: $\mathcal{R} > 0$

In Fig. 2.4 we exhibit solutions for the function $W(\varphi)$ corresponding to generic RG flows for a bulk potential given by (2.6.1) and for $\mathcal{R} > 0$. To be specific, we have set $\Delta_- = 1.2$, but our observations will hold more generally.

- The main result is that for every value of φ_0 between $\varphi_{\max} = 0$ and $\varphi_{\min} = 1$ there exists a unique solution to the equations (2.2.4-2.2.6) corresponding to an RG flow originating from the UV fixed point at $\varphi_{\max} = 0$ and ending at φ_0. For illustration, in Fig. 2.4 we have chosen to display five such solutions labelled by $W_i(\varphi)$ with $i = 1, \ldots, 5$, that differ in the value of the IR endpoint φ_0. However, there is no solution for a flow with $\mathcal{R} > 0$ with an endpoint at $\varphi_0 = \varphi_{\min}$ exactly. In contrast, such a flow arises for $\mathcal{R} = 0$ and we have included the corresponding superpotential W_{flat} in the figure.

- Note that the solutions $W_i(\varphi)$ diverge when approaching their corresponding IR end points. The divergence is of the form $\sim (\varphi_0 - \varphi)^{-1/2}$ as expected for a RG flow with $\mathcal{R} > 0$ (see sec. 2.5.2). Recall that this divergence does not imply a singularity in the bulk geometry.

- Returning to Fig. 2.4, in the vicinity of the UV fixed point the solutions are described by the family of solutions collectively denoted by $W_-(\varphi)$ in section 2.4. These solutions depend on the two continuous parameters $\mathcal{R}$ and C. This is consistent with the existence of a unique solution corresponding to a RG flow for every φ_0. Picking a solution with the correct IR behavior for a RG flow fixes one combination of the two parameters. The remaining freedom is then equivalent to the choice of IR end point φ_0.

- Given a numerical solution, we can extract the corresponding values of $\mathcal{R}$ and C explicitly by fitting the UV region with the asymptotics (2.4.2-2.4.4). An interesting observation is that there exists an inverse relation between $\mathcal{R}$ and φ_0, i.e. flows with endpoints closer to the UV fixed points exhibit larger values of $\mathcal{R}$. Further, $\mathcal{R}$ diverges when φ_0 approaches the UV fixed point. On the other hand, when the IR endpoint approaches $\varphi_{\min}$ the value of $\mathcal{R}$ asymptotes to zero. In fact, for the potential considered here the evolution of $\mathcal{R}$ with φ_0 is monotonic and displayed in Fig. 2.5a.

- For completeness, we also exhibit C as a function of φ_0 in Fig. 2.5b. We find that C is negative, but its behavior is otherwise similar to that of $\mathcal{R}$. In particular, its absolute value increases with decreasing φ_0 and

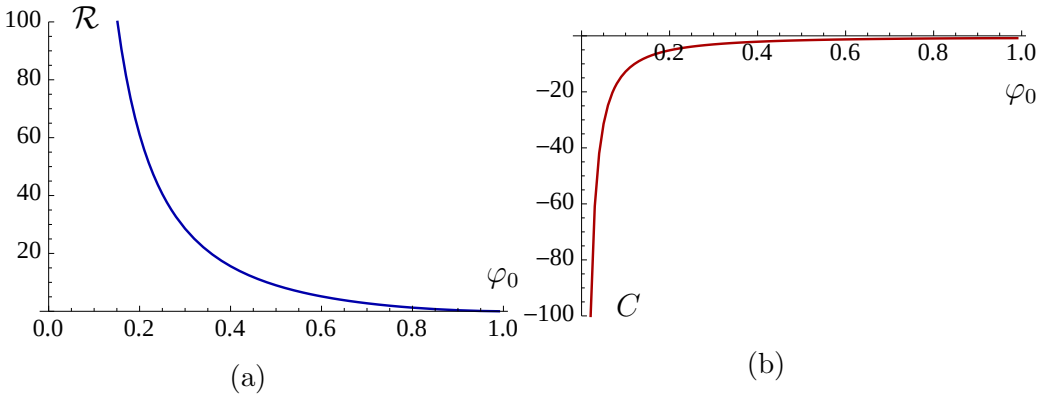

Figure 2.5: QFT on S^d: Dimensionless curvature $\mathcal{R}$ and dimensionless vev C as a function of IR endpoint φ_0 for the potential (2.6.1) with $\Delta_- = 1.2$. Both these quantities diverge as φ_0 approaches the UV fixed point at $\varphi = 0$.

diverges when $\varphi_0 \to 0$. However, as $\varphi_0 \to \varphi_{\rm min}$ we find numerically that $C \neq 0$.

- Given a solution $W_i(\varphi)$, we can also determine the corresponding scale factor $e^{A(u)}$ and scalar field profile $\varphi(u)$. This introduces the remaining integration constant φ_- into the solution. In figure 2.6 we plot the scale factors $e^{A(u)}$ and the scalar field profile $\varphi(u)$ corresponding to the solutions $W_1(\varphi)$, $W_2(\varphi)$ and $W_3(\varphi)$ in figure 2.4. The scale factor $e^{A(u)}$ shrinks to zero at a finite value of u, in agreement with our identification of φ_0 with an IR endpoint. The scalar field arrives at the IR value φ_0 at that point.

The above findings can be summarized as follows. Consider a field theory with fixed source φ_- on a background with fixed curvature $R^{\rm uv}$, such that $\mathcal{R} = R^{\rm uv}|\varphi_-|^{-2/\Delta_-}$ is fixed. The flow will end at a value φ_0, which is determined by $\mathcal{R}$. The larger the value of $\mathcal{R}$, the closer this end point φ_0 will be to $\varphi_{\rm max}$. The remaining parameter C is then determined by the requirement that the solution is has the correct (regular) behavior at the endpoint.

QFT on AdS_d: $\mathcal{R} < 0$

We repeat the above analysis for the case with $\mathcal{R} < 0$. We will find that many properties observed for positive $\mathcal{R}$ also hold for negative $\mathcal{R}$. In this case however the IR endpoint at φ_0 is replaced by an IR *turning point* for both φ and A (see section 2.5.3). There are also other important differences which we will highlight. To be specific, we will again work with the potential

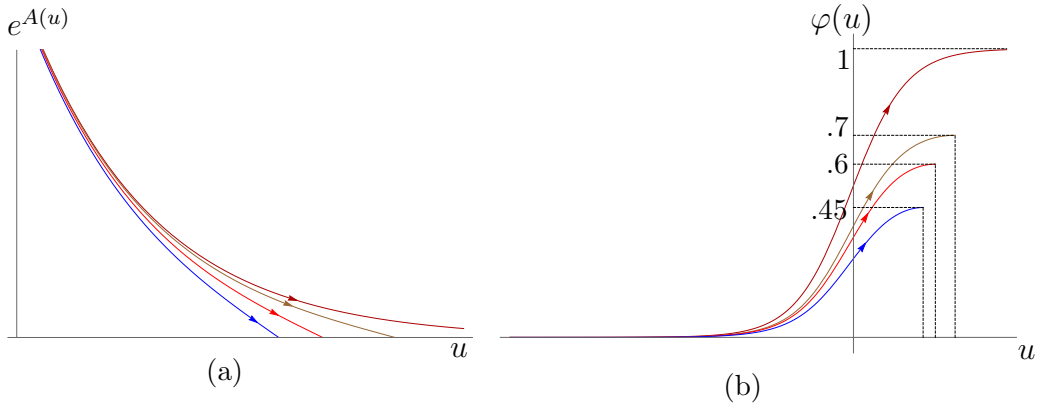

Figure 2.6: (a): Scale factor e^A as a function of u for the flows denoted by 1,2,3 in Fig. 2.4. For the flat case, the scale factor is depicted as the dark red curve and only shrinks to zero at $u \to \infty$. For the positive curvature cases, the scale factor e^A shrinks to zero at finite values of u. (b): Scalar field $\varphi(u)$ as a function of u. For the flat case, the scalar field arrives at the minimum of the potential at $\varphi = 1$ at the end of the flow. Here it is denoted by the darker red line. For the curved cases, the scalar field does not reach the minimum. The figure shows the scalar field profile for flows denoted by 1,2,3 in Fig. 2.4.

given by (2.6.1). In the following, we collect our observations. It will be convenient to distinguish the cases $\Delta_- < 1$ and $\Delta_- > 1$.

- For $\Delta_- < 1$ there exists a unique solution to equations (2.2.4-2.2.6) corresponding to a *monotonic* RG flow for every value of IR turning point $\varphi_0 \in [0, \varphi_{\rm min}]$. This is identical to what we have found for flows with $\mathcal{R} > 0$, and for any Δ_-.

- For $\Delta_- > 1$ an RG flow solution exists for every value of IR turning point $\varphi_0 \in [0, \varphi_{\rm min}]$, but these are not necessarily monotonic. In particular, we find that generic flows can only have $\varphi_0 \in [\varphi_c, \varphi_{\rm min}]$, where $\varphi_c > \varphi_{\rm max}$ is determined by the specific choice of potential. On the other hand, flows with $\varphi_0 \in [0, \varphi_c]$ exist, but are non-monotonic: the scalar field $\varphi(u)$ starts from 0 towards *negative* values, before turning around, crossing $\varphi = 0$ again and reaching a value $\varphi_0 \in [0, \varphi_c]$. We will refer to such solutions as *bouncing* flows and they will be discussed in more detail in section 2.6.3. Note that these bouncing flows are dual to a different class of theories than the monotonic flows, since the UV source must have a different sign in the two cases.

- In Fig. 2.7 we display three solutions for $W(\varphi)$ with $\mathcal{R} < 0$. The

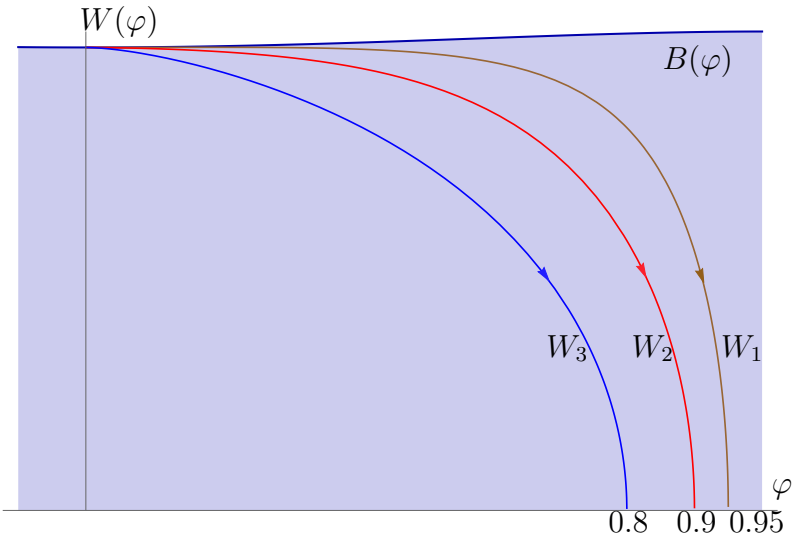

Figure 2.7: Solutions for $W(\varphi)$ with $\mathcal{R} < 0$ and for the potential (2.6.1) with $\Delta_- = 1.2$. The three solutions $W_i(\varphi)$ with $i = 1, 2, 3$ have different IR turning points φ_0. For negative curvature case, the function $W(\varphi)$ can go into the area below the critical curve $B(\varphi) = \sqrt{-3V(\varphi)}$ which is the shaded region.

results are obtained for the potential (2.6.1) with $\Delta_- = 1.2$. The three solutions labelled by W_1, W_2 and W_3 differ in the value of their corresponding IR turning point φ_0. Note that $W(\varphi)$ goes to zero at φ_0, with infinite slope as expected from the analytical results in sec. 2.5.3. The inverse scale factor $e^{A(u)}$ reaches a minimum at the loci where W vanishes (see Fig. 2.8). This is due to the fact that A reaches a minimum at the turning point.

- Returning to figure 2.7, in the vicinity of the UV fixed point the solutions are again described by the family of solutions collectively denoted by $W_-(\varphi)$ in section 2.4. We can extract the constants $\mathcal{R}$ and C for generic flows. As in the positive curvature case, we find that the absolute value $|\mathcal{R}|$ increases monotonically with a decrease in the value of the IR (turning) point φ_0. For $\Delta_- < 1$ we find that the increase in $|\mathcal{R}|$ continues until $\varphi_0 \to 0$ at which point $|\mathcal{R}|$ diverges. This changes for $\Delta_- > 1$. In this case $|\mathcal{R}|$ already diverges when $\varphi_0 \to \varphi_c$ for some positive value φ_c. This is shown in Fig. 2.9a, where we display $\mathcal{R}$ as a function of φ_0 for the potential (2.6.1) with $\Delta_- = 1.2$. In this example we find that $\varphi_c \approx 0.49$. The reason for this behavior is that the flow ending at φ_c corresponds to a theory with vanishing source φ_-, which in turn implies that $\mathcal{R} = R^{\rm uv}|\varphi_-|^{-2/\Delta_-}$ diverges. The rose-colored area in Fig. 2.9a corresponds to $\varphi < \varphi_c$, which is the region where direct

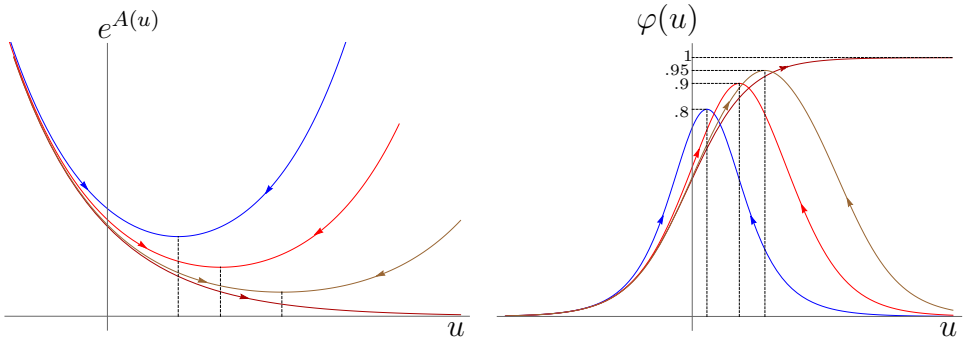

Figure 2.8: (a): $e^{A(u)}$ vs. u and (b) $\varphi(u)$ vs. u corresponding to the flows in Fig. 2.7. The coloring is the same as in Fig. 2.7. The dark red curve corresponds to the solution for the flat case. The vertical lines represent the reflection points.

flows cannot arrive. Flows with turning points in this region leave the UV fixed point at $\varphi = 0$ to the left before reversing direction. We will discuss such bouncing flows in more detail in section 2.6.3.

- For completeness, we display C as a function of φ_0 in Fig. 2.9b. The results are again obtained for the potential (2.6.1) with $\Delta_- = 1.2$. For $\varphi_0 \to \varphi_{\text{min}}$ the parameter C takes some finite value. The value of C then increases monotonically with decreasing φ_0 until C diverges for $\varphi_0 \to \varphi_c$. This can be understood as the divergence of $C = \frac{\Delta_-}{d}\langle\mathcal{O}\rangle|\varphi_-|^{-\Delta_+/\Delta_-}$ for $\varphi_- \to 0$. The rose-colored region again corresponds to the area $\varphi < \varphi_c$ where direct flows cannot end.

To summarize, generic flows for $\mathcal{R} < 0$ exhibit many phenomena already observed for $\mathcal{R} > 0$. In particular, the inverse relation between $|\mathcal{R}|$ and φ_0 persists. A new phenomenon is the appearance of bouncing solutions for $\Delta_- > 1$. We will discuss these solutions in detail in section 2.6.3.

2.6.2 The holographic β-function

Having discussed generic flow solutions for $W(\varphi)$ and $S(\varphi)$, let us now turn to the holographic β-function defined in (2.2.11). In Fig. 2.10 we plot examples of the holographic β-function for generic flows in the potential (2.6.1) with $\Delta_- = 1.2$. The dark red curve is $\beta_{\text{flat}}(\varphi) = -2(d-1)W'(\varphi)/W(\varphi)$ for a flat flow. The remaining curves $\beta_i(\varphi)$ with $i = 1, 2, 3$ correspond to RG flow solutions with $\mathcal{R} = 0.09,\ 1.29,\ 7.14$ respectively. Note that the β-functions

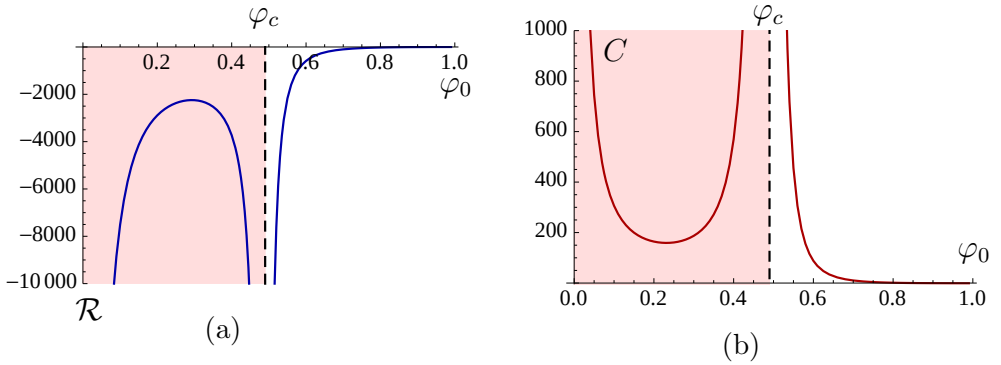

Figure 2.9: QFT on AdS_d: dimensionless curvature $\mathcal{R} = R^{\mathrm{uv}}|\varphi_-|^{-2/\Delta_-}$ and dimensionless vev $C = \frac{\Delta_-}{d}\langle\mathcal{O}\rangle|\varphi_-|^{-\Delta_+/\Delta_-}$ vs. φ_0 for the potential (2.6.1) with $\Delta_- = 1.2$. Flows with turning points in the rose-colored region leave the UV fixed point at $\varphi = 0$ to the left before bouncing and finally ending at positive φ_0. Flows with turning points in the white region are direct: They leave the UV fixed point at $\varphi = 0$ to the right and do not exhibit a reversal of direction. The flow with turning point φ_c on the border between the bouncing/non-bouncing regime corresponds to a theory with vanishing source φ_-. As a result, both $\mathcal{R}$ and C diverge at this point.

show the same asymptotic behavior in the UV, i.e.

$$\beta(\varphi) = -\Delta_-\varphi + \ldots + \mathcal{O}\left(\mathcal{R}\,|\varphi|^{1+\frac{2}{\Delta_-}}\right), \tag{2.6.2}$$

where we have indicated the first non-trivial curvature correction at small curvature. Moving away from the UV fixed point at $\varphi = 0$, the β-functions begin to change due to the curvature. The departure from β_{flat} is the more pronounced, the higher the value of $\mathcal{R}$. Most notably, depending on the value of $\mathcal{R}$, the various β-functions vanish at different values of φ_0. Using results from sections 2.4.2 and 2.5.2, we find that the β-functions exhibit the following asymptotic form near their respective IR end-points:

$$\mathcal{R} = 0: \qquad \beta_{\mathrm{flat}} = \Delta_-^{\min}(\varphi_{\min} - \varphi) + \mathcal{O}\big((\varphi_{\min} - \varphi)^2\big), \tag{2.6.3}$$

$$\mathcal{R} > 0: \qquad \beta_i = -2(\varphi_{0,i} - \varphi) + \mathcal{O}\big((\varphi_{0,i} - \varphi)^{3/2}\big), \quad \text{for} \quad i = 1, 2, 3, \tag{2.6.4}$$

where $\varphi_{0,i}$ are the respective end-points of the flows. The difference in IR behavior between flat flows and flows with $\mathcal{R} > 0$ can be understood as follows. For flat flows, IR fixed-points are determined by the potential, as they correspond to minima of V. Correspondingly, the vanishing of β_{flat} at the fixed point is set by $\Delta_-^{\min}$, which depends on the potential at the minimum.

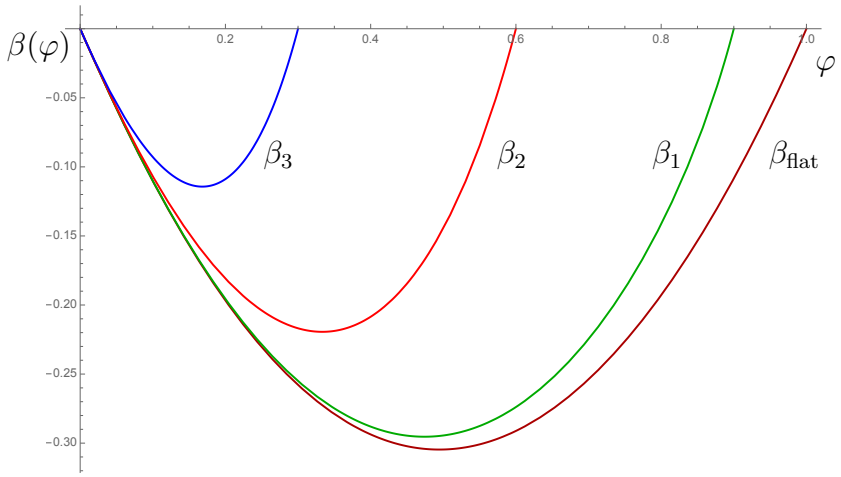

Figure 2.10: Solutions for $\beta(\varphi) = -2(d-1)\frac{S(\varphi)}{W(\varphi)}$ with $\mathcal{R} \geq 0$ and for the potential (2.6.1) with $\Delta_- = 1.2$. The three solutions $\beta_i(\varphi)$ with $i = 1, 2, 3$ differ in the value of their IR endpoint φ_0.

In contrast, for flows with $\mathcal{R} > 0$, it is the existence of non-zero curvature which cuts off the flows in the IR, rather than a property of the potential. As a result, the behavior of β_i in the IR does not depend on the behavior of the potential at the IR end-point. In fact, the behavior $\beta_i = -2(\varphi_{0,i} - \varphi)$ for $\mathcal{R} > 0$ is universal regardless of V and $\mathcal{R}$. The effect of non-zero curvature $\mathcal{R}$ is to fix the value of the IR end point $\varphi_{0,i}$.

Last, we comment on flows with $\mathcal{R} < 0$. The behavior of $\beta(\varphi)$ in the UV is again given by (2.6.2). However, at the turning point φ_0 the β-function does not vanish, but remains finite. Using our expressions from sec. 2.5.3 one finds

$$\beta(\varphi_0) = d(d-1)\frac{|V'(\varphi_0)|}{V(\varphi_0)}\,. \tag{2.6.5}$$

This indicates that the turning points φ_0 in the negative curvature case are not fixed points of an RG flow.

2.6.3 Bouncing Solutions

Bouncing solutions are made possible by the fact that at a generic point $W(\varphi)$ and $S(\varphi)$ may be multivalued. We have already observed in the previous section that bounces are generic for negative curvature. Here we present a few more examples.

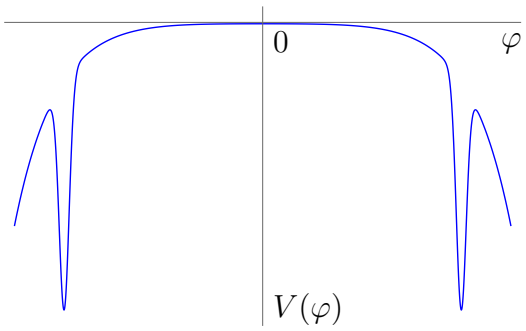

Figure 2.11: Plot of the potential (2.6.6) with parameters $\Delta_+ = 2.91$, $\sigma = 0.01$, $c = 2000$, $\Gamma = 2/\sqrt{3}$, $\varphi_* = 4$.

QFT on S^d: $\mathcal{R} > 0$

The potential (2.6.1), did not exhibit multivalued $W(\varphi)$ and $S(\varphi)$ for the positively curved case. We now consider the potential:

$$V = -\frac{\Delta_+(d-\Delta_+)}{2\ell^2}\varphi^2 + \frac{d(d-1)}{\ell^2}\left(\frac{\Gamma}{2}\varphi^2 - \cosh(\Gamma\varphi)\right) \qquad (2.6.6)$$
$$- \frac{|c|}{\ell^2}\left(e^{-\frac{(\varphi-\varphi_*)^2}{2\sigma}} + e^{-\frac{(\varphi+\varphi_*)^2}{2\sigma}} + e^{-\frac{\varphi_*^2}{2\sigma}}\left(\frac{1}{\sigma} - \frac{\varphi_*^2}{\sigma^2}\right)\varphi^2 - 2e^{-\frac{\varphi_*^2}{2\sigma}}\right).$$

which depends on the parameters Δ_+, Γ, φ_* and c. The potential is an inverted parabola superimposed on an inverted cosh. In addition, there are two inverted Gaussians with peaks at $\pm\varphi_*$ and whose height and width can be adjusted using c and σ. The potential thus has a maximum at $\varphi = 0$. In addition, we choose the parameters Γ, c and σ such that there are also two minima close to $\pm\varphi_*$. The parameter Δ_+ is consistent with the definition of $\Delta_\pm$ in (2.4.5), i.e. it is given by (2.4.5) with $m^2 = V''|_{\varphi=0}$. A plot of this potential is shown in Fig. 2.11 for parameters $\Delta_+ = 2.91$, $\sigma = 0.01$, $c = 2000$, $\Gamma = 2/\sqrt{3}$, $\varphi_* = 4$. This potential is constructed with the intention to give rise to bouncing solutions. The two Gaussians introduce two steep features in the potential, which exhibit solution with bounces.

Fig. 2.12 shows two bouncing solutions $W_1(\varphi)$ and $W_2(\varphi)$ with $\mathcal{R} > 0$. For comparison, we also plot W_{flat}, which is the bouncing solution in the same potential for $\mathcal{R} = 0$. The flows in Fig. 2.12 originate from a UV fixed point at a maximum of V at $\varphi_{\max} = 0$, departing towards negative values of φ. The flows then exhibit a bounce, reverse direction and eventually flow to the regime with $\varphi > 0$. Depending on the precise form of the potential for $\varphi > 0$, the flows may bounce again (even repeatedly), diverge, or approach an IR end point.

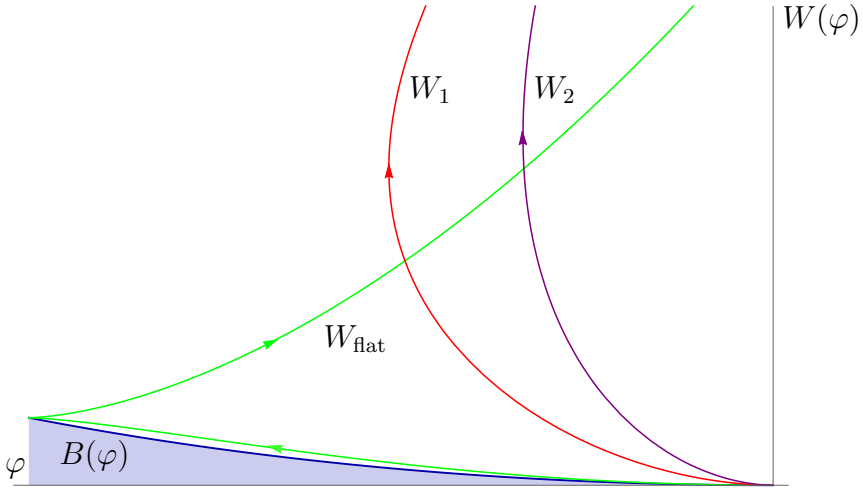

Figure 2.12: Solutions for $W(\varphi)$ for flows exhibiting a single bounce for the potential (2.6.6) with $\Delta_+ = 2.91$, $\sigma = 0.01$, $c = 2000$, $\Gamma = 2/\sqrt{3}$, $\varphi_* = 4$. $W_{1,2}$ are solutions with $\mathcal{R}_2 > \mathcal{R}_1 > 0$, while W_{flat} is the solution in the same potential with $\mathcal{R} = 0$. The shaded area is the region below the critical curve $B(\varphi) = \sqrt{-3V(\varphi)}$.

For $\mathcal{R} = 0$ the bounce locus is the critical curve, i.e. $W_{\text{flat}}(\varphi_B) = B(\varphi_B)$. In addition $W'_{\text{flat}} \sim \pm(\varphi - \varphi_B)^{1/2}$ in the vicinity of a bounce. As shown in [5], these two properties are shared by all bouncing solutions for $\mathcal{R} = 0$.

For $\mathcal{R} > 0$ we can make the following observations:

- For $\mathcal{R} > 0$ the bounce locus does not lie on the critical curve (1.4.13). Instead we find that $W(\varphi_B) > B(\varphi_B)$ for $\mathcal{R} > 0$ (see Fig. 2.12). Another interesting observation is that $W' \sim \pm(\varphi - \varphi_B)^{-1/2}$ in the vicinity of a bounce for $\mathcal{R} \neq 0$. Thus, while W' changes sign at the bounce, it also diverges at this point.

- We can also determine the values $\mathcal{R}_1$ and $\mathcal{R}_2$ corresponding to the two flows W_1 and W_2. Here we have $\mathcal{R}_2 > \mathcal{R}_1$. Studying further bouncing flows with $\mathcal{R} \neq 0$ the following behavior emerges: the larger the value of $|\mathcal{R}|$, the closer bounces occur to the UV fixed point.

- For completeness, we also plot the functions S and the inverse scale factor e^{-2A} corresponding to the two solutions W_1 and W_2. This is shown in figures 2.13a and 2.13b respectively. Note that e^{-2A} takes finite values throughout, including at the bouncing locus φ_B. The bulk geometry is thus perfectly regular along the flow including the bounces.

We can summarize our findings as follows. Consider a field theory with

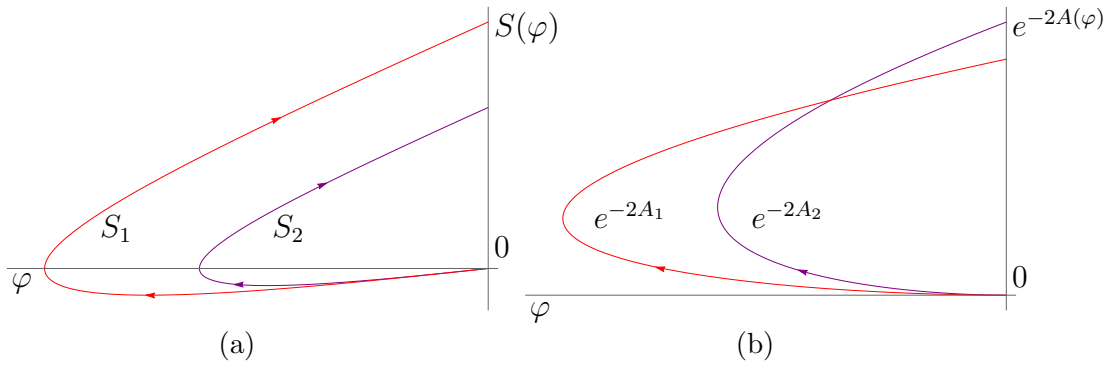

Figure 2.13: Plots of $S_{1,2}(\varphi)$ and $e^{-2A_{1,2}(\varphi)}$ corresponding to the two solutions $W_{1,2}(\varphi)$ in figure 2.12. The solutions are obtained for the potential (2.6.6) with $\Delta_+ = 2.91$, $\sigma = 0.01$, $c = 2000$, $\Gamma = 2/\sqrt{3}$, $\varphi_* = 4$.

fixed UV source φ_- and defined on a manifold with UV curvature $R^{\rm uv}$. One observation of this section is that for a suitable potential V, solutions corresponding to RG flows with bounces exist. Decreasing $R^{\rm uv}$ (and thus $\mathcal{R} = R^{\rm uv}|\varphi_-|^{-2/\Delta_-}$), the bounce moves further away from the UV fixed point and approaches the critical curve $B(\varphi)$. For $R^{\rm uv} \to 0$ the bounce eventually reaches the critical curve. On the contrary, increasing $R^{\rm uv}$ moves the bounce towards the UV fixed point.

QFT on AdS$_d$: $\mathcal{R} < 0$

Bouncing solutions also exist for $\mathcal{R} < 0$, i.e. for field theories defined on negatively curved manifolds. Our observations from above also hold here: Bounce loci φ_B do not occur on the critical curve, but now we have $W(\varphi_B) < B(\varphi_B)$ for $\mathcal{R} < 0$ (see Fig. 2.14). Similarly, increasing $|\mathcal{R}|$ moves φ_B towards the UV fixed point. For example, for the two flows W_1 and W_2 in Fig. 2.14 we have $\mathcal{R}_2 > \mathcal{R}_1$.

An important difference to the case $\mathcal{R} > 0$ is that for $\mathcal{R} < 0$ bouncing solutions are generic. Let us explain what we mean by this. For $\mathcal{R} > 0$ bouncing solutions may exist in suitable potentials, but given a generic potential, one does not expect the existence of bouncing solutions. This is to be contrasted with the situation for $\mathcal{R} < 0$. There any potential with at least one maximum with $\Delta_- > 1$ will allow for bouncing solutions.

This can be understood analytically from the results of appendix H. There we study solutions for flows in purely quadratic potentials, where we restricted our focus to flows that end or turn close to the UV fixed point where they originated from. The main observation of relevance here is as follows: we find that for $\mathcal{R} < 0$ such flows will always bounce if $\Delta_- > 1$. Now note

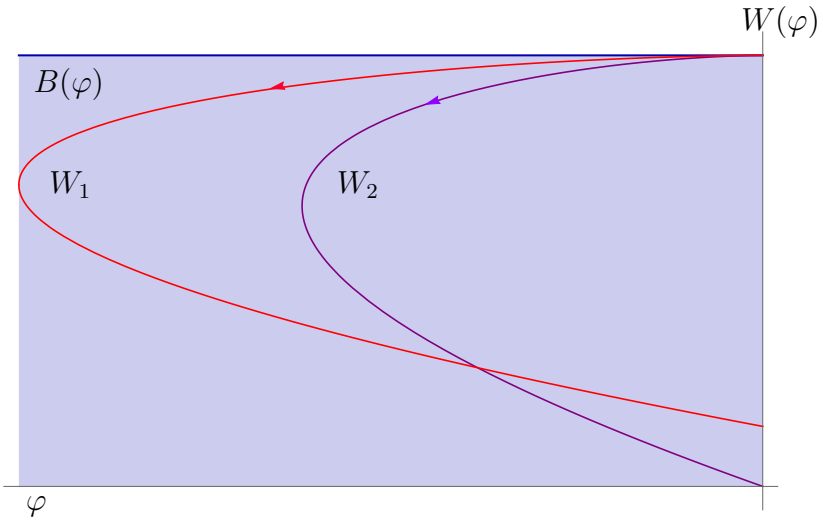

Figure 2.14: Plot of solutions for $W(\varphi)$ for flows exhibiting a single bounce for the potential (2.6.6) with $\Delta_+ = 2.91$, $\sigma = 0.01$, $c = 2000$, $\Gamma = 2/\sqrt{3}$, $\varphi_* = 4$. $W_{1,2}$ are solutions with $\mathcal{R} < 0$, and $|\mathcal{R}_2| > |\mathcal{R}_1|$.

that sufficiently close to a maximum the potential can always be approximated by a quadratic function, and the results from appendix H will hold. Thus we expect that for $\Delta_- > 1$ flows with turning points sufficiently close to this maximum will necessarily bounce. This is indeed what we observe numerically.

Thus, for $\mathcal{R} < 0$ bounces can occur in very simple potentials, like the quadratic-quartic potential in (2.6.1) and which we will discuss in the following. However, now we will consider this potential for the range $\varphi \in [-\varphi_{\min}, \varphi_{\min}] = [-1, 1]$. As we have seen in section 2.6.1, for negative curvature and $\Delta_- > 1$ there exists a critical value φ_c for the IR turning point below which the solution goes through a bounce before reaching the turning point. The critical value φ_c depends on the details of the potential: for example, a numerical analysis shows that, for $\Delta_- = 1.2$, $\varphi_c = 0.49$, while for $\Delta_- = 1.4$ $\varphi_c = 0.63$.

We will now examine how the quantities $\mathcal{R}$ and C vary as the endpoint of the flow φ_0 is varied from $\varphi_{\max} = 0$ to $\varphi_{\min} = 1$. For $\Delta_- = 1.2$ this has already been discussed for the non-bouncing flows with $\varphi_0 \gtrsim 0.49$. We will now complement these plots with the results for bouncing flows, i.e. for $|\varphi_0| \lesssim 0.49$. This is shown in fig. 2.9.

Interestingly, in addition to the usual divergence in $\mathcal{R}$ and C for $\varphi_0 \to \varphi_{\max}$ we find that both $\mathcal{R}$ and C also diverge when $\varphi_0 \to \varphi_c$, i.e. when φ_0 approaches the boundary between bouncing and non-bouncing flows. This can be understood as follows. Non-bouncing flows with turning points in

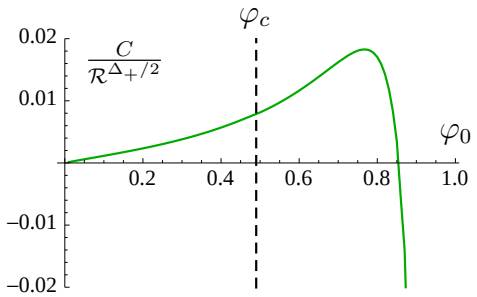

Figure 2.15: QFT on AdS_d: $C/\mathcal{R}^{\Delta_+/2}$ vs. φ_0 for the potential (2.6.1) with $\Delta_- = 1.2$. Flows with turning points in the rose-colored region exhibit a bounce.

$\varphi_0 > \varphi_c$ correspond to flows that leave the UV fixed point to the right, and as a consequence have $\varphi_- > 0$. Bouncing flows with $\varphi_0 < \varphi_c$ leave the UV fixed point to the left before turning around, and thus have $\varphi_- < 0$. Thus, when φ_0 passes through φ_c the source has to change sign. Note that in terms of the physical UV curvature $R^{\rm uv}$ and the vev $\langle\mathcal{O}\rangle$ the two quantities $\mathcal{R}$ and C can be written as:

$$\mathcal{R} = \frac{R^{\rm uv}}{|\varphi_-|^{2/\Delta_-}}\,, \qquad C = \frac{\Delta_-}{d}\frac{\langle\mathcal{O}\rangle}{|\varphi_-|^{\Delta_+/\Delta_-}}\,, \tag{2.6.7}$$

The divergence for $\varphi_0 \to \varphi_c$ can thus be interpreted as follows. To change sign the source has to pass through zero. As long as $R^{\rm uv}$ and $\langle\mathcal{O}\rangle$ remain finite, letting $\varphi_- \to 0$ makes both $\mathcal{R}$ and C diverge.

This interpretation can be checked by plotting the quantity

$$\chi \equiv \frac{\langle\mathcal{O}\rangle}{(R^{\rm uv})^{\Delta_+/2}} = \frac{d}{\Delta_-}\frac{C}{\mathcal{R}^{\Delta_+/2}}\,, \tag{2.6.8}$$

which is manifestly independent of φ_- and should thus be finite for $\varphi_0 \to \varphi_c$. This is indeed what we observe. In fig. 2.15 we plot $\frac{\Delta_-\chi}{d}$ vs. φ_0 for the potential (2.6.1) with $\Delta_- = 1.2$. We find that χ is finite and continuous when φ_0 passes through φ_c.

In this chapter, we have discussed holographic RG flow solutions with curved slices, corresponding to QFTs living on curved space-times and showed different RG flows for various potentials. In the next three chapters, we will discuss different applications of the holographic RG flows on curved manifolds discussed in this chapter.

Chapter 3

F-functions from holography

3.1 Introduction

In the previous chapter, we have discussed the holographic RG flows on maximally symmetric manifolds, in particular on spheres. The study there can be used in turn to study QFTs defined on spheres. In this chapter, we will discuss properties of QFTs on spheres in the context of F-theorems.

By the AdS/CFT dictionary, we can find the partition function of the boundary field theory from the dual on-shell action. A fundamental property of QFT is that the number of degrees of freedom decreases under renormalization group flow. The quantitative description of this phenomenon is the subject of the so called 'c-theorems'. The first ingredient of any c-theorem is to identify a c-quantity that measures the number of degrees of freedom of the QFTs at the UV and IR fixed points of the RG flow. The second ingredient is a c-function with the property that it interpolates monotonically between the UV and IR values of the c-quantity along the flow.

For field theories in an even number of space-time dimensions suitable c-quantities can be identified with coefficients of the Weyl anomaly. In $d = 2$ Zamolodchikov proposed a suitable c-function, which at the fixed points reduces to the Weyl anomaly coefficient c [61]. In $d = 4$ it is the anomaly coefficient a which plays the role of the c-quantity [62]. A proof of monotonicity under RG flow was presented in [63], therefore establishing the a-theorem in $d = 4$. In odd space-time dimensions the Weyl anomaly is absent, and hence a different approach to the c-theorem is required.

Progress in this direction was made by relating the c-theorem to entropic considerations. In [64] it was shown that the c-theorem in $d = 2$ can be derived from strong subadditivity of an entanglement entropy. In [35, 45] it was observed that the c-quantity in any dimension (even and odd) can be

defined as the universal contribution to an entanglement entropy across a suitably chosen surface.[1]

The case of the c-theorem in $d = 3$, also referred to as the F-theorem, received particular attention. It was suggested in [43, 44, 66] that the role of the c-quantity can be played by (the finite part of) the free energy of the theory on the 3-sphere, $F = -\ln|Z_{S^3}|$. For CFTs the free energy on S^3 coincides with the entanglement entropy across a spherical surface [67], hence providing a link to the entropic formulation of [35, 45]. The free energy on S^3 was also proposed as a possible c-function (henceforth F-function) in $d = 3$, with the radius of the sphere as the parameter along the RG flow [43, 44, 66]. A generalisation of the sphere partition function beyond $d = 3$ was suggested as a definition for a c-function in general d [68] (see also [69]). Evidence for the F-theorem in both supersymmetric and non-supersymmetric theories can be found in [44, 66, 70, 43, 71, 72].

However, there exist problems with the identification of the free energy with the F-function. In [66] one curious observation was that for the simple case of a free massive scalar on S^3 the free energy failed to interpolate monotonically between UV and IR (see also [73]). Only by performing an ad-hoc subtraction of a suitably chosen function it could be made monotonic, suggesting that the free energy on S^3 fails to be a universally valid F-function.

A more successful definition of the F-function employs an appropriately defined entanglement entropy. In [74] Liu and Mezei constructed a quantity termed 'Renormalized Entanglement Entropy' (REE), whose functional dependence on the size of the entangling surface is interpreted as describing the RG flow of the entanglement entropy with distance scale. At the fixed points of a flow the REE reduces to the central charge of the corresponding CFT. For *Poincaré-invariant* field theories in $d = 3$ space-time dimensions the REE was proven to decrease monotonically from UV to IR in [75], suggesting that the REE can play the role of the F-function in $d = 3$. A different approach for isolating the finite contribution to the entanglement entropy based on mutual information was proposed in [76].

The study of c-theorems and in particular the F-theorem remains an active field with many directions for further study. For example, the question of stationarity of the F-function at fixed points is currently unresolved with evidence against stationarity found in [77]. For a recent work on the construction of c-functions in defect CFTs see [78].

In this chapter we will address open questions regarding the F-theorem,

[1] For a recent review of entanglement entropy in holography and its application to RG flows and c-theorems see [65].

both in its formulation in terms of the free energy on S^3, and in its entropic formulation. Although the (UV-finite part of the) free energy on a sphere and the REE coincide at fixed points, the formulation of the F-theorem in terms of the free energy on S^3 [43, 44, 66] seems problematic. As stated above, the free energy on S^3 fails to be monotonic even for the case of a free massive scalar [66, 73], thus calling into question its identification as a universally valid F-function. The same conclusion was reached in the context of holographic RG flows in [79].

Another open question concerns the entropic formulation. In this case an F-function can be defined as the REE across a spherical surface [74]. While this was proven to be monotonic under RG flow for Poincaré invariant theories, the status of the REE as an F-function beyond Poincaré-invariant theories is unclear. For example, in [80] the behaviour of the REE under renormalization group flow was examined for the theory of a conformally coupled scalar on dS_3. In this case the REE fails to exhibit monotonicity and it is hence not a good F-function on dS_3 (see also [73]).

Finally, it is not clear if and how the two formulations of the F-theorem are related. In particular, while the two definitions in terms of the entanglement entropy and free energy coincide in the UV and IR [67], it is not known to what extent this relation should persist along the RG flow. While the F-theorem in three dimensions is by now well established in terms of the entanglement entropy, an alternative formulation directly in terms of the sphere partition function may still be desirable as this quantity may be easier to compute in practice for non-conformal field theories and it may evade some of the difficulties in the computation of the entanglement entropy in the presence of a regulator [76].

Motivated by the discussion above, in this chapter we will address the following questions:

1. Can a true F-function be constructed from the free energy on S^3?

2. How can a good F-function be constructed from an entanglement entropy for theories on dS_3?

3. How are the formulations of the F-function in terms of the free energy on S^3 and in terms of an entanglement entropy related? In particular, under what circumstances do they coincide along the whole flow rather than only at the UV and IR end points?

Here we will use holography to address these questions. Throughout this chapter we will make use of the understanding of holographic RG flows for field theories on curved manifolds described in chapter 2.

3.2 On-shell action and free energy

In this section we will present various quantities which will be instrumental in the construction of the F-functions, as well as their renormalization.

The basic quantity considered in this section is the (regularised or renormalized) bulk on-shell action, which is the action given in (1.4.2) evaluated on solutions to the field equations (2.1.5)–(2.1.7). This functional reduces to a function of boundary values, $S_{\text{on-shell}} = S_{\text{on-shell}}(\varphi_-, R^{(\zeta)})$. However, the need for regularisation and/or renormalization of this quantity introduces a dependence on extra parameters: a UV cut-off, or a choice of boundary counterterms.

As discussed in section 1.3.4 in the dual field theory, the on-shell action has a different interpretation depending whether one is using standard or alternative holographic dictionary.

- In the standard dictionary, the on-shell action is related to the *free energy* of the theory as[2]

$$F(j, R) \equiv -S_{\text{on-shell}}(\varphi_-, R^{(\zeta)}) \,, \tag{3.2.1}$$

  with the source j identified with φ_-.

- In the alternative dictionary, the on-shell action is identified, rather than with the free energy, with its Legendre transform with respect to the source j, i.e. the *quantum effective potential* $\Gamma(\langle\mathcal{O}\rangle, \mathcal{R})$ of the theory, which depends on the operator vev $\langle\mathcal{O}\rangle$ rather than the source j. That is, in alternative quantisation we have

$$\Gamma(\langle\mathcal{O}\rangle, R^{(\zeta)}) \equiv -S_{\text{on-shell}}(\varphi_-, R^{(\zeta)}) \,, \tag{3.2.2}$$

  where φ_- is now identified with $\langle\mathcal{O}\rangle$.

This distinction will be important later on. However, for simplicity, we will be referring to the on-shell action as *free energy*, thereby assuming the standard dictionary, unless stated explicitly otherwise.

The appropriately renormalized free energy, which will be computed in subsection 3.2.2, will be the starting point for constructing our proposals for F-functions in section 3.3.

[2] In a thermodynamic interpretation of our system one may define the thermodynamic free energy F_{th} as $\beta F_{\text{th}} = S_{\text{on-shell},E}$ with β the appropriate inverse temperature and $S_{\text{on-shell},E}$ the Euclidean on-shell action. Note that this thermodynamic free energy F_{th} differs from the free energy F defined here.

3.2.1 The free energy of a holographic RG flow

We begin by writing the expression for the free energy F for a field theory on S^d, by using the definition (3.2.1), where $S_{\text{on-shell}}$ is given by (1.4.2) evaluated on a solution.

The on-shell action can be expressed as a functional over $A(u)$ (we refer readers to appendix F for details of the derivation). This leads to the following expression for the free energy,

$$F = 2(d-1)M^{d-1}V_d \left[e^{dA}\dot{A}\right]_{\text{UV}} - \frac{2M^{d-1}R}{d}V_d \int_{\text{UV}}^{\text{IR}} du\, e^{(d-2)A(u)}\,, \qquad (3.2.3)$$

where we defined

$$V_d \equiv \int \mathrm{d}^d x\sqrt{|\zeta|} = \text{Vol}(S^d)\,, \qquad (3.2.4)$$

and $R = R^{(\zeta)} = R^{UV} = \frac{d(d-1)}{\alpha^2}$ in our convention. The integration in (3.2.3) is over the entire geometry of the holographic RG flow from the boundary at $u \to -\infty$ (referred to as UV) to the interior at some finite u_0 (referred to as IR). There is a similar contribution as the first term in equation (3.2.3) from the IR. Because of regularity of the IR end-point, the contribution vanishes, as can be easily seen using equation (2.5.13).

Integrating up to the boundary gives rise to UV-divergences and hence we will cut off the integration in the UV at some finite value $u = \ell \log \epsilon$. Hence, whenever we write 'UV' in the following, this implies that the corresponding quantity is to be evaluated at

$$u_\epsilon \equiv \ell \log \epsilon \qquad \text{or} \qquad \varphi_\epsilon \equiv \varphi(\ell \log \epsilon)\,. \qquad (3.2.5)$$

It will be convenient to rewrite the free energy given in (3.2.3) in terms of the functions $W(\varphi)$, $S(\varphi)$ and $T(\varphi)$. The resulting expression will be more amenable to numerical analysis as well as analytical considerations compared to (3.2.3). As a first step, we write

$$V_d = \int \mathrm{d}^d x\sqrt{|\zeta|} = \frac{2\pi^{\frac{d+1}{2}}}{\Gamma(\frac{d+1}{2})}\,\alpha^d = \tilde{\Omega}_d\, R^{-\frac{d}{2}}\,, \quad \text{with} \quad \tilde{\Omega}_d \equiv \frac{2d^{\frac{d}{2}}(d-1)^{\frac{d}{2}}\pi^{\frac{d+1}{2}}}{\Gamma(\frac{d+1}{2})}\,. \qquad (3.2.6)$$

Inserting this into (3.2.3) and using the definitions (2.2.1)–(2.2.3) the free energy (3.2.3) can be written as

$$F = -M^{d-1}\tilde{\Omega}_d \left(\left[T^{-\frac{d}{2}}(\varphi)W(\varphi)\right]_{\text{UV}} + \frac{2}{d}\int_{\text{UV}}^{\text{IR}} d\varphi\, S^{-1}(\varphi)T^{-\frac{d}{2}+1}(\varphi) \right)\,. \qquad (3.2.7)$$

We now rewrite the second term. In particular note that we can express[3]

$$\frac{2}{d}\, S^{-1}(\varphi) T^{-\frac{d}{2}+1}(\varphi)\, \mathrm{d}\varphi = -\mathrm{d}\left(T^{-\frac{d}{2}+1}(\varphi) U(\varphi)\right) , \tag{3.2.8}$$

in terms of a function $U(\varphi)$ which satisfies

$$SU' - \frac{d-2}{2(d-1)} WU = -\frac{2}{d} . \tag{3.2.9}$$

As this is a first order differential equation, solving for U introduces in principle one integration constant, which we will refer to as B. However, this will be fixed by a IR condition as we will see shortly. Using the near-boundary expansions of W and S given in (2.4.2) and (2.4.3), we can derive the near-boundary behaviour of U from (3.2.9):

$$U(\varphi) \underset{\varphi\to 0}{=} \ell \left[\frac{2}{d(d-2)} + B|\varphi|^{(d-2)/\Delta_-} + \mathcal{O}\big(\mathcal{R}|\varphi|^{2/\Delta_-}\big) \right] . \tag{3.2.10}$$

Notice that the dependence on the integration constant C through W and S, only enters U at subleading order in the near-boundary expansion. Thus, in the vicinity of the UV, we find that there is a family of solutions for U, which we will denote by $U_{B,\mathcal{R}}$.

The regular IR expansion acts as a boundary condition for the differential equation (3.2.9). It is given by the regularity condition

$$U(\varphi) \underset{\varphi\to\varphi_0}{=} U_0 \sqrt{|\varphi-\varphi_0|} + \mathcal{O}\big(|\varphi-\varphi_0|\big) , \tag{3.2.11}$$

where $U_0 = \frac{4}{d(d-1)S_0}$ and S_0 was defined in (2.5.11). This fixes the integration constant B appearing in U uniquely in terms of φ_0. Therefore, by introducing the function $U(\varphi)$ we did not introduce any extra freedom or new parameter. As a result, B becomes a function of φ_0, $B(\varphi_0)$. As $\mathcal{R}$ is a function of φ_0, we can trade the dependence on φ_0 in $B(\varphi_0)$ with a dependence on $\mathcal{R}$ which, contrary to φ_0, is one of the boundary data, and write $B \equiv B(\mathcal{R})$. As shown in sec. 3.4, $B(\mathcal{R})$ computes an appropriately defined entanglement entropy.

Going back to the computation of the free energy, using (3.2.8) the second term in (3.2.7) becomes:

$$\frac{2}{d}\int_{\mathrm{UV}}^{\mathrm{IR}} d\varphi\, S^{-1}(\varphi) T^{-\frac{d}{2}+1}(\varphi) = -\big[T^{-\frac{d}{2}+1}(\varphi)U(\varphi)\big]_{\mathrm{IR}} + \big[T^{-\frac{d}{2}+1}(\varphi)U(\varphi)\big]_{\mathrm{UV}} . \tag{3.2.12}$$

[3]To avoid confusion, in eq. (3.2.8) we denote the differential symbol by d, while the number of (boundary) space-time dimensions is written as d. In the remainder of this analysis there is little danger of confusion and so we revert to using d for both differentials and the number of dimensions.

One can check that the contribution from the IR to the above expression vanishes, by inserting the corresponding near-IR expansions for $T(\varphi)$ and $U(\varphi)$ given in (2.5.10) and (3.2.11). This is ensured by the regularity conditions on $U(\varphi)$ at the IR end-point.[4] Collecting all results, we arrive at an expression for F which is purely a UV boundary term:

$$F = -M^{d-1}\tilde{\Omega}_d \left(\left[T^{-\frac{d}{2}}(\varphi_\epsilon) W(\varphi_\epsilon) \right] + \left[T^{-\frac{d}{2}+1}(\varphi_\epsilon) U(\varphi_\epsilon) \right] \right) . \tag{3.2.13}$$

In the following, we will write the divergent terms in (3.2.13) explicitly. To this end, we introduce an energy cutoff λ_ϵ which is defined as

$$\lambda_\epsilon = \frac{e^{A(u_\epsilon)}}{\ell} . \tag{3.2.14}$$

Furthermore, we introduce the quantities $\gamma^\epsilon_{\mu\nu}$ and φ^ϵ_-, which correspond to the sources for the metric and the dilaton at the cutoff-surface at u_ϵ. These are defined as:

$$\gamma_{\mu\nu}(u_\epsilon) = \gamma^\epsilon_{\mu\nu}\, \ell^2\, \lambda_\epsilon^2 , \qquad \varphi_\epsilon = \varphi^\epsilon_-\, \lambda_\epsilon^{-\Delta_-} , \tag{3.2.15}$$

where the induced metric $\gamma_{\mu\nu}(u)$ is given in (2.1.3). Note that with our definition of the cutoff (3.2.14) the source metric at the cutoff-surface $\gamma^\epsilon_{\mu\nu}$ is identical to the UV boundary metric $\zeta_{\mu\nu}$:

$$\gamma^\epsilon_{\mu\nu} = \gamma_{\mu\nu}(u_\epsilon)\, \ell^{-2} \lambda_\epsilon^{-2} = \zeta_{\mu\nu}\, e^{2A(u_\epsilon)}\, e^{-2A(u_\epsilon)} = \zeta_{\mu\nu} . \tag{3.2.16}$$

In contrast, for finite ϵ the cutoff-source φ^ϵ_- departs from the UV source φ_-, and only reduce to it for $\epsilon \to 0$:

$$\lim_{\epsilon\to 0} \varphi^\epsilon_- = \varphi_- . \tag{3.2.17}$$

As $\gamma^\epsilon_{\mu\nu} = \zeta_{\mu\nu}$ the scalar curvature associated with the cutoff metric is just the UV curvature R. However, it will be useful to also define the corresponding dimensionless curvature $\mathcal{R}_\epsilon$ in units of the cutoff source φ^ϵ_- as

$$\mathcal{R}_\epsilon \equiv R\, |\varphi^\epsilon_-|^{-2/\Delta_-} , \quad \text{which satisfies} \quad \lim_{\epsilon\to 0} \mathcal{R}_\epsilon = \mathcal{R} . \tag{3.2.18}$$

[4] While for W IR regularity is a necessary condition for the regularity of the bulk solution, the regularity of U is a choice, but a particularly convenient one as it allows to write the free energy purely as a UV boundary term. Any other choice of the integration constant in the U-equation would have given the same numerical result for F, but this would arise by a combination of UV and IR terms [34]. This goes against the spirit of holography, in which one should be able to write the field theory partition function purely in terms of UV boundary data.

Similarly, we define a dimensionless cutoff Λ_ϵ as

$$\Lambda_\epsilon \equiv \frac{\lambda_\epsilon}{|\varphi_-^\epsilon|^{1/\Delta_-}} = \frac{e^{A(\ell \log \epsilon)}}{\ell\,|\varphi_-^\epsilon|^{1/\Delta_-}}\,, \tag{3.2.19}$$

i.e. Λ_ϵ corresponds to the energy cutoff λ_ϵ in units of the cutoff source φ_-^ϵ. It is important to note that the quantities φ_-^ϵ and λ_ϵ (rather than φ_- and $\zeta_{\mu\nu}$) are the correct set of covariant boundary data one should fix in the cut-off gravitational theory, i.e. they fix the induced metric and the value of the scalar field at the cutoff surface. It is therefore natural to write the cutoff free energy in terms of these quantities.

We are now in a position to enumerate the divergent terms in (3.2.13) explicitly. As a first step we insert the near-boundary expansions for $W(\varphi)$ and $U(\varphi)$. Further, noting that $T(\varphi) = R^{(\gamma)}(\varphi)$ the free energy in (3.2.13) becomes:

$$\begin{aligned} F = -M^{d-1}\tilde{\Omega}_d \Bigg\{ & \quad \big(R^{(\gamma)}(\varphi_\epsilon)\big)^{-\frac{d}{2}} \left[\frac{2(d-1)}{\ell} + \frac{\Delta_-}{2\ell}\varphi_\epsilon^2 + \frac{C}{\ell}\,|\varphi_\epsilon|^{d/\Delta_-} + \dots\right] \\ & + \big(R^{(\gamma)}(\varphi_\epsilon)\big)^{-\frac{d}{2}+1} \left[\frac{\ell}{d-2} + B\ell|\varphi_\epsilon|^{\frac{(d-2)}{\Delta_-}} + \dots\right] + \mathcal{O}\Big(\ell^3\big(R^{(\gamma)}(\varphi_\epsilon)\big)^{-\frac{d}{2}+2}\Big)\Bigg\}. \end{aligned} \tag{3.2.20}$$

This can then be written as an expansion in terms of Λ_ϵ and $\mathcal{R}_\epsilon$ as follows. From our above definitions we have that

$$R^{(\gamma)}(\varphi_\epsilon) = \ell^{-2}\,\mathcal{R}_\epsilon \Lambda_\epsilon^{-2} \tag{3.2.21}$$

$$|\varphi_\epsilon| = \Lambda_\epsilon^{-\Delta_-}\,. \tag{3.2.22}$$

Inserting this into (3.2.20) we can write the free energy as a double expansion in $\mathcal{R}_\epsilon$ and Λ_ϵ.

As the structure of the UV-divergent terms depends on the number of dimensions d, it is easiest to give results for a specific value for d. Therefore, in the remainder of this section we turn to our main case of interest and work with $d = 3$.

The unrenormalized free energy in $d = 3$

Starting with (3.2.20) and using (3.2.21) and (3.2.22) we find the following result for $d = 3$:

$$F^{d=3}(\Lambda_\epsilon, \mathcal{R}_\epsilon) = -(M\ell)^2\tilde{\Omega}_3 \Bigg\{ \quad \mathcal{R}_\epsilon^{-3/2}\Big[4\Lambda_\epsilon^3\Big(1+\mathcal{O}\big(\Lambda_\epsilon^{-2\Delta_-}\big)\Big) + C(\mathcal{R}_\epsilon)\Big] \\ + \mathcal{R}_\epsilon^{-1/2}\Big[\Lambda_\epsilon\Big(1+\mathcal{O}\big(\Lambda_\epsilon^{-2\Delta_-}\big)\Big) + B(\mathcal{R}_\epsilon)\Big] + \mathcal{O}\Big(\mathcal{R}_\epsilon^{1/2}\Lambda_\epsilon^{-1}\Big)\Bigg\}. \tag{3.2.23}$$

We can then make the following observations:

- There is a leading divergence of the form $\sim \Lambda_\epsilon^3$ and a subleading divergence $\sim \Lambda_\epsilon$. Depending on the precise value of Δ_- there may be many further divergent terms. However, all UV-divergent terms either come with a curvature factor $\mathcal{R}_\epsilon^{-3/2}$ or $\mathcal{R}_\epsilon^{-1/2}$. Moreover, the integration constants $B(\mathcal{R}_\epsilon)$ and $C(\mathcal{R}_\epsilon)$ only contribute finite terms. This observation will be important later. It is a manifestation of the well-known fact in holographic renormalization that UV divergences are universal and vevs only contribute to finite terms in the on-shell action.

- The most important part of F as far as the F-theorem is concerned is what we will refer to as the 'universal contribution'. This is the Λ_ϵ-independent piece of (3.2.23), in the limit that the cutoff is taken to infinity:

$$\begin{aligned} F^{d=3}_{\text{univ}} &= \lim_{\epsilon\to 0}\Big[-(M\ell)^2\tilde{\Omega}_3\big(\mathcal{R}_\epsilon^{-3/2}C(\mathcal{R}_\epsilon) + \mathcal{R}_\epsilon^{-1/2}B(\mathcal{R}_\epsilon)\big)\Big] \\ &= -(M\ell)^2\tilde{\Omega}_3\left(\mathcal{R}^{-3/2}C(\mathcal{R}) + \mathcal{R}^{-1/2}B(\mathcal{R})\right). \end{aligned} \tag{3.2.24}$$

  This depends on the boundary parameter $\mathcal{R}$ and on the (curvature-dependent) parameters $C(\mathcal{R})$ and $B(\mathcal{R})$, which in turn are related to the following field theoretic quantities: $C(\mathcal{R})$ is related to a vev in standard quantisation:

$$C(\mathcal{R}) = \frac{\Delta_-}{d}\langle\mathcal{O}\rangle|\varphi_-|^{-\frac{\Delta_+}{\Delta_-}}, \tag{3.2.25}$$

  while $B(\mathcal{R})$ computes an appropriately defined entanglement entropy (see sec. 3.4). In addition, for $\mathcal{R}\to 0$ one can show (see app. J.2) that

$B(\mathcal{R})$ is related to a derivative with respect to curvature of the vev $\langle\mathcal{O}\rangle$ as:

$$B(\mathcal{R})\big|_{\mathcal{R}=0} = 2\,\frac{\partial C(\mathcal{R})}{\partial\mathcal{R}}\bigg|_{\mathcal{R}=0} = \frac{2\Delta_-}{d}|\varphi_-|^{-\frac{\Delta_+-2}{\Delta_-}}\,\frac{\partial}{\partial R}\langle\mathcal{O}\rangle\bigg|_{R=0}\,, \quad (3.2.26)$$

where the last equality holds for fixed φ_-.

3.2.2 The renormalized free energy

The universal contribution to the free energy written in equation (3.2.24) can be affected by finite local counterterms. Therefore, to obtain the finite part of the free energy in a systematic and unambiguous way, we need to resort to holographic renormalization.

In holographic renormalization of a general dilaton-gravity theory, the counterterms can be conveniently organised in terms of curvature invariants associated with the induced metric $\gamma_{\mu\nu}$, multiplied by suitable functions of the scalar field [30]. The intrinsic curvature appears up to a maximum power of $d/2$ (plus logarithmic contributions associated to anomalies) for d even and $(d-1)/2$ for d odd. For example, the first two counterterms are given by

$$F_{ct}^{(0)} = M^{d-1}\int_{\rm UV} d^dx\sqrt{|\gamma|}\,W_{ct}(\varphi)\,, \quad (3.2.27)$$

$$F_{ct}^{(1)} = M^{d-1}\int_{\rm UV} d^dx\sqrt{|\gamma|}\,R^{(\gamma)}U_{ct}(\varphi)\,, \quad (3.2.28)$$

$$\vdots$$

and these are all the counterterms needed in $d=3$. The functions W_{ct} and U_{ct} satisfy the equations[5]

$$\frac{d}{4(d-1)}W_{ct}^2 - \frac{1}{2}\big(W_{ct}'\big)^2 = -V\,, \quad (3.2.29)$$

$$W_{ct}'\,U_{ct}' - \frac{d-2}{2(d-1)}\,W_{ct}\,U_{ct} = -1\,. \quad (3.2.30)$$

These are equivalent to the "flat" superpotential equation with $T=0$ and to (a rescaled version of) the "flat" U-equation (3.2.9) with $S(\varphi)$ replaced by W'. Therefore they track the flat space holographic RG flow.

As we will be exclusively interested in the case $d=3$ in this chapter, the two counterterms (3.2.27) and (3.2.28) are sufficient and we hence refrain

[5]The eq. (3.2.29) for W_{ct} is equivalent to the EOM for W in the case $R=0$.

from giving explicit expressions of counterterms at higher orders in $R^{(\gamma)}$, but they can be found in [30].

Equations (3.2.29) and (3.2.30) determine the functions W_{ct} and U_{ct} up to two integration constants, which we call C_{ct} and B_{ct}, respectively and which we can choose at will. A particular choice of these constants corresponds to a choice of renormalization scheme. It will also be useful to record the expansion of the functions W_{ct} and U_{ct} in the vicinity of the UV boundary. In particular, close to a UV fixed point at $\varphi = 0$ the functions W_{ct} and U_{ct} can be expanded in powers of φ as follows, [81, 82, 40]:

$$W_{0,ct}(\varphi) = \frac{2(d-1)}{\ell} + \frac{\Delta_-}{2\ell}\varphi^2 + \frac{C_{ct}}{\ell}|\varphi|^{d/\Delta_-} + \dots , \tag{3.2.31}$$

$$U_{ct}(\varphi) = \frac{\ell}{d-2} + \ell\, B_{ct}\, |\varphi|^{(d-2)/\Delta_-} + \dots , \tag{3.2.32}$$

where C_{ct} and B_{ct} now appear explicitly.

The renormalized free energy is then given by the free energy (3.2.13) with all necessary counterterms added. For $d = 3$ this gives

$$F^{d=3,\text{ren}}(\mathcal{R}|B_{ct}, C_{ct}) = \lim_{\Lambda_\epsilon \to \infty} \left[F^{d=3}(\Lambda_\epsilon, \mathcal{R}_\epsilon) + F^{(0)}_{ct} + F^{(1)}_{ct} \right] . \tag{3.2.33}$$

where we explicitly emphasised the fact that the dependence on Λ_ϵ has been traded with a dependence on counterterms.

Renormalized free energy for $d = 3$

As a first step, it will be convenient to rewrite the counterterms (3.2.27) and (3.2.28) as follows. Using the fact that

$$R^{(\gamma)} = T\,, \qquad \text{and} \qquad \sqrt{-\gamma} = R^{d/2} T^{-d/2} \sqrt{-\zeta}\,, \tag{3.2.34}$$

the counterterms become

$$F^{(0)}_{ct} = M^{d-1} \tilde{\Omega}_d \left[T^{-\frac{d}{2}}(\varphi)\, W_{ct}(\varphi) \right]_{\text{UV}}\,, \tag{3.2.35}$$

$$F^{(1)}_{ct} = M^{d-1} \tilde{\Omega}_d \left[T^{-\frac{d}{2}+1}(\varphi)\, U_{ct}(\varphi) \right]_{\text{UV}}\,, \tag{3.2.36}$$

where $\tilde{\Omega}_d$ is defined in (3.2.6). Using this we find the following expression for the renormalized free energy in $d = 3$:

$$F^{d=3,\text{ren}} = -M_p^2 \tilde{\Omega}_3 \left(\left[T^{-\frac{3}{2}}(\varphi) \big(W(\varphi) - W_{ct}(\varphi) \big) \right]_{\text{UV}} + \left[T^{-\frac{1}{2}}(\varphi) \big(U(\varphi) - U_{ct}(\varphi) \big) \right]_{\text{UV}} \right) . \tag{3.2.37}$$

Inserting the expressions for the UV expansions for T, W, W_{ct}, U and U_{ct} from (2.4.4), (2.4.2), (3.2.31), (3.2.10), (3.2.32) we finally arrive at

$$F^{d=3,\text{ren}}(\mathcal{R}|B_{ct},C_{ct}) = -(M\ell)^2\tilde{\Omega}_3\Big[\mathcal{R}^{-3/2}\big(C(\mathcal{R})-C_{ct}\big)+\mathcal{R}^{-1/2}\big(B(\mathcal{R})-B_{ct}\big)\Big]. \tag{3.2.38}$$

This now shows the explicit dependence of the free energy on the two renormalization constants C_{ct} and B_{ct}.

3.2.3 Expressions at small and large curvature

We begin by collecting the results from the previous sections. There we presented expressions for the free energy on S^3. In particular, we have the following expressions for the cutoff-regulated and renormalized quantities:

$$\begin{aligned} F(\Lambda_\epsilon,\mathcal{R}_\epsilon) = -(M\ell)^2\tilde{\Omega}_3\Bigg\{ &\quad \mathcal{R}_\epsilon^{-3/2}\Big[4\Lambda_\epsilon^3\Big(1+\mathcal{O}\big(\Lambda_\epsilon^{-2\Delta_-}\big)+C(\mathcal{R}_\epsilon)\Big)\Big] \\ &+\mathcal{R}_\epsilon^{-1/2}\Big[\Lambda_\epsilon\Big(1+\mathcal{O}\big(\Lambda_\epsilon^{-2\Delta_-}\big)+B(\mathcal{R}_\epsilon)\Big)\Big]+\mathcal{O}\Big(\mathcal{R}_\epsilon^{1/2}\Lambda_\epsilon^{-1}\Big)\Bigg\}, \end{aligned} \tag{3.2.39}$$

$$F^{\text{ren}}(\mathcal{R}|B_{ct},C_{ct}) = -(M\ell)^2\tilde{\Omega}_3\Big[\mathcal{R}^{-3/2}\big(C(\mathcal{R})-C_{ct}\big)+\mathcal{R}^{-1/2}\big(B(\mathcal{R})-B_{ct}\big)\Big], \tag{3.2.40}$$

where we now suppress the superscript $d=3$ to remove clutter.

Generally, we will have to revert to numerical methods to evaluate these quantities. However, for both large and small curvature we can make analytical progress. In particular, as shown in appendix H, we can extract the behaviour of $C(\mathcal{R})$ and $B(\mathcal{R})$ analytically for $\mathcal{R}\to\infty$ and $\mathcal{R}\to 0$. It is these functions that determine the $\mathcal{R}$-dependence of the renormalized free energy F^{ren}, the universal contribution F_{univ} to the cutoff-regulated free energy, and ultimately our candidate F-functions.

Hence, in this section we will summarise the results for $C(\mathcal{R})$ and $B(\mathcal{R})$ in the regimes $\mathcal{R}\to\infty$ and $\mathcal{R}\to 0$ obtained in appendix H, and determine the resulting expressions for F^{ren}. The corresponding expressions for F_{univ} can be computed analogously from (3.2.24).

Large curvature results: $\mathcal{R} \to \infty$

From the calculations in Appendix H.1 we obtain:

$$C(\mathcal{R}) \underset{\mathcal{R}\to\infty}{=} \mathcal{O}\big(\mathcal{R}^{3/2-\Delta_-}\big)\,, \qquad B(\mathcal{R}) \underset{\mathcal{R}\to\infty}{=} -8\pi^2\tilde{\Omega}_3^{-2}\,\mathcal{R}^{1/2}\left(1+\mathcal{O}\big(\mathcal{R}^{-\Delta_-}\big)\right)\,. \tag{3.2.41}$$

Inserting this into equation (3.2.39)–(3.2.40) we obtain the corresponding large-curvature asymptotics for the free energy. To be brief, we give explicit expressions for the renormalized quantities only. Therefore, for $\mathcal{R} \to \infty$ we obtain:

$$F^{\rm ren} \underset{\mathcal{R}\to\infty}{=} (M\ell)^2\left(8\pi^2+\tilde{\Omega}_3 B_{ct}\mathcal{R}^{-1/2}+\tilde{\Omega}_3 C_{ct}\mathcal{R}^{-3/2}+\mathcal{O}(\mathcal{R}^{-\Delta_-})\right)\,. \tag{3.2.42}$$

Therefore, $F^{\rm ren}$ is finite for $\mathcal{R} \to \infty$ approaching the value $8\pi^2(M\ell)^2$.

We identify this value as the free energy (or central charge) of the UV CFT. The reason is as follows. For fixed R taking $\mathcal{R} \to \infty$ corresponds to the limit of vanishing source, i.e. $|\varphi_-| \to 0$. Hence the value of the (renormalized) free energy obtained for $\mathcal{R} \to \infty$ can be identified with that of the corresponding CFT.

The above observation gives rise to the following general result. For a CFT associated with an extremum of the potential at $\varphi_{\rm CFT}$ the (renormalized) free energy is given by

$$F_{\rm CFT} = 8\pi^2(M\ell_{\rm CFT})^2\,, \qquad \text{with} \qquad \ell^2_{\rm CFT} \equiv -\frac{6}{V(\varphi_{\rm CFT})}\,. \tag{3.2.43}$$

This is valid regardless whether the extremum is a maximum or a minimum of the potential. Also note that the renormalized value of the free energy of a CFT is unambiguous, i.e. there is no scheme-dependence.

Small curvature expansion: $\mathcal{R} \to 0$

From the analysis in appendix H.2 one finds:

$$C(\mathcal{R}) \underset{\mathcal{R}\to 0}{=} C_0 + C_1\mathcal{R} + \mathcal{O}\big(\mathcal{R}^2\big) + \mathcal{O}\big(\mathcal{R}^{3/2-\Delta_-^{\rm IR}}\big)\,, \tag{3.2.44}$$

$$B(\mathcal{R}) \underset{\mathcal{R}\to 0}{=} B_0\left(1+\mathcal{O}\big(\mathcal{R}\big)\right) - 8\pi^2\tilde{\Omega}_3^{-2}\frac{\ell^2_{\rm IR}}{\ell^2}\,\mathcal{R}^{1/2}\left(1+\mathcal{O}\big(\mathcal{R}^{-\Delta_-^{\rm IR}}\big)\right)\,, \tag{3.2.45}$$

where we have defined

$$\ell^2_{\rm IR} \equiv -\frac{d(d-1)}{V(\varphi_{\rm IR})}\,, \qquad \Delta_-^{\rm IR} = \frac{1}{2}(d-\sqrt{d^2+4\ell^2_{\rm IR}V''(\varphi_{\rm IR})})\,, \tag{3.2.46}$$

where $\varphi_{\rm IR}$ is the minimum of the potential. Note that $\Delta_-^{\rm IR} < 0$ since $V''(\varphi_{\rm IR}) > 0$.

The quantities C_0, B_0 and C_1 appearing in equations (3.2.44)–(3.2.45) are numerical coefficients. The quantity C_0 is the flat-space value of the vev $\langle\mathcal{O}\rangle$ and C_1 is the coefficient of the first curvature correction to $\langle\mathcal{O}\rangle$. The coefficient B_0 corresponds to the flat-space limit of an appropriately defined entanglement entropy (see sec. 3.4).[6]

This leads to the following expression for the renormalized free energy:

$$F^{\rm ren} \underset{\mathcal{R}\to 0}{=} -(M\ell)^2\tilde{\Omega}_3\big(C_0 - C_{ct}\big)\mathcal{R}^{-3/2} - (M\ell)^2\tilde{\Omega}_3\big(B_0 + C_1 - B_{ct}\big)\mathcal{R}^{-1/2} + 8\pi^2(M\ell_{\rm IR})^2 + \mathcal{O}(\mathcal{R}^{-\Delta_-^{\rm IR}}) + \mathcal{O}(\mathcal{R}^{1/2})\,. \tag{3.2.47}$$

Note that in general $F^{\rm ren}$ diverges for $\mathcal{R} \to 0$. The leading divergence is of the form $\mathcal{R}^{-3/2}$ and it can be understood as a volume divergence. This is the statement that the free energy is an extensive quantity and grows with the volume of the S^3, i.e. $\mathrm{Vol}(S^3) \sim \mathcal{R}^{-3/2}$ for fixed φ_-. The same IR divergence also occurs in the unrenormalized quantity $F(\Lambda_\epsilon, \mathcal{R}_\epsilon)$. The coefficient of that divergence is the free-energy density of the flat theory.

In addition to the divergent terms, the expression (3.2.47) also exhibits a finite contribution. From (3.2.43) we identify this term as the central charge of the IR CFT associated with the IR fixed point at the minimum of the potential. Interestingly, while this central charge is a property of the IR CFT only, here it emerges from the free energy of a holographic RG flow solution from the UV fixed point to this IR.

These observations suggest that we may be able to construct F-functions (depending on $\mathcal{R}$) out of the free energy, which interpolate between the central charges of the UV and IR CFTs, if we can isolate a quantity which generalises the finite contribution also away from the fixed points. This is what we will propose in the next section.

3.3 Constructing F-functions from the free energy

Having collected all the necessary ingredients, we can finally turn to constructing candidate F-functions. We start with a definition of the F-theorem.

[6] In fact, for our setup one finds that $B_0 = 2C_1$, This follows from a thermodynamic relation between the free energy on S^3 and an appropriately defined entanglement entropy and will be explained in sec. 3.4 and app. J.2.

We then explain how the F-theorem is related to holographic RG flows[7]. Finally, using the results from section 3.2 we propose several candidate F-functions and check their viability numerically.

3.3.1 Definitions and strategy

The F-theorem [44] is a statement about Lorentz-invariant quantum field theories in $d = 3$ and their behaviour under renormalization group flow. In its minimal form, it is concerned with properties of two conformal field theories which are connected by an RG flow. It states that at both the UV and IR fixed points one can define a quantity F such that

$$F_{\mathrm{UV}} \geq F_{\mathrm{IR}} \,. \tag{3.3.1}$$

A refined version demands that there exists a function $\mathcal{F}(\mathcal{R})$, with $\mathcal{R}$ some parameter along the flow, which exhibits the following properties:

- At the fixed points of the flow, the function $\mathcal{F}(\mathcal{R})$ takes the values $\mathcal{F}_{\mathrm{UV}}$ and $\mathcal{F}_{\mathrm{IR}}$ respectively.

- The function $\mathcal{F}(\mathcal{R})$ evolves monotonically along the flow, i.e.

$$\frac{d}{d\mathcal{R}}\mathcal{F}(\mathcal{R}) \geq 0 \,, \tag{3.3.2}$$

  for a parameter $\mathcal{R}$ that decreases monotonically when going from UV to IR.

- It is also expected that $\mathcal{F}(\mathcal{R})$ should be stationary at the fixed points of the RG flow. This expectation arises from the observation that the Zamolodchikov c-function in $d = 2$ is stationary at the fixed points. However, as pointed out in [77], there exist F-function candidates that satisfy the first two requirements (correct values in UV/IR, monotonicity), but violate stationarity. We hence leave it open whether the F-function should be stationary at the fixed points and focus on the other two conditions in this work.

Here we will explore several candidate F-functions in a holographic setting for a field theory on S^3. We lay out our strategy in the following:

[7] This idea was already explored in [79]. As we will see, the key reason that work gave a negative result lies in how infrared divergences are treated

1. In the holographic context, the UV theory is the CFT associated with a maximum $\varphi_{\rm max}$ of the bulk potential V. The IR CFT will be associated with a neighbouring minimum $\varphi_{\rm min}$:

$$\begin{aligned} \text{CFT}_{\rm UV} \quad &\longleftrightarrow \quad \varphi(u) = \varphi_{\rm UV} = \varphi_{\rm max} = const.\,, \\ \text{CFT}_{\rm IR} \quad &\longleftrightarrow \quad \varphi(u) = \varphi_{\rm IR} = \varphi_{\rm min} = const.\,. \end{aligned}$$

2. We identify the F-quantity with the renormalized free energy of the corresponding CFT. This can be calculated as follows. Note that at an extremum of V the bulk geometry is AdS_4. The scale factor is then given by

$$A_{\rm UV}(u) = \ln\left(-\frac{\ell_{\rm UV}}{\alpha}\sinh\frac{u+c_{\rm UV}}{\ell_{\rm UV}}\right), \quad \text{with} \quad \ell_{\rm UV}^2 = -\frac{6}{V(\varphi_{\rm UV})} \tag{3.3.3}$$

for the UV CFT and associated AdS space, and

$$A_{\rm IR}(u) = \ln\left(-\frac{\ell_{\rm IR}}{\alpha}\sinh\frac{u+c_{\rm IR}}{\ell_{\rm IR}}\right), \quad \text{with} \quad \ell_{\rm IR}^2 = -\frac{6}{V(\varphi_{\rm IR})}\,. \tag{3.3.4}$$

for the IR CFT and its associated AdS space.

The UV and IR values of the F-quantity are then given by the renormalized action evaluated on these solutions. From (3.2.43) it follows that this is given by:[8]

$$F_{\rm UV} = 8\pi^2(M\ell_{\rm UV})^2\,, \qquad F_{\rm IR} = 8\pi^2(M\ell_{\rm IR})^2\,. \tag{3.3.5}$$

As $\ell_{\rm UV} > \ell_{\rm IR}$ these indeed satisfy $F_{\rm UV} \geq F_{\rm IR}$.

3. It is the dimensionless curvature $\mathcal{R}$ which will play the role of the parameter along the flow, which we will also refer to as curvature-RG flow to distinguish it from the holographic RG flow in u. The candidate F-functions will be specific functionals for a given holographic flow solution $A(u), \varphi(u)$. To be precise, we will consider F-functions constructed out of the (renormalized) free energy introduced in section 3.2. As pointed out there, given a flow solution $A(u), \varphi(u)$ with UV data R, φ_- these functionals only depend on the UV sources via the dimensionless combination $\mathcal{R}$. As a result, the candidate F-functions we will consider will only depend on UV sources via $\mathcal{R}$, i.e.

$$\mathcal{F}(\mathcal{R}) \equiv \mathcal{F}\left[A_{R,\varphi_-}(u),\, \varphi_{R,\varphi_-}(u)\right]\,. \tag{3.3.6}$$

[8]Note that for a CFT the value of the on-shell action is uniquely defined, i.e. there is no scheme-dependence. Different schemes (in $d = 3$) correspond to theories with different coefficients for the finite counterterms $\sim \int d^3x\,\sqrt{\zeta}\,|\varphi_-|^{3/\Delta_-}$ and $\sim \int d^3x\,\sqrt{\zeta}\,R\,|\varphi_-|^{1/\Delta_-}$. However, for a CFT $\varphi_- = 0$ and no such finite counterterms exist.

4. In terms of curvature-RG flow in $\mathcal{R}$, the notion of UV and IR are defined as follows. By UV we refer to the limit $\mathcal{R} \to \infty$. The corresponding UV value for the F-function is the functional $\mathcal{F}$ evaluated on a holographic RG flow solution $A(u)$, $\varphi(u)$ with end point $\varphi_0 \to \varphi_{\rm UV}$. Moving away from the UV corresponds to letting $\mathcal{R}$ decrease, which is equivalent to evaluating $\mathcal{F}$ over solutions $A(u), \varphi(u)$ with end points that successively move away from $\varphi_{\rm UV}$. The IR is defined as $\mathcal{R} \to 0$. The related solutions $A(u), \varphi(u)$ exhibit $\varphi_0 \to \varphi_{\rm IR}$, i.e. the end point approaches a minimum of the potential, and the corresponding value $\mathcal{F}(\mathcal{R})$ is the functional evaluated on this solution.[9]

The upshot is: To calculate $\mathcal{F}(\mathcal{R})$ along the RG flow defined by $\mathcal{R}$ we have to evaluate the functional $\mathcal{F}$ over a family of holographic RG flow solutions whose IR end points φ_0 move successively from $\varphi_{\rm UV}$ to $\varphi_{\rm IR}$.

3.3.2 Candidate F-functions

In this section, we will propose several suitable candidate F-functions. The building blocks will be both the renormalized and unrenormalized free energy, with the relevant expressions collected in (3.2.39)–(3.2.40). Our candidate F-functions will be constructed to satisfy two criteria:

1. Any candidate F-function has to be free of both UV and IR divergences.

2. In the UV ($\mathcal{R} \to \infty$) and the IR ($\mathcal{R} \to 0$) the F-functions should reproduce the free energy of the corresponding UV and IR CFTs, i.e.

$$\mathcal{F}(\mathcal{R}) \underset{\mathcal{R}\to\infty}{\longrightarrow} F_{\rm UV} = 8\pi^2 (M\ell_{\rm UV})^2 \,, \tag{3.3.7}$$

$$\mathcal{F}(\mathcal{R}) \underset{\mathcal{R}\to 0}{\longrightarrow} F_{\rm IR} = 8\pi^2 (M\ell_{\rm IR})^2 \,. \tag{3.3.8}$$

We begin by examining the various divergent pieces present in the free energy. The unrenormalized free energy given in (3.2.39) exhibits UV-divergent terms, which in terms of the dimensionless cutoff Λ_ϵ defined in (3.2.19) take the following schematic form:

$$\Lambda_\epsilon\text{-dependent terms in } F(\Lambda_\epsilon, \mathcal{R}_\epsilon): \quad \sim \mathcal{R}_\epsilon^{-1/2}(\Lambda_\epsilon + \ldots) \quad \text{and} \quad \sim \mathcal{R}_\epsilon^{-3/2}(\Lambda_\epsilon^3 + \ldots) \,.$$

[9] Note that this notion of UV and IR in terms of $\mathcal{R} \to \infty$ and $\mathcal{R} \to 0$ differs from the usual definition of UV fixed point and IR end point for a single holographic flow solution. For a single holographic RG flow the terms UV and IR refer to the limits ($u \to -\infty$, $\varphi \to \varphi_{\rm UV}$) and ($u \to u_0$, $\varphi \to \varphi_0$), respectively.

In addition, the unrenormalized free energy contains terms which do not depend on Λ_ϵ, but diverge when $\mathcal{R}_\epsilon \to 0$. These are IR divergences associated with a diverging volume of S^3. The relevant terms take the following schematic form (see app. H.2 for details):

$$\text{IR-divergent terms in } F(\Lambda_\epsilon, \mathcal{R}_\epsilon): \quad \sim \mathcal{R}_\epsilon^{-1/2}(B_0^\epsilon + C_1^\epsilon)\big|_{\mathcal{R}_\epsilon \to 0} \quad \text{and} \quad \sim \mathcal{R}_\epsilon^{-3/2} C_0^\epsilon\big|_{\mathcal{R}_\epsilon \to 0}\,,$$

with C_0^ϵ, B_0^ϵ and C_1^ϵ numerical constants.

Alternatively, we can work with the renormalized free energy F^{ren}. While this is free of UV-divergences, F^{ren} still exhibits IR divergent terms. In this case, these are schematically given by (see (3.2.47)):

$$\text{IR-divergent terms in } F^{\text{ren}}(\mathcal{R}|B_{ct}, C_{ct}): \quad \sim \mathcal{R}^{-1/2}(B_0 + C_1 - B_{ct})\big|_{\mathcal{R}\to 0} \quad \text{and} \quad \sim \mathcal{R}^{-3/2}(C_0 - C_{ct})\big|_{\mathcal{R}\to 0}\,.$$

As one can observe from the above equations, both UV-divergent as well as IR-divergent terms come with the same functional dependence on $\mathcal{R}$ or $\mathcal{R}_\epsilon$, collectively denoted by $\mathcal{R}_{(\epsilon)}$. That is, the problematic terms come with a factor $\mathcal{R}_{(\epsilon)}^{-3/2}$ or $\mathcal{R}_{(\epsilon)}^{-1/2}$. A similar observation, regarding the entanglement entropy, has also been made for theories in flat space-time in [74]. There it was shown that the divergent contribution to the entanglement entropy across a scalable surface (with, say, scale a) only come with several distinct powers of that scale a. The same holds in our case for the free energy, with the scale a given by the curvature R. The main difference is that here the field theory itself is defined on curved space-time with constant scalar curvature R.

The challenge for constructing a viable F-function now is to isolate the finite contributions to the free energy or the entanglement entropy, i.e. we need to ensure that both UV-cutoff-dependent terms as well as the explicitly IR-divergent terms do not enter into the F-function. There are at least two ways of doing this:

1. For one, we can remove any contribution with curvature dependence $\mathcal{R}_{(\epsilon)}^{-3/2}$ or $\mathcal{R}_{(\epsilon)}^{-1/2}$ by acting on F or F^{ren} (collectively written as $F^{(\text{ren})}$) with an appropriate differential operator, similarly to what was done

in [74]. In particular, we define[10]

$$\mathcal{D}_{3/2} \equiv \left(\frac{2}{3}\,\mathcal{R}_{(\epsilon)}\,\frac{\partial}{\partial \mathcal{R}_{(\epsilon)}} + 1\right), \quad \text{and} \quad \mathcal{D}_{1/2} \equiv \left(2\,\mathcal{R}_{(\epsilon)}\,\frac{\partial}{\partial \mathcal{R}_{(\epsilon)}} + 1\right). \tag{3.3.9}$$

These satisfy

$$\mathcal{D}_{3/2}\mathcal{R}_{(\epsilon)}^{-3/2} = 0\,, \qquad \mathcal{D}_{1/2}\mathcal{R}_{(\epsilon)}^{-1/2} = 0\,, \tag{3.3.10}$$

and hence remove the divergent contributions while leaving terms with any other power of $\mathcal{R}_{(\epsilon)}$ intact.

2. By working with the renormalized quantity F^{ren} we can guarantee the absence of UV-divergences. The observation then is that we can remove the remaining IR-divergent pieces by choosing a suitable renormalization scheme. This amounts to an appropriate specific choice of renormalization parameters which we will call $B_{ct,0}$ and $C_{ct,0}$:

$$B_{ct,0} \equiv B(0) + \left.\tfrac{\partial C(\mathcal{R})}{\partial \mathcal{R}}\right|_{\mathcal{R}=0} = B_0 + C_1\,, \qquad C_{ct,0} \equiv C(0) = C_0\,. \tag{3.3.11}$$

In order to make clear that these renormalization conditions are well-defined in terms of the dual field theory language, we show in appendix J.2 that this choice of renormalization conditions is equivalent to requiring that certain correlation functions involving the renormalized stress-tensor $T^{\text{ren}}_{\mu\nu}$ of the boundary theory vanish for $R \to 0$.

We are now in a position to propose candidate F-functions. To be specific, we begin with F-functions constructed out of the renormalized free energy F^{ren}. This has two IR-divergent terms, one at order $\mathcal{R}^{-3/2}$ and one at order $\mathcal{R}^{-1/2}$. As stated above, each of these terms can be removed in two ways, either by differentiation or with the help of counterterms. This gives four possibilities for removing divergent pieces and we hence define the four

[10] That is, for a function of $\mathcal{R}$ these are defined in terms of derivatives with respect to $\mathcal{R}$, while for a function of $\mathcal{R}_\epsilon$ these act as derivatives with respect to $\mathcal{R}_\epsilon$. In the cut-off theory, taking the derivative with respect to $\mathcal{R}_\epsilon$ is the same as taking a derivative with respect to R with φ^ϵ_- and the cutoff fixed. This is the correct thing to do if we want to compare theories with different curvatures while fixing all other boundary data. In contrast, in the renormalized theory the derivative with respect to $\mathcal{R}$ is what is needed to vary the curvature at fixed φ_-.

divergence-free quantities $\mathcal{F}_{1,2,3,4}(\mathcal{R})$ constructed from $F^{\rm ren}$:

$$\mathcal{F}_1(\mathcal{R}) \equiv \mathcal{D}_{1/2}\,\mathcal{D}_{3/2}\,F^{\rm ren}(\mathcal{R}|B_{ct},C_{ct})\,, \tag{3.3.12}$$
$$\mathcal{F}_2(\mathcal{R}) \equiv \mathcal{D}_{1/2}\qquad F^{\rm ren}(\mathcal{R}|B_{ct},C_{ct,0})\,, \tag{3.3.13}$$
$$\mathcal{F}_3(\mathcal{R}) \equiv \qquad \mathcal{D}_{3/2}\,F^{\rm ren}(\mathcal{R}|B_{ct,0},C_{ct})\,, \tag{3.3.14}$$
$$\mathcal{F}_4(\mathcal{R}) \equiv \qquad\qquad F^{\rm ren}(\mathcal{R}|B_{ct,0},C_{ct,0})\,. \tag{3.3.15}$$

with $\mathcal{D}_{1/2}$, $\mathcal{D}_{3/2}$ defined in (3.3.9) and $B_{ct,0}$, $C_{ct,0}$ given in (3.3.11). As we will check explicitly at the end of this section, for $\mathcal{R}\to\infty$ and $\mathcal{R}\to 0$ the functions $\mathcal{F}_{1,2,3,4}$ reduce to $F_{\rm UV}$ and $F_{\rm IR}$, respectively. As a result, they pass the minimum test and are four good candidate F-functions.

An important observation is that the functions $\mathcal{F}_{1,2,3,4}$ can be written entirely in terms of $\mathcal{R}$, $B(\mathcal{R})$ and $C(\mathcal{R})$ (as well as the counter-terms). In particular, inserting (3.2.40) into (3.3.12)–(3.3.12) one obtains

$$\mathcal{F}_1(\mathcal{R}) = -(M\ell)^2\,\tilde{\Omega}_3\;\frac{4}{3}\mathcal{R}^{1/2}\Big(2B'+C''+\mathcal{R}B''\Big)\,, \tag{3.3.16}$$
$$\mathcal{F}_2(\mathcal{R}) = -(M\ell)^2\,\tilde{\Omega}_3\;2\mathcal{R}^{-3/2}\Big(-(C-C_{ct,0})+\mathcal{R}C'+\mathcal{R}^2B'\Big)\,, \tag{3.3.17}$$
$$\mathcal{F}_3(\mathcal{R}) = -(M\ell)^2\,\tilde{\Omega}_3\;\frac{2}{3}\mathcal{R}^{-1/2}\Big((B+C'-B_{ct,0})+\mathcal{R}B'\Big)\,, \tag{3.3.18}$$
$$\mathcal{F}_4(\mathcal{R}) = -(M\ell)^2\,\tilde{\Omega}_3\;\mathcal{R}^{-3/2}\Big((C-C_{ct,0})+\mathcal{R}(B-B_{ct,0})\Big)\,, \tag{3.3.19}$$

where $\tilde{\Omega}_3$ is defined in (3.2.6). Here we suppressed the argument of $B(\mathcal{R})$ and $C(\mathcal{R})$ to reduce clutter and $'$ refers to a derivative with respect to $\mathcal{R}$.

Similarly, we can start with the unrenormalized free energy $F(\Lambda_\epsilon,\mathcal{R}_\epsilon)$. This again has divergent terms at order $\mathcal{R}_\epsilon^{-3/2}$ and $\mathcal{R}_\epsilon^{-1/2}$. Here, from the various options for cancelling these terms, we can only apply the method involving differentiation. However, one can check that this does not give rise to a new F-function. Applying the derivatives $\mathcal{D}_{3/2}$ and $\mathcal{D}_{1/2}$ to (3.2.23) and subsequently taking the cutoff to infinity one finds:

$$\begin{aligned}\lim_{\Lambda_\epsilon\to\infty}\mathcal{D}_{1/2}\,\mathcal{D}_{3/2}\,F(\Lambda_\epsilon,\mathcal{R}_\epsilon) &= \lim_{\Lambda_\epsilon\to\infty}\left[-(M\ell)^2\tilde{\Omega}_3\frac{4}{3}\mathcal{R}_\epsilon^{1/2}\Big(2B'(\mathcal{R}_\epsilon)+C''(\mathcal{R}_\epsilon)+\mathcal{R}_\epsilon B''(\mathcal{R}_\epsilon)\Big)\right]\\ &= -(M\ell)^2\,\tilde{\Omega}_3\;\frac{4}{3}\mathcal{R}^{1/2}\Big(2B'(\mathcal{R})+C''(\mathcal{R})+\mathcal{R}B''(\mathcal{R})\Big)\\ &= \mathcal{F}_1(\mathcal{R})\,.\end{aligned} \tag{3.3.20}$$

As a result, the functions $\mathcal{F}_{1,2,3,4}$ defined in (3.3.12)–(3.3.15) exhaust the possibilities for candidate F-functions that can be constructed directly from the free energy on S^3 by the procedures mentioned above.

One can show explicitly that all our candidate F-functions reduce to $F_{\rm UV}$ and $F_{\rm IR}$ in the UV ($\mathcal{R} \to \infty$) and IR ($\mathcal{R} \to 0$), respectively. For example, using the results in sec. 3.2.3 we find the following behaviour for $\mathcal{R} \to \infty$:

$$\mathcal{F}_1(\mathcal{R}) \underset{\mathcal{R}\to\infty}{=} F_{\rm UV} + \mathcal{O}(\mathcal{R}^{-\Delta_-})\,, \tag{3.3.21}$$

$$\mathcal{F}_2(\mathcal{R}) \underset{\mathcal{R}\to\infty}{=} F_{\rm UV} + \mathcal{O}(\mathcal{R}^{-\Delta_-}) + (M\ell_{\rm UV})^2\tilde{\Omega}_3\, C_{ct,0}\, \mathcal{R}^{-3/2}\,, \tag{3.3.22}$$

$$\mathcal{F}_3(\mathcal{R}) \underset{\mathcal{R}\to\infty}{=} F_{\rm UV} + \mathcal{O}(\mathcal{R}^{-\Delta_-}) + (M\ell_{\rm UV})^2\tilde{\Omega}_3\, B_{ct,0}\, \mathcal{R}^{-1/2}\,, \tag{3.3.23}$$

$$\mathcal{F}_4(\mathcal{R}) \underset{\mathcal{R}\to\infty}{=} F_{\rm UV} + \mathcal{O}(\mathcal{R}^{-\Delta_-}) + (M\ell_{\rm UV})^2\tilde{\Omega}_3\, B_{ct,0}\, \mathcal{R}^{-1/2} + (M\ell_{\rm UV})^2\tilde{\Omega}_3\, C_{ct,0}\, \mathcal{R}^{-3/2}\,, \tag{3.3.24}$$

We can also make another observation. From the above it follows that all our candidate F-functions are also stationary in the UV, i.e. they obey $\partial_{\mathcal{R}}\mathcal{F}_i|_{\mathcal{R}\to\infty} = 0$.

Similarly, using the results in sec. 3.2.3 the F-functions behave for $\mathcal{R} \to 0$ as

$$\mathcal{F}_i(\mathcal{R}) \underset{\mathcal{R}\to 0}{=} F_{\rm IR} + \mathcal{O}(\mathcal{R}^{-\Delta_-^{\rm IR}}) + \mathcal{O}(\mathcal{R}^{1/2})\,, \qquad i = 1\ldots 4\,. \tag{3.3.25}$$

Finally, we need to check whether our functions $\mathcal{F}_i(\mathcal{R})$ decrease monotonically with RG flow. Only if this is the case we can declare success and present them as good F-functions. In section (3.3.4) we will test our proposal numerically on some simple but generic examples and show that all the proposed F-functions are indeed monotonic. This lends support to our proposal, and further tests (and eventually a proof) will be left for future work.

3.3.3 An F-function from holographic RG flow in flat space-time

Before testing our proposal on examples, in this section we will review a different type of F-function which arises from holographic RG flow in *flat* space-time. This was originally constructed by Liu and Mezei [74] starting from the entanglement entropy across a spherical region in flat space.

The construction is as follows. We consider a ball of radius α in a flat space-time quantum field theory, and compute the entanglement entropy between the points inside the ball and those outside the ball, which we will denote by $S_{\rm FEE}(\alpha)$ This quantity is both UV divergent and, once UV-regulated, has a large-volume divergence as $\alpha \to \infty$, just like the free energy we have been studying in this section. Liu and Mezei proposed as an F-function the

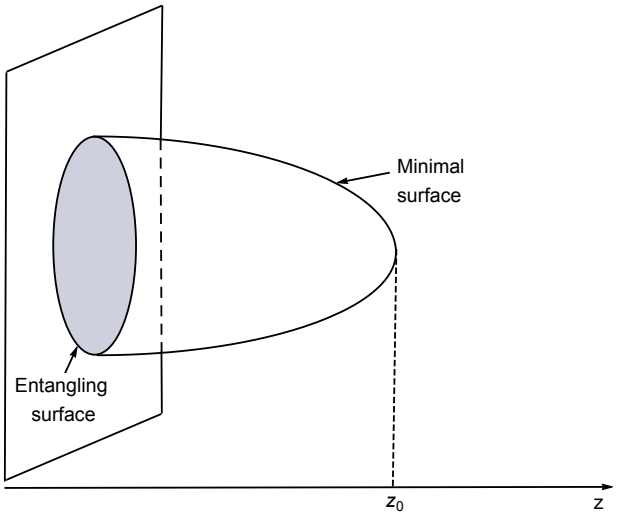

Figure 3.1: Cartoon of the minimal surface to compute the entanglement entropy in flat space. The coordinate z is the holographic direction in conformal coordinates.

"Renormalized entanglement entropy" (REE), which we will denote by $\mathcal{F}_0$, and which is defined as

$$\mathcal{F}_0(\alpha) = \left(\alpha \frac{d}{d\alpha} - 1\right) S_{\rm FEE}(\alpha) \ , \tag{3.3.26}$$

It was subsequently proven to be a good F-function in [75], i.e. it interpolates monotonically between the values of the CFT central charge at the end-points of the flat-space RG flow.

In a field theory with a holographic dual, the entanglement entropy across a region of space is computed via the Ryu-Takayanagi prescription [83]: one picks a $(d-2)$-dimensional surface on the AdS boundary which coincides with the entangling surface and extends it to a geodesic $(d-1)$-dimensional surface in the bulk. The entanglement entropy is then computed in terms of the minimal surface area $\mathcal{A}$ by

$$S_{\rm FEE}(\alpha) = \mathcal{A}/4G_{d+1} \ , \tag{3.3.27}$$

where G_{d+1} is Newton's constant in $(d+1)$ dimensions.

In the case we are discussing, for $d = 3$, the entangling surface is a circle of radius α, and the situation is described schematically in Figure 3.1. The details of the calculation are given in Appendix I. Notice that for this calculation we consider the vacuum, flat-space RG flow theory, whose metric

is (here it is convenient to use conformal coordinates),

$$ds^2 = \rho(z)\left(dz^2 + \eta_{\mu\nu}dx^\mu dx^\nu\right) . \tag{3.3.28}$$

where $\rho(z)$ is related to the scale factor introduced in (2.1.1) as $\rho(z) = e^{A(u(z))}$.

To calculate the minimal surface $\mathcal{A}$ we need to choose a solution $\rho(z)$ relevant to the problem at hand. Here this is $\rho(z) = e^{A_{\rm flat}(u(z))}$ where $A_{\rm flat}(u)$ is a holographic RG flow solution for a field theory in flat space-time. The minimal surface area is then calculated as

$$\mathcal{A} = 2\pi \int_\epsilon^{z_0} dz\; a^2(z) r(z) \sqrt{1 + (r'(z))^2}, \tag{3.3.29}$$

where $r(z)$ describes the embedding of the Ryu-Takayanagi minimal surface, and z_0 is the point where the latter smoothly caps-off. The geodesic equation and regularity conditions for $r(z)$ are described in appendix I. The entanglement entropy $S_{\rm FEE}$ then follows from (3.3.27).

As in the case of the on-shell action studied in sec. 3.2 we find that in holography the entanglement entropy $S_{\rm FEE}$ is a function of the dimensionless combination $\mathcal{R} = R|\varphi_-|^{-2/\Delta_-}$. Then the REE can be written as

$$\mathcal{F}_0(\mathcal{R}) = -\mathcal{D}_{1/2} S_{\rm FEE}(\mathcal{R}) . \tag{3.3.30}$$

where $\mathcal{D}_{1/2}$ is the differential operator defined in eq. (3.3.9).

As with the other F-functions, the REE of Liu and Mezei (3.3.30) can be computed numerically in specific examples. A numerical comparison between our candidate F-functions and $\mathcal{F}_0$ will be performed in the next section.

3.3.4 Numerical tests of monotonicity

To test our proposal, in this section we will evaluate the candidate F-functions $\mathcal{F}_i(\mathcal{R})$ with $i = 1, 2, \ldots 4$ for a set of example RG flows. In our holographic setting this amounts to choosing a dilaton potential. Here we will work with the potential:

$$V(\varphi) = -\frac{6}{\ell_{\rm UV}^2} - \frac{\Delta_-(3-\Delta_-)}{2\ell_{\rm UV}^2}\,\varphi^2 + \frac{\lambda}{\ell_{\rm UV}^2}\,\varphi^4 . \tag{3.3.31}$$

This potential has a maximum at $\varphi_{\rm UV} = 0$ and a minimum at $\varphi_{\rm IR} = \sqrt{\frac{\Delta_-(3-\Delta_-)}{4\lambda}}$. We can also define a quantity $\ell_{\rm IR}$ as in (3.2.46) which by definition satisfies $\ell_{\rm IR} < \ell_{\rm UV}$. For definiteness, in the following we will set

$$\ell_{\rm IR}^2 = b\,\ell_{\rm UV}^2 \quad \text{with} \quad b = 0.9 , \tag{3.3.32}$$

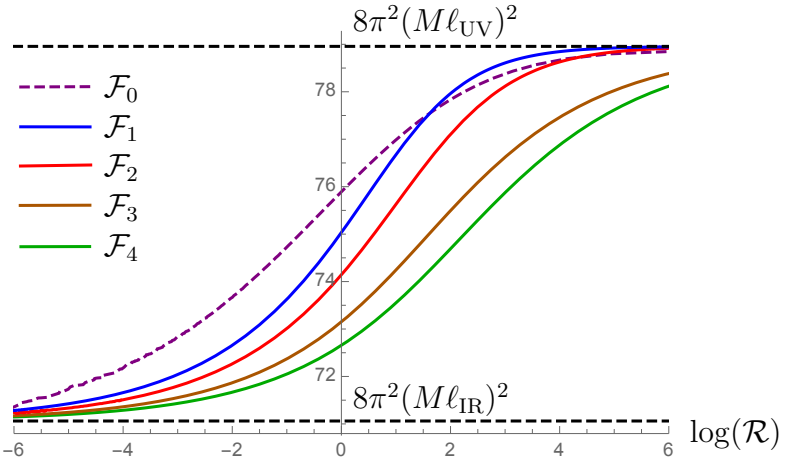

Figure 3.2: F-functions $\mathcal{F}_{1,2,3,4}$ defined in (3.3.12)–(3.3.15) and Liu-Mezei F-function $\mathcal{F}_0$ (i.e. the REE of [74]) vs. $\log(\mathcal{R})$ for a holographic model with dilaton potential (3.3.31) and $\Delta_- = 1.2$.

which we can do by choosing

$$\lambda = \frac{\Delta_-^2(3-\Delta_-)^2\, b}{96(1-b)}\,. \tag{3.3.33}$$

Then, in the following, we will also set $M\ell_{\rm UV} = 1$. With this potential we can vary the dimensions of perturbing operators and therefore we can check various different flows.

To construct solutions, and compute the corresponding on-shell action, in the whole range of $\mathcal{R}$ we proceed as follows. We pick a value φ_0 with $\varphi_{\rm max} < \varphi_0 < \varphi_{\rm min}$ and solve equations (2.2.7), (2.2.8) and (3.2.9) subject to the boundary conditions (2.5.11) and (3.2.11) to obtain a solution for the functions $W(\varphi)$, $S(\varphi)$ and $U(\varphi)$. From the near-boundary (i.e. $\varphi \to \varphi_{\rm UV} = 0$) behaviour of $W(\varphi)$, $S(\varphi)$ and $U(\varphi)$ we can then extract the corresponding values of $\mathcal{R}_0$, $C(\mathcal{R}_0)$ and $B(\mathcal{R}_0)$, respectively.[11] By varying the end point φ_0 from $\varphi_{\rm UV}$ to $\varphi_{\rm IR}$ and repeating the analysis we can hence extract $C(\mathcal{R})$ and $B(\mathcal{R})$ as functions of $\mathcal{R}$. This is summarised schematically below:

$$\begin{array}{l}\text{Choose a value for } \varphi_0 \longrightarrow W(\varphi),\ S(\varphi),\ U(\varphi) \longrightarrow \text{ choose new value for } \varphi_0 \longrightarrow \ldots \\ \qquad\qquad\qquad\qquad\quad \downarrow \quad\ \downarrow \quad\ \downarrow \\ \qquad\qquad\qquad\qquad\quad \mathcal{R}_0 \quad C(\mathcal{R}_0) \quad B(\mathcal{R}_0)\end{array}$$

Once we have $C(\mathcal{R})$ and $B(\mathcal{R})$ as functions of $\mathcal{R}$ we can determine the

[11] See (2.4.2), (2.4.3) and (3.2.10) for the near-boundary expansions of $W(\varphi)$, $S(\varphi)$ and $U(\varphi)$, respectively.

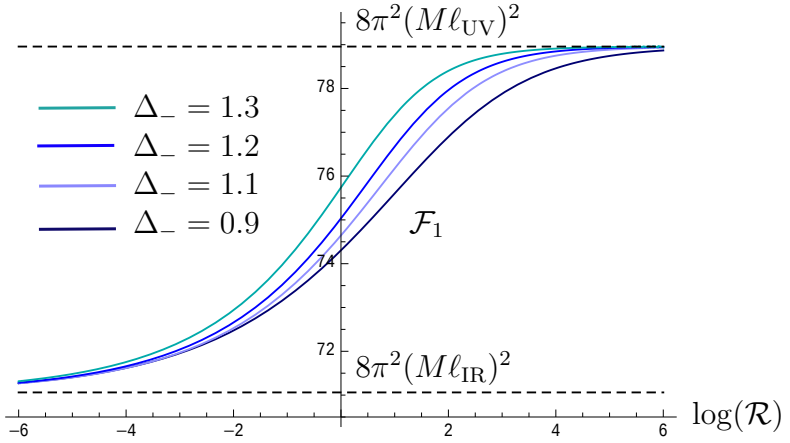

Figure 3.3: $\mathcal{F}_1$ vs. $\log(\mathcal{R})$ for a holographic model with dilaton potential (3.3.31) and $\Delta_- = 0.9$ (dark blue), 1.1, (light blue), 1.2 (blue) and 1.3 (cyan).

counterterms $B_{ct,0}$ and $C_{ct,0}$ from (3.3.11). Finally, using (3.3.16)–(3.3.19) we can compute the functions $\mathcal{F}_i(\mathcal{R})$.

In figure 3.2 we plot $\mathcal{F}_{1,2,3,4}$ vs. $\log(\mathcal{R})$ for the potential (3.3.31) with $\Delta_- = 1.2$. For comparison, we also display the Liu-Mezei F-function [74] labelled by $\mathcal{F}_0(\mathcal{R})$ and given in (3.3.30) for a flat-space RG flow in the same potential (3.3.31) with $\Delta_- = 1.2$.[12] We make the following observations.

- In the UV ($\mathcal{R} \to \infty$) all four candidate F-functions asymptote to $F_{\rm UV} = 8\pi^2(M\ell_{\rm UV})^2$ as expected. Similarly, in the IR ($\mathcal{R} \to 0$) all four candidate F-functions approach $F_{\rm IR} = 8\pi^2(M\ell_{\rm IR})^2$.

- Most importantly, all four candidate F-functions interpolate monotonically between $F_{\rm UV}$ and $F_{\rm IR}$, that is we observe

$$\frac{\partial \mathcal{F}_i(\mathcal{R})}{\partial \mathcal{R}} \geq 0\,, \quad i = 1,2,3,4\,. \tag{3.3.34}$$

  Hence every one of $\mathcal{F}_{1,2,3,4}$ is a good F-function.

- We can also understand the qualitative differences between the plots for $\mathcal{F}_{1,2,3,4}$. By equations (3.3.21)–(3.3.24), for $\Delta_- = 1.2$ the functions $\mathcal{F}_{1,2}$ behave as $\mathcal{F}_{1,2} = F_{\rm UV} + \mathcal{O}(\mathcal{R}^{-1.2})$ for large $\mathcal{R}$, while $\mathcal{F}_{3,4}$ behave as $\mathcal{F}_{3,4} = F_{\rm UV} + \mathcal{O}(\mathcal{R}^{-0.5})$. As a result, we expect $\mathcal{F}_{3,4}$ to fall off faster than $\mathcal{F}_{1,2}$ when decreasing $\mathcal{R}$. This is exactly what we observe in fig. 3.2.

[12] In the case of $\mathcal{F}_0(\mathcal{R})$, the quantity $\mathcal{R}$ refers to the curvature of the spherical entangling surface in units of φ_- and *not* the curvature of the background space-time, which is flat in this case.

- The REE of Liu and Mezei $\mathcal{F}_0(\mathcal{R})$ is also a good F-function, interpolating monotonically between $F_{\rm UV}$ and $F_{\rm IR}$. Note, however, that it does not coincide with any of our F-functions $\mathcal{F}_{1,2,3,4}(\mathcal{R})$, which are manifestly different as functions of $\mathcal{R}$. In other words, the formulation of the F-function in $d = 3$ in terms of a flat-space entanglement entropy across a ball with radius α and in terms of the free energy on S^3 with radius α differ as functions of α.

These observations persist beyond the example with $\Delta_- = 1.2$. In figure 3.3 we plot $\mathcal{F}_1$ vs. $\log(\mathcal{R})$ for a holographic model with dilaton potential (3.3.31) and $\Delta_- = 0.9$, 1.1, 1.2 1.3. In all cases $\mathcal{F}_1(\mathcal{R})$ is a good F-function, interpolating monotonically between $F_{\rm UV}$ and $F_{\rm IR}$. The same is true for $\mathcal{F}_{2,3,4}$, but we refrain from plotting the results explicitly.

3.3.5 Alternative quantisation and the effective potential as an F-function

So far we have worked with holographic theories in what we referred to as 'standard quantisation'. That is, we identified the dimension Δ of the operator $\mathcal{O}$ perturbing the UV CFT with Δ_+. By doing so we restricted our analysis to (in $d = 3$)

$$\frac{3}{2} < \Delta < 3\,. \tag{3.3.35}$$

For such theories we found four potentially good F-functions $\mathcal{F}_{1,2,3,4}(\mathcal{R})$, which can be constructed from the free energy on S^3. The parameter along the RG flow is $\mathcal{R}$, which is the value of the curvature R of the background space-time of the field theory in units of the operator source φ_-.

The question then arises, how the F-theorem is realised for theories perturbed by an operator $\mathcal{O}$ with dimension $\Delta < 3/2$. In particular, how can one define good F-functions for such theories? We can answer this question by switching to 'alternative quantisation'. This amounts to identifying the dimension Δ of $\mathcal{O}$ with Δ_-. In general dimension d, this possibility exists in the range $d/2 - 1 < \Delta_- < d/2$. In this range, using the identification $\Delta = \Delta_-$ we can cover the region

$$\frac{1}{2} < \Delta < \frac{3}{2}\,. \tag{3.3.36}$$

The main point to note is that by swapping the scheme of quantisation none of the calculations and expressions we obtained so far are changed in any way. All that changes is the interpretation of the various expressions. As

we will argue presently, the functions $\mathcal{F}_{1,2,3,4}(\mathcal{R})$ defined in (3.3.12)–(3.3.15) will still be good F-functions for $\Delta < 3/2$. However, the interpretation in terms of field theory quantities will change when swapping the quantisation scheme.

For one, in alternative quantisation φ_- is identified with the vev of $\mathcal{O}$ and hence $\mathcal{R} = R\,|\varphi_-|^{-2/\Delta_-}$ is now the *boundary curvature in units of the operator vev*. It is this quantity which is now the parameter describing the RG flow.

Secondly, note that while in (3.3.12)–(3.3.15) the functions $\mathcal{F}_{1,2,3,4}(\mathcal{R})$ were constructed from what we referred to as the free energy $F^{(\mathrm{ren})}$, this language was tacitly assuming standard quantisation (as we have specified at the beginning of section 3.2). In fact, the functions $\mathcal{F}_{1,2,3,4}(\mathcal{R})$ can also be defined in the more general terms of the Euclidean on-shell action,

$$\mathcal{F}_1(R) \equiv \mathcal{D}_{1/2}\,\mathcal{D}_{3/2}\,S^{\mathrm{ren}}_{\text{on-shell},E}(\mathcal{R}|B_{ct},C_{ct})\,, \tag{3.3.37}$$

$$\mathcal{F}_2(R) \equiv \mathcal{D}_{1/2}\qquad S^{\mathrm{ren}}_{\text{on-shell},E}(\mathcal{R}|B_{ct},C_{ct,0})\,, \tag{3.3.38}$$

$$\mathcal{F}_3(R) \equiv \qquad \mathcal{D}_{3/2}\,S^{\mathrm{ren}}_{\text{on-shell},E}(\mathcal{R}|B_{ct,0},C_{ct})\,, \tag{3.3.39}$$

$$\mathcal{F}_4(R) \equiv \qquad\qquad S^{\mathrm{ren}}_{\text{on-shell},E}(\mathcal{R}|B_{ct,0},C_{ct,0})\,. \tag{3.3.40}$$

This does not require a distinction between standard and alternative quantisation.

In standard quantisation one has $S^{(\mathrm{ren})}_{\text{on-shell},E} = F^{(\mathrm{ren})}$ and (3.3.37)–(3.3.40) reduce to (3.3.12)–(3.3.15).

In alternative quantisation the on-shell action corresponds to the *quantum effective potential* Γ^{ren}, i.e. the Legendre transform of the free energy. To illustrate this, we momentarily separate $\mathcal{R}$ into R and φ_-. Then, in alternative quantisation, one has

$$S^{\mathrm{ren}}_{\text{on-shell},E}(R,\varphi_-) = \Gamma^{\mathrm{ren}}(R,\varphi_-)\,, \tag{3.3.41}$$

with Γ^{ren} a function of R and the vev φ_-. The free energy is denoted by $F^{\mathrm{ren}}(R,j)$, where j is the source. This is then related to $\Gamma^{\mathrm{ren}}(R,\varphi_-)$ as

$$\Gamma^{\mathrm{ren}}(R,\varphi_-) = F^{\mathrm{ren}}\big(R,j(\varphi_-)\big) - \int d^3x\sqrt{\gamma^{(0)}}\,j(\varphi_-)\,\varphi_-\,, \tag{3.3.42}$$

where $j(\varphi_-)$ is defined by

$$\left.\frac{\delta F(R,j)}{\delta j}\right|_{j(\varphi_-)} - \varphi_- = 0\,. \tag{3.3.43}$$

The key observation is that the functions defined in (3.3.37)–(3.3.40) are good F-functions (in the examples we considered in the previous section),

regardless what quantisation is chosen. In standard quantisation they correspond to F-functions for theories where the perturbing operator has dimension $\frac{3}{2} < \Delta < 3$. Using alternative quantisation, the same expressions now give F-functions for theories where the perturbing operator has dimension $\frac{1}{2} < \Delta < \frac{3}{2}$.

This for example implies that the F-functions $(\mathcal{F}_1, \mathcal{F}_2, \mathcal{F}_3, \mathcal{F}_4)$ for $\Delta_- = 1.2$ plotted in fig 3.2 have two interpretations. Using standard quantisation, they can be understood as F-functions for a theory with $\Delta = 3 - \Delta_- = 1.8$ with the parameter $\mathcal{R}$ the curvature in units of the source. Using alternative quantisation they become F-functions for a theory with $\Delta = \Delta_- = 1.2$ with $\mathcal{R}$ the curvature in units of the vev.

There is another interesting consequence of the observations in this section. Our results imply that, depending on the operator dimension Δ, we have to construct F-functions differently in terms of field-theoretic quantities. In particular, our findings suggest that for $\Delta > 3/2$ it is the free energy F that acts as a F-functions while for $\Delta < 3/2$ it is the quantum effective potential Γ that should be used. In section 3.5.2 we will find that this indeed solves long-standing puzzles regarding the F-theorem for the free massive boson.

3.4 De Sitter entanglement entropy and the F-theorem

In this section we make the connection between the quantities introduced so far (namely the various versions of the UV-finite free energy) and the entanglement entropy across a spherical surface in de Sitter space. The latter quantity has been discussed earlier in field theoretical context [80] as well as in holography [67, 84]. Here, both the free energy and the entanglement entropy are determined as functionals of corresponding holographic RG flows for theories in curved space-time. In this setting we will observe that the de Sitter entanglement entropy corresponds to one of the contributions to the free energy. In the de Sitter static patch, this relation translates into the relation between free energy and the *thermodynamic* entropy, computed by the area law. This is very interesting as it suggests that standard QFT on a fixed de Sitter background, and non-dynamical gravity satisfy thermodynamics equations that relate the on-shell action to the entanglement entropy.

As it was observed in [80], starting from the (unrenormalized) entanglement entropy and performing a similar subtraction as the one proposed by Liu and Mezei in flat space, one can in principle obtain new candidate F-

functions. We will show that the resulting F-functions are already part of the set we defined in section 3.3.2.

3.4.1 Entanglement entropy for a spherical surface in de Sitter space

Here we derive an expression for the entanglement entropy across a spherically symmetric surface for a theory in dS_d. While we will be once more mainly interested in expressions for $d = 3$, we will work in general d when possible. In a holographic setup, this amounts to computing the holographic entanglement entropy across a $(d-2)$-dimensional spherical surface on the dS_d boundary of our $(d+1)$-dimensional space-time.

To this end, consider our metric ansatz (2.1.1) for a field theory on dS_d with the following choice of (global) coordinates on dS_d:

$$ds^2 = du^2 + e^{2A(u)}\left[-dt^2 + \alpha^2 \cosh^2(t/\alpha)\left(d\theta^2 + \sin^2\theta d\Omega_{d-2}^2\right)\right] \tag{3.4.1}$$

where $d\Omega_{d-2}^2$ is the metric on a $(d-2)$-dimensional unit sphere. In global coordinates the de Sitter metric describes a S^{d-1} that starts infinite in the infinite past, decreases size until a minimum size of the order of the de Sitter curvature, and then increases again and becomes of infinite size in the infinite future.

We now wish to calculate the static entanglement entropy for an entangling surface on the boundary QFT given by $\theta|_{u\to-\infty} = \frac{\pi}{2}$ and $t = 0$. This splits the spatial S^{d-1} into the two hemispheres that touch at the entangling surface that is the equator (which is a S^{d-2}).

To calculate this in our holographic setting, we use the prescription of Ryu and Takayanagi [83]. We hence need to find the minimal surface in the bulk which has the entangling surface as the boundary. The entanglement entropy is then given by

$$S_{\mathrm{EE}} = \frac{\gamma}{4G_{d+1}} \tag{3.4.2}$$

where γ is the area of the minimal surface whose boundary is the entangling surface at $u \to -\infty$, and G_{d+1} is Newton's constant in $(d+1)$ dimensions.

In the Euclidean signature of the calculation, the $t = 0$ slice is the S^{d-1} corresponding to the equator of the S^d slice. The entangling surface is then an S^{d-2} at fixed $\theta = \pi/2$, dividing the S^{d-1} in two halves. One can show (see app. G) that the minimal Ryu-Takayanagi surface is described by the curve $\theta(u) = \pi/2$. The geometric setup is shown in figure 3.4 (for $d = 3$ and fixed t).

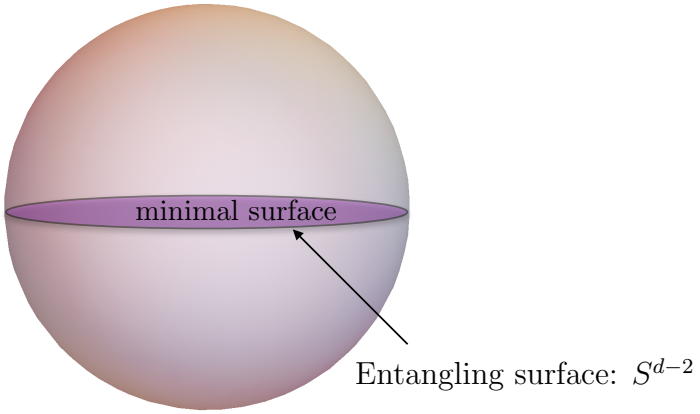

Figure 3.4: Sketch of the minimal surface which has the spherical surface $\theta = \pi/2$ as its boundary.

The detailed calculation is presented in appendix G and here we just quote the result, which can also be found in [84]:

$$S_{\rm EE} = M^{d-1}\frac{2R}{d}V_d\int_{\rm UV}^{\rm IR} du\, e^{(d-2)A(u)}\,, \tag{3.4.3}$$

where V_d is the volume of the d-dimensional sphere of radius α.

We can now make the following observation. The expression (3.4.3) for the entanglement entropy is identical to the 2nd term of the free energy (3.2.3). As a result, we find that here the entanglement entropy $S_{\rm EE}$ is related to the free energy F on S^d as

$$S_{\rm EE} = 2(d-1)M_p^{d-1}V_d\left[e^{dA}\dot{A}\right]_{\rm UV} - F\,. \tag{3.4.4}$$

We will exploit this connection frequently in the following. We can also show that, just as F, the entanglement entropy $S_{\rm EE}$ only depends on the UV curvature R only through the dimensionless combination $\mathcal{R}$.

3.4.2 Thermal interpretation

Equation (3.4.4) is suggestive that there should be a thermal interpretation to the entanglement entropy, and that the first term on the right hand side

should have the interpretation of an internal energy, to reproduce a relation of the form[13]

$$S = \beta U_{\rm th} - \beta F_{\rm th} \tag{3.4.5}$$

for some appropriate definition of the inverse temperature β and internal energy $U_{\rm th}$.

In fact, as shown in [67], the thermal interpretation becomes manifest if we go to the static patch of the de Sitter slice, by a coordinate transformation which does not involve the radial coordinate. Writing the d-dimensional de Sitter slices in static coordinates, the bulk metric reads

$$ds^2 = du^2 + e^{2A(u)}\left[-\left(1-\frac{r^2}{\alpha^2}\right)d\tau^2 + \left(1-\frac{r^2}{\alpha^2}\right)^{-1}dr^2 + r^2 d\Omega_{d-2}^2\right] . \tag{3.4.6}$$

where α is the de Sitter radius and $0 < r < \alpha$. The details and the explicit coordinate transformation is given in Appendix J.1.

The metric (3.4.6) has a horizon at $r = \alpha$, whose associated temperature is

$$T = \frac{1}{2\pi\alpha} \tag{3.4.7}$$

and whose entropy, computed via the horizon area, coincides with the expression for $S_{\rm EE}$ in equation (3.4.3),

$$S_{\rm th} \equiv \frac{\text{Area}}{4G_{d+1}} = S_{\rm EE}\,, \tag{3.4.8}$$

as shown in appendix J.1.

The final ingredient is the identification of $U_{\rm th}$ in equation (3.4.5): for static metrics, this corresponds to the ADM mass of the solution. A simple computation (see again appendix J.1) shows that

$$\beta U_{\rm th} = 2(d-1)M_P^{d-1}\left[e^{dA(u)}\dot{A}(u)\right]_{\rm UV} V_d. \tag{3.4.9}$$

Using the identification (3.4.8)–(3.4.9), equation (3.4.4) takes the first-law form (3.4.5). From this relation, as shown in appendix J.2, one can derive an identity relating the scalar-vev and curvature-vev parameters $C(\mathcal{R})$ and $B(\mathcal{R})$. For $d = 3$ this is given by

$$C'(\mathcal{R}) = \frac{1}{2}B(\mathcal{R}) - \mathcal{R}B'(\mathcal{R})\,, \tag{3.4.10}$$

[13]Recall that our "free energy" is related to the usual thermodynamic free energy by a factor β, i.e. $F = \beta F_{\rm th}$. See footnote 12.

with $'$ denoting a derivative with respect to $\mathcal{R}$. In the limit $\mathcal{R} \to 0$ of this equation one obtains a relation between the leading term in B and the first curvature correction to C in the small $\mathcal{R}$ limit, as defined in equations (3.2.44)–(3.2.45):

$$C_1 = \frac{1}{2} B_0 \tag{3.4.11}$$

3.4.3 Renormalized entanglement entropies and associated F-functions

The entanglement entropy given in (3.4.3) is UV-divergent and we hence regulate it. Subsequently, we also define a renormalized entanglement entropy by adding appropriate counterterms.

The procedure parallels the one used in the case of the free energy, using the dimensionless cutoff Λ_ϵ defined in equation (3.2.19). The entanglement entropy can then be written as a function of Λ_ϵ and $\mathcal{R}_\epsilon$. To be specific, we now again restrict to $d = 3$ to find:

$$S_{\rm EE}^{d=3}(\Lambda_\epsilon, \mathcal{R}_\epsilon) = (M\ell)^2 \tilde{\Omega}_3 \left\{ \mathcal{R}_\epsilon^{-1/2} \left[\frac{2}{3} \Lambda_\epsilon \Big(1 + \mathcal{O}\big(\Lambda_\epsilon^{-2\Delta_-}\big) + B(\mathcal{R}_\epsilon) \Big) \right] + \mathcal{O}\Big(\mathcal{R}_\epsilon^{1/2} \Lambda_\epsilon^{-1} \Big) \right\}, \tag{3.4.12}$$

where $\tilde{\Omega}_3$ was defined in (3.2.6). The function $B(\mathcal{R})$ is the same that appeared before in expressions for the free energy. Note that here all divergent terms have the same curvature dependence, i.e. they are accompanied by a factor $\mathcal{R}_\epsilon^{-1/2}$.

We can now also define a renormalized entanglement entropy by adding appropriate counterterms to (3.4.12) and taking the limit $\Lambda_\epsilon \to +\infty$. Note that the quantity we define this way differs from and should not be confused with the 'Renormalized Entanglement Entropy' (REE) of Liu and Mezei defined in [74]. Here we will proceed as in the case of the free energy and add appropriate counterterms.

Counterterms for the entanglement entropy should be defined in terms of an integral over the entangling surface or a related surface (see e.g. [85]). In particular, on the boundary, our entangling 'surface' is given by S^{d-2} with radius α. However, using the relation (3.4.4), note that for our setup the entanglement entropy (3.4.3) can be written in terms of quantities which are proportional to the volume of S^d (with radius α) rather than the volume of the entangling surface S^{d-2}. As a result, we will be able to write down

counterterms as integrals over S^d. These expressions will however only hold for the setup discussed here, but this is all that we need.

Given the relation (3.4.4) between $S_{\rm EE}$ and the free energy, the analysis is similar to the one performed in section 3.2.2 for the free energy. We will hence be brief and give the main results. As a first step we rewrite the integral appearing in (3.4.3) in terms of the functions $T(\varphi)$ and $U(\varphi)$, where $U(\varphi)$ was introduced before in (3.2.9):

$$\begin{aligned} S_{\rm EE} &= M^{d-1}\frac{2R}{d}{\rm Vol}(S^d)\int_{\rm UV}^{\rm IR} du\, e^{(d-2)A(u)} \\ &= M^{d-1}\tilde{\Omega}_d\left[T^{-\frac{d}{2}+1}(\varphi)\,U(\varphi)\right]_{\rm UV}, \end{aligned} \tag{3.4.13}$$

and with $\tilde{\Omega}_d$ defined in (3.2.6). Then, as in the case of the free energy, we can cancel divergences with the help of an appropriately defined function $\tilde{U}_{ct}(\varphi)$. In $d=3$ this will remove all the divergences. Hence, in $d=3$ we can write the renormalized entanglement entropy as follows:

$$S_{\rm EE}^{d=3,{\rm ren}} = M_p^2\tilde{\Omega}_3\left[T^{-\frac{1}{2}}(\varphi)\big(U(\varphi)-\tilde{U}_{ct}(\varphi)\big)\right]_{\rm UV}, \tag{3.4.14}$$

where $\tilde{U}_{ct}(\varphi)$ has to satisfy

$$W_{ct}'\,\tilde{U}_{ct}' - \frac{d-2}{2(d-1)}\,W_{ct}\,\tilde{U}_{ct} = -\frac{2}{d}, \tag{3.4.15}$$

and W_{ct} a solution to (3.2.29). The function $\tilde{U}_{ct}(\varphi)$ will contain an integration constant which we will denote by $\tilde{B}_{ct}$. Fixing a value for $\tilde{B}_{ct}$ is equivalent to choosing a renormalization scheme.

Finally, inserting the near-boundary expansion for T, U and $\tilde{U}_{ct}$ this becomes[14]

$$S_{\rm EE}^{d=3,{\rm ren}}(\mathcal{R}|\tilde{B}_{ct}) = (M\ell)^2\tilde{\Omega}_3\,\mathcal{R}^{-1/2}\big(B(\mathcal{R})-\tilde{B}_{ct}\big), \tag{3.4.16}$$

where we also indicated that $S_{\rm EE}^{d=3,{\rm ren}}$ is a function of $\mathcal{R}$ that further depends on our choice for the parameter $\tilde{B}_{ct}$. In the following, we will work exclusively in $d=3$. Thus, the superscript $d=3$ on $S_{\rm EE}^{d=3,{\rm ren}}$ is henceforth obsolete and will be dropped to remove clutter.

As for the renormalized free energy, we can obtain large-curvature and small curvature asymptotics for the renormalized entanglement entropy (see

[14]Note that $\tilde{U}_{ct}$ satisfies the same equation as U_{ct}, (3.2.30), rescaled by a constant factor $2/d$. As a result, the near-boundary expansion of $\tilde{U}_{ct}$ will be given by the rescaled expression for U_{ct} in (3.2.32), but with B_{ct} replaced by $\tilde{B}_{ct}$.

appendix H for details):

$$S_{\rm EE}^{\rm ren} \underset{\mathcal{R}\to\infty}{=} -(M\ell)^2\left(8\pi^2 + \tilde{\Omega}_3\tilde{B}_{ct}\mathcal{R}^{-1/2} + \mathcal{O}(\mathcal{R}^{-\Delta_-})\right) \tag{3.4.17}$$

$$S_{\rm EE}^{\rm ren} \underset{\mathcal{R}\to 0}{=} -(M\ell)^2\tilde{\Omega}_3\big(B_0 - \tilde{B}_{ct}\big)\mathcal{R}^{-1/2} - 8\pi^2(M\ell_{\rm IR})^2\left(1 + \mathcal{O}(\mathcal{R}^{-\Delta_-^{\rm IR}})\right) + \mathcal{O}(\mathcal{R}^{1/2})\,, \tag{3.4.18}$$

The leading IR (i.e. small-$\mathcal{R}$) divergence in $S_{\rm EE}^{\rm ren}$ scales as $\mathcal{R}^{-1/2}$. The reason is that the entanglement entropy scales with the volume of the entangling surface, which is given by $\mathrm{Vol}(S^1) \sim \mathcal{R}^{-1/2}$ for fixed φ_-. Hence, the divergence of $S_{\rm EE}^{\rm ren}$ can also be understood as a volume-divergence, but this time of the entangling surface. Note that a similar IR divergence (i.e. $\sim \mathcal{R}^{-1/2}$) also occurs in the unrenormalized quantity $S_{\rm EE}(\Lambda_\epsilon, \mathcal{R}_\epsilon)$.

The finite term for $\mathcal{R} \to 0$ is the same for $F^{\rm ren}$ and $S_{\rm EE}^{\rm ren}$ up to an overall sign and is given by $\pm 8\pi^2(M\ell_{\rm IR})^2$. The same is true for the UV limit as $\mathcal{R} \to +\infty$. This suggests that one can also construct candidate F-functions starting from the entanglement entropy, once the IR divergence is eliminated. Similarly to the case of the free energy discussed in section (3.3.2) we can either use the derivative operator $\mathcal{D}_{1/2}$ defined in (3.3.9) (since only the $\mathcal{R}^{-1/2}$ appears) acting on equation (3.4.16), or choose an appropriate scheme such that the first term in the IR expansion (3.4.18) vanishes. This gives rise to the following two candidate F-functions:

$$\mathcal{F}_5(\mathcal{R}) \equiv -\mathcal{D}_{1/2}\; S_{EE}^{\rm ren}(\mathcal{R}|\tilde{B}_{ct}) = \lim_{\Lambda_\epsilon\to\infty}\Big[- \mathcal{D}_{1/2}\, S_{\rm EE}(\Lambda_\epsilon, \mathcal{R}_\epsilon)\Big]\,, \tag{3.4.19}$$

$$\mathcal{F}_6(\mathcal{R}) \equiv \qquad - S_{\rm EE}^{\rm ren}(\mathcal{R}|\tilde{B}_{ct,0})\,, \tag{3.4.20}$$

where

$$\tilde{B}_{ct,0} \equiv B(0) = B_0. \tag{3.4.21}$$

Note that $\mathcal{F}_5$ is the analogue of Liu and Mezei's 'Renormalized Entanglement Entropy' (REE) defined in [74], but for a theory defined on dS_3. It can either be defined in terms of the renormalized or the unrenormalized entanglement entropy. As one can check from (3.4.17) and (3.4.18), both $\mathcal{F}_5$ and $\mathcal{F}_6$ reduce to $F_{\rm UV}$ and $F_{\rm IR}$ in the UV and IR, respectively. From equation (3.4.16) it follows that we can write $\mathcal{F}_{5,6}$ in terms of $B(\mathcal{R})$ as follows:

$$\mathcal{F}_5(\mathcal{R}) = -(M\ell)^2\,\tilde{\Omega}_3\; 2\,\mathcal{R}^{1/2}\,B'(R)\,, \tag{3.4.22}$$

$$\mathcal{F}_6(\mathcal{R}) = -(M\ell)^2\,\tilde{\Omega}_3\;\mathcal{R}^{-1/2}\big(B(R) - \tilde{B}_{ct,0}\big)\,, \tag{3.4.23}$$

where again $'$ denotes an $\mathcal{R}$-derivative.

As it turns out, equations (3.4.22) and (3.4.23) do not give rise to new F-functions compared to those defined from the free energy. Rather, as we will show below

$$\mathcal{F}_5(\mathcal{R}) \equiv \mathcal{F}_1(\mathcal{R}), \quad \mathcal{F}_6(\mathcal{R}) \equiv \mathcal{F}_3(\mathcal{R}), \tag{3.4.24}$$

where $\mathcal{F}_1$ and $\mathcal{F}_3$ are defined in equations (3.3.12) and (3.3.14).

The relations (3.4.24) follow from the thermodynamic relation discussed in the previous subsection,

$$S_{\rm EE} = \beta U_{\rm th} - \beta F_{\rm th} \tag{3.4.25}$$

if $\beta U_{\rm th}$ is identified with the space-time integral of the boundary stress tensor. As we show in detail in appendix J.2, the relation (3.4.25) is equivalent to the following two identities

$$\mathcal{D}_{3/2}\, F(\Lambda_\epsilon, \mathcal{R}_\epsilon) = -S_{EE}(\Lambda_\epsilon, \mathcal{R}_\epsilon)\,, \tag{3.4.26}$$

$$\mathcal{D}_{3/2}\, F^{\rm ren}(\mathcal{R}|B_{ct}, C_{ct}) = -S^{\rm ren}_{EE}\big(\mathcal{R}\big|\tfrac{2}{3}\, B_{ct}\big)\,, \tag{3.4.27}$$

together with the relation

$$B_{ct,0} = \frac{3}{2}\tilde{B}_{ct,0}\,, \tag{3.4.28}$$

between the counterterm parameters $B_{ct,0}$ and $\tilde{B}_{ct,0}$.

These in turn imply the identities (3.4.24). For example, starting with (3.4.19) and using (3.4.26) and (3.3.20) one finds

$$\mathcal{F}_5(\mathcal{R}) \overset{(3.4.19)}{=} \lim_{\Lambda_\epsilon\to\infty}\Big[-\mathcal{D}_{1/2}\, S_{\rm EE}(\Lambda_\epsilon, \mathcal{R}_\epsilon)\Big] \overset{(3.4.26)}{=} \lim_{\Lambda_\epsilon\to\infty}\Big[\mathcal{D}_{1/2}\,\mathcal{D}_{3/2}\, F(\Lambda_\epsilon, \mathcal{R}_\epsilon)\Big] \overset{(3.3.20)}{=} \mathcal{F}_1(\mathcal{R})\,. \tag{3.4.29}$$

Similarly, starting with (3.4.20) and using (3.4.27), (3.4.28) and (3.3.14) one obtains

$$\begin{aligned}\mathcal{F}_6(\mathcal{R}) &\overset{(3.4.20)}{=} -S^{\rm ren}_{\rm EE}(\mathcal{R}|\tilde{B}_{ct,0}) \overset{(3.4.27)}{=} \mathcal{D}_{3/2}\, F^{\rm ren}(\mathcal{R}|\tfrac{3}{2}\tilde{B}_{ct,0}, C_{ct}) \\ &\overset{(3.4.28)}{=} \mathcal{D}_{3/2}\, F^{\rm ren}(\mathcal{R}|B_{ct,0}, C_{ct}) \overset{(3.3.14)}{=} \mathcal{F}_3(\mathcal{R})\,.\end{aligned} \tag{3.4.30}$$

3.5 Free field theories

Here we will check whether our four proposals for F-functions also work more generally beyond a holographic setting. Therefore, we turn to free field theories where many results can be obtained analytically. We find that all our F-functions are monotonic in $d = 3$ for a massive fermion (corresponding to $\Delta_{\rm UV} = 2$) and for a massive scalar ($\Delta_{\rm UV} = 1$). In the latter case the UV dimension of the deforming operator ϕ^2 is less than $d/2$ and therefore, according to our prescription, the F-functions must be constructed from the quantum effective potential, rather than from the free energy. This leads indeed to monotonic F-functions, contrary to what one has been observed using either the free energy on the sphere (see [66]) or the entanglement entropy on dS_3 (see [80]).

3.5.1 Free fermion on S^3

Here we consider the theory of a free massive fermion on S^3 with action given by

$$S_D = \int d^3 \sqrt{\zeta} \, \left[i\psi^\dagger \not{D} \psi - im\psi^\dagger \psi \right] , \tag{3.5.1}$$

where again $\zeta_{\mu\nu}$ is a metric on S^3 with curvature $R = 6/\alpha^2$. This is a conformal theory perturbed by the operator $\psi^\dagger\psi$ with source m. The dimension of the perturbing operator is therefore

$$\Delta[\psi^\dagger\psi] = 2 > \frac{3}{2} \, . \tag{3.5.2}$$

According to our observations from holography (see sec. 3.3.5), we expect that the free energy can be used for constructing good F-functions.

Following [66] the free energy can be written as

$$F_D = -\sum_{n=1}^{\infty} n(n+1) \, \log \left[\left(n + \frac{1}{2} \right)^2 + (\alpha m)^2 \right] , \tag{3.5.3}$$

which only depends on m and α through the dimensionless combination (αm). To make contact with the notation in the previous sections, here we identify

$$\mathcal{R} = (\alpha m)^{-2} \, , \tag{3.5.4}$$

which is (proportional to) the curvature in units of the source.[15]

For $m \to 0$ ($\mathcal{R} \to \infty$ for fixed α) the theory given by (3.5.1) becomes conformal. In this case the free energy (3.5.3) was evaluated explicitly in [66]. Using zeta-function renormalization one finds

$$F_{D,\mathrm{UV}} = \frac{\log 2}{4} + \frac{3\zeta(3)}{8\pi^2}\,, \tag{3.5.5}$$

which we will refer to as the 'UV' value.

On the other hand, for $m \to \infty$ ($\mathcal{R} \to 0$ for fixed α), the theory becomes non-dynamical and empty. We hence expect the corresponding value of the free energy to be

$$F_{D,\mathrm{IR}} = 0\,. \tag{3.5.6}$$

A good F-function should then interpolate monotonically between the values $F_{D,\mathrm{UV}}$ and $F_{D,\mathrm{IR}}$ when going from the UV ($\mathcal{R} \to \infty$) to the IR ($\mathcal{R} \to 0$).

To this end, we now evaluate the free energy for an arbitrary value of $\mathcal{R}$. We start from the following observation in [66]. There it was shown that, upon zeta-function renormalization, the free energy satisfies

$$\frac{\partial F_D^{\mathrm{ren}}}{\partial(\alpha m)^2} = \frac{4(\alpha m)^2+1}{\alpha m}\,\pi\,\tanh\left(\pi\alpha m\right). \tag{3.5.7}$$

With the help of this, we can then write the zeta-function renormalized free energy in terms of an integral as

$$F_D^{\mathrm{ren}}(\mathcal{R}) = F_{D,\mathrm{UV}} + \int_0^{1/\mathcal{R}} dx\,\frac{4x+1}{\sqrt{x}}\,\pi\,\tanh\left(\pi\sqrt{x}\right). \tag{3.5.8}$$

This expression will be sufficient for both the analytical and numerical evaluations in this section. By construction, $F_D^{\mathrm{ren}}(\mathcal{R})$ reduces to $F_{D,\mathrm{UV}}$ in the UV, i.e. for $\mathcal{R} \to \infty$. However, in the IR ($\mathcal{R} \to 0$) the expression (3.5.8) does not reproduce $F_{D,\mathrm{IR}}$, but rather diverges. In particular, one finds

$$F_D^{\mathrm{ren}}(\mathcal{R}) \underset{\mathcal{R}\to 0}{=} \frac{\pi}{3}\mathcal{R}^{-3/2} + \frac{\pi}{4}\mathcal{R}^{-1/2} + (\text{vanishing for } \mathcal{R} \to 0)\,. \tag{3.5.9}$$

These can again be understood as volume-divergences, with the leading divergent term proportional to the dimensionless volume $\mathcal{R}^{-3/2}$.

[15] The curvature in units of the source is given by $6(\alpha m)^{-2}$, which differs from the expression in (3.5.4) by a factor of 6. By defining $\mathcal{R}$ as in (3.5.4) we can avoid a proliferation of factors of $\sqrt{6}$ in the following expressions without affecting the monotonicity properties.

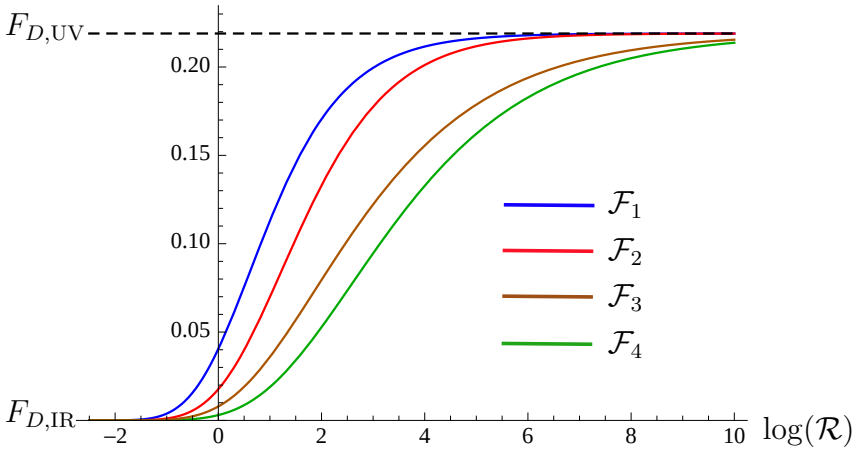

Figure 3.5: $\mathcal{F}_{1,2,3,4}$ given in (3.5.11)–(3.5.14) vs. $\log(\mathcal{R})$ for a theory of a free fermion on S^3. The black dashed line indicates the value of $F_{D,\mathrm{UV}}$ given in (3.5.5).

Here we used zeta function renormalization to arrive at a finite expression for F_D^{ren}. However, we could have equally renormalized the free energy by adding specific covariant counterterms to the action (3.5.1). In this case our expression for F_D^{ren} would be scheme-dependent, with different renormalization schemes parameterised by two real numbers c_{ct} and b_{ct}. These parameters are the coefficients of the two *finite* (i.e. UV-cutoff-independent) counterterms

$$F_{ct,1}^{\mathrm{finite}} = c_{ct} \int d^3x \sqrt{\zeta}\, m^3 = 2\pi^2\, c_{ct}\, \mathcal{R}^{-3/2}\,, \tag{3.5.10}$$
$$F_{ct,2}^{\mathrm{finite}} = b_{ct} \int d^3x \sqrt{\zeta}\, Rm = 12\pi^2\, b_{ct}\, \mathcal{R}^{-1/2}\,.$$

As we show in appendix K,[16] zeta-function renormalization is equivalent to renormalization via counterterms, with a particular choice of c_{ct} and b_{ct}. However, we can always change renormalization scheme by adding terms of the form (3.5.10) to F_D^{ren}. In the following, we will now exploit this to construct the equivalents of the F-functions discussed in the context of holography in section 3.3.

As explained in Section 3.3.2, we can remove the two divergent terms $\sim \mathcal{R}^{-3/2}$ and $\sim \mathcal{R}^{-1/2}$ either with the help of a differential operator, or by subtracting them with the help of counterterms.[17] In analogy with the

[16] In app. K, we work with the theory of a free massive scalar on S^3. However, our findings can be easily generalised for the case of the Dirac fermion.

[17] This is to add the counterterms (3.5.10) with $c_{ct} = -1/(6\pi)$ and $b_{ct} = -1/(48\pi)$.

functions $\mathcal{F}_{1,2,3,4}$ in (3.3.12)–(3.3.15), here we can define four F-functions as follows:[18]

$$\mathcal{F}_1(\mathcal{R}) = \mathcal{D}_{1/2}\,\mathcal{D}_{3/2}\;\; F_D^{\rm ren}(\mathcal{R})\,, \tag{3.5.11}$$

$$\mathcal{F}_2(\mathcal{R}) = \mathcal{D}_{1/2}\qquad \left(F_D^{\rm ren}(\mathcal{R}) - \frac{\pi}{3}\mathcal{R}^{-3/2}\right), \tag{3.5.12}$$

$$\mathcal{F}_3(\mathcal{R}) = \qquad \mathcal{D}_{3/2}\left(F_D^{\rm ren}(\mathcal{R}) - \frac{\pi}{4}\mathcal{R}^{-1/2}\right), \tag{3.5.13}$$

$$\mathcal{F}_4(\mathcal{R}) = \qquad\qquad \left(F_D^{\rm ren}(\mathcal{R}) - \frac{\pi}{3}\mathcal{R}^{-3/2} - \frac{\pi}{4}\mathcal{R}^{-1/2}\right), \tag{3.5.14}$$

with $\mathcal{D}_{1/2}$ and $\mathcal{D}_{3/2}$ given in (3.3.9). As one can check explicitly, the functions $\mathcal{F}_{1,2,3,4}$ reduce to the values $F_{D,\rm UV}$ and $F_{D,\rm IR}$ for $\mathcal{R}\to\infty$ and $\mathcal{R}\to 0$, respectively. In addition, by evaluating them numerically, one finds that all four functions $\mathcal{F}_{1,2,3,4}$ interpolate monotonically between the UV and IR values (see fig. 3.5). Therefore, all four functions $\mathcal{F}_{1,2,3,4}(\mathcal{R})$ in (3.5.11)–(3.5.14) are good F-functions for the free fermion. We find that our proposals for constructing F-functions also hold beyond the context of holographic theories.

3.5.2 Free boson on S^3

We now turn to the case of a free boson on S^3. The action is given by

$$S_S = \frac{1}{2}\int d^3x\,\sqrt{\zeta}\,\left[(\nabla\phi)^2 + \frac{R}{8}\,\phi^2 + m^2\phi^2\right], \tag{3.5.15}$$

where $R = 6/\alpha^2$ is again the scalar curvature of the S^3. This is a CFT perturbed by the operator ϕ^2 with source $\frac{1}{2}m^2$. The dimension of the perturbing operator is given by

$$\Delta[\phi^2] = 1 < \frac{3}{2}\,. \tag{3.5.16}$$

If our findings from holographic theories are correct, then a good F-function can be constructed from the quantum effective potential for the scalar (i.e. the Legendre transform of the free energy with respect to the source). We will check this explicitly by first examining the suitability of the free energy as a F-function before turning to its Legendre transform.

[18] The function $\mathcal{F}_4$ given in (3.5.14) has already been confirmed to be a good F-function for the free fermion in [66].

The free energy as a candidate F-function

As shown in [66], the free energy can be written as the following infinite sum:

$$F_S = \frac{1}{2}\sum_{n=1}^{\infty} n^2 \log\left[n^2 - \frac{1}{4} + (\alpha m)^2\right] , \tag{3.5.17}$$

which depends on α and m only through the dimensionless combination (αm). In the following, it will also be useful to define

$$\chi = (\alpha m)^{-2} , \tag{3.5.18}$$

which is proportional to the curvature in units of the source. We do not use the label $\mathcal{R}$ for consistency with our holographic results earlier. There, for theories with $\Delta < 3/2$, the quantity $\mathcal{R}$ denoted the curvature in units of the vev, not the source. Here we maintain this convention.

We can now work in analogy of the free fermion discussed above. For $m \to 0$ ($\chi \to \infty$ at fixed α) the theory becomes conformal. For this case the sum in (3.5.17) was evaluated [66]. Using zeta-function renormalization one finds

$$F_{S,\mathrm{UV}} = \frac{1}{16}\left(2\log 2 - \frac{3\zeta(3)}{\pi^2}\right) . \tag{3.5.19}$$

For $m \to \infty$ ($\chi \to 0$ at fixed α) the theory becomes empty and we expect.

$$F_{S,\mathrm{IR}} = 0 . \tag{3.5.20}$$

A good F-function should reduce to these values in the limits $\chi \to \infty$ and $\chi \to 0$, respectively.

Using zeta-function renormalization, it was also shown in [66] that the renormalized free energy satisfies

$$\frac{\partial F_S^{\mathrm{ren}}}{\partial(\alpha m)^2} = -\frac{\pi}{4}\sqrt{(\alpha m)^2 - \frac{1}{4}}\,\coth\left(\pi\sqrt{(\alpha m)^2 - \frac{1}{4}}\right) . \tag{3.5.21}$$

Therefore, we can again write the zeta-function renormalized free energy as an integral. Here one finds

$$F_S^{\mathrm{ren}}(\chi) = F_{S,\mathrm{UV}} - \frac{\pi}{4}\int_0^{1/\chi} dx\,\sqrt{x^2 - \frac{1}{4}}\,\coth\left(\pi\sqrt{x^2 - \frac{1}{4}}\right) , \tag{3.5.22}$$

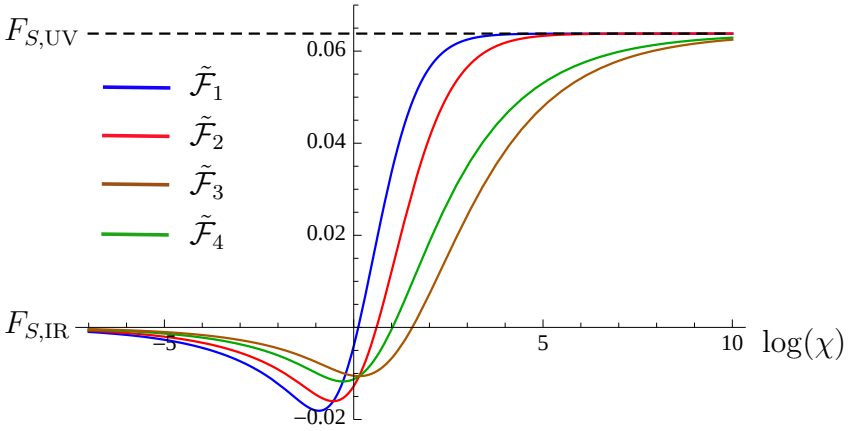

Figure 3.6: $\tilde{\mathcal{F}}_{1,2,3,4}$ given in (3.5.24)–(3.5.27) vs. $\log(\chi)$ with $\chi = (\alpha m)^{-2}$ for a theory of a free massive scalar on S^3. The black dashed line indicates the value of $F_{S,\mathrm{UV}}$ given in (3.5.5).

which by definition reduces to $F_{S,\mathrm{UV}}$ for $\chi \to \infty$. The expression (3.5.22) again has IR divergences, which come with powers of $\chi^{-3/2}$ and $\chi^{-1/2}$. In particular, one finds

$$F_S^{\mathrm{ren}}(\chi) \underset{\chi\to 0}{=} -\frac{\pi}{6}\chi^{-3/2} + \frac{\pi}{16}\chi^{-1/2} + (\text{vanishing for } \chi \to 0)\,. \tag{3.5.23}$$

We can again define finite candidate F-functions, where the divergent terms are removed by differentiation or subtraction or a combination thereof. By analogy with (3.3.12)–(3.3.15) we hence define the following for candidate F-functions constructed from the free energy (3.5.22):

$$\tilde{\mathcal{F}}_1(\chi) = \mathcal{D}^{\chi}_{1/2}\,\mathcal{D}^{\chi}_{3/2}\;\; F_S^{\mathrm{ren}}(\chi)\,, \tag{3.5.24}$$

$$\tilde{\mathcal{F}}_2(\chi) = \mathcal{D}^{\chi}_{1/2}\qquad \left(F_S^{\mathrm{ren}}(\chi) + \frac{\pi}{6}\chi^{-3/2}\right), \tag{3.5.25}$$

$$\tilde{\mathcal{F}}_3(\chi) = \qquad \mathcal{D}^{\chi}_{3/2}\left(F_S^{\mathrm{ren}}(\chi) - \frac{\pi}{16}\chi^{-1/2}\right), \tag{3.5.26}$$

$$\tilde{\mathcal{F}}_4(\chi) = \qquad\qquad \left(F_S^{\mathrm{ren}}(\chi) + \frac{\pi}{6}\chi^{-3/2} - \frac{\pi}{16}\chi^{-1/2}\right), \tag{3.5.27}$$

where $\mathcal{D}^{\chi}_{1/2}$ and $\mathcal{D}^{\chi}_{3/2}$ are defined as in (3.3.9), but with $\mathcal{R}$ replaced by χ. By construction all four functions $\tilde{\mathcal{F}}_{1,2,3,4}$ reduce to the values $F_{S,\mathrm{UV}}$ and $F_{S,\mathrm{IR}}$ for $\chi \to \infty$ and $\chi \to 0$, respectively. However, a numerical evaluation shows that they do *not* interpolate monotonically between the UV and IR. As shown in figure 3.6 all four functions $\tilde{\mathcal{F}}_{1,2,3,4}$ fail to exhibit monotonicity. Therefore, they are not good F-functions for the free scalar.

The fact that the free energy does not straightforwardly give rise to a good F-function for the free scalar has been observed before. In [66] it was already found that the function $\tilde{\mathcal{F}}_4(\chi)$ defined in (3.5.27) is not monotonic in χ. To overcome this, a different subtraction of IR-divergent pieces was suggested. While this indeed solved the problem, the necessary subtraction is introduced ad hoc leaving the question unanswered how a good F-function can be constructed systematically.

Similar problems for constructing a good F-function for the free massive scalar were found in [80]. There the authors examined the equivalent of the 'Renormalized Entanglement Entropy' (REE) of Liu and Mezei [74] for the theory of a free massive scalar on dS_3, again observing non-monotonicity. As can be deduced from the calculations in [80], the relations (3.4.26) and (3.4.27) between the dS_3 entanglement entropy and the free energy on S^3 also hold for the free massive scalar. As a result, our function $\tilde{\mathcal{F}}_1(\chi)$ defined in (3.5.24) is nothing but the REE on dS_3 studied in [80]. The failure of finding monotonicity of the REE on dS_3 can then be understood as part of the more general failure of the free energy as an F-function for the free scalar on S^3.

Faced with this obstacle, we will now follow the intuition gained from our holographic analyses and consider the quantum effective potential rather than the free energy as an F-function for the free scalar. Interestingly, we will find that this will indeed give rise to a monotonic function interpolating between the UV and IR, thus answering the question how a good F-function for the free scalar on S^3 or dS_3 can be constructed.

The quantum effective potential as a candidate F-function

We define the quantum effective potential as the Legendre transformation of the free energy with respect to the source m^2. While we found that the free energy only depends on the radius α and the source m^2 through the combination $(\alpha m)^2$, it will be convenient to write it in the following as $F_S^{\text{ren}}(\alpha, m^2)$, with radius and source appearing as separate arguments.

We begin by defining a quantity $G_S^{\text{ren}}(\alpha, \psi, m^2)$ as the Legendre transformation of the free energy with respect to m^2 as follows:

$$\begin{aligned} G_S^{\text{ren}}(\alpha, \psi, m^2) &= F_S^{\text{ren}}(\alpha, m^2) + \int d^3x \, \sqrt{\zeta}\, m^2 \psi \\ &= F_S^{\text{ren}}(\alpha, m^2) + 2\pi^2 \, (\alpha m)^2 (\alpha \psi) \,, \end{aligned} \tag{3.5.28}$$

where we have used that α and m^2 are constant in space-time and $\int d^3x \sqrt{\zeta} = 2\pi^2\alpha^3$. Here we introduced the variable ψ 'dual' to the source m^2, and which

will be proportional to the vev of the operator ϕ^2. Extremising with respect to m^2 gives

$$\frac{\partial F_S^{\rm ren}}{\partial(\alpha m)^2} + 2\pi^2 \alpha\psi = 0\,, \tag{3.5.29}$$

which can be inverted to find $m^2(\psi)$. The quantum effective potential $\Gamma_S^{\rm ren}(\alpha,\psi)$ is then given by

$$\Gamma_S^{\rm ren}(\alpha,\psi) \equiv G_S^{\rm ren}(\alpha,\psi,m^2(\psi))\,. \tag{3.5.30}$$

Note that in (3.5.28) and (3.5.29) the source m^2 only appears in the combination $(\alpha m)^2$. Similarly ψ only appears in the combination $(\alpha\psi)$. We already defined $\chi = (\alpha m)^{-2}$ as the dimensionless curvature in units of the source. Now, we also define

$$\mathcal{R} \equiv (\alpha\psi)^{-2} \tag{3.5.31}$$

as the curvature in units of the vev, in analogy with our holographic analysis for theories with $\Delta < 3/2$. Notice that we can write (3.5.28) and (3.5.29) using only the dimensionless combinations χ and $\mathcal{R}$ as variables without ever having to refer to α, m^2 or ψ individually. Also using the fact that the free energy is a function of χ only, $F_S^{\rm ren}(\alpha,m^2) = F_S^{\rm ren}(\chi)$, this implies that the quantum effective potential (3.5.30) is only a function of $\mathcal{R}$, i.e.

$$\Gamma_S^{\rm ren}(\alpha,\psi) = \Gamma_S^{\rm ren}(\mathcal{R})\,. \tag{3.5.32}$$

The inversion required for finding $m^2(\psi)$ can only be done numerically, which, given expression (3.5.21) is a straightforward exercise. However, for small and large ψ we can also obtain analytical results. In particular, we find

$$m^2(\psi) \underset{\psi\to 0}{=} \frac{16\psi}{\alpha}\Big(1+\mathcal{O}(\psi)\Big)\,, \tag{3.5.33}$$

$$m^2(\psi) \underset{\psi\to \infty}{=} 64\pi^2\psi^2\Big(1+\mathcal{O}(\psi^{-2})\Big)\,. \tag{3.5.34}$$

Therefore, for $\psi \to 0$ we find $m^2(\psi) \to 0$ and for $\psi \to \infty$ we observe $m^2(\psi) \to \infty$.

We can then make the following observations. For $\psi \to 0$ ($\mathcal{R} \to \infty$ at fixed α) the second term in (3.5.28) vanishes and correspondingly

$$\Gamma_S^{\rm ren}(\mathcal{R}\to\infty) = F_S^{\rm ren}(\chi\to\infty) \to F_{S,\rm UV}\,. \tag{3.5.35}$$

Therefore, in the UV limit $\mathcal{R} \to \infty$ the quantum effective potential reduces to the value of the free energy of a conformal scalar on S^3.

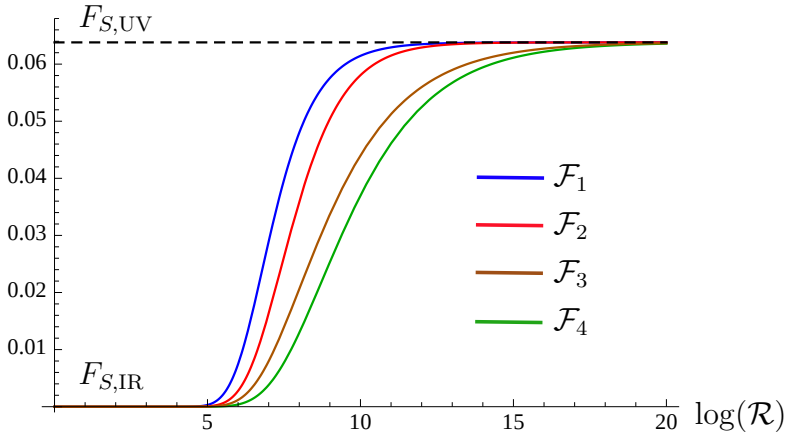

Figure 3.7: $\mathcal{F}_{1,2,3,4}$ given in (3.5.37)–(3.5.40) vs. $\log(\mathcal{R})$ for a theory of a free massive scalar on S^3. The black dashed line indicates the value of $F_{S,\mathrm{UV}}$ given in (3.5.19).

For $\psi \to \infty$ ($\mathcal{R} \to 0$ at fixed α) the quantum effective action exhibits divergences which come with powers $\mathcal{R}^{-3/2}$ and $\mathcal{R}^{-1/2}$. These can be found by inserting (3.5.23) and (3.5.34) into (3.5.28) and expressing everything in terms of $\mathcal{R}$. One obtains

$$\Gamma_S^{\mathrm{ren}}(\mathcal{R}) \underset{\mathcal{R}\to 0}{=} \frac{128\pi^4}{3}\mathcal{R}^{-3/2} + \frac{\pi^2}{2}\mathcal{R}^{-1/2}\,. \tag{3.5.36}$$

We now have all the ingredients to construct the analogues of the F-functions in (3.3.37)–(3.3.40) for the free scalar on S^3. Here these are given by

$$\mathcal{F}_1(\mathcal{R}) = \mathcal{D}_{1/2}\,\mathcal{D}_{3/2}\;\;\Gamma_S^{\mathrm{ren}}(\mathcal{R})\,, \tag{3.5.37}$$

$$\mathcal{F}_2(\mathcal{R}) = \mathcal{D}_{1/2}\qquad\left(\Gamma_S^{\mathrm{ren}}(\mathcal{R}) - \frac{128\pi^4}{3}\mathcal{R}^{-3/2}\right), \tag{3.5.38}$$

$$\mathcal{F}_3(\mathcal{R}) = \qquad\mathcal{D}_{3/2}\left(\Gamma_S^{\mathrm{ren}}(\mathcal{R}) - \frac{\pi^2}{2}\mathcal{R}^{-1/2}\right), \tag{3.5.39}$$

$$\mathcal{F}_4(\mathcal{R}) = \qquad\qquad\left(\Gamma_S^{\mathrm{ren}}(\mathcal{R}) - \frac{128\pi^4}{3}\mathcal{R}^{-3/2} - \frac{\pi^2}{2}\mathcal{R}^{-1/2}\right), \tag{3.5.40}$$

with $\mathcal{D}_{1/2}$ and $\mathcal{D}_{3/2}$ given in (3.3.9) and $\Gamma_S^{\mathrm{ren}}(\mathcal{R})$ defined in (3.5.30). These are four candidate F-functions constructed from the quantum effective potential (i.e. the Legendre transform of the free energy with respect to the source m^2). They are functions of $\mathcal{R}$, the (dimensionless) curvature in units of the vev $\langle\phi^2\rangle$.

The candidate F-functions pass the test with flying colours. As one can check explicitly, they reduce to the values $F_{S,\mathrm{UV}}$ and $F_{S,\mathrm{IR}}$ in the limits $\mathcal{R} \to$

∞ and $\mathcal{R} \to 0$, respectively. In fig. 3.7 we then plot $\mathcal{F}_{1,2,3,4}$ vs. $\log(\mathcal{R})$. The main observation is that all four functions (3.5.37)–(3.5.40) interpolate monotonically between $F_{S,\mathrm{UV}}$ and $F_{S,\mathrm{IR}}$. Therefore, the functions $\mathcal{F}_{1,2,3,4}(\mathcal{R})$ defined in (3.5.37)–(3.5.40) are indeed good F-functions for the free scalar on S^3.

To conclude, for the case of the free massive boson on S^3 good F-functions can be constructed from the quantum effective potential, as suggested by our holographic analysis. The free energy fails to interpolate monotonically between $F_{S,\mathrm{UV}}$ and $F_{S,\mathrm{IR}}$ as observed in [66] and reviewed at the beginning of this section. For the massive fermion on S^3 our holographic findings imply that a good F-function can be constructed from the free energy, which we confirmed explicitly in sec. 3.5.1. To test our F-function proposals further one can check if anything goes wrong if one uses the quantum effective potential to construct an F-function for the free massive fermion. As the calculation is very similar to the analysis presented in this section we do not include it in this work and only quote the result. Interestingly, one finds that the analogues of (3.5.37)–(3.5.40) are *not* monotonic in the fermionic case. This suggests that, when implementing our proposals, the choice between free energy and quantum effective potential is exclusive in the sense that only one leads to a good F-function for a given theory. We leave further investigations of this matter to future work.

Chapter 4

Holographic quantum phase transitions driven by curvature

The holographic RG flows on curved manifolds discussed in chapter 2 are dual to vacua of the boundary field theory. In the framework of holography there may be multiple RG flows that originate from a single UV fixed point but flow to different IR end points. From the field theory point of view this corresponds to a theory that exhibits multiple vacua, with a one-to-one correspondence between the number of flows and the number of vacua.

This behavior was described in [5] for holographic RG flows of field theories on flat manifolds. There it was observed that in addition to a flow from a maximum to the nearest minimum, there may also exist flows that *skip* the nearest minimum to end at the next minimum. We find that this situation persists if we add non-zero curvature: at a fixed curvature and UV source there may be multiple RG flow emanating from the same UV fixed point, but terminating at different IR end points. The different flows are distinguished by the subleading term in Eq. (2.4.2) which determines the vev of the dual operator.

The various flows correspond to different saddle points of the action and are hence in one-to-one correspondence with vacua of the field theory. In the case of multiple flows the question then arises which of these ground states is the true vacuum. In the dual gravitational picture this is equivalent to the questions which saddle point is dominant in the gravitational path integral. This can be answered by comparing the free energies associated with the various vacua and identifying the ground state with the lowest free energy as the true vacuum. In the example presented in [5], the skipping flow is the true vacuum.

If we vary the value of R^{uv} the RG flows deform and the vevs and free energies of the various vacua change. Interestingly, under a variation of R^{uv}

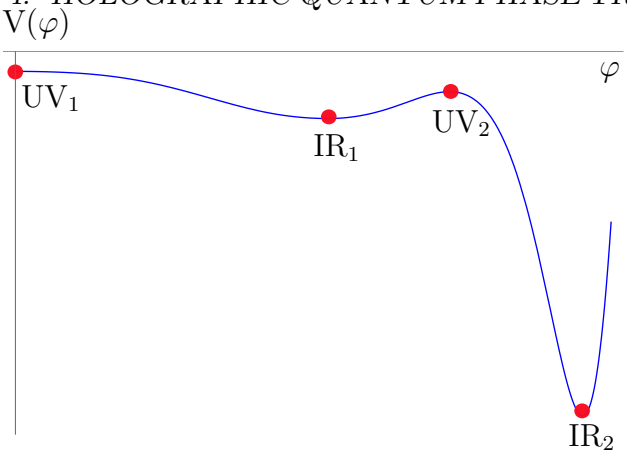

Figure 4.1: Plot of the degree-12 potential which allows skipping solutions. This potential has several extrema which are denoted as UV_1, UV_2, IR_1 and IR_2.

the identification of the true vacuum may change, i.e. the system may exhibit a phase transition. This corresponds to a *quantum* phase transition as our system is at zero temperature. The control parameter in this case is the curvature R^{uv}.

In the following, we choose a specific example based on a suitably chosen potential exhibiting multiple RG flows originating from the same UV fixed point. For this example we study the evolution of the free energies for the various flows under a change of curvature. Ultimately, we will observe a change of sign of the free energy difference between the different saddle points, indicating the existence of a phase transition driven by curvature.

4.1 Skipping flows

To illustrate the concept of skipping flows, we set $d = 4$ and consider a potential which is a polynomial of degree 12, whose explicit form is not essential and can be found in [5]. A plot of (part of) this potential is shown in figure 4.1. It has several extrema, denoted by UV_1, UV_2, IR_1 and IR_2 In this section, we will determine the possible RG flows as we increase the dimensionless UV curvature parameter, $\mathcal{R}$.

Flat case: $\mathcal{R} = 0$

We first consider the RG flow solutions for the QFT in flat space-time. The corresponding solutions for $W(\varphi)$ are shown in Fig. 4.2. In this case, there are three RG flows in total, two originating from UV_1 and one from UV_2.

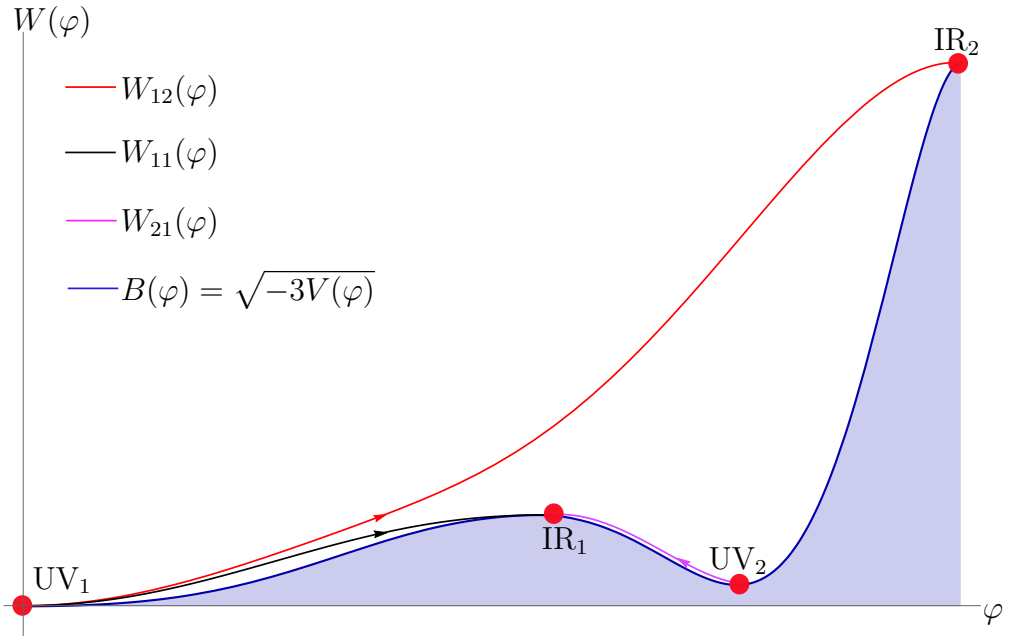

Figure 4.2: The plot represents the function $W(\varphi)$ corresponding to the three regular holographic RG flow solutions arising from the potential in figure 4.1. Two of them are standard interpolating from UV_1 to IR_1 and from UV_2 to IR_1. The third one skips IR_1 and ends up at IR_2. The shaded region is the forbidden region below the critical curve $B(\varphi)$. The arrows represent the direction of the flow from the UV to the IR.

We will focus on the flows emanating from UV_1. Among the two RG flows emanating from the UV_1, the one denoted by $W_{11}(\varphi)$ interpolates between UV_1 and the nearest minimum to the right IR_1. The second flow denoted $W_{12}(\varphi)$ skips the fixed point IR_1 and ends at IR_2.

To decide which solution is the dominant saddle point in the path integral, we need to compare their corresponding free energies at fixed boundary condition φ_-. As described in [5] the flow with the higher value of vev parameter C is the dominant saddle point: this is the skipping flow, as the solution with larger C has a larger $W(\varphi)$ in the UV. Consequently, the skipping flow represents the true ground-state of the dual QFT in flat space-time.

Although our focus will be on flows starting at UV_1, for completeness we briefly discuss the flow from UV_2, also depicted in Fig. 4.2. There is a single flow which starts from UV_2, denoted as $W_{21}(\varphi)$, and it interpolates between the UV_2 and IR_1. There is no solution starting from UV_2 and ending at IR_2 as there can be at most one flow that can end at a given IR point from a given direction. This is because regular solutions in the IR do not admit small deformations [5]. Here the fixed point IR_2 is already "taken" by the

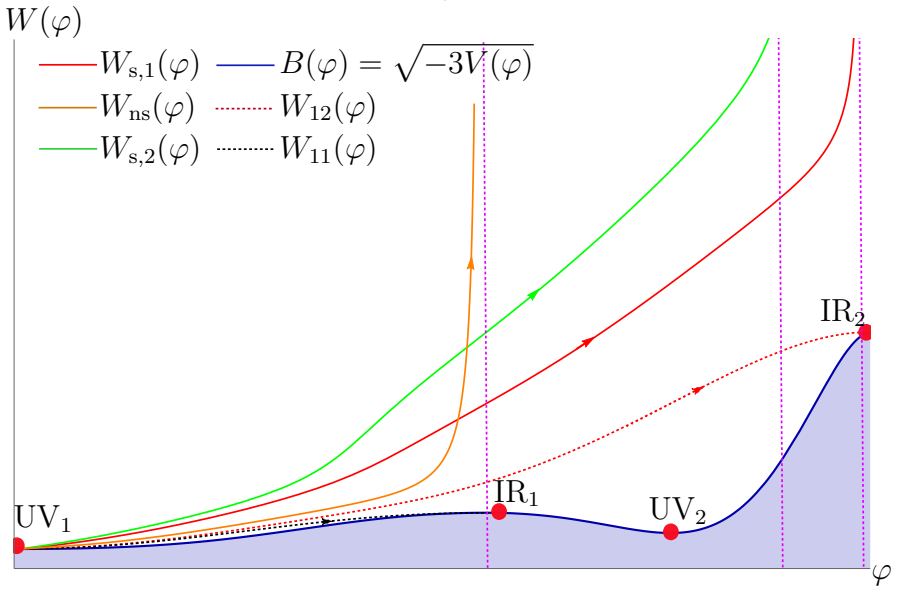

Figure 4.3: The solid lines represent the function $W(\varphi)$ corresponding to the three different solutions starting from UV_1 which exist at small positive curvature. Two of them (red and green curves) are skipping flows and the third one (orange curve) is non-skipping. For comparison, we also show the flat RG flows (dashed curves)

skipping flow $W_{12}(\varphi)$.

We now turn on positive curvature on the d-dimensional slice and see how this affects the various RG flows solutions presented above.

Finite curvature $\mathcal{R} > 0$; Flows from UV_1

Turning on a small positive curvature, there are now three flows (instead of the two at $\mathcal{R} = 0$) emanating from UV_1 and shown in the Fig. 4.3. Two of them are skipping the nearest possible IR region (between $\varphi = 0$ and IR_1) and end up near IR_2. These two are denoted as $W_{s,1}(\varphi)$ and $W_{s,2}(\varphi)$ and represented as red and green curves respectively in the Fig. 4.3. The third flow is the non-skipping flow and denoted as $W_{ns}(\varphi)$. It starts from UV_1 and ends up in the region between $\varphi = 0$ and IR_1. The two flows $W_{ns}(\varphi)$ and $W_{s,1}(\varphi)$ are deformations of the corresponding flat flows (represented as the dotted black and red curves in Fig. 4.3) and end slightly before the respective IR fixed points. The flow $W_{s,2}(\varphi)$ on the other hand is a new branch which only exists for non-zero curvature.

As $\mathcal{R}$ is increased, the flows are deformed as shown in Fig. 4.4. The IR end points of the skipping flows $W_{s,2}(\varphi)$ and $W_{s,1}(\varphi)$, move towards each other, up to a critical value of $\mathcal{R}$ where the two solutions merge. Above this

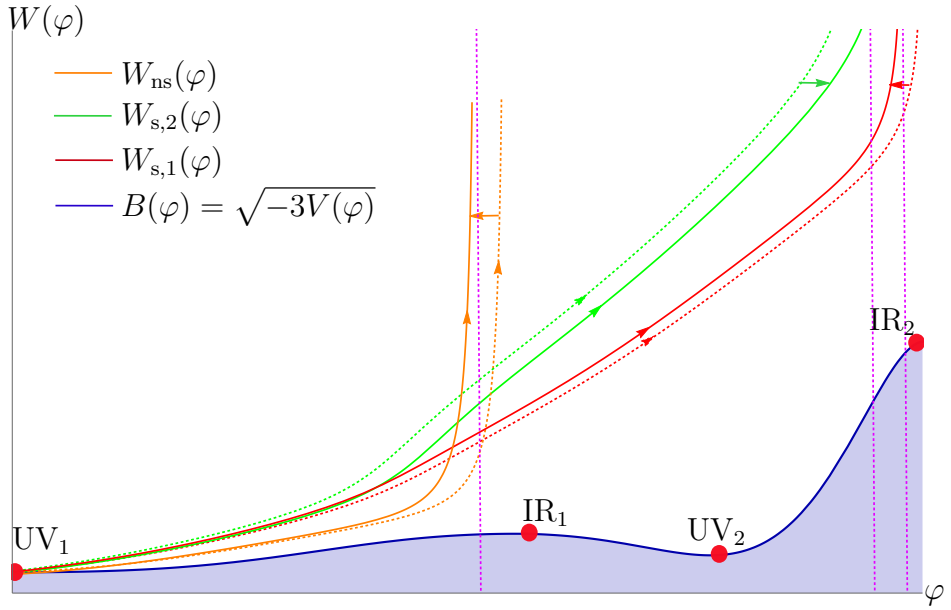

Figure 4.4: As the curvature is increased, IR end points of the skipping flows move toward each other. The non-skipping IR end point moves closer to UV$_1$.

value, the skipping solution disappears and only the non-skipping flow is left. The IR end point of the non-skipping flow $W_{\rm ns}(\varphi)$ moves to the left from the IR$_1$ and it approaches the UV fixed point point UV$_1$ as $\mathcal{R}$ is increased, as expected in the generic case.

Finite curvature: $\mathcal{R} > 0$; Flows from UV$_2$

For completeness, we will also describe the flows starting from UV$_2$ as we increase the curvature. In the flat case, there was only one such flow, with a negative source (see $W_{21}(\varphi)$ in Fig. 4.2). If the curvature is slightly increased, this flow splits into two. One starts from UV$_2$ and ends in the region between IR$_1$ and UV$_2$. This is shown as the red curve $\mathrm{W}_{2nb,n}(\varphi)$ in Fig. 4.5. The other flow, represented as the red curve $\mathrm{W}_{2b,n}(\varphi)$ in Fig. 4.6, starts form UV$_2$, *bounces* in the region between IR$_1$ and UV$_2$ and ends in the region $\varphi >$ UV$_2$. These two flows, namely the non-bouncing flow and the bouncing flow with negative source, exist for all values of curvature.

Beyond a certain value of the curvature, two new solutions appear that emanate from UV$_2$ in addition to the bouncing and the non-bouncing flows. These have a positive source and have no $\mathcal{R} = 0$ counterpart. They end in region $\varphi >$ UV$_2$. They are shown as the red curves $W_{2nb,p}(\varphi)$ in Fig. 4.7.

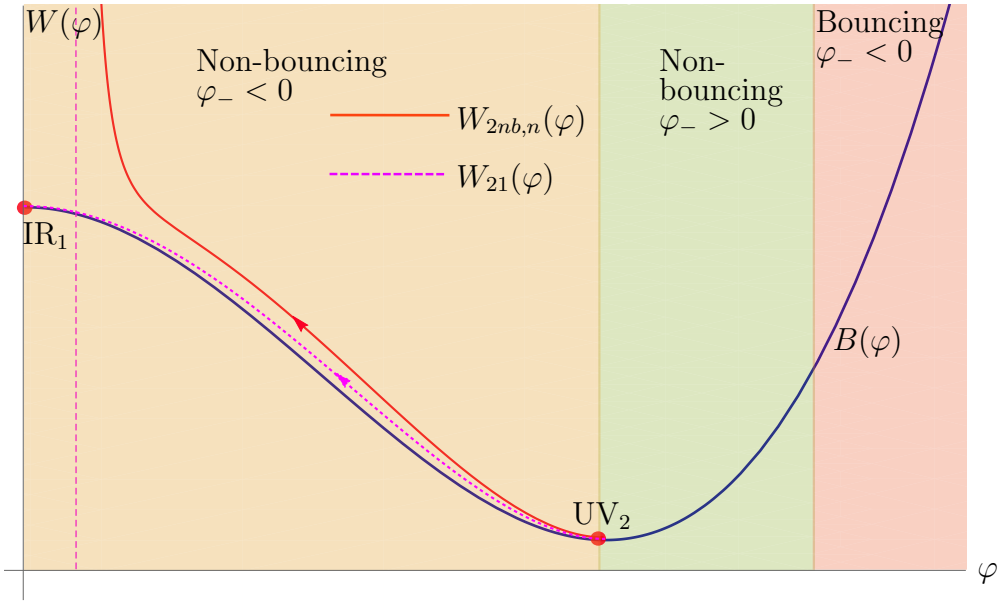

Figure 4.5: Function $W_{2nb,n}(\varphi)$ for a non-bouncing flows starting from UV_2. In this case the source is negative. This type of flow comes from a curvature deformation of the flat case flow W_{21} and exists for all values of the curvature.

Full space of solutions

Fig. 4.8, shows the dimensionless UV curvature parameter $\mathcal{R}$ as a function of the IR end point φ_0 of the flow. Non-skipping flows start from UV_1 and the end in the leftmost blue region. This type of solution exists for all values of curvature. On the other hand, skipping flows from UV_1 end up in the rightmost purple region, and they come in two branches (i.e. there are two different endpoints in the right purple region for a given value of $\mathcal{R}$). These skipping flows exist up to a maximum value of curvature, where the two branches merge.

We also display the results for flows starting from UV_2 in Fig. 4.8. Flows with a negative source (i.e. going towards the left of UV_2) either end in the light brown region, or bounce and then end in the red region. Both these bouncing and non-bouncing solutions originate as deformations of the "flat" flow $W_{21}(\varphi)$ (see Figures 4.5 and 4.6), and exist for any positive value of $\mathcal{R}$.

A particularly interesting set of flows from UV_2 are those with end points in the green region in Fig. 4.8. Note that all flows in this region have $\mathcal{R} \geq \mathcal{R}_{\mathrm{min}}$ for some minimal value of the dimensionless curvature. This implies that these flows do not arise from a continuous deformation of a flat flow. In fact, there is no flat flow from UV_2 with positive source. This was explained in [5] as arising from the fact that there is already a regular flow terminating

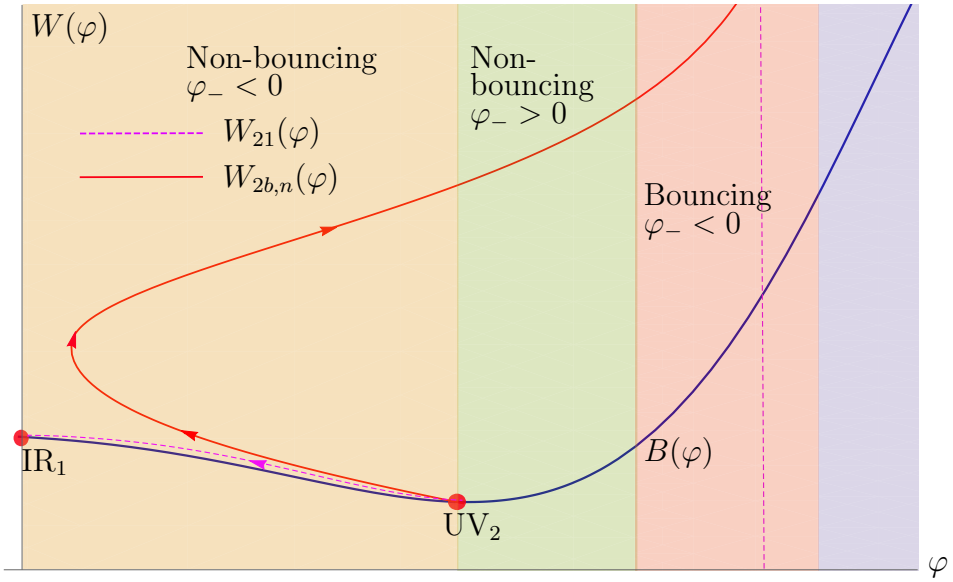

Figure 4.6: Function $W_{2b,n}(\varphi)$ for a bouncing flows starting from UV_2. For bouncing flows, the source is negative. This type of flow also comes from a curvature deformation of the flat case flow W_{21} (dotted line) and exist for all values of the curvature.

at IR_2 from the left, and therefore no other regular flows can also arrive from the same side. The solutions with end points in the green region in Fig. 4.8 thus correspond to new vacua which do not exist for $\mathcal{R} = 0$, but appear when $\mathcal{R}$ becomes large enough.

The fact that there is a regular flow starting at UV_2 for negative coupling (towards the left of UV_2) but not positive coupling (towards the right of UV_2) has analogues in QFT. Both for YM and $\lambda\phi^4$ theory the coupling must have a fixed sign. The theories do not exist for negative g^2_{YM} or negative λ. Something similar also happens here. The unusual occurence however is that the theory with the 'wrong' sign exists for sufficiently large space-time curvature. In a sense positive curvature cures the sickness of the flat theory. It would be interesting to understand this phenomenon better and find examples of a similar behavior in QFT.

Notice that there are several values of the endpoint where the curvature parameter diverges. Two of them correspond to the UV fixed points UV_1 and UV_2, in line with the generic behavior found in section 2.6. The third one (namely the point φ_* in Fig. 4.8 separating the green and red regions) is more interesting. Across this point the source changes sign. For the endpoint exactly at φ_* the solution must have zero source, implying that for finite R^{uv}, the quantity $\mathcal{R}$ diverges (recall the definition in equation (2.4.16))

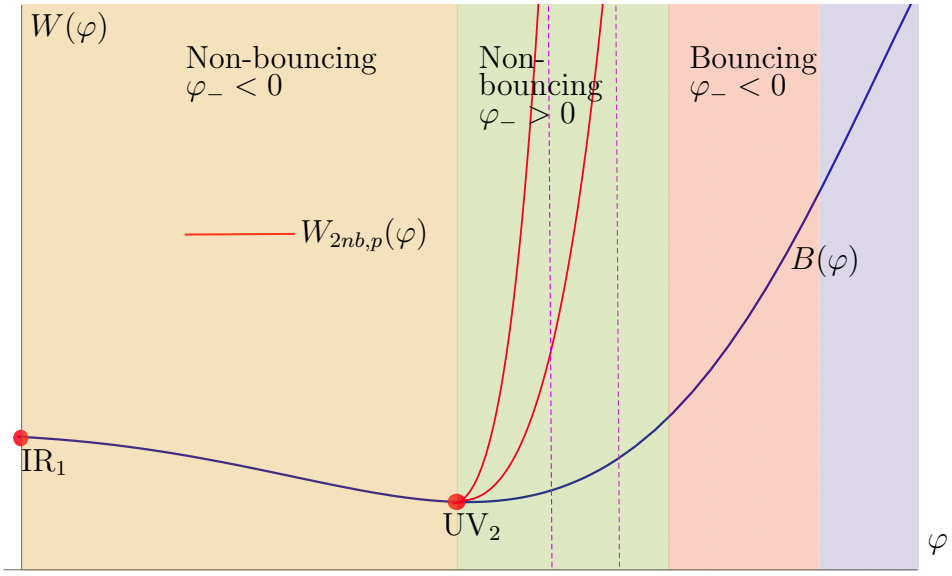

Figure 4.7: Two non-bouncing flows $W_{2nb,p}(\varphi)$ from UV_2 with identical value of $\mathcal{R}$. Interestingly, flows of this type only exist for $\mathcal{R} > \mathcal{R}_{\min}$, i.e. when the dimensionless curvature is larger than some minimal value. As a result, such flows do not come from a curvature deformation of a $\mathcal{R} = 0$ flow.

as we approach φ_*. This fact has a remarkable consequence: It implies that, above some positive threshold value for the curvature, there exist RG flows with no source (i.e. of the W_+ branch, the ones driven by a vev) starting at UV_2 and ending at φ_*. Compare this to the flat case, where regular vev flows are highly non-generic, and require a fine-tuned potential.

Note that there seems to exist an endpoint for flows with $\mathcal{R} = 0$ that does not coincide with an extremum of the potential. This is the point $\varphi_!$ in Fig. 4.8 separating the purple and red regions. However, one finds that this endpoint cannot be reached by a flow from UV_1 or UV_2. To illustrate this, let us consider what happens for flows ending in both the red and purple regions of Fig. 4.8 when we let $\varphi_0 \to \varphi_!$. Flows ending in the red region of Fig. 4.8 leave UV_2 to the left before bouncing and reversing direction (see Fig. 4.6). Taking $\varphi_0 \to \varphi_!$ the bounce point occurs closer and closer to IR_1, coinciding with IR_1 for $\varphi_0 = \varphi_!$. Once this happens the two branches of the previously bouncing solution become two independent RG flows. For one, there is the flow starting from UV_2 and ending at IR_1 (denoted by W_{21} in Fig. 4.9). This is a zero-curvature flow from extremum to extremum. The 2nd branch of the bouncing flow now becomes a flow starting at the minimum associated with IR_1 and ending at $\varphi_!$. This is shown as W_{3+} in Fig. 4.9. The minimum thus plays the role of a UV fixed point, which we label UV_3 in Fig. 4.9. This

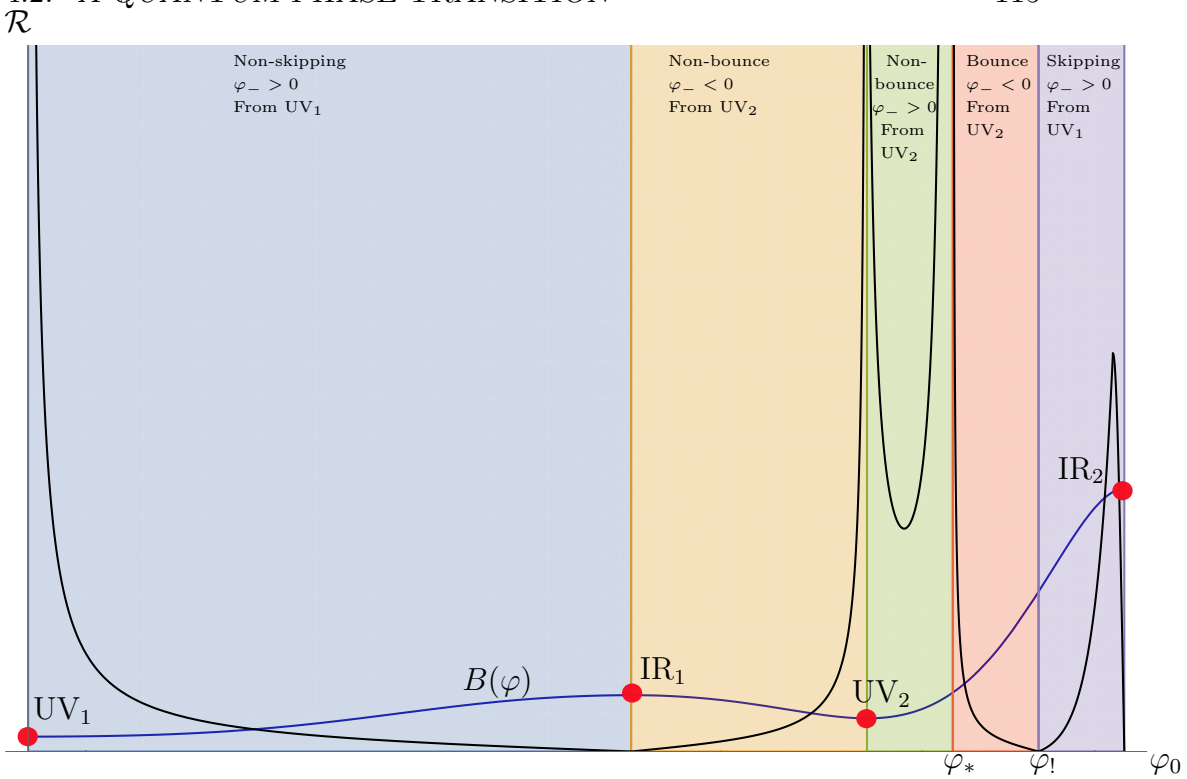

Figure 4.8: Dimensionless curvature $\mathcal{R}$ vs. flow end point φ_0. The leftmost blue region is the IR region where non-skipping flows from UV$_1$ can end. The rightmost purple area is the IR region for skipping flows from UV$_1$. The light brown region is the IR region for flows starting from UV$_2$ with a negative source and no bounces along the flow. The green area is the IR region for flows starting from UV$_2$ with a positive source. The red region is the IR region for flows from UV$_2$ with a negative source but which exhibit a bounce. The blue line is the critical curve $B(\varphi) = \sqrt{-3V(\varphi)}$.

corresponds to a W_+ solution in the language of section 2.4 with fixed value $\mathcal{R} = R^{\rm uv}|\varphi_+|^{-2/\Delta_+} \neq 0$. We can make an analogous observation for flows ending in the purple region, which originate from UV$_1$ and skip IR$_1$. Taking $\varphi_0 \to \varphi_!$ the flows miss IR$_1$ with ever decreasing distance, and pass through IR$_1$ for $\varphi_0 = \varphi_!$. Again, in this case we should not continue the flow beyond IR$_1$, which becomes the endpoint. This corresponds to the solution W_{11} in Fig. 4.9.

4.2 A quantum phase transition

We have observed that there are more than one flows with the same dimensionless UV curvature parameter, $\mathcal{R}$, and now we will focus on flows

which start from UV_1 and have the same source. These correspond to three branches of solutions contained in the blue and purple regions in figure 4.8. Beyond a certain value of the curvature, only the non-skipping solution in the blue region exists, so this solution it is necessarily the ground state. On the other hand, as we mentioned at the beginning of this section, at zero curvature one of the *skipping* solutions is the true ground state. This suggests that varying $\mathcal{R}$ we should encounter a phase transition.

To determine which solution is the dominant vacuum, we need to compare their free energies. The computation of the free energy has been discussed in length in section 3.2.1 of the previous chapter. It was mentioned that the free energy is UV divergent and this divergence can be removed by holographic renormalization. The number of counter-terms depends on the space-time dimensions and in the previous chapter the main focus was on $d = 3$. In this chapter we are interested in $d = 4$ and the renormalized free energy is

$$F^{d=4,ren}(\mathcal{R}|B_{ct}, C_{ct}) = \lim_{\epsilon\to 0}\left[F + F^{(0)}_{ct} + F^{(1)}_{ct} + F^{(2)}_{ct}\right] \tag{4.2.1}$$

where $F, F^{(0)}_{ct}, F^{(1)}_{ct}$ were defined in (3.2.13), (3.2.27) and (3.2.28) respectively. The new counter-term for $d = 4$ is

$$F^{(2)}_{ct} = -M_P^{d-1}\int_{\mathrm{UV}} d^dx\sqrt{|\gamma|}\,(R^{(\gamma)})^2\frac{\ell^3}{48\Delta_-}\log(\varphi)\ . \tag{4.2.2}$$

To compare the free energies, we evaluate expression (4.2.1) numerically, supplemented by the appropriate counter-terms and we set $B_{ct} = C_{ct} = 0$. The numerical evaluation of the free energy difference between the two skipping solutions and the non-skipping solution is shown in Fig. 4.10, which clearly shows that we are in presence of a first order quantum phase transition driven by space-time curvature. A similar phase transition was observed in [86, 87] where temperature is the driving parameter.

At zero curvature, one of the skipping solutions dominates, and the second one becomes degenerate with the non-skipping solution. As the curvature is increased, the difference between the free energies decreases. At a certain value of the dimensionless curvature, $\mathcal{R} = \mathcal{R}_c$, the free energy difference changes sign. (In our example we find $\mathcal{R}_c \approx 80$.) Now, the non-skipping solution is the dominant saddle point in the path integral. Finally, the two skipping solutions merge at a maximal value $\mathcal{R}$ and disappear for larger values of the curvature.

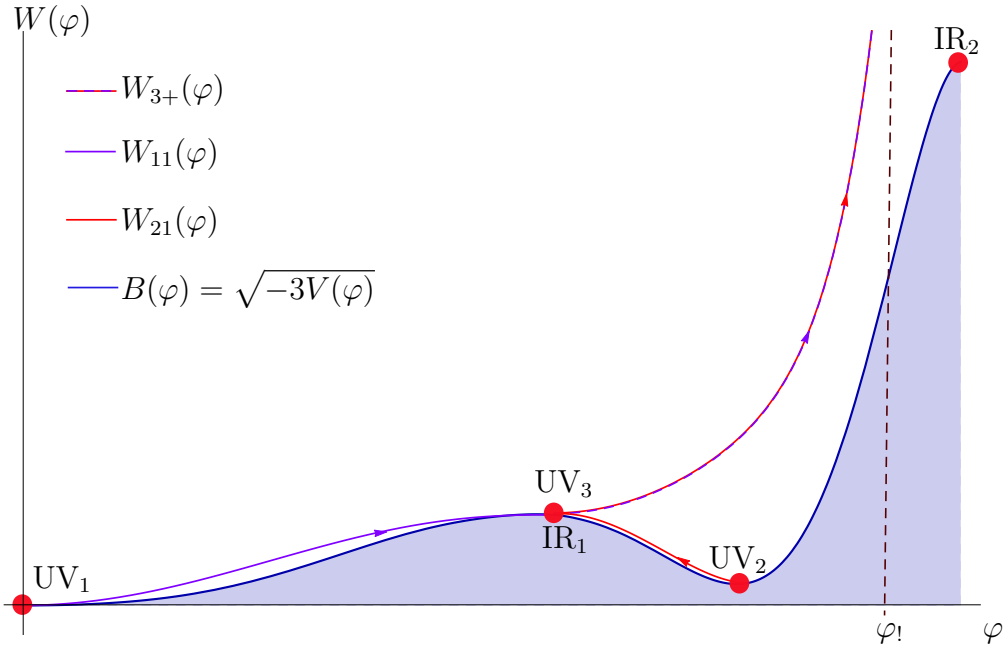

Figure 4.9: RG flows with IR endpoint $\varphi_0 \to \varphi_!$. When the endpoint φ_0 approaches $\varphi_!$ flows from both UV_1 and UV_2 pass by closely to IR_1, passing through IR_1 exactly for $\varphi_0 = \varphi_!$. This is shown by the purple and red curves. Beyond IR_1 both these solutions coincide, which is denoted by the colored dashed curve. These have the following interpretation. The flows from UV_1 and UV_2 should not be continued beyond IR_1, which becomes the IR endpoint for the zero curvature flows W_{11} and W_{21}. The remaining branch (the colored dashed curve) is now an independent flow denoted by W_{3+}. This is a flow from a UV fixed point at a minimum of the potential (denoted by UV_3 above) to $\varphi_!$ and corresponds to a W_+ solution in the notation of section 2.4 with fixed value $\mathcal{R} = R^{\mathrm{uv}}|\varphi_+|^{-2/\Delta_+} \neq 0$. While flows from UV_1 and UV_2 can end arbitrarily close to $\varphi_!$, the endpoint $\varphi_0 = \varphi_!$ cannot be reached from UV_1 or UV_2.

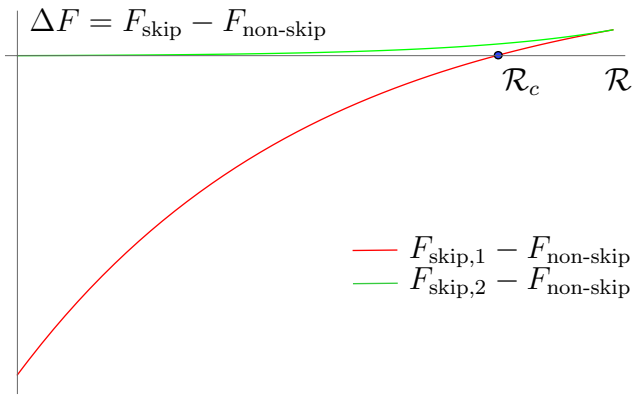

Figure 4.10: Free energy difference between the skipping and the non-skipping solution. For a fixed curvature, there are two skipping solutions for which the function $W(\varphi)$ was denoted as $W_{s,1}(\varphi)$ and $W_{s,2}(\varphi)$ (they were denoted as red and green curves respectively in figures 4.3 and 4.4). In this figure, the red curve corresponds to the free energy difference between the $W_{s,1}(\varphi)$ solution and the non-skipping solution. The green curve corresponds to the free energy difference between the $W_{s,2}(\varphi)$ solution and the non-skipping solution $W_{ns}(\varphi)$.

Chapter 5

De Sitter and Anti-de Sitter branes in self-tuning models

In chapter 2, we have discussed in details the holographic RG flows on maximally symmetric manifolds which can be either flat, dS or AdS in Lorentzian signature. These solutions can be used to study a system when a brane (a codimension-one hypersurface) is embedded in the bulk. On both sides of the brane, solutions are the holographic RG flows. Introduction of the brane requires matching solutions of both sides, known as Israel's junction conditions. In this chapter we study a bulk-brane system and look for solutions when the brane is curved.

5.1 Braneworlds and holography

Soon after its first introduction in [12, 15, 16], it has been clear that the holographic gauge/gravity duality is intimately linked to a new way of thinking about modified gravity and beyond the standard model phenomenology which was being developed around the same time: the idea of the braneworld [88, 89, 90]. In these models, several problems of the Standard Model or its high-energy completion were addressed by postulating that the observed particles and fields are confined to a four-dimensional hypersurface (*brane*) embedded in a higher-dimensional space-time (*bulk*). The connection to holography, observed in [91, 92, 93], stems from the fact that the bulk was often taken to be (a portion of) Anti-de Sitter space, which may be given a dual interpretation in terms of a strongly coupled, large-N, four-dimensional field theory. Since then, holographic duality and braneworld phenomenology have often been two complementary sides of model building.

One of the earliest applications of braneworlds in this context was aimed

at addressing the various naturalness problems which afflict the Standard Model and General Relativity, both from the particle physics side (electroweak hierarchy problem) and from the cosmology side (cosmological constant problem(s)).

On the one hand, cosmological applications led to departures from solutions describing a static flat brane in a static bulk, and prompted the study of braneworld cosmology [94, 95, 96]. The connection between braneworld models and gravity modifications was proposed as a way to model the observed current acceleration of the universe [97, 98].

On the other hand, it was proposed to use braneworld models to resolve the clash between the huge vacuum energy resulting from quantum effective field theory calculations and the smallness of the observed cosmological constant of the current de Sitter-like epoch. These proposal aimed at realising a *self-tuning* mechanism, first proposed in [99, 100], in which, contrary to purely four-dimensional models, the vacuum energy from quantum loops has no effect on the curvature of the brane, which is perceived as (almost) flat by four-dimensional observers [101, 102].

Although in principle appealing, the models which were proposed at the time all had issues related to the apparent inevitability of naked singularities in the bulk and/or an impossibility to have both a successful self-tuning mechanism and the existence of an effective four-dimensional gravity on the brane[6].

Recently, a novel framework was developed, which revisits the self-tuning braneworld approach [7] and which uses holography as a guiding principle for model building. It consists of a general two-derivative Einstein-dilaton bulk theory, and a codimension-one brane whose effective world-volume action contains all possible two-derivative terms (namely a brane potential for the scalar, an induced kinetic term for the scalar and an Einstein-Hilbert term for the induced metric) preserving four-dimensional diffeomorphism invariance. The bulk action is expected to be dual to a strongly coupled, large-N four-dimensional QFT, while the brane action is expected to contain the Standard Model fields as its localized fluctuations.

In the spirit of *semi-holography* (see e.g. [103]), asymptotically anti-de Sitter solutions of this theory are interpreted as a purely four-dimensional theory in which the bulk geometry is dual to a strongly interacting UV conformal field theory (CFT), deformed by a relevant operator (dual to the bulk scalar) and coupled to a weakly interacting Standard Model sector (the brane), a setup whose dual version was advocated in [104].

In the model described above, the brane separates the bulk geometry into two regions: one side connects to an asymptotically AdS conformal boundary (UV of the field theory dual). On the other side of the brane, the geometry

may flow to another, regular, asymptotically AdS region (in which case the field theory flows to an IR conformal fixed point).[1] The two sides of the geometry must obey the bulk Einstein-dilaton equations and the connection across the brane must satisfy Israel's junction conditions. Induced four-dimensional gravity on the brane is recovered in a range of distance scales via the DGP mechanism [105, 106] thanks to the localized Einstein-Hilbert term in the brane action.[2]

The use of holography as a guideline for model-building, in order to organise the space of solutions, has allowed to solve or alleviate some of the difficulties of the earlier models. In particular, holography can give a consistent meaning to certain kinds of bulk singularities [107]. These are indeed necessary to construct holographic duals of confining theories [26, 27, 108], and they may be consistently eliminated by uplifting to higher dimensions [109, 110].

As it was shown in [7], for rather generic choices of the bulk and brane potentials, enforcing the holographic interpretation of the model results in a self-tuning mechanism for the four-dimensional cosmological constant. The model admits solutions in which the geometry on the brane is flat, regardless of the vacuum energy arising from quantum loops of the brane fields. The brane is stabilized in the bulk at an equilibrium position, which is dynamically determined by the bulk geometry and brane potentials via Israel's junction conditions. Under certain general conditions, all fluctuations around the equilibrium position have positive energy.

The fact that the framework proposed in [7] allows self-tuning flat solutions opens new questions, and at the same time offers new possibilities for model building. In [7], brane flatness and four-dimensional Poincaré invariance were imposed by design on the solution ansatz, and the self-tuning mechanism corresponds to the existence of stabilized solutions with this symmetry. It is important however to explore, in the same context, other solutions in which the brane has non-zero curvature and/or has a time-dependent (cosmological) induced metric. One reason is to understand how these solutions compete with the flat solution (which represents the Poincaré-invariant vacuum). In addition, because we currently live in an accelerating universe, obtaining a positively curved (e.g. de Sitter) metric on a brane is phenomenologically important. Finally, it is important to clarify what is responsible, from the dual field theory perspective, for obtaining a curved brane geometry.

In this chapter, we look for solutions of the self-tuning framework in

[1] It may also have a mild (resolvable) naked singularity, according to the Gubser criterion.

[2] This term is generated via quantum effects of the brane localized fields.

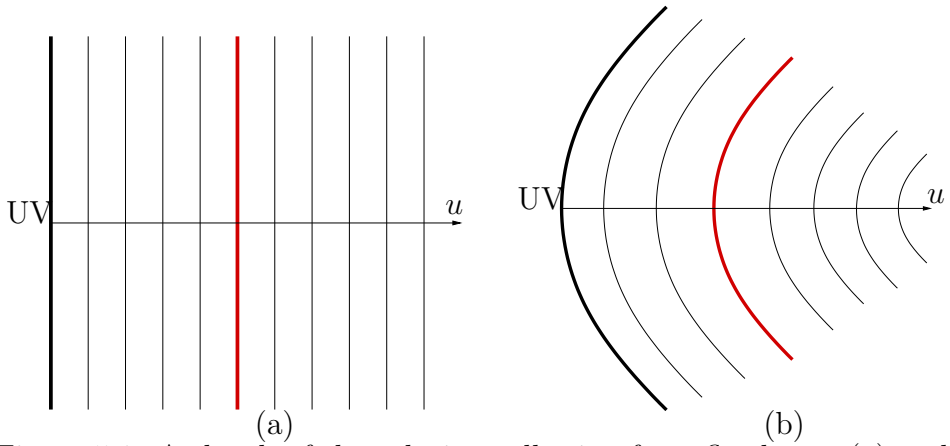

Figure 5.1: A sketch of the solutions allowing for a flat brane (a) and those allowing for a curved brane (b). The thick black line represents the conformal boundary of AdS, whereas the brane is represented in red. The direction u is the holographic direction, and the thin black lines are constant-u hypersurfaces. The brane metric is inherited from the UV boundary metric (up to a rescaling).

which the brane has a curved geometry. Our first result can be formulated as follows: no *vacuum* curved-brane solutions generically exist[3]. A non-trivial brane geometry can be obtained if one modifies the UV boundary conditions on the bulk fields, such that they allow domain wall solutions with constant curvature radial slices. In the dual QFT language this amounts to changing the dual QFT. As we shall see, a de Sitter brane geometry will be possible when the domain wall solution is sliced by de Sitter slices. In this case, the bulk geometry is dual to a QFT defined on a constant positive curvature manifold. For an AdS brane geometry, the bulk geometry is a domain wall with negative curvature slices, and the UV field theory is a CFT with an additional defect [57, 111].

Prompted by the above result, we set forward to study curved domain wall geometries, and we ask the question whether stabilized curved brane solutions do arise. We focus in particular on maximally symmetric geometries, in which both the bulk and the brane preserve four-dimensional de Sitter (dS) or Anti-de Sitter (AdS) invariance. The structure of these solutions is sketched in figure 5.1, in which we show a comparison between the flat solutions studied in [7] and the curved embeddings we discuss in this chapter.

As far as the bulk is concerned, the corresponding solutions describe holographic RG flows on maximally symmetric spaces and they were discussed

[3]By "vacuum" solution here we mean one where the bulk has 4d Poincaré invariance, representing the ground state of the dual QFT.

in chapter 2. The introduction of the brane amounts to gluing together two bulk RG-flow solutions of the type described there, to impose regularity on the IR side of the solution and to solve at the same time for the brane position and the UV part of the geometry in such a way that Israel's junction conditions are satisfied.

In these solutions, the metric on the brane is the same (up to a scaling factor, which depends on the position in the bulk) as the UV metric to which the dual CFT is coupled. For example, a de Sitter brane solution can exist only if the dual CFT is set on de Sitter space, and similarly for Anti-de Sitter. In the latter case, the holographic interpretation is more subtle because, in addition to the usual boundary conditions in the radial direction, one has also to introduce boundary conditions at the boundary of the slices. As discussed in [8] (see also [57] for a previous similar discussion) this introduces a codimension-one defect in the dual field theory.

Although the type of geometry of the brane is fixed by the boundary conditions, the magnitude of the brane curvature and its position in the bulk are determined dynamically by the field equations and the junction conditions. We refer to this as *self-stabilisation*, which is the curved counterpart of the self-tuning mechanism found in [7].[4]

There is an alternative realisation of the same solutions, which can be obtained via a bulk coordinate transformation, in which the leading UV asymptotics correspond instead to a flat metric, but the scalar sources are varying in space or time. This leads to an inequivalent description in terms of the dual QFT: instead of a boundary QFT living on a curved spacetime, we have a flat-space QFT driven by a time-varying (in the dS case) or space-dependent (in the AdS case) source. The two descriptions however result in the same brane geometry. Although in the bulk the two solutions are related by a coordinate transformation, the latter acts non-trivially on the boundary, and it leads therefore to an inequivalent theory with different boundary sources. In most of the chapter we will work with the curved-CFT description with constant scalar sources.

5.2 A curved brane in a warped bulk

In this chapter, we will consider Einstein-scalar theory in $d+1$ dimensions, coupled to a d-dimensional dynamical hypersurface (*brane*)

$$S = S_{bulk} + S_{brane} \ . \tag{5.2.1}$$

[4] We reserve the phrase *self-tuning* for the flat solutions, in which the effective cosmological constant on the brane is dynamically set to zero.

The bulk action is given in (1.4.2) whereas the brane action is

$$S_{brane} = M_P^{d-1} \int d^d x \sqrt{-\gamma} \left(-W_B(\varphi) - \frac{1}{2} Z(\varphi) \gamma^{\mu\nu} \partial_\mu \varphi \partial_\nu \varphi + U(\varphi) R_B \right) . \tag{5.2.2}$$

The framework above was considered in [7] as a way to describe, in a gravity dual language, the interaction between weakly coupled physics (e.g. the Standard Model) localized on the brane, and a strongly coupled, large N CFT, described by the bulk geometry. In this context, the functions $W_B(\varphi), Z(\varphi)$ and $U(\varphi)$ may be thought as generated by integrating out the brane-localized fields. In particular the function $W_B(\varphi)$ contains contributions from the brane vacuum energy.

It was shown in [7] that, rather generically, this kind of models allow self-tuning solutions, in which the brane geometry is flat, regardless of the value of the brane vacuum energy. In that work, the bulk geometry enjoyed four-dimensional Poincaré invariance of constant-u hypersurfaces, which was inherited by the brane.

In this chapter, we will move beyond flat brane solutions, and ask the question, what kind of non-trivial brane geometries one can obtain within the same framework. After some general considerations, we will then restrict our attention to *constant curvature* brane geometries, i.e. either de Sitter or Anti-de Sitter. We will not study the most general solution of the model specified by the action (5.2.1), but we will restrict to situations in which the bulk is static, leaving more general time-dependent geometries for future work.

The simplest possibility to move in this direction is to look for a solution in which the curvature is due solely to the embedding of the brane, and the bulk geometry retains its four-dimensional Poincaré invariance. In this ansatz, the boundary conditions (which define the dual CFT data) are the same[5] as those studied in [7]. As we will show in section 5.2.1 however, for generic bulk and brane potentials, no solution of this kind exists. This leads us to generalize the bulk ansatz, in a way described in chapter 2:

$$ds^2 = du^2 + e^{2A(u)} \zeta_{\mu\nu} dx^\mu dx^\nu \ , \tag{5.2.3}$$

where $\zeta_{\mu\nu}$ is the slicing metric.

In general, a co-dimension-one brane configuration preserving space-rotations is described by an embedding of the form[6] $F(u, \tau) = 0$ for some function F,

[5] In the dual CFT language such a solution would constitute an alternative state of the same theory which gave the self-tuning vacuum.

[6] For definiteness, here we focus on a "cosmological" brane, whose induced metric depends non-trivially on the time-coordinate τ. Similar considerations apply a static curved brane, after trading τ for one of the space coordinates.

or more explicitly by giving a trajectory in the holographic direction,

$$u = u_\star(\tau). \tag{5.2.4}$$

The situation considered in [7] was the case of a static, flat brane located at $u = u_\star$ and separating two different geometries (one for $u < u_\star$, one for $u > u_\star$) of the form (5.2.3) with flat slices, $\zeta_{\mu\nu} = \eta_{\mu\nu}$, and different scale factors. Here, we want to look at more general solutions which allow for a *curved* brane.

5.2.1 (No) Curved brane in a flat-sliced bulk

First, we address the question whether a constant curvature brane can be embedded in a flat-sliced bulk, i.e. we take the bulk geometry to be the same as in [7],

$$ds^2 = du^2 + e^{2A(u)}\eta_{\mu\nu}dx^\mu dx^\nu, \quad \varphi = \varphi(u) \tag{5.2.5}$$

but look for a more general brane embedding, specified by a non-trivial function $u_\star(\tau)$. Such a solution would result in a curved "cosmological" brane. The bulk scale factor and scalar field on each side of the brane are a priori different solutions of the the bulk Einstein's equation,

$$(A, \varphi) = \begin{cases} (A_-(u), \varphi_-(u)) & u < u_\star(\tau) \\ \\ (A_+(u), \varphi_+(u)) & u > u_\star(\tau) \end{cases} \tag{5.2.6}$$

Israel's junction conditions then dictate how the left and right solutions must be glued across the brane. The question is whether, for a given bulk theory and a given choice of brane potentials, it is possible to find a non-trivial embedding function such that Israel's junction conditions are satisfied.

In general, the answer is negative: as we show in detail in Appendix L, for generic choices of the brane potentials, no solutions to the junction conditions may be found: for a non-trivial embedding function $u_\star(\tau)$ the junction conditions require that all world-volume terms in the brane action (5.2.2) must vanish[7]. As we discuss in Appendix L, for *special* choices of the brane potentials however, non-trivial solutions may be found. These have the curious property that, although these solutions are exact, there is no backreaction of the brane onto the bulk (*evanescent branes*). For example, if

[7]This may still lead to interesting physics if we can treat the brane as a probe, as is the case in the so called *mirage cosmology* [112, 113]. In this case the trajectory $u_\star(t)$ is determined by extremizing the world-volume action in a fixed background, ignoring the backreaction on the bulk. However this is not our goal here, as we want to keep the backreaction intact.

W_B, U and Z are positive constants, then a de Sitter embedding of the brane exists if the bulk is Poincaré-AdS space-time with constant scalar field. More generally, it may be possible to tune the brane potentials so that a certain FWR embedding is possible in a given bulk solution. These special cases however require the brane potentials to be tuned to specific functions so that the corresponding brane embedding is compatible with the bulk solution. Although this is interesting, this goes against our general philosophy, which consists in taking the bulk and brane data as unrelated and as generic as possible.

Given the result above, we have two possibilities for obtaining a curved brane embedding:

1. We can keep a flat UV metric $\zeta_{\mu\nu} = \eta_{\mu\nu}$ but generalise the bulk ansatz (5.2.3), embedding a non-trivial brane trajectory $u_\star(\tau)$ in a time-dependent bulk of the general form

$$ds^2 = n^2(u,\tau)du^2 + \beta^2(u,\tau)d\tau^2 + \gamma^2(u,\tau)\delta_{ij}dx^i x^j \tag{5.2.7}$$

   We can then impose boundary conditions such that the metric reduces asymptotically to the form

$$ds^2 \simeq du^2 + e^{-\frac{2u}{\ell}}\left[\zeta_{\mu\nu} + \ldots\right]dx^\mu dx^\nu, \qquad u \to -\infty \tag{5.2.8}$$

   with $\zeta_{\mu\nu} = \eta_{\mu\nu}$, with time-dependent corrections entering only at subleading orders.

2. Alternatively, we can study solutions in which the brane is static, and at a fixed position $u = u_\star$, in a static bulk solution like (5.2.3) where each slice is curved. The induced metric on the brane will inherit the curvature of the corresponding constant-u slice. This choice necessarily leads to a near-boundary expansion of the metric like in (5.2.8), with a curved UV metric, which amounts to couple the dual UV CFT to a curved background[8]. Note that this involves different AdS boundary conditions and is therefore not in the same class of solutions as asymptotically flat conditions. However, as we will see in subsection 5.2.4,

[8]The same considerations applies to a more general class of bulk metrics than (5.2.3), of the form

$$ds^2 = du^2 - \beta^2(u)d\tau^2 + a^2(\tau)\gamma_{ij}(u)dx^i dx^j. \tag{5.2.9}$$

These metrics have the property that any surface at $u = u_\star$ has a fixed FRW geometry, which can be brought in standard form after a world-volume coordinate transformation acting on (τ, x_i). However different constant-u slices differ by more than just an overall rescaling. One can easily show that, also in this case, the near-boundary expansion leads to a non-trivial time-dependent UV metric.

it is possible to rewrite these solutions in terms of a flat space CFT, which however is coupled to time- or space-dependent external sources.

In the rest of this chapter we will explore the second option, and embed the brane as a static hypersurface in a bulk metric of the form (5.2.3), where $\zeta_{\mu\nu}$ is identified with the metric of the dual UV CFT. However these solutions are not unrelated to the first option described above: as we will discuss in more detail in section 5.2.4, a coordinate transformation can bring a solution of the form (5.2.3) to one of the form (5.2.7) with flat asymptotic conditions, at the cost of introducing a time- or space-dependence in the scalar field at leading order in the near-boundary expansion. In the holographic dual language, this situation describes a CFT living on flat space, but driven by a varying scalar source.

5.2.2 The junction conditions

We are now in the position to introduce the brane as an interface between two geometries of the form (5.2.3). The dynamics of the brane is encoded in the junction conditions, as we explain below.

We consider solutions where the geometry to one side of the brane connects to an UV-type region, and the other to an IR-type region. To distinguish between the two sides, we label the metric and scalar field on the two sides of the brane by g_{ab}^{UV}, g_{ab}^{IR} and $\varphi^{UV}, \varphi^{IR}$. When a quantity X exhibits a jump across the position of the brane, this will be written as $\big[X\big]_{IR}^{UV}$. The Israel matching conditions then result in the following two requirements:

1. The metric and scalar field are continuous across the brane:

$$\Big[g_{ab}\Big]_{IR}^{UV} = 0\,, \qquad \Big[\varphi\Big]_{UV}^{IR} = 0\,. \tag{5.2.10}$$

2. The extrinsic curvature as well as the normal derivative of φ are discontinuous:

$$\Big[K_{\mu\nu} - \gamma_{\mu\nu}K\Big]_{UV}^{IR} = \frac{1}{\sqrt{-\gamma}}\frac{\delta S_{brane}}{\delta\gamma^{\mu\nu}}, \qquad \Big[n^a\partial_a\varphi\Big]_{UV}^{IR} = -\frac{1}{\sqrt{-\gamma}}\frac{\delta S_{brane}}{\delta\varphi}. \tag{5.2.11}$$

Here $\gamma_{\mu\nu} = e^{2A(u)}\zeta_{\mu\nu}$ is the induced metric, $K_{\mu\nu}$ is the extrinsic curvature of the brane with $K = \gamma^{\mu\nu}K_{\mu\nu}$ the trace, and n^a is a unit vector normal to the brane with orientation towards the IR.

For our setup given in (5.2.2) the equations (5.2.11) become

$$\Big[K_{\mu\nu}-\gamma_{\mu\nu}K\Big]^{IR}_{UV}=\bigg[\frac{1}{2}W_B(\varphi)\gamma_{\mu\nu}+U(\varphi)G^B_{\mu\nu}-\frac{1}{2}Z(\varphi)\partial_\mu\varphi\partial_\nu\varphi \\ +\frac{1}{4}Z(\varphi)\gamma_{\mu\nu}(\partial\varphi)^2+\left(\gamma_{\mu\nu}\gamma^{\rho\sigma}\nabla_\rho\nabla_\sigma-\nabla_\mu\nabla_\nu\right)U(\varphi)\bigg]_{\varphi_\star}, \tag{5.2.12}$$

$$\Big[n^a\partial_a\varphi\Big]^{IR}_{UV}=\left[\frac{dW_B}{d\varphi}-\frac{dU}{d\varphi}R_B+\frac{1}{2}\frac{dZ}{d\varphi}(\partial\varphi)^2-\frac{1}{\sqrt{-\gamma}}\partial_\mu\left(Z\sqrt{-\gamma}\gamma^{\mu\nu}\partial_\nu\varphi\right)\right]_{\varphi_\star}, \tag{5.2.13}$$

where ∇_μ, $G^B_{\mu\nu}$ and R_B are the covariant derivative, Einstein tensor and Ricci scalar computed from the induced metric and $\varphi_\star(x^\mu)\equiv\varphi(u_\star,x^\mu)$ is the scalar field at the position of the brane. Furthermore, for our setting we find:

$$K_{\mu\nu}=\dot{A}\gamma_{\mu\nu},\qquad K_{\mu\nu}-\gamma_{\mu\nu}K=-(d-1)\dot{A}\gamma_{\mu\nu}=\frac{1}{2}W\gamma_{\mu\nu},\qquad n^a\partial_a\varphi=\dot{\varphi}=S\,. \tag{5.2.14}$$

From the induced metric on the brane $\gamma_{\mu\nu}=e^{2A}\zeta_{\mu\nu}$, we find that $R^B_{\mu\nu}=R^{(\zeta)}_{\mu\nu}$ and $R_B=e^{-2A}R^{(\zeta)}$, where $R^{(\zeta)}$ is the slicing curvature associated with the metric $\zeta_{\mu\nu}$. Hence

$$G^B_{\mu\nu}=G^\zeta_{\mu\nu}=\frac{1}{2}(2-d)\kappa\,e^{-2A}\gamma_{\mu\nu}=\frac{2-d}{2d}\,T\gamma_{\mu\nu}\,, \tag{5.2.15}$$

where we have used the definitions (2.2.1)–(2.2.3). We introduce W_{UV},S_{UV} and W_{IR},S_{IR} as the functions W and S for the UV and the IR regions, respectively. Using these quantities we can then write the junction conditions (5.2.12)–(5.2.13) as:

$$W_{IR}-W_{UV}\big|_{\varphi_*}=W_B+\frac{(2-d)}{d}\,U\,T\bigg|_{\varphi_\star}, \tag{5.2.16}$$

$$S_{IR}-S_{UV}\big|_{\varphi_*}=W_B{}'-U'\,T|_{\varphi_\star}\,. \tag{5.2.17}$$

From the continuity of the metric (5.2.10), we can infer that the scale factor is continuous across the brane and the same is true for the function $T(\varphi)$,

$$T_{UV}(\varphi_\star)=T_{IR}(\varphi_\star)\ . \tag{5.2.18}$$

Using the continuity of T and φ across the brane, it follows from (2.2.5) that

$$\frac{d}{2(d-1)}W^2_{UV}-S^2_{UV}\Big|_{\varphi_\star}=\frac{d}{2(d-1)}W^2_{IR}-S^2_{IR}\Big|_{\varphi_\star} \tag{5.2.19}$$

We can write the conditions (5.2.16)–(5.2.17) as

$$W_{UV}|_{\varphi_*} = W_{IR} - W_B - \frac{2-d}{d} U T_{IR}\Big|_{\varphi_\star} \tag{5.2.20}$$

$$S_{UV}|_{\varphi_*} = S_{IR} - W_B' + U' T_{IR}|_{\varphi_\star} \ . \tag{5.2.21}$$

From the equation of motion we can write

$$Q^2 W_{UV}^2 - S_{UV}^2 - 2T_{UV} + 2V = 0 \tag{5.2.22}$$

where $Q^2 = \frac{d}{2(d-1)}$. Using eqs. (5.2.20)–(5.2.21) and using the fact that T and φ are continuous, we can express everything in terms of IR quantities. Using also $Q^2 W_{IR}^2 - S_{IR}^2 - 2T_{IR} + 2V = 0$ and after a bit of algebra we obtain the condition:

$$\Bigg[-2Q^2 W_{IR}\left(W_B + \frac{2-d}{d} U T_{IR}\right) + Q^2 \left(W_B + \frac{2-d}{d} U T_{IR}\right)^2 + 2S_{IR}\left(W_B' - U' T_{IR}\right) - \left(W_B' - U' T_{IR}\right)^2 \Bigg]_{\varphi_\star} = 0 \ . \tag{5.2.23}$$

Notice that all functions of φ involved in this equation are in principle known, in terms of a few input quantities: V, W_B and U are fixed by the choice of the action; W_{IR}, S_{IR} and T_{IR} are determined by regularity, plus the choice of the endpoint φ_0 of the IR solution. Therefore, once the underlying model and φ_0 are chosen, (5.2.23) provides a transcendental equation for the brane position $\varphi_\star$, which generically has a finite number of solutions (including the possibility of no solution).

Once $\varphi_\star$ is determined, we can use equations (5.2.20)–(5.2.21) as initial conditions for W_{UV} and S_{UV}, to be used in the system of differential equations (2.2.7)–(2.2.8) which determines the solution for W and S in the UV and the corresponding values of $\mathcal{R}$ and C (the dimensionless curvature and vev parameters).

To summarize, one can use the following algorithmic procedure to solve the system from the IR, across the brane, to the UV:

$$\text{choice of } \varphi_0 \ \to \ W_{IR}, S_{IR} \ \to \ \varphi_\star \ \to \ W_{UV}, S_{UV} \ \to \ \mathcal{R}, C \tag{5.2.24}$$

The only control parameter here is φ_0, which determines everything else. In particular, the choice of φ_0 at an IR extremum of the potential would result in the flat-sliced solution with $\mathcal{R} = 0$. For the case when the flat solution IR is reached as $\varphi \to \infty$, things are more subtle, as we will see in section 5.3.

5.2.3 Junction rules

Here we discuss what are the geometric rules to patch together two geometries across the brane, and which types of junctions give rise to a sensible holographic interpretation.

In the positive or zero curvature case, the flow of $A(u)$ is monotonically decreasing from the UV to the IR. Since $\dot{A} \propto -W$, the scalar function $W(\varphi)$ cannot change sign.[9] At the junction, we must require that one side of the brane actually connects to a UV region, and the other to an IR region. This implies that the flow of $A(u)$ must not change direction, i.e. $\dot{A}$ should not change sign, across the brane. Since at the brane position $\dot{A}_{UV} \propto -W_{UV}(\varphi_\star)$ and $\dot{A}_{IR} \propto -W_{IR}(\varphi_\star)$, we must discard solutions in which $W_{UV}(\varphi_\star)$ and $W_{IR}(\varphi_\star)$ have opposite signs. If that were the case, we would be joining two UV or two IR regions.

The above constraint does not apply to solutions with negatively curved slices: in this case $\dot{A}$ (and W) can change sign in the bulk, and there is no reason why it should not change sign across the brane. In fact, in this case, both sides of the brane eventually reach a UV region.

Next, since we will solve the matching conditions in field space, rather than in coordinate space, we need to understand towards which side (i.e. direction of increasing or decreasing φ away from $\varphi_\star$) one should follow the solution $W_{UV}(\varphi)$ on the UV side of the brane. As we discussed at the end of the previous subsection, if we start from the IR side of the solution, the junction conditions determine the pair of initial conditions $(S_{UV}(\varphi_\star), W_{UV}(\varphi_\star))$ for the system (5.2.20)–(5.2.21), and we need to know if we should keep the solution for $\varphi > \varphi_\star$ or $\varphi < \varphi_\star$. To understand what the correct choice is, recall that in our conventions the coordinate u runs in the same direction on both sides of the brane, and we take it to be increasing from the UV to the IR. Therefore if the brane is at $u_\star$, the IR side is $u > u_\star$, and the UV side is $u < u_\star$. Then, to be consistent with this choice, it is the sign of $\dot{\varphi}(u_\star) \equiv S_{UV}(\varphi_\star)$ which decides which one is the right direction to follow on the UV side:

- If $S_{UV}(\varphi_\star) > 0$, then $\dot{\varphi}(u_\star) > 0$ at the brane, and we should take the UV solution such that φ increases towards the brane, i.e. the solution W_{UV}, S_{UV} for $\varphi_{UV} < \varphi_\star$.

- Conversely, if $S_{UV}(\varphi_\star) < 0$, we should take the other part of the solution, the one with $\varphi_{UV} > \varphi_\star$.

This junction rule is summarized graphically in figure 5.2.

[9] Since the overall sign of W can be changed by sending $u \to -u$, we will always choose

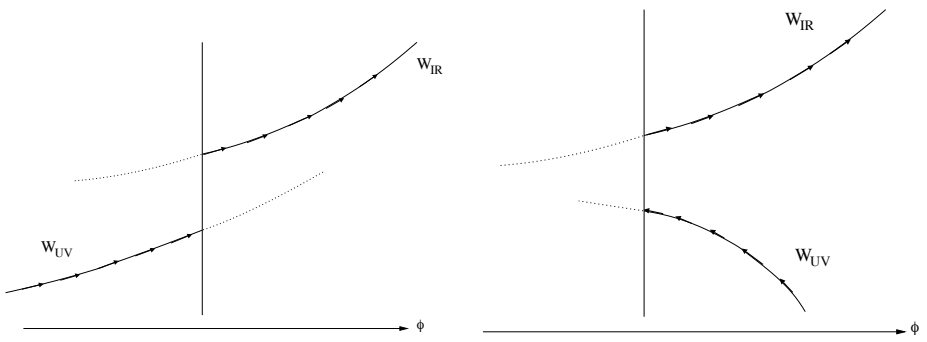

$S_{UV}(\varphi_\star) > 0$ $S_{UV}(\varphi_\star) < 0$

Figure 5.2: Junction rules in field space. The vertical solid line indicates the locus of the brane.

Finally, due to stability requirements of the solution, some care is needed when choosing the combination of bulk and brane potentials appearing in the action. Because we will not pursue phenomenological applications here, and in general we will not worry about whether the functions chosen can lead to physics compatible with observation (e.g. the presence of four-dimensional gravity in the brane), we will try to require that at least the flat solutions be free of ghosts and tachyonic instabilities. Although this does not straightforwardly guarantee stability of the curved solutions, there are strong indications that this is the case, at least for the positive curvature solutions, as discussed in section 4.5 of [8].

That there are no instabilities in the bulk is automatically guaranteed if the scalar field kinetic term has the correct sign, and there are no violations of the BF bound in the UV or in the IR. However, some unstable modes can still arise due to the brane fluctuations. For the flat case, the analysis of [7] showed that there are very simple *sufficient* conditions which guarantee the absence of ghosts and tachyonic instabilities for the self-tuning flat brane solutions. These are:

$$U(\varphi_\star) > 0, \qquad Z(\varphi_\star) > 0 \tag{5.2.25}$$

$$\frac{W_B(\varphi_\star)}{W_{IR}(\varphi_\star)W_{UV}(\varphi_\star)} > \frac{U(\varphi_\star)}{3}, \tag{5.2.26}$$

$$Z(\varphi_\star)\left(\frac{W_B(\varphi_\star)}{W_{IR}(\varphi_\star)W_{UV}(\varphi_\star)} - \frac{U(\varphi_\star)}{3}\right) > \left(\frac{dU}{d\varphi}\right)^2_{\varphi_\star}, \tag{5.2.27}$$

$W > 0$ for definiteness.

$$W''_{IR}(\varphi_\star) - W''_{UV}(\varphi_\star) < W''_B(\varphi_\star). \tag{5.2.28}$$

Conditions (5.2.25) are also *necessary*: violating either of them would guarantee the presence of either a spin-2 or a spin-0 ghost. On the other hand, the other conditions are only sufficient, but if they are violated the stability analysis becomes much more involved, and requires a detailed perturbation analysis of the full bulk solution.

Since here we will not aim to build explicit, realistic phenomenological models, we will not always strictly enforce the conditions (5.2.26)–(5.2.28), not to limit too much the scope of the examples we study.

5.2.4 Curved CFT boundary metrics vs. variable scalar sources

In this section we briefly comment on a possible alternative realisation of the solutions described so far, in terms of a dual CFT living in *Minkowski* space, but coupled to a non-trivial time-dependent (for dS branes) or space-dependent (for AdS) external source.

In the UV region, the bulk metric (5.2.3) takes the asymptotic form (5.2.8), where $\zeta_{\mu\nu}$ is the metric to which the dual CFT is coupled, and in the examples described above is (A)dS$_d$. It is well known (see e.g. [59]) that one can foliate AdS$_{d+1}$ by either Minkowski, dS$_d$ or AdS$_d$. From the bulk point of view, these choices only differ by a coordinate transformation. From the dual field theory point of view, however, different coordinate choices lead to different physical theories, as the appropriate coordinate transformation acts non-trivially on the conformal boundary and it changes both the metric and the scalar sources.[10] Therefore, we can use these coordinate transformations to find new solutions with a different holographic interpretation. In the rest of this section we consider the case of a dS brane for definiteness.

Let us therefore consider dS-sliced domain walls. Going from a curved to a flat foliation by a coordinate transformation is only possible if the bulk is *exactly* AdS$_{d+1}$, not only asymptotically. However, we can still perform a coordinate transformation to new radial and time coordinates (ρ, t) of the form

$$u = f(\rho, t), \qquad \tau = g(\rho, t), \tag{5.2.29}$$

such that close to the UV boundary it changes a dS slicing into a flat one. If we take τ to be the conformal time coordinate in the de Sitter metric ansatz,

[10] A well-known example of this phenomenon is the difference between global and Poincaré AdS coordinates, which give a different structure of the conformal boundary metric and describe a dual field theory on $R \times S^{d-1}$, and $R^{1,d-1}$, respectively.

i.e. $\zeta_{\mu\nu} = \frac{H^2}{\tau^2}\eta_{\mu\nu}$, f and g can be two arbitrary smooth functions constrained only by demanding that their asymptotic form leads to a flat UV metric in the new coordinates (ρ, t), $\zeta_{\mu\nu} = \eta_{\mu\nu}$, in the limit $u \to -\infty$. This imposes the following constraints,

$$f(\rho,t) \to \rho - \ell \ln\left(-\frac{t}{\ell}\right), \qquad g(\rho,t) \to t, \qquad \rho \to -\infty, \tag{5.2.30}$$

where $-\infty < t < 0$ (see e.g. section 4.4 of [8] for the full coordinate transformation, from which the limits (5.2.30) can be easily obtained).

In the original coordinates (u, τ) the brane was located at the equilibrium position $u = u_\star$. In the new coordinates this will result in a non-trivial trajectory,

$$f(\rho,t) = u_\star \quad \Rightarrow \quad \rho = \rho_\star(t). \tag{5.2.31}$$

The important point is that, by construction,

1. The junction conditions are still satisfied, since they have tensorial nature;

2. The induced metric on the brane is diffeomorphic to the original one before the change of coordinates.

This implies that we have an alternative embedding of the same dS brane, which is now moving in an asymptotically AdS space-time whose asymptotic boundary has a flat metric source. The dual field theory lives therefore in flat space.

This is not the end of the story however: recall that the bulk has also a non-trivial scalar field profile. In the old coordinates (u, τ) this is described by a function $\varphi(u)$, which becomes a time-dependent function $\varphi(\rho, t)$ in the new coordinates. This has an important implication: writing the near-boundary scalar field asymptotics (2.4.10) in the new coordinates using (5.2.30), we find

$$\varphi(\rho,t) \simeq \varphi_- \left(\frac{\ell}{|t|}\right)^{\Delta_-} \ell^{\Delta_-} e^{\Delta_-\rho/\ell} + \dots \qquad \rho \to -\infty. \tag{5.2.32}$$

In the holographic dictionary, this implies that the CFT is coupled to a *time-dependent* external source

$$j = \left(\frac{\ell}{|t|}\right)^{\Delta_-} \varphi_- \tag{5.2.33}$$

The source is switched on from $j = 0$ at early times and increases in time as a power-law. Thus, in this language, cosmological de Sitter expansion of the

brane is driven by a time-dependent source in a flat-space CFT. This gives an alternative (and, from the CFT standpoint, inequivalent) description of the solutions we are discussing.

Notice that the only case in which one can embed a dS brane in a flat CFT with no sources is the Karch-Randall-like setup, where the bulk is AdS (in any coordinates), with no scalar field. In this case a non-zero brane tension and/or induced Einstein term generically require patching together two AdS spaces with different curvatures, as was the case in [114, 115, 116].

5.3 IR exponential potential

We now present implementations of the self-stabilisation mechanism in one example model characterized by an infinite range of the bulk field φ. Other models with a IR fixed point are discussed in [10]. Here and in what follows we set $d = 4$. A particular model will be characterised by a choice of bulk potential $V(\varphi)$ and the brane quantities $W_B(\varphi)$ and $U(\varphi)$. While the functions V, W_B and U should be determined from a microscopic model, this goes beyond the scope of this analysis. Instead, the functions will be chosen by hand and the consequences for self-stabilisation studied. Also, we will not be interested in constructing phenomenologically viable models, as this also goes beyond the scope of this investigation. The main goal of this section is to study the viability and efficacy of self-stabilisation in this holographic setting with non-zero UV curvature. In particular, we wish to answer the following questions:

1. How do self-stabilising solutions with non-zero UV curvature differ from the self-tuning solutions with vanishing UV curvature studied in [7]?

2. How does the brane curvature R_B depend on the UV curvature $R^{(\zeta)}$? E.g. can R_B be small while $R^{(\zeta)}$ is large (in suitable units) and vice versa.

3. Can the brane curvature R_B be small in units of the 4d Planck mass M_4 on the brane without the need of tuning of model parameters?

To be specific, we choose:

$$V(\varphi) = \frac{1}{\ell^2}\left[-12 - \varphi^2\left(\frac{1}{2}\Delta(4-\Delta) - \frac{b^2}{4}\right) - V_1 \sinh^2\left(\frac{b\varphi}{2}\right)\right], \qquad (5.3.1)$$

with $2 < \Delta < 4$ and $V_1 > 0$ and b another (dimensionless) parameter. We will set $\ell = 1$ in the following. The maximum of V is at $\varphi_{\max} = 0$, which, in

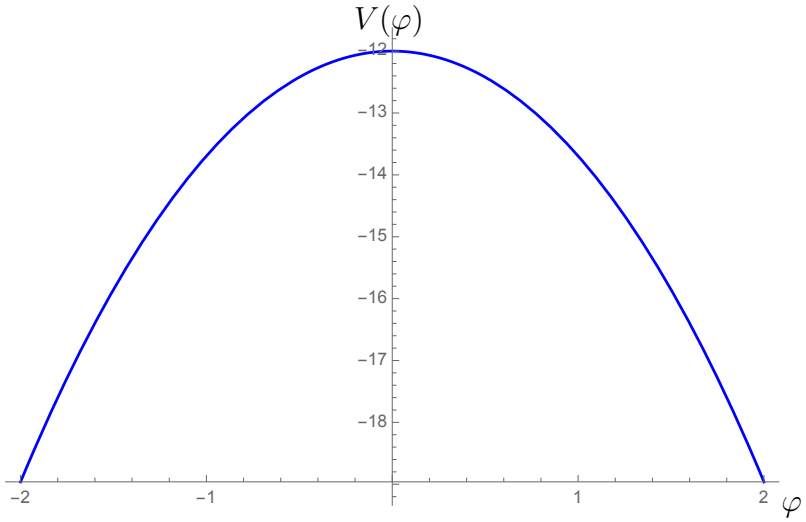

Figure 5.3: The bulk potential (5.3.1) with $\Delta = 2.8$, $\ell = 1$ and $b = 1.2\sqrt{\frac{2}{3}}$.

the language of holographic RG flows, is a UV fixed point with corresponding UV CFT. In this framework the parameter Δ is interpreted as the dimension of the operator perturbing this UV CFT. However, as there are no minima the IR is only reached for $|\varphi| \to \infty$. A plot of this potential is displayed in Fig. 5.3. One reason for choosing a potential with unlimited range in φ is as follows. In [7], for the case of a flat brane, it was observed that bulk potentials with a finite range for φ do not easily exhibit self-tuning solutions satisfying the stability criterion (5.2.26), at least not without some fine-tuning of parameters. However, for potentials with infinite range in φ this difficulty can be overcome, as was shown for the case of a flat brane in [7] using an example based on bulk potential (5.3.1).

To allow comparisons with the results in [7] we choose a brane potential with the same mathematical form. Hence we will work with the following brane quantities:

$$W_B(\varphi) = \Lambda^4 \left[-1 - \frac{\varphi}{s} + \left(\frac{\varphi}{s}\right)^2 \right], \qquad U(\varphi) = const\,, \tag{5.3.2}$$

where Λ and s are numerical parameters (as we have set $\ell = 1$). The brane potential is chosen such that it has at least one zero for $\varphi > 0$. The position of the zero is controlled by s. Again, absent any prior knowledge regarding $U(\varphi)$ we take it to be constant for simplicity.

5.3.1 Analytical results

Before moving on to numerical studies, we collect analytical results for the asymptotic region $\varphi \to \infty$. Note that apart from a region in the vicinity of $\varphi_{\max} = 0$ the potential is well-approximated by an exponential. As a result, an analytical understanding of solutions for an exponential potential will turn out to be very helpful for the interpretation of our numerical findings.

Therefore, we collect analytical solutions for an exactly exponential bulk potential. To be specific, we will consider

$$V = -V_\infty \exp(b\varphi) \,, \tag{5.3.3}$$

which is the asymptotic form of (5.3.1) for $\varphi \to \infty$ if we identify $V_\infty = V_1/4$. For $\varphi \to \infty$ the bulk solutions fall into three classes.

1. **Continuous branch**:
   For one there exists a family of solutions of the form

   $$W \simeq W_0\, e^{Q\varphi} \,, \quad S \simeq W' \,, \quad T \simeq T_0\, e^{Q\varphi} \,, \quad \text{where} \quad Q = \sqrt{\frac{2}{3}} \,. \tag{5.3.4}$$

   In this case W_0 and T_0 are free parameters. The existence of this branch of solutions requires

   $$b < 2Q = 2\sqrt{\frac{2}{3}} \,. \tag{5.3.5}$$

   This branch also exists for flat solutions (albeit with $T_0 = 0$) . For $\varphi \to \infty$ these solutions exhibit an unacceptable singularity according to Gubser's criterion [107]. For more details on this class of solutions see e.g. [5].

2. **A special solution with $S = W'$**:
   There exists an isolated solution of the form

   $$W = W_0\, e^{b\varphi/2} \,, \quad S = W' \,, \quad T = 0 \,, \quad \text{with} \quad W_0 = \sqrt{\frac{8V_\infty}{4Q^2 - b^2}} \,, \tag{5.3.6}$$

   with Q defined as in (5.3.4). Again, this solution only exists for

   $$b < 2Q = 2\sqrt{\frac{2}{3}} \,. \tag{5.3.7}$$

   This is the special flat solution satisfying Gubser's criterion, giving rise to an acceptable IR singularity.

3. **A special solution with $S = W/(3b)$:**
Finally, the equations of motion (2.2.4)–(2.2.6) also admit the solution

$$W = W_0\, e^{b\varphi/2}, \quad S = \frac{W}{3b}\,, \quad T = T_0\, e^{b\varphi}\,, \tag{5.3.8}$$
$$\text{with} \quad W_0 = \sqrt{6V_\infty}\,, \quad T_0 = \left[2b^2 - \frac{4}{3}\right] V_\infty\,.$$

This solution exists for any value of b, but we observe that the sign of the function T depends on b as follows:

$$b > \sqrt{\frac{2}{3}} \quad \Leftrightarrow \quad T > 0\,,$$
$$b < \sqrt{\frac{2}{3}} \quad \Leftrightarrow \quad T < 0\,,$$
$$b = \sqrt{\frac{2}{3}} \quad \Leftrightarrow \quad T = 0\,.$$

For $b^2 = 2/3$ the solution of type 3 discussed and the one of type 2 discussed above are identical.

Here we see that non-zero curvature gives rise to a new solution reaching the asymptotic IR region $\varphi \to +\infty$, for which $W(\varphi)$ has the same exponential growth but different overall magnitude as the special, flat solution, and for which $S \neq W'$. Depending on the value of b these solution are found either for $R > 0$ only, or for $R < 0$ only.

Intriguingly, the critical value separating these cases, $b = \sqrt{2/3}$, is the same which separates confining from non-confining theories. This may signal interesting consequences in regards to confining holographic theories on curved manifolds, whose analysis we leave for further investigation.

5.3.2 Numerical studies

We now return to a study of the model with the full bulk potential (5.3.1) and brane quantities (5.3.2). In particular, we now solve numerically for solutions of the bulk-brane system. For definiteness, we will choose the following values for the parameters:

$$\Delta = 2.9\,, \quad \Lambda = 3\,, \quad s = 8\,, \quad V_1 = 1\,, \quad U = 10^{-4}\,, \tag{5.3.9}$$

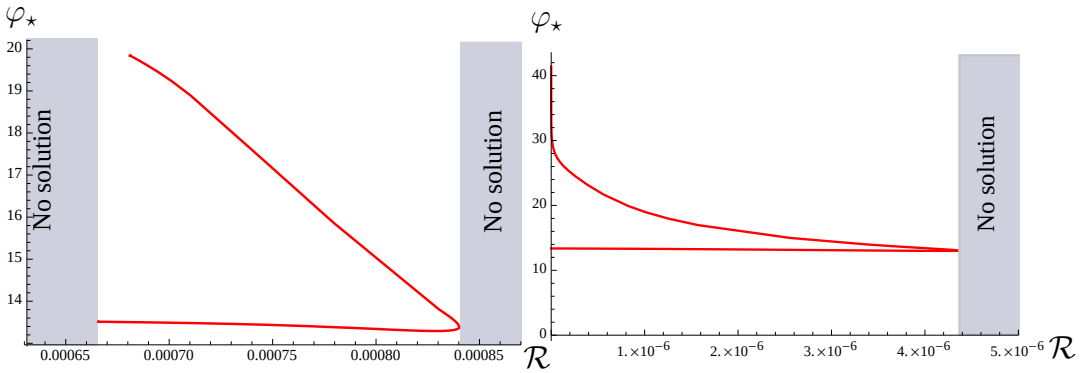

(a) (b)

Figure 5.4: Equilibrium brane position $\varphi_\star$ vs. $\mathcal{R}$ for $\mathcal{R} > 0$. Results are obtained for bulk potential (5.3.1), brane quantities (5.3.2) and parameter values (5.3.9). The left figure (a) is for $b = 1.1 \times \sqrt{2/3}$ and the right figure (b) is for $b = 0.9 \times \sqrt{2/3}$.

but these values are in no way special. However, a small numerical value for U will turn out to be favourable for satisfying the stability criteria (5.2.26) and (5.2.27). We then perform the analysis for two different values of b. In particular, we will study the cases

$$b = 1.1\sqrt{2/3} \quad \text{and} \quad b = 0.9\sqrt{2/3}\,. \tag{5.3.10}$$

We will restrict our analysis to solutions with positive UV curvature $\mathcal{R} > 0$, as this will exhibit all the phenomena that we wish to illustrate with this example. In fig. 5.4 we show the space of solutions by plotting the equilibrium brane position $\varphi_\star$ vs. $\mathcal{R}$. In fig. 5.4a we show the results for $b = 1.1\sqrt{2/3}$ while the results for $b = 0.9\sqrt{2/3}$ are displayed in fig. 5.4b.

One common observation for both values of b is that solutions only exist for a very narrow range in $\mathcal{R}$. In particular, we find that solutions only exist for the following values of $\mathcal{R}$:

$$\begin{aligned} b = 1.1\sqrt{2/3}: &\quad \text{solutions exist for} \quad 0.00066 \lesssim \mathcal{R} \lesssim 0.00084 \quad \text{and} \quad \mathcal{R} = 0\,, \\ b = 0.9\sqrt{2/3}: &\quad \text{solutions exist for} \quad 0 \leq \mathcal{R} \lesssim 4.5 \cdot 10^{-6}\,. \end{aligned}$$

That is, for $b = 0.9\sqrt{2/3}$ we only find solutions with very small absolute values of $\mathcal{R}$. For $b = 1.1\sqrt{2/3}$ solutions with finite $\mathcal{R}$ can only exist in a very narrow band of width $\Delta\mathcal{R} \sim 2 \cdot 10^{-4}$ about the central value $\mathcal{R} \sim 7.5 \cdot 10^{-4}$.[11]

[11] Here we collect further, but less important observations. For one, we find that there are typically two solutions for the equilibrium position $\varphi_\star$ if $\mathcal{R}$ permits a solution. Also, for completeness, note that for $\mathcal{R} \to 0$ the lower branch in fig. 5.4b is continuously connected to a solution with $\mathcal{R} = 0$, whereas this is not the case for the upper branch.

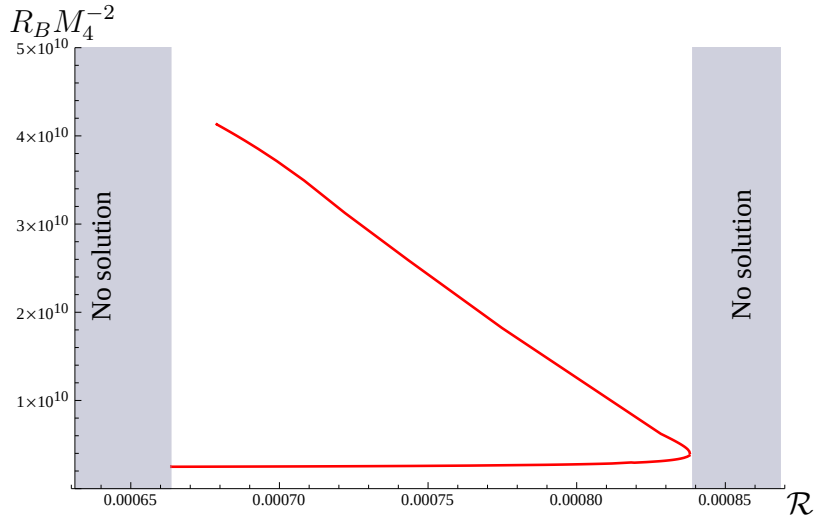

Figure 5.5: The brane curvature $R_B M_4^{-2}$ vs. $\mathcal{R}$ for $b = 1.1 \times \sqrt{2/3}$. Results are obtained for bulk potential (5.3.1), brane quantities (5.3.2) and parameter values (5.3.9).

We can understand all these observations with the help of the analytical results collected in the previous section. To this end note that, for all the solutions, the brane finds it equilibrium position at a value of φ where the bulk potential is well approximated by an exponential.[12] As a result, immediately to the left and the right of the brane the bulk solutions will, at leading order, be given by the solutions collected in section 5.3.1. More precisely, as the potential is not exactly exponential, the solutions in the full potential will be given by those in sec. 5.3.1 up to some small corrections. With this we can explain the results in fig. 5.4 as follows.

- On the IR side of the brane all solutions for $b = 1.1\sqrt{2/3}$ are small perturbations of the special solution of type $S = W/(3b)$ (case 3) in the classification of sec. 5.3.1. As this is a unique solution only a small subset of solution leaving the UV fixed point will asymptote to this solution. This explains the narrow range in $\mathcal{R}$ for which solutions exist. In addition, for $b = 1.1\sqrt{2/3}$ this type of solution has $T \neq 0$, which implies that $\mathcal{R} \neq 0$. Hence we do not expect these solutions to exist for arbitrarily small values of $\mathcal{R}$, which is exactly what we observe. In

[12]Note from fig. 5.4 that for all the solutions obtained the brane equilibrium position takes values $\varphi_\star \gtrsim 13$. There the bulk potential is well-approximated by

$$V = -\frac{V_1}{4} e^{b\varphi} \left(1 + \mathcal{O}(\varphi^2 e^{-b\varphi})\right).$$

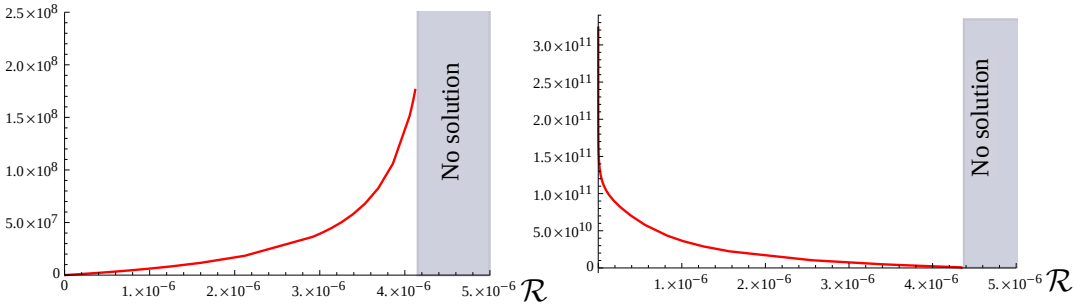

Figure 5.6: The brane curvature $R_B M_4^{-2}$ vs. $\mathcal{R}$ for $b = 0.9 \times \sqrt{2/3}$. Results are obtained for bulk potential (5.3.1), brane quantities (5.3.2) and parameter values (5.3.9). The plots (a) and (b) exhibit results for the two branches of solutions separately.

other words, there is a gap in solutions for $\mathcal{R} > 0$.

- In contrast for $b = 0.9\sqrt{2/3}$ the solutions on the IR side of the brane are small perturbations of the special solution of type $S = W'$ (case 2) in the classification of sec. 5.3.1.[13] Note that this type of solution has $T = 0$ exactly, which would imply $\mathcal{R} = 0$. Since the potential is not exactly exponential, the solutions are only approximately of type 2 and finite but small values of $\mathcal{R}$ are allowed. This is exactly what we observe in fig. 5.4.

Next, we study the brane curvature across our space of solutions. For $b = 1.1\sqrt{2/3}$ we plot $R_B M_4^{-2}$ vs. $\mathcal{R}$ in fig. 5.5. The main observation is that, unless $\mathcal{R} = 0$, the brane curvature R_B is always finite and never small. (In fact, for our unrealistic choice of brane parameters it is also extremely super-Planckian.) There is no continuous limit where $R_B M_4^{-2} \to 0$.

For $b = 0.9\sqrt{2/3}$ the findings are qualitatively different. We display the corresponding results for $R_B M_4^{-2}$ vs. $\mathcal{R}$ in fig. 5.6. In particular, in fig. 5.6a we show results for the lower branch in fig. 5.4a, while fig. 5.6b contains the data for the upper branch of fig. 5.4a. Most importantly, the lower branch exhibits a limit $R_B \to 0$ for $\mathcal{R} \to 0$ which is continuously connected to a solution with $R_B = 0$ and $\mathcal{R} = 0$. On the other branch of solutions (fig. 5.6b) R_B is never zero and potentially diverges for $\mathcal{R} \to 0$.[14]

[13] For $b = 0.9\sqrt{2/3}$ solutions of type 3 have $T < 0$ and hence $\mathcal{R} < 0$. As we restrict our attention to configurations with $\mathcal{R} > 0$ we cannot find solutions of type 3 for $b = 0.9\sqrt{2/3}$.

[14] We could not determine this decisively in our numerical analysis. While we observe that both $\varphi_\star$ and $R_B M_4^{-2}$ increase on this branch when $\mathcal{R}$ is decreased, we can neither

Last, we comment on the stability of the solutions obtained here. In [7] a set of sufficient criteria (5.2.25)–(5.2.28) was derived which guarantee the perturbative stability of a *flat* brane solution. Here we do find a branch which in the limit $\mathcal{R} \to 0$ is connected continuously to a flat brane solution. By an explicit calculation we find that this solution satisfies the stability criteria (5.2.25)–(5.2.27), but not (5.2.28). This is not necessarily fatal, as (5.2.28) is only a sufficient condition for stability. However, a more detailed analysis is necessary to conclusively determine the stability of this solution, which is beyond the scope of this analysis. We further expect the stability properties of the flat solution also to extend to the branch of curved brane solutions connected to the flat solution. The reason is that the solutions exhibit *positive* boundary or brane curvature, which we do not expect to aversely affect stability.

We are now in a position to summarise our findings for the model studied in this section.

1. We find the space of solutions in $\mathcal{R}$ to be highly restricted. The reason is that for large φ for all solutions have to asymptote to one of the two unique solutions. In our case these are the two special solutions for an exponential bulk potential described in sec. 5.3.1. Only a small subset of solutions departing from the UV fixed point will asymptote to such a solution and all lie within a narrow range in $\mathcal{R}$.

2. We again find a branch of solutions that in the limit $\mathcal{R} \to 0$ is connected continuously to a flat brane solution with $\mathcal{R} = 0$ and $R_B = 0$. Here we made sure that flat brane limit satisfies the criteria (5.2.25)–(5.2.27) for perturbative stability. It does not satisfy the sufficient condition (5.2.28).

exclude nor confirm whether this continues for arbitrarily small values of $\mathcal{R}$.

Chapter 6

Conclusions

6.1 Summary of the results

In this thesis, we studied two-derivative Einstein-scalar theory in $(d+1)$-dimensions:

$$S[g,\varphi] = M_P^{d-1} \int du\, d^d x\, \sqrt{|g|} \left(R^{(g)} - \frac{1}{2}\partial_a\varphi\partial^a\varphi - V(\varphi) \right) + S_{GHY} \quad (6.1.1)$$

and considered solutions with a scalar field profile $\varphi = \varphi(u)$ and a metric ansatz given by

$$ds^2 = du^2 + e^{2A(u)}\zeta_{\mu\nu}dx^\mu dx^\nu\,, \quad (6.1.2)$$

where the bulk is foliated by maximally symmetric space-times with positive or negative curvature. With our work, we have extended the systematic analysis of flat RG flows presented in [5]. Via gauge/gravity duality, the ansatz (6.1.2) describes RG flows of field theories defined on manifolds with constant positive curvature (S^d or dS_d, depending on the signature) or constant negative curvature (H^d, AdS_d). In this thesis, we presented two applications of the holographic RG flows on curved manifolds. The main results of these studies are summarized below.

6.1.1 Holographic RG flows on curved manifolds

In chapter 2, we have studied the holographic RG flows on maximally symmetric manifolds. What we have found is as follows.

To make the connection between the bulk geometry and the RG flows, first we defined two independent scalar functions $W(\varphi)$ and $S(\varphi)$ which satisfy:

$$W(\varphi(u)) \equiv -2(d-1)\frac{dA(u)}{du}\,, \qquad S(\varphi(u)) \equiv \frac{d\varphi(u)}{du}\,. \quad (6.1.3)$$

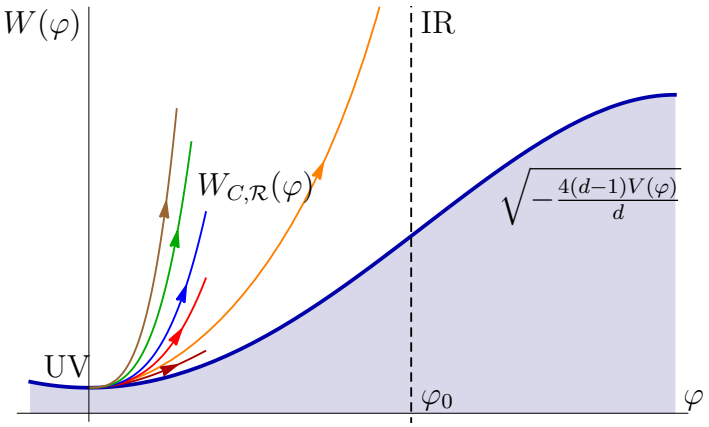

Figure 6.1: Family of solutions $W_{C,\mathcal{R}}(\varphi)$ in the vicinity of a UV fixed point located at a maximum of the potential. For a field theory with a given UV value of the source and fixed R^{uv} only a finite number of these solutions (here only one) can be completed into a flow reaching an IR end point at φ_0. The shaded region below the blue curve is not accessible for $R^{\text{uv}} \geq 0$.

In terms of these functions the equations of motion became a set of non-linear first order differential equations (2.2.7) and (2.2.8). The holographic β-function can be expressed in terms of $W(\varphi)$ and $S(\varphi)$:

$$\beta(\varphi) \equiv \frac{d\varphi}{dA} = -2(d-1)\frac{S(\varphi)}{W(\varphi)}\,. \tag{6.1.4}$$

The holographic RG flows coincide with the space of regular solutions of $W(\varphi)$ and $S(\varphi)$ which depends on the sources of the boundary field theory R^{UV} and φ_-.

It is a well-known result from holography that, when the boundary theory is in flat space, UV fixed points are associated with extrema of the potential V. This persists at finite boundary curvature ($R^{\text{uv}} \neq 0$).

- Maxima of V: For maxima of V, we found solutions describing a relevant deformation away from a UV fixed point. Such solutions came as *two-parameter families* $W_{C,\mathcal{R}}(\varphi)$, $S_{C,\mathcal{R}}(\varphi)$, where C and $\mathcal{R}$ are dimensionless parameters related to the vev of the deforming operator and to the UV value of the scalar curvature R^{uv}, respectively. At most a finite subset of these solutions can be extended to globally regular solutions corresponding to RG flows. This is shown schematically in figure 6.1.

- Minima of V: Flows away from a minimum of V also exist and are driven by the vev of an irrelevant operator [5]. There is only one free

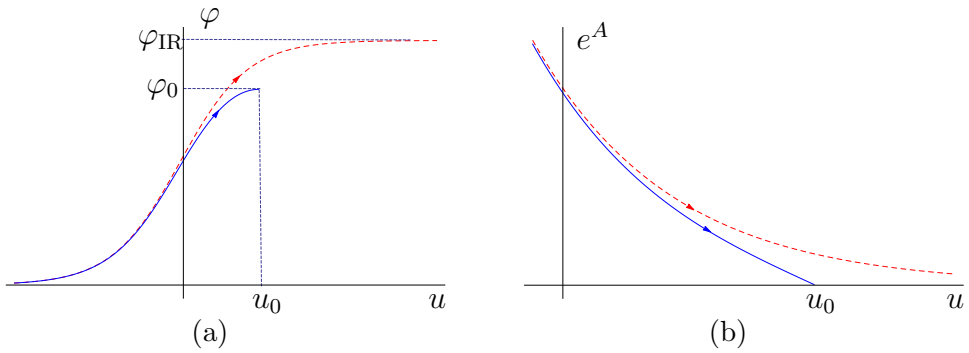

Figure 6.2: The solid lines show the scalar field (left) and scale factor (right) profiles of a positive curvature RG flow geometry, from the UV ($u \to -\infty$, $\varphi \to 0$) to the IR endpoint ($u = u_0$, $\varphi = \varphi_0$). The dashed lines represent the solutions with zero curvature, extending all the way to $u \to +\infty$ and to the IR fixed point at $\varphi = \varphi_{\rm IR}$.

parameter $\mathcal{R}$ related to $R^{\rm uv}$. These solutions are all *badly singular* in generic theories and can only be extended to globally regular solutions in special cases.

The behavior in the innermost region of the geometry (far from the UV boundary) depends on the sign of the curvature $R^{\rm uv}$ of the boundary metric.

- For field theories on manifolds with $R^{\rm uv} > 0$, non-singular flows stop at an IR endpoint, where $e^A \to 0$, φ takes on a finite value φ_0, and $S(\varphi) = \dot{\varphi} = 0$. At the endpoint, the function W diverges as $W \sim |\varphi - \varphi_0|^{-1/2}$. This behavior is shown schematically in figures 6.1 (function W) and 6.2 (scalar field and scale factor). The bulk geometry is regular and becomes approximately AdS_{d+1} when approaching the IR endpoint. An important remark is that, when the field theory curvature is non-vanishing, the IR endpoint *cannot* be located at a minimum of the scalar potential.

- For field theories on manifold with $R^{\rm uv} < 0$, the flow eventually reaches a turning point φ_0 where both $A(u)$ and $\varphi(u)$ invert their direction, but the value of e^A remains finite. These points are characterized by $S(\varphi_0) = W(\varphi_0) = 0$. As u increases past the turning point, the geometry connects back to the boundary of AdS_{d+1}. Therefore, in this case, there is no IR endpoint, but rather an IR "throat" connecting two boundary regions. This behavior is shown schematically in Figure 6.3. This situation was already discussed in [60] in the case of pure gravity. As it was pointed out there, the two UV regions are part of

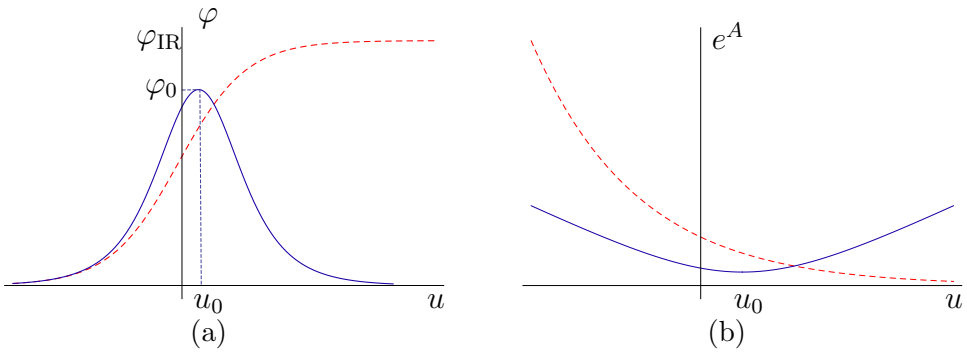

Figure 6.3: The solid lines show the scalar field (left) and scale factor (right) profiles of a negative curvature RG flow geometry, from the left boundary ($u \to -\infty$, $\varphi \to 0$) to the turning point ($u = u_0$, $\varphi = \varphi_0$), to the right boundary ($u \to +\infty$, $\varphi \to 0$). The solution is symmetric around u_0. The dashed lines represent the zero-curvature solution interpolating from the UV boundary to the IR fixed point at $\varphi = \varphi_{IR}$, and featuring a monotonic scale factor.

the same AdS_{d+1} boundary, and are connected via the AdS_d boundary of the codimension-one slices.

In general, any point φ_0 can be an IR end point ($R^{\rm uv} > 0$) or turning point ($R^{\rm uv} < 0$), as long as φ_0 is not an extremum of V. However, for a given curvature $R^{\rm uv}$, and for every value φ_0, there is a unique solution corresponding to a flow ending at φ_0 and connecting to the UV boundary. Such points, for $R^{\rm uv} > 0$, are the fixed points of the flow, where the associated β-function, defined in (6.1.4), vanishes as discussed in section 2.6.2

We have constructed several examples of curved holographic RG flow solutions that start from a UV fixed point at a maximum of the potential, and have a regular interior where the geometry displays the general features described in the previous paragraphs.

The value φ_0 (be it an endpoint or a turning point) for a given regular flow is determined by the values of $R^{\rm uv}$ and φ_- governing the leading UV asymptotics. More precisely, the value φ_0 is completely determined by the dimensionless combination $\mathcal{R} \equiv R^{\rm uv}|\varphi_-|^{2/(d-\Delta)}$, where Δ is the dimension of the dual operator corresponding to φ.

In particular, the following observations hold for generic potentials and either sign of the curvature: *Increasing* $|R^{\rm uv}|$ while keeping the UV source φ_- fixed causes the IR endpoint (or turning point) φ_0 to move closer to the starting point of the flow at the UV maximum. Conversely, *decreasing* $|R^{\rm uv}|$ while keeping the the UV source φ_- fixed causes φ_0 to move away from the starting point of the flows at the UV maximum. For $R^{\rm uv} \to 0$ the IR endpoint

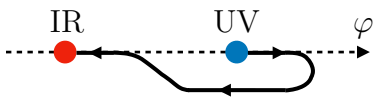

Figure 6.4: Schematic structure of a field theory with an RG flow exhibiting a "bounce".

(or turning point) approaches a minimum of V.

In the simplest RG flow solutions, the scalar field is monotonic between the UV fixed point and the IR critical point φ_0, which typically is reached before the (would-be flat) IR fixed point (as in figure 6.2a). This is, however, not always the case. For example, already in the flat case it was shown in [5] that holographic RG flows may exhibit phenomena which seem exotic from the point of view of QFT perturbation theory. For one, holographic RG flows may *bounce*, i.e. the flow may reverse direction in coupling constant space (see fig. 6.4) without stopping.

In this work we found that flows exhibiting bounces persist for field theories on curved manifolds. Interestingly, for field theories on AdS_4 we found that bounces are generic features of RG flows if the UV operator dimension is $3 < \Delta < 4$. This is unlike the situation in the flat or positively curved case, where this does not occur generically.

6.1.2 F-functions from holography

In chapter 3, we presented how to construct holographically F-functions in $d = 3$. In that chapter we provided evidence, from both holography and free theories, that for 3d QFTs it is indeed possible to construct monotonic F-functions starting from the free energy on S^3 and avoid the difficulties encountered in the past. As we showed, this is possible as long as one properly takes into account the following two considerations:

1. As the sphere path integral is UV divergent one has to work with renormalized quantities to define anything meaningful. Away from the fixed points, this introduces a scheme dependence of the resulting finite functions. In a generic scheme, the renormalized sphere free energy is finite but non-monotonic, as simple holographic examples have already shown [79]. The key is to adopt renormalization schemes which, at the same time as the UV divergences, remove also the IR divergences associated with taking the volume of the S^3 to infinity. We have identified four different schemes which accomplish this: three of them involve acting with differential operators (in the curvature) on the regulated partition

function; the last one consists of a specific choice of counterterms, and in particular can be related to specific renormalization conditions on correlators of the *flat space* field theory.

2. Defining the subtraction procedure as outlined above is not enough. We found the definition of the F-function is different depending on the dimension Δ of the relevant operator which deforms the CFT away from the UV fixed point. We have found that, if $\Delta > 3/2$, then the F-functions are given by the (renormalized) free energy. If $\Delta < 3/2$ on the other hand, they have to be defined with the same subtractions, but on its Legendre transform, i.e. the quantum effective potential. It is here that holography has played a crucial role, as this would have been very hard to guess from purely field theoretical considerations. Instead, the natural quantity to work with on the gravity side is the on-shell action, and it is the same quantity which, depending on Δ, plays the role of either the QFT free energy or its Legendre transform.

We have found evidence that one can construct a good F-function from the de Sitter entanglement entropy. Like in the case of the free energy or its Legendre transform, an appropriate subtraction procedure has to be used, either by applying a differential operator à la Liu and Mezei, or by a counterterm subtraction. We found that for $\Delta > 3/2$ the corresponding F-functions coincide with a subset of those constructed from the free energy on S^3, while for $\Delta < 3/2$ they correspond to a subset of those obtained from the Legendre transform of the free energy.

6.1.3 Quantum phase transitions driven by boundary curvature

In chapter 4 we studied a quantum phase transition driven by the UV curvature. A field theory on a curved manifold, defined by a value of the UV source φ_- and of the UV curvature $R^{\rm uv}$ may display several saddle points, which in the holographic dual framework correspond to different RG flow geometries. The true vacuum can be determined by calculating the free energies of the flows corresponding to the various saddle points. The solution with the lowest free energy is the true vacuum.

The example we discussed is based on a potential which was already studied in [5] in the flat case. Its main feature is to allow two regular flows in the zero-curvature case, one connecting two neighboring (UV and IR) fixed points, the second *skipping* the closest available IR fixed point and ending at a fixed point at larger field value. This is represented schematically in fig. 6.5.

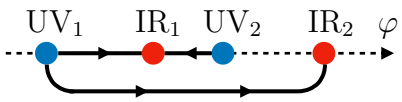

Figure 6.5: Schematic structure of a field theory which presents multiple RG-flows: In particular, there are two flows starting at the fixed point UV_1, one going to the closer IR fixed point IR_1, the second skipping IR_1 and ending at IR_2.

In [5], it was found that, for the theory in flat space, the preferred ground state is the skipping solution. Turning on a small positive curvature, the skipping and non-skipping solutions persist, their free-energy difference decreases up to a critical value $\mathcal{R}_c$ where it changes sign: for $\mathcal{R} > \mathcal{R}_c$ the dominant saddle point is now the shorter (non-skipping) flow. Finally, skipping flows disappear beyond a finite value larger than $\mathcal{R}_c$ (see figure 4.10).

This is the typical structure of a first order phase transition, where a stable phase becomes unstable then disappears, as a function of a control parameter. Usually these kinds of phase transitions are driven by temperature (e.g. Hawking-Page transition for global AdS-Schwarzschild black holes). Here it takes place at zero temperature and is driven by one of the "couplings" of the UV theory.

6.1.4 Self-stabilisation of curved brane

In chapter 5, we studied self-stabilising solutions of a 4-dimensional brane embedded into a 5-dimensional bulk, where the curvature of the brane is adjusted dynamically. This was in the spirit of self-tuning mechanisms of the cosmological constant in braneworld scenarios [101, 102, 6, 7], with the difference that we were not exclusively interested in solutions where the brane is flat. For simplicity, we considered the background of the CFT to be a (locally) maximally symmetric 4-dimensional space-time (dS_4, $\mathcal{M}_4$ or AdS_4) which we characterise by its scalar curvature $R^{(\zeta)}$: curvature associated to the slicing metric $\zeta_{\mu\nu}$.

The first observation was that generic self-stabilising solutions with $R^{(\zeta)} = 0$ (i.e. $\zeta_{\mu\nu} = \eta_{\mu\nu}$) only exist if the world-volume of the brane is also flat. That is, if the boundary CFT resides on Minkowski space, the world-volume of the brane is also given by Minkowski space, which is the scenario studied previously in [7]. Exceptions exist, but are non-generic as they require a tuning of model-parameters (e.g. a precise choice of the dilaton potential on the brane, see appendix L for details). This no-go result can also be overcome if the 5d bulk is not static , but time-dependent. However, in this case the

dual interpretation in terms of RG flows does not apply any more.

To find self-stabilising solutions with a curved brane in a static bulk, one is hence forced to modify the UV boundary conditions of the bulk fields. In chapter 5, we mainly did so by choosing $R^{(\zeta)} \neq 0$. We then worked with a simple brane embedding in which the brane geometry is inherited from the boundary. For a bulk described by (6.1.2) this amounts to locating the brane at some fixed $u = u_\star$. This choice is equivalent to restricting to branes with maximally symmetric world-volume with scalar curvature R_B. The brane curvature is then related to $R^{(\zeta)}$ as

$$R_B = R^{(\zeta)}\, e^{-2A(u_\star)}\,. \tag{6.1.5}$$

To find solutions for a brane with world-volume given by (A)dS$_4$, the boundary CFT has to reside on (A)dS$_4$.

There exists an alternative realisation of the same solutions, which can be obtained via a bulk coordinate transformation. In this formulation the boundary metric is flat ($R^{(\zeta)} = 0$), but the scalar sources are no longer constant on the boundary: they now vary in space or time. As a result, the holographic interpretation is also modified. Instead of the boundary QFT living on a curved space-time, we then have a flat-space QFT driven by a time-varying (in the dS case) or space-dependent (in the AdS case) source. In the dS case one requires the source j to vary as $j \sim |t|^{\Delta-d}$, where t is the de Sitter conformal time on the brane and Δ is the dimension of the relevant operator deforming the CFT.

We then studied how the brane curvature R_B depends on $R^{(\zeta)}$ quantitatively. This was done mostly numerically by searching for self-stabilising solutions while scanning over all possible values of $R^{(\zeta)}$. To perform a numerical analysis, we have to specify a particular model by choosing a bulk dilaton potential $V(\varphi)$, a brane dilaton potential $W_B(\varphi)$, and the (dilaton-dependent) Newton's 'constant' term $U(\varphi)$ on the brane. Given a UV completion of our model, these functions can in principle be determined, but this goes beyond the scope of this work. For the numerical study we chose an exponential potential on the brane and we have found that: the space of solutions in $\mathcal{R}$ is highly restricted and there is a branch of solutions that in the limit $\mathcal{R} \to 0$ is connected continuously to a flat brane solution with $\mathcal{R} = 0$ and $R_B = 0$.

6.2 Open questions and outlook

From the point of view of field theory, this work offers a new (holographic) insight on RG flows on curved manifolds. It also opens new directions to

explore. We mention some of these in the following.

We have seen that positive curvature flows end at points of maximal symmetry. From the gravity side, this symmetry is just the full set of AdS isometries. However, it is unclear how this symmetry is realized on the field theory side, since (unlike in the case of flat IR fixed points) it does not obviously reduce to conformal transformations (or rather conformal isometries) on the field theory coordinates. It would be interesting to investigate this further.

One important question is whether the solutions discussed in this work are perturbatively stable. In the case of flat sections, it was shown in [5] that, regardless of the details of the bulk geometries, solutions which reach an IR fixed point are stable under small perturbations. This includes bouncing solutions, as the bounce does not introduce any particular features in the fluctuation equations which may trigger instabilities. In the curved case the situation is less clear. To reach the same conclusion one would have to develop a complete fluctuation analysis around the ansatz (6.1.2). This is an important direction to explore in the future work. Another important question concerns the boundary conditions and stability for solutions in which the field theory is on a negatively curved space. When the field theory space-time is AdS_d, the solution is not single valued on the boundary, but it must contain a defect along the portion of the AdS_{d+1} boundary which corresponds to the AdS_d boundary . This can be avoided by quotienting the AdS_d slices by a finite group, but as argued in [60], this may introduce perturbative instabilities. It would be interesting to understand these issues in more detail.

There remain many directions for further investigation in the context of F-theorem. An open question concerns the relation of our proposed F-functions to the one obtained from the Renormalized Entanglement Entropy (REE) of a spherical region in the Minkowski QFT [74]. For a CFT at a fixed point, the corresponding F-quantity coincides with the one defined from both the free energy and the de Sitter entanglement entropy. This follows from the fact that, for a CFT, one can use a conformal transformation to map the spherical region in flat space to a similar region in de Sitter [67]. Away from the fixed point however this no longer holds, and we show explicitly that the F-functions obtained from the free energy differ from the flat space REE. It would be interesting to understand whether these are related in some deeper way.

It will be interesting to gather additional evidence that the functions $\mathcal{F}_{1,2,3,4}(\mathcal{R})$ defined in (3.3.12)–(3.3.15) are indeed good F-functions. While we checked this explicitly for a wide range of theories in holography and for free field theories, further tests are desirable. In the context of holography, we

worked with bottom-up four-dimensional models, and it would be interesting to check whether our proposal holds in top-down models from string theories. For three-dimensional field theories, there are many examples of gravity dual holographic RG flows in gauged $N = 8$, $d = 4$ supergravity [117, 118, 119, 120], and their M-theory uplifts[121, 122]. One could also consider three-dimensional theories with flavor, whose RG flows were studied e.g. in [123, 124, 125] (in the quenched flavor limit) and [126]. The quenched flavor case looks particularly treatable, as one does not need to find the curved domain wall solution in the full 11-dimensional bulk theory, but only restrict to the contribution to the F-functions from the flavor degrees of freedom coming from the D6 branes wrapped on $\mathrm{AdS}_4 \times S^7$ using curved slicing of AdS_4, and use the flavor mass as the deformation parameter.

Further open question is to what extent an F-theorem exists in higher odd dimensions, i.e. $d = 5, 7, \ldots$. Several proposals for F-functions in higher odd dimensions exist [35, 45, 66, 68] and evidence for an F-theorem in $d = 5$ can be found in [127, 128]. However, so far there is no proof of monotonicity for dimensions with $d \geq 5$. The F-functions introduced in this work, while constructed for $d = 3$, allow for a straightforward generalisation to any odd d and are hence suitable for exploring the F-theorem beyond $d = 3$.

The bulk-brane setup studied here is a promising framework for further phenomenological investigation. However, before a realistic model can be constructed, there are several open questions that should be addressed. For one, it is important to determine to what extent our results are general, or model-dependent. In particular, is it a generic feature of this construction that $R_B \ll M_4^2$ *only* occurs when perturbing a solution for a flat brane? In addition, more work is also needed regarding the theoretical foundations of the model. It would be desirable if the quantities $V(\varphi)$, $W_B(\varphi)$ and $U(\varphi)$ could be constrained, either by direct calculation or from physical principles. For example, it is expected that consistency with quantum gravity gives stringent constraints on the physics of scalar fields [129, 130, 131, 132, 133, 134, 135], restricting their field range and even constraining the shape of the potential. It would be interesting to study to what extent these conditions, also known as 'swampland conjectures', can be used to constrain this model.

An important question regards the stability of the solutions obtained here. The perturbative stability of self-stabilising solutions for a *flat* brane was analysed in [7]. The result of this analysis is a set of certain sufficient conditions for stability involving the bulk solutions and the brane quantities evaluated at the position of the brane. Here, we expect that the presence of *positive* brane curvature will not introduce any additional instabilities (see [8] for more details). Hence we expect any solutions, which can be obtained from a stable flat brane solution by turning on positive (boundary and brane) cur-

vature to be stable. On the other hand, the presence of *negative* (boundary and brane) curvature may introduce new instabilities. In this case, perturbative stability has to be checked explicitly case by case, which goes beyond the scope of this work. As our priority in this work was to explore the space of self-stabilising solutions rather than to perform realistic model-building, the solutions explored in this work do not always satisfy all of the sufficient conditions for stability. For example, the solutions in sec. 5.3 satisfy all but one of the sufficient stability conditions. This does not imply that these solutions are necessarily unstable, but a more detailed analysis is required.

Last, some of our findings may have interesting applications in the study of holographic RG flows. In particular, certain bulk solutions studied in the theory with $V(\varphi) \sim -\exp(\varphi)$ should be relevant for the study of the RG behaviour of confining theories [27] on curved backgrounds in holography.

Appendix A

Curvature Invariants

In this appendix we record expressions for various curvature invariants. In particular, for the metric (2.1.1), we will compute R, $R_{AB}R^{AB}$ and $R_{ABCD}R^{ABCD}$ and we will express them in terms of the functions W, S and T defined in (2.2.1)–(2.2.3).

Ricci scalar
The expression for the Ricci scalar is found as,

$$R = -\left[2d\ddot{A}(u) + d(d+1)\dot{A}^2(u)\right] + e^{-2A(u)}R^{(\zeta)} \tag{A.1}$$

which in terms of $W(\varphi)$, $S(\varphi)$ and $T(\varphi)$ can be written as,

$$R = \frac{d}{d-1}W'S - \frac{d(d+1)}{4(d-1)^2}W^2 + T = \frac{S^2}{2} + \frac{d+1}{d-1}V \ . \tag{A.2}$$

In the last step we have used equations (2.2.4)–(2.2.6) to simplify. This shows that the scalar curvature diverges when the potential $V(\varphi)$ diverges or when $S(\varphi)$ diverges.

Ricci squared
The square of the Ricci tensor is given as,

$$\begin{aligned} R_{AB}R^{AB} = d^2\left(\ddot{A}(u) + \dot{A}^2(u)\right)^2 + \frac{(R^{(\zeta)})^2}{d}e^{-4A(u)} - 2R^{(\zeta)}e^{-2A(u)}(\ddot{A}(u) \\ + d\dot{A}^2(u)) + d\left(\ddot{A}(u) + d\dot{A}^2(u)\right)^2. \end{aligned} \tag{A.3}$$

On shell, this can be written in terms of V and S as

$$R_{AB}R^{AB} = d^2\left(\frac{S^2}{2d} + \frac{V}{d(d-1)}\right)^2 + \frac{dV^2}{(d-1)^2}. \tag{A.4}$$

This also diverges when $V(\varphi) \to \infty$ or when $S(\varphi)$ diverges.

Riemann squared
The so-called Kretschmann scalar is found as,

$$R_{ABCD}R^{ABCD} = 4d\left(\ddot{A}(u) + \dot{A}^2(u)\right)^2 + 2d(d-1)\left(\frac{e^{-2A(u)}}{\alpha^2} - \dot{A}^2(u)\right)^2. \tag{A.5}$$

Using the equations of motion this can be written as,

$$R_{ABCD}R^{ABCD} = \frac{4}{d}\left(\frac{S^2}{2} + \frac{V}{d-1}\right)^2 + \frac{1}{2d(d-1)}\left(S^2 - 2V\right)^2. \tag{A.6}$$

Again, this diverges whenever the potential $V(\varphi)$ or the function $S(\varphi)$ diverge.

Appendix B

Properties of the functions W, S and T

B.1 Positive curved case (S^d or $\mathbf{dS}_d$)

1. There are two branches of solutions W and S at a generic point. On a single branch the signs of S and W' coincide. This can be seen from Eq. (2.2.4) which we can write as:

$$SW' = S^2 + \frac{2}{d}T \ . \tag{B.1.1}$$

The RHS is always positive. Therefore the signs of S and W' must be same. The two possible signs for S and W' give rise to the two branches.

2. The absolute value of $W(\varphi)$ is bounded by the critical curve $B(\varphi) = \sqrt{-\frac{4(d-1)}{d}V(\varphi)}$ and on this critical curve the two functions $S(\varphi)$ and $T(\varphi)$ go to zero. This can be shown from Eq. (2.2.5) which we can write as

$$\frac{d}{2(d-1)}W^2 = S^2 + 2T - 2V \geq -2V \ . \tag{B.1.2}$$

Therefore, we can write,

$$W^2(\varphi) \geq -\frac{4(d-1)}{d}V(\varphi) = B^2(\varphi). \tag{B.1.3}$$

On the critical curve $\frac{d}{2(d-1)}W^2(\varphi) = -2V(\varphi)$. So Eq. (2.2.5) can be written as

$$S^2 + 2T = 0 \ . \tag{B.1.4}$$

This is a sum of two positive numbers which can be zero iff the individual contributions are zero. Hence, on the critical curve, the functions $S(\varphi)$ and $T(\varphi)$ vanish.

3. Bounces cannot happen on the critical curve. Let us assume that along a flow originating from a UV fixed point a bounce occurs at $\varphi = \varphi_*$, which happens to lie on the critical curve. From property 2, we see that at $\varphi = \varphi_*$, $T(\varphi_*) = 0$. But we started from the UV, which is also on the critical curve and consequently had $T(\varphi_{UV}) = 0$. So $T(\varphi)$ is starting from a value of 0 and ending with a value of 0. This cannot happen because $\frac{dT}{du} = \frac{TW}{d-1} \geq 0$ (assuming $W \geq 0$). Instead, a bounce can happen when $S = 0$ and

$$W^2 = \frac{2(d-1)}{d}(2T - 2V) \quad \text{where } T > 0 \ . \tag{B.1.5}$$

B.2 Positive and negative curved case

4. The functions $W(\varphi)$, $S(\varphi)$ and $T(\varphi)$ satisfy the following relation:

$$T'S = \frac{TW}{d-1} \ . \tag{B.2.1}$$

This comes from the definition of the functions $W(\varphi)$, $S(\varphi)$ and $T(\varphi)$. We can take a u-derivative of $T = e^{-2A(u)}R^{(\zeta)}$ and then use the definitions (2.2.3)–(2.2.1) .

5. At the zeros of the function $S(\varphi)$, the geometry is approximately maximally symmetric. We can express the Ricci tensor in terms of the function $S(\varphi)$. The only non-zero components of the Ricci tensor are:

$$R_{uu} = \left(\frac{S^2}{2} + \frac{V}{d-1}\right) g_{uu}, \tag{B.2.2}$$

$$R_{\mu\nu} = \frac{V}{d-1} g_{\mu\nu}. \tag{B.2.3}$$

Let S be zero at a value $\varphi = \varphi_*$. Then at this point the Ricci tensor can be written as

$$R_{AB} = \frac{V(\varphi_*)}{d-1} g_{AB}. \tag{B.2.4}$$

Therefore the space is maximally symmetric near the zeros of S. As the potential is negative, this space is approximately AdS.

6. Symmetry properties. Let $W(\varphi)$, $S(\varphi)$ and $T(\varphi)$ satisfy the equations (2.2.4)–(2.2.6) for a generic potential $V(\varphi)$. Then

$$\bar{S}(\varphi) = -S(\varphi) \ , \tag{B.2.5}$$
$$\bar{W}(\varphi) = -W(\varphi) \ , \tag{B.2.6}$$
$$\bar{T}(\varphi) = T(\varphi) \tag{B.2.7}$$

are also solutions of the equations (2.2.4)–(2.2.6). The scale factor and the curvature invariants behave as

$$\bar{A}(u) = A(u) \ , \tag{B.2.8}$$
$$\bar{R}(\varphi) = R(\varphi) \ , \tag{B.2.9}$$
$$\bar{R}_{AB}\bar{R}^{AB}(\varphi) = R_{AB}R^{AB}(\varphi) \ , \tag{B.2.10}$$
$$\bar{R}_{ABCD}\bar{R}^{ABCD}(\varphi) = R_{ABCD}R^{ABCD}(\varphi) \ . \tag{B.2.11}$$

This means that we have two equivalent copies of geometries below and above the φ axis.

If $V(\varphi)$ is an even function of φ, then

$$\tilde{S}(\varphi) = -S(-\varphi) \ , \tag{B.2.12}$$
$$\tilde{W}(\varphi) = W(-\varphi) \ , \tag{B.2.13}$$
$$\tilde{T}(\varphi) = T(-\varphi) \ , \tag{B.2.14}$$

satisfy the equations (2.2.4)–(2.2.6). This is because the above relations imply

$$\tilde{S}'(\varphi) = S'(-\varphi) \ , \tag{B.2.15}$$
$$\tilde{W}'(\varphi) = -W'(-\varphi) \ , \tag{B.2.16}$$

and we also have that $V'(\varphi) = -V'(-\varphi)$. The scale factor and the curvature invariants behave as

$$\tilde{A}(u) = A(u) \ , \tag{B.2.17}$$
$$\tilde{R}(\varphi) = R(-\varphi) \ , \tag{B.2.18}$$
$$\tilde{R}_{AB}\tilde{R}^{AB}(\varphi) = R_{AB}R^{AB}(-\varphi) \ , \tag{B.2.19}$$
$$\tilde{R}_{ABCD}\tilde{R}^{ABCD}(\varphi) = R_{ABCD}R^{ABCD}(-\varphi) \ . \tag{B.2.20}$$

This shows we have two equivalent copies of geometries on the positive and negative side of φ axis.

Appendix C

Near boundary solution: Small curvature expansion

In this appendix we will collect analytical expressions for $W(\varphi)$, $S(\varphi)$ and $T(\varphi)$ describing the geometry in the vicinity of the boundary of the asymptotically AdS_{d+1} space-time.

It will be advantageous to organize the solution as a perturbative expansion in R^{uv}, expanding about the result for $R^{\mathrm{uv}} = 0$. The reason is as follows. We will find that for asymptotically AdS_{d+1} space-times *a near-boundary expansion of the quantities* φ, A, W, S and T *will automatically give rise to an expansion in* R^{uv}. We have already encountered this in (2.3.6) where we expanded the scale factor $A(u)$ for AdS_{d+1} in the vicinity of the boundary. We found that R^{uv} enters the expansion exclusively in the combination $R^{\mathrm{uv}}e^{2u/\ell}$. Expanding $A(u)$ in powers of $e^{2u/\ell}$ in the vicinity of the boundary at $u \to -\infty$ is thus is equivalent to expanding in powers of R^{uv}. This observation will also hold more generally for asymptotically AdS_{d+1} space-times.

Consequently, we will expand $W(\varphi)$, $S(\varphi)$ and $T(\varphi)$ as follows:

$$W(\varphi) = \sum_{n=0}^{\infty} W_n (\ell^2 R^{\mathrm{uv}})^n \,, \tag{C.1}$$

$$S(\varphi) = \sum_{n=0}^{\infty} S_n (\ell^2 R^{\mathrm{uv}})^n \,, \tag{C.2}$$

$$T(\varphi) = \sum_{n=0}^{\infty} T_n (\ell^2 R^{\mathrm{uv}})^{n+1} \,, \tag{C.3}$$

where ℓ will be identified with the AdS length scale of the asymptotically AdS_{d+1} bulk space-time. Note that the expansion of $T(\varphi) \equiv R^{\mathrm{uv}}e^{-2A(\varphi)}$ starts at linear order in R^{uv}. We proceed by inserting the above expansions

into the equations of motion (2.2.4)–(2.2.6) and solve these order by order in $R^{\rm uv}$.

Calculating S_n

Inserting the above expansions into (2.2.4) the resulting equations at order $(R^{\rm uv})^0$ and $(R^{\rm uv})^1$ can be rewritten as

$$S_0 = W_0' \,, \tag{C.4}$$

$$S_1 = -\frac{2}{d}\frac{T_0}{W_0'} + W_1' \,, \tag{C.5}$$

where we assumed $S_0 \neq 0$ as we are interested in non-zero flows. In virtue of (C.4) we will freely replace S_0 by W_0' whenever convenient. Eq. (C.5) will allow us to calculate S_1 once T_0, W_0 and W_1 have been determined.

Calculating T_n

Note that we can write

$$\begin{aligned} -2A &= -2A_0 + \frac{1}{d-1}\int_{\varphi_0}^{\varphi} \frac{W}{S}\mathrm{d}\varphi \\ &= -2A_0 + \frac{1}{d-1}\int_{\varphi_0}^{\varphi} \frac{W_0}{S_0}\mathrm{d}\varphi - \frac{\ell^2 R^{\rm uv}}{d-1}\int_{\varphi_0}^{\varphi} \frac{S_1 W_0 - S_0 W_1}{S_0^2}\,\mathrm{d}\varphi + \dots \end{aligned} \tag{C.6}$$

$$= -2A_0 + \frac{1}{d-1}\int_{\varphi_0}^{\varphi} \frac{W_0}{W_0'}\mathrm{d}\varphi - \frac{\ell^2 R^{\rm uv}}{d-1}\int_{\varphi_0}^{\varphi} \frac{S_1 W_0 - W_0' W_1}{(W_0')^2}\,\mathrm{d}\varphi + \dots \,, \tag{C.7}$$

where we defined $A_0 \equiv A(\varphi_0)$ for some φ_0. Despite the explicit appearance φ_0 above, the result is independent of φ_0. Then, from the defining expression $T \equiv R^{\rm uv} e^{-2A}$ we obtain

$$T_0 = \ell^{-2}\, e^{-2A_0} e^{\frac{1}{d-1}\int_{\varphi_0}^{\varphi} \frac{W_0}{W_0'} d\varphi} \,, \tag{C.8}$$

$$T_1 = -\ell^{-2}\, e^{-2A_0} e^{\frac{1}{d-1}\int_{\varphi_0}^{\varphi} \frac{W_0}{W_0'} d\varphi} \frac{1}{d-1}\int_{\varphi_0}^{\varphi} \frac{S_1 W_0 - W_0' W_1}{(W_0')^2}\, d\varphi \,. \tag{C.9}$$

We will calculate T_0 explicitly in section C.1.

Calculating W_n

Inserting the expansions into (2.2.5) we obtain the following two equations at the orders $(R^{\text{uv}})^0$ and $(R^{\text{uv}})^1$:

$$\frac{d}{4(d-1)}W_0^2 - \frac{1}{2}(W_0')^2 = -V\,, \tag{C.10}$$

$$W_1' - \frac{d}{2(d-1)}\frac{W_0}{W_0'}W_1 + \frac{d-2}{d}\frac{T_0}{W_0'} = 0\,. \tag{C.11}$$

Inserting our expression (C.8) for T_0 into the last equation, this can be integrated to give

$$W_1 = e^{\frac{d}{2(d-1)}\int_{\varphi_0}^{\varphi}\frac{W_0}{W_0'}}\left(\tilde{C}_1 + \frac{2-d}{d}\,e^{-2A_0}\int_{\varphi_0}^{\varphi}\frac{e^{\frac{2-d}{2(d-1)}\int_{\varphi_0}^{\varphi}\frac{W_0}{W_0'}}}{W_0'}\right)\,, \tag{C.12}$$

where $\tilde{C}_1$ is an integration constant.

Overall, given a solution for W_0 and W_0' we can now determine W_1 and T_0, which in turn will allow us to calculate S_1 and finally T_1. While these results will be sufficient for the scope of this work, the analysis in this appendix can in principle be extended to determine the coefficients W_n, S_n and T_n to an arbitrarily high order.

C.1 Extrema of V

Here we will derive solutions for W, S and T in the vicinity of extrema of the potential, using the small curvature expansion introduced in section C.[1] To this end, it will be sufficient to consider the potential

$$V = -\frac{d(d-1)}{\ell^2} - \frac{m^2}{2}\varphi^2 + \mathcal{O}(\varphi^3)\,, \tag{C.1.1}$$

where we will choose $m^2 > 0$ for maxima and $m^2 < 0$ for minima.

Calculating W_0

At order $(R^{\text{uv}})^0$ the analysis of our system reduces to a study of holographic RG flows for field theories on flat manifolds. This has been studied extensively in the past and we can hence be brief. For details we will refer readers

[1] This is consistent as long as extrema of the potential coincide with the boundary of the bulk space-time. We check this explicitly when discussing the resulting geometries in section 2.4.

to e.g. [5]. To be specific, at order $(R^{\rm uv})^0$ we have $W = W_0$, $S = S_0 = W_0'$ and $T = 0$. Thus at order $(R^{\rm uv})^0$ the solution is completely determined by W_0.

We can determine W_0 by solving (C.10). In the vicinity of the extremum of V at $\varphi = 0$ this can be done by writing W_0 as a regular expansion in powers of φ. There exist two independent solutions, which we will label by the two subscripts $(\pm)$:

$$W_{0,\pm}^{\rm reg} = \frac{2(d-1)}{\ell} + \frac{\Delta_\pm}{2\ell}\varphi^2 + \mathcal{O}(\varphi^3)\,, \qquad \text{(C.1.2)}$$
$$\text{with} \quad \Delta_\pm = \frac{1}{2}\left(d \pm \sqrt{d^2 - 4m^2\ell^2}\right)\,.$$

Terms in $W_{0,\pm}^{\rm reg}$ of order φ^3 and higher will depend on cubic and higher terms in V, which we ignore in the vicinity of extrema.

The solution permits a continuous deformation δW_{01} as long as the deformation is subleading compared to $W_{0,\pm}^{\rm reg}$. We will make this condition precise at the end of this section. The deformation can be determined by inserting $W_0 = W_{0,\pm}^{\rm reg} + \delta W_{01}$ into (C.10) and solving for δW_{01}:

$$\delta W_{01} = \frac{C}{\ell}\exp\left(\frac{d}{2(d-1)}\int^\varphi \mathrm{d}\varphi \frac{W_{0,\pm}^{\rm reg}}{(W_{0,\pm}^{\rm reg})'}\right) = \frac{C}{\ell}\,|\varphi|^{\frac{d}{\Delta_\pm}}\left[1 + \mathcal{O}(\varphi)\right]\,, \qquad \text{(C.1.3)}$$

where we introduced the dimensionless integration constant C. Putting everything together, we thus obtain:

$$W_0 = \frac{2(d-1)}{\ell} + \frac{\Delta_\pm}{2\ell}\varphi^2 + \mathcal{O}(\varphi^3) + \frac{C}{\ell}\,|\varphi|^{\frac{d}{\Delta_\pm}}\left[1 + \mathcal{O}(\varphi) + \mathcal{O}(C)\right]\,. \qquad \text{(C.1.4)}$$

From this we also have that

$$S_0 = W_0' = \frac{\Delta_\pm}{\ell}\varphi + \mathcal{O}(\varphi^2) + \frac{Cd}{\Delta_\pm \ell}\,|\varphi|^{\frac{d}{\Delta_\pm}-1}\left[1 + \mathcal{O}(\varphi) + \mathcal{O}(C)\right]\,. \qquad \text{(C.1.5)}$$

We can now return to the question under which circumstances the deformation $\propto C$ is permitted. To this end consider eq. (2.2.9) which involves S only and which any solution for S must satisfy. It is easy to check that the corresponding equation at order $(\mathcal{R}^{\rm uv})^0$ is only satisfied by S_0 if the linear term in (C.1.5) dominates over the term involving C. This implies that solutions for S and W permit a deformation only if

$$\frac{d}{\Delta_\pm} > 2\,. \qquad \text{(C.1.6)}$$

If this is not the case, no deformation is permitted, which is equivalent to setting $C = 0$.

Calculating T_0:

Given the expression for W_0 in (C.1.4), we can now proceed to determining T_0 from (C.8). In particular, the exponent in (C.8) is given by

$$\begin{aligned} &-2A(\varphi_0) + \frac{1}{(d-1)} \int_{\varphi_0}^{\varphi} \mathrm{d}\varphi \, \frac{W_0}{W_0'} \\ &= -2A(\varphi_0) + \frac{2}{\Delta_\pm} \int_{\varphi_0}^{\varphi} \frac{\mathrm{d}\varphi}{\varphi} \left[1 + \mathcal{O}(\varphi) + \mathcal{O}(C|\varphi|^{d/\Delta_\pm - 2})\right] , \end{aligned} \tag{C.1.7}$$

where we have used (C.1.4) to get to the second line. One unattractive feature is the explicit appearance of the arbitrary parameter φ_0. In particular, there is physical information in $A(\varphi_0)$ which is obscured by this notation. Thus, in the following, we will explain how we can remove φ_0 from the expression for T_0. The idea is to trade the arbitrary parameter φ_0 for φ_- or φ_+ which are physical parameters of the boundary field theory.

To this end, given our expression (C.1.4) for W_0, let us calculate the corresponding solutions for $A(u)$ and $\varphi(u)$ using $W_0 = -2(d-1)\dot{A}$ and $W_0' = \dot{\varphi}$:

$$\varphi(u) = \begin{cases} \varphi_+ \, \ell^{\Delta_+} \, e^{\Delta_+ u/\ell} + \mathcal{O}(e^{2\Delta_- u/\ell}) & (+)\text{-branch}, \\ \varphi_- \, \ell^{\Delta_-} \, e^{\Delta_- u/\ell} + \mathcal{O}(e^{2\Delta_- u/\ell}, e^{\Delta_+ u/\ell}) & (-)\text{-branch}, \end{cases} \tag{C.1.8}$$

$$A(u) = \bar{A} - \frac{u}{\ell} + \mathcal{O}(e^{2\Delta_\pm u/\ell}, e^{du/\ell}) , \tag{C.1.9}$$

where we introduced φ_+, φ_- and $\bar{A}$ as integration constants.[2] We can always set $\bar{A} = 0$ as argued in section 2.3 and we will do so in the following. As explained in section 2.4, φ_- is interpreted as the UV value of source for the operator $\mathcal{O}$ in the boundary field theory. The parameter φ_+ is related to the vev of $\mathcal{O}$ as follows: $\langle \mathcal{O} \rangle = (2\Delta_+ - d)\varphi_+$. Using these expressions we can now invert $\varphi(u)$ and insert the result into $A(u)$ to arrive at an expression for $A(\varphi_0)$:

$$\begin{aligned} A(\varphi_0) &= -\frac{1}{\Delta_\pm} \ln\left(\frac{\varphi_0}{\varphi_\pm \ell^{\Delta_\pm}}\right) + \mathcal{O}(\varphi_0^a) \\ &= -\frac{1}{\Delta_\pm} \int_{\varphi_\pm \ell^{\Delta_\pm}}^{\varphi_0} \frac{\mathrm{d}\varphi}{\varphi} + \mathcal{O}(\varphi_0^a) . \end{aligned} \tag{C.1.10}$$

Here a is an exponent that will depend on the precise values of $\Delta_\pm$. The most important fact for this analysis is that $a > 0$, as can be verified explicitly.

[2] The leading terms in $\varphi(u)$ and $A(u)$ will turn out to be universal, i.e. higher order corrections in R^{uv} to W and S will not affect the leading terms.

Inserting this expression for $A(\varphi_0)$ into (C.1.7) we find

$$\begin{aligned}
&-2A(\varphi_0)+\frac{2}{\Delta_\pm}\int_{\varphi_0}^{\varphi}\frac{\mathrm{d}\varphi}{\varphi}\,\left[1+\mathcal{O}(\varphi)+\mathcal{O}(C|\varphi|^{d/\Delta_\pm-2})\right]\\
&=\frac{2}{\Delta_\pm}\int_{\varphi_\pm\ell^{\Delta_\pm}}^{\varphi_0}\frac{\mathrm{d}\varphi}{\varphi}+\frac{2}{\Delta_\pm}\int_{\varphi_0}^{\varphi}\frac{\mathrm{d}\varphi}{\varphi}+\int_{\varphi_0}^{\varphi}\mathrm{d}\varphi\left[\mathcal{O}(\varphi^0)+\mathcal{O}(C\varphi^{d/\Delta_\pm-3})\right]+\mathcal{O}(\varphi_0^a)\\
&=\frac{2}{\Delta_\pm}\int_{\varphi_\pm\ell^{\Delta_\pm}}^{\varphi}\frac{\mathrm{d}\varphi}{\varphi}+\int_{\varphi_0}^{\varphi}\mathrm{d}\varphi\left[\mathcal{O}(\varphi^0)+\mathcal{O}(C\varphi^{d/\Delta_\pm-3})\right]+\mathcal{O}(\varphi_0^a)\\
&=\frac{2}{\Delta_\pm}\ln\left(\frac{\varphi}{\varphi_\pm\ell^{\Delta_\pm}}\right)+\int_{\varphi_0}^{\varphi}\mathrm{d}\varphi\left[\mathcal{O}(\varphi^0)+\mathcal{O}(C\varphi^{d/\Delta_\pm-3})\right]+\mathcal{O}(\varphi_0^a)\,. \qquad \text{(C.1.11)}
\end{aligned}$$

The main observation is that we can now remove φ_0 by setting $\varphi_0 \to 0$.[3] There is no danger of picking up a divergence from the integral. (Recall that the term involving C is only present if $d/\Delta_\pm > 2$.) The lower limit of the integral simply becomes 0 while the term $\mathcal{O}(\varphi_0^a)$ simply vanishes as $a > 0$. We are thus finally in a position to state the result for T_0. Using (C.1.11) in (C.8) we obtain:

$$T_0=\ell^{-4}\left(\frac{\varphi}{\varphi_\pm}\right)^{\frac{2}{\Delta_\pm}}\left[1+\mathcal{O}(\varphi)+\mathcal{O}(C|\varphi|^{d/\Delta_\pm-2})\right]\ . \qquad \text{(C.1.12)}$$

Thus, in the vicinity of an extremum we find that T has an expansion of the form

$$\begin{aligned}
T_\pm(\varphi)=\ell^{-2}\left(R^{\mathrm{uv}}|\varphi_\pm|^{-2/\Delta_\pm}\right)\,|\varphi|^{2/\Delta_\pm}\,\big[1+\mathcal{O}(\varphi)+\mathcal{O}(C|\varphi|^{d/\Delta_\pm-2})\\
+\mathcal{O}(\ell^2R^{\mathrm{uv}})\big]\ . \qquad \text{(C.1.13)}
\end{aligned}$$

Here we wish to highlight the appearance of the dimensionless combination of quantities $R^{\mathrm{uv}}|\varphi_\pm|^{-2/\Delta_\pm}$. This is not a coincidence. In fact, we will find that in W, S and T the quantity R^{uv} will exclusively appear in the combination $R^{\mathrm{uv}}|\varphi_\pm|^{-2/\Delta_\pm}$. Thus, it will be useful in assigning a label to this particular combination and we hence define

$$\mathcal{R}=\begin{cases} R^{\mathrm{uv}}|\varphi_+|^{-2/\Delta_+} & \text{on the (+)-branch}\\ R^{\mathrm{uv}}|\varphi_-|^{-2/\Delta_-} & \text{on the (−)-branch}\end{cases}\ . \qquad \text{(C.1.14)}$$

Strictly speaking, we should understand the small curvature expansions in (C.1)–(C.3) as expansions in $\mathcal{R}$.

[3] However, we could in principle also choose some finite value for φ_0. It is easy to check that this would have the same effect as a shift in the integration constant $\bar{A}$.

Calculating W_1 and S_1:

Given our expressions (C.1.4) and (C.1.12) for W_0 and T_0 we are now in a position to calculate W_1 and S_1 from (C.12) and (C.5), respectively. Starting with W_1, after some work one finds

$$W_1 = \frac{1}{d\ell^3}\left(\frac{\varphi}{\varphi_\pm}\right)^{\frac{2}{\Delta_\pm}}\left[1+\mathcal{O}(\varphi)+\mathcal{O}(C|\varphi|^{d/\Delta_\pm-2})\right] + \frac{C_1}{\ell}|\varphi|^{d/\Delta_\pm}\left[1+\mathcal{O}(\varphi)+\mathcal{O}(C|\varphi|^{d/\Delta_\pm-2})\right] \tag{C.1.15}$$

Most importantly, any dependence on the arbitrary parameter φ_0 appearing in (C.12) can be absorbed into the integration constant C_1. Another observation is that the term $C_1|\varphi|^{d/\Delta_\pm}$ in W_1 combines with the term $C|\varphi|^{d/\Delta_\pm}$ in W_0 and thus C_1 does not represent an independent integration constant.

We are now in a position to calculate S_1. We obtain:

$$S_1 = \frac{C_1 d}{\Delta_\pm \ell}|\varphi|^{\frac{d}{\Delta_\pm}-1}\left[1+\mathcal{O}(\varphi)+\mathcal{O}\left(C|\varphi|^{\frac{d}{\Delta_\pm}-2}\right)\right]+\frac{1}{\ell}\mathcal{O}\left(|\varphi|^{\frac{2}{\Delta_\pm}+1}\right) + \frac{1}{\ell}\mathcal{O}\left(C|\varphi|^{\frac{2+d}{\Delta_\pm}-1}\right). \tag{C.1.16}$$

Here, the term involving C_1 will combine with the corresponding term in S_0. We also determined the leading order in φ of the terms not containing C_1. One can check that the exact numerical coefficients will depend on the cubic and quartic terms in the potential, and which we hence leave implicit.

C.2 Summary

Putting everything together, we are now in a position to write down expressions for W, S and T in the vicinity of an extremum of V and up to order

$R^{\rm uv}$ (or $\mathcal{R}$):

$$W_\pm(\varphi) = \frac{1}{\ell}\left[2(d-1) + \frac{\Delta_\pm}{2}\varphi^2 + \mathcal{O}(\varphi^3)\right] \tag{C.2.1}$$
$$+ \frac{\mathcal{R}}{d\ell}\,|\varphi|^{\frac{2}{\Delta_\pm}}\,\left[1 + \mathcal{O}(\varphi) + \mathcal{O}(C) + \mathcal{O}(\mathcal{R})\right]$$
$$+ \frac{C}{\ell}\,|\varphi|^{\frac{d}{\Delta_\pm}}\,\left[1 + \mathcal{O}(\varphi) + \mathcal{O}(C) + \mathcal{O}(\mathcal{R})\right],$$
$$S_\pm(\varphi) = \frac{\Delta_-}{\ell}\varphi\,\left[1 + \mathcal{O}(\varphi)\right] + \frac{Cd}{\Delta_-\ell}\,|\varphi|^{\frac{d}{\Delta_-}-1}\,\left[1 + \mathcal{O}(\varphi) + \mathcal{O}(C)\right], \tag{C.2.2}$$
$$+ \frac{1}{\ell}\mathcal{O}\left(\mathcal{R}|\varphi|^{\frac{2}{\Delta_-}+1}\right) + \frac{1}{\ell}\mathcal{O}\left(\mathcal{R}C|\varphi|^{\frac{2+d}{\Delta_-}-1}\right)$$
$$T_\pm(\varphi) = \ell^{-2}\mathcal{R}\,|\varphi|^{\frac{2}{\Delta_-}}[1 + \mathcal{O}(\varphi) + \mathcal{O}(C) + \mathcal{O}(\mathcal{R})], \tag{C.2.3}$$

where $\mathcal{R}$ has been defined in (C.1.14). While we write $\mathcal{O}(C)$ and $\mathcal{O}(\mathcal{R})$ to remove clutter when possible, it is to be understood that C and $\mathcal{R}$ are always accompanied by an appropriate power in φ. Also, we absorbed the integration constant C_1 into C. Further, if $d/\Delta_\pm < 2$ we have to set $C = 0$, otherwise S is not a solution of (2.2.9). While this is the most general result for an extremum of V, we now look at maxima and minima of V in turn.

Maxima of V

At a maximum of V we have:

$$\frac{d}{2} < \Delta_+ < d\,, \qquad 0 < \Delta_- < \frac{d}{2}\,, \tag{C.2.4}$$
$$1 < \frac{d}{\Delta_+} < 2\,, \qquad \frac{d}{\Delta_-} > 2\,. \tag{C.2.5}$$

As $d/\Delta_+ < 2$ we have to set $C = 0$ in the $(+)$-branch of solutions. This is not required for the $(-)$-branch as we have $d/\Delta_- > 2$. The resulting solutions are shown in discussed in section 2.4.1.

Minima of V

At a minimum of V we have:

$$\Delta_+ < d\,, \qquad \Delta_- < 0\,, \tag{C.2.6}$$
$$\frac{d}{\Delta_+} < 1\,, \qquad \frac{d}{\Delta_-} < 0\,. \tag{C.2.7}$$

As $d/\Delta_+ < 2$ we have to set $C = 0$ in the $(+)$-branch of solutions. However, on the $(-)$-branch we have $\Delta_- < 0$ and as a result, any term involving C or $\mathcal{R}$ in (C.2.1)–(C.2.3) diverges! To arrive at an acceptable solution, we have to set both C and $R^{\rm uv}$ (and thus $\mathcal{R}$) to zero. We then recover the solution for RG flows for field theories on flat manifolds. A more comprehensive discussion of the solutions on both the $(+)$ and $(-)$-branches can be found in the main text in section 2.4.2.

Appendix D

Solution in the vicinity of minima of V

Here we will examine solutions for $A(u)$ and $\varphi(u)$ in the vicinity of a minimum. In particular, we will be interested in flows starting or ending at the minimum. The potential is given by (2.4.1) with $m^2 < 0$. As we work in the vicinity of the minimum, we will express solutions as a perturbation about the solution for an AdS fixed point:

$$A(u) = A_0(u) + \epsilon^2 A_2(u) + \mathcal{O}(\epsilon^4)\,, \tag{D.1}$$
$$\varphi(u) = 0 + \epsilon\varphi_1(u) + \mathcal{O}(\epsilon^3)\,, \tag{D.2}$$

with

$$A_0(u) = \begin{cases} \ln\left(-\frac{\ell}{\alpha}\sinh\frac{u+c}{\ell}\right) & S^d \text{ or } \mathrm{dS}_d \\ -\frac{u+c}{\ell} & \mathcal{M}_d \\ \ln\left(\frac{\ell}{\alpha}\cosh\frac{u+c}{\ell}\right) & \mathrm{AdS}_d \end{cases} . \tag{D.3}$$

With this ansatz we proceed to solving the equations of motion (2.1.5)–(2.1.7) order by order in ϵ. To be specific, at order $\mathcal{O}(\epsilon)$ we obtain:

$$\ddot{\varphi}_1 + d\dot{A}_0\dot{\varphi}_1 + m^2\varphi_1 = 0\,. \tag{D.4}$$

Minima as UV fixed points First, we wish to show that a minimum can indeed give rise to a UV fixed point. At a UV fixed point the scale factor diverges as $A(u) \to \infty$ which is the case for $u \to -\infty$. A flow leaving a UV fixed point will thus correspond to a solution to (D.4) subject to the boundary conditions $\varphi_1(u \to -\infty) \to 0$ and $\dot{\varphi}_1(u \to -\infty) \to 0$.

We can discuss the case of dS, AdS and Minkowski slices in a unified way, due to $A_0(u \to -\infty) \to -\frac{u}{\ell}$ for all three cases. Thus, for $u \to -\infty$ (D.4)

becomes

$$\ddot{\varphi}_1 - \frac{d}{\ell}\dot{\varphi}_1 + m^2\varphi_1 = 0\,, \tag{D.5}$$

which is solved by

$$\varphi_1(u) = c_1\, e^{\Delta_- u/\ell} + c_2\, e^{\Delta_+ u/\ell} + \dots\,, \tag{D.6}$$

where $c_{1,2}$ are integration constants and $\Delta_\pm$ have been defined before in (2.4.5). This is just the usual asymptotic form of the scalar field in the vicinity of a UV fixed point, with c_1 related to the source of the perturbing operator and c_2 related to its vev. However, note that for $m^2 < 0$ we have $\Delta_- < 0$ while $\Delta_+ > d$. The boundary conditions hence require that we set $c_1 = 0$. As a result, flows away from a UV fixed point at a minimum of the potential are purely driven by a vev. As the leading behavior of φ is determined by Δ_+, solutions with minima as UV fixed points are associated with the (+)-branch of solutions for W, S and T.

Minima as IR fixed points For the case of Minkowski slicings it is well-known that minima of the potential can be identified as IR fixed points, a fact we will confirm presently. We define an IR endpoint as the locus where the scale factor diverges as $A(u) \to -\infty$. For the case of flat slicings this occurs for $u \to \infty$. The relevant equation is again (D.5), but the boundary conditions now read $\varphi_1(u \to \infty) \to 0$ and $\dot{\varphi}_1(u \to \infty) \to 0$. The general solution is, as before, given by (D.6), but the boundary conditions now require that $c_2 = 0$ instead. Thus, for $R^{\text{uv}} = 0$ minima of the potential can play the role of IR endpoints of RG flows. When rewritten in terms of W, S and T, this is a solution on the (−)-branch.

In the following we will show that in space-times with a curved foliation RG flows cannot end at a minimum of the potential. For the case of dS and AdS slicings the IR is identified with $u \to -c_{\text{IR}}$ where the bulk geometry asymptotes to AdS_{d+1}:

$$A_0(u) \underset{u\to -c_{\text{IR}}}{\to} \begin{cases} \ln\left(-\frac{\ell}{\alpha}\sinh\frac{u+c_{\text{IR}}}{\ell_{\text{IR}}}\right) & S^d \text{ or } \text{dS}_d \\ \ln\left(\frac{\ell}{\alpha}\cosh\frac{u+c_{\text{IR}}}{\ell_{\text{IR}}}\right) & \text{AdS}_d \end{cases}\,. \tag{D.7}$$

For the following analysis it will be useful to introduce the coordinate $w \equiv \frac{u+c_{\text{IR}}}{\ell_{\text{IR}}}$. In the remainder of this subsection we will also define $\dot{} \equiv \frac{d}{dw}$. RG flows ending at an IR endpoint at the minimum of the potential will then correspond to solutions to (D.4) subject to the boundary conditions $\dot{\varphi}_1(w = 0) = 0$ and $\varphi(w = 0) = 0$.

In the vicinity of the IR locus equation (D.4) becomes

$$S^d \text{ or } \mathrm{dS}_d\text{:} \qquad \ddot{\varphi}_1 + d\left(\frac{1}{w} + \frac{w}{3} + \mathcal{O}(w^3)\right)\dot{\varphi}_1 + m^2\ell_{\mathrm{IR}}^2\varphi_1 = 0\,, \tag{D.8}$$

$$\mathrm{AdS}_d\text{:} \qquad \ddot{\varphi}_1 + d\left(w - \frac{w^3}{3} + \mathcal{O}(w^5)\right)\dot{\varphi}_1 + m^2\ell_{\mathrm{IR}}^2\varphi_1 = 0\,. \tag{D.9}$$

Solving and implementing the boundary condition $\dot{\varphi}_1(w=0)=0$ we find

$$S^d \text{ or } \mathrm{dS}_d\text{:} \qquad \varphi_1(w) = c_1\left(1 - \frac{m^2\ell_{\mathrm{IR}}^2}{2(d+1)}w^2 + \mathcal{O}(w^4)\right)\,, \tag{D.10}$$

$$\mathrm{AdS}_d\text{:} \qquad \varphi_1(w) = c_1\left(1 - \frac{m^2\ell_{\mathrm{IR}}^2}{2}w^2 + \mathcal{O}(w^4)\right)\,, \tag{D.11}$$

with c_1 the remaining constant of integration. Note that the only way of satisfying the second boundary condition $\varphi_1(w=0)=0$ is to set $c_1 = 0$, which causes $\varphi(w)$ to vanish identically. *Hence there are no solutions that smoothly arrive at a minimum of the potential for S^d/dS_d and AdS_d slicings.* The only solutions that exist for $R^{\mathrm{uv}} \neq 0$ are solutions with $\varphi = 0$, i.e. conformal fixed points. Most importantly, there are no RG flows for $R^{\mathrm{uv}} \neq 0$ that end at a fixed point at a minimum of the potential. This is equivalent to the absence of the $(-)$-branch of solutions for W, S and T in the vicinity of a minimum of V for $R^{\mathrm{uv}} \neq 0$.

Appendix E

Extremal points of the first order flow equations

We will start by examining the critical power behavior for the first order functions that is allowed by the equations of motion (2.2.4)–(2.2.6). Then we will proceed to examine the solutions in the regime where the flow stops. To find where the flow of φ stops, we need to find (finite) points φ_0 where S vanishes.

We parametrize S as

$$S \simeq C_0 \, (\varphi_0 - \varphi)^a \quad , \quad \varphi \to \varphi_0 \quad , \quad a > 0 \tag{E.1}$$

We assume without loss of generality that φ is approaching to φ_0 from the left, i.e. $\varphi < \varphi_0$. As the flow does not end up at the minimum at the presence of curvature, φ_0 is a generic point and therefore

$$V(\varphi) = V_0 + V_1(\varphi_0 - \varphi) + V_2(\varphi_0 - \varphi)^2 + \mathcal{O}((\varphi_0 - \varphi)^3) \ . \tag{E.2}$$

Near φ_0 the various terms of (2.2.9) behave as follows

$$\begin{aligned} &S^4 \sim (\varphi_0 - \varphi)^{4a}, \quad S^3 S'', S^2 S'^2 \sim (\varphi_0 - \varphi)^{4a-2}, \quad S^2 V \sim (\varphi_0 - \varphi)^{2a}, \\ &S S' V' \sim (\varphi_0 - \varphi)^{2a-1}, \quad S^2 V'' \sim (\varphi_0 - \varphi)^{2a}, \quad V'^2 \sim (\varphi_0 - \varphi)^0. \end{aligned} \tag{E.3}$$

It is apparent that near φ_0, if $a = 1/2$, then to leading order Eq. (2.2.9) is satisfied. After getting the leading order power law behavior, it is clear that the functions have a square root series expansion near the IR end-point. For brevity, let us write $x = \varphi_0 - \varphi$. Let us also write the following expansions

near $x = 0$:

$$S(x) = \sqrt{x}\left(S_0 + S_1\sqrt{x} + S_2 x + \cdots\right) \ , \tag{E.4}$$

$$W(x) = \frac{1}{\sqrt{x}}\left(W_0 + W_1\sqrt{x} + W_2 x + \cdots\right) \ , \tag{E.5}$$

$$T(x) = \frac{1}{x}\left(T_0 + T_1\sqrt{x} + T_2 x + \cdots\right) \ , \tag{E.6}$$

$$V(x) = V_0 + V_1 x + V_2 x^2 + \cdots \ . \tag{E.7}$$

Now we can use Eqs. (2.2.7) and (2.2.8) to find the various coefficients. There are two cases which are generic.

Case (a):

$$S_0^2 = 2V_1 \ , S_1 = \frac{-dW_1}{3(d-1)} \ , S_2 = \frac{36(d-1)\left((d-1)V_2 + V_0\right) + d(d+9)W_1^2}{36(d-1)^2 S_0} \tag{E.8}$$

$$W_0 = 0 \ , \quad W_1 = \text{arbitrary} \ , \quad W_2 = -\frac{4(d-1)V_0 + dW_1^2}{d(d-1)S_0} \tag{E.9}$$

$$T_0 = 0 \ , \quad T_1 = 0 \ , T_2 = \frac{dW_1^2}{4(d-1)} + V_0 \ , T_3 = -\frac{W_1\left(4(d-1)V_0 + dW_1^2\right)}{2(d-1)^2 S_0} \tag{E.10}$$

In this case $\ddot{\varphi} = \frac{1}{2}\frac{d}{dx}S^2 = S_0^2 = 2V_1 \neq 0$. So the flow does not stop here. We will find that this corresponds to a bouncing solution. Note that $S_0 = \pm\sqrt{2V_1}$, i.e. there are two branches. These will be the two branches those meet at the bouncing point. As $V_0 < 0$ we find that T can be both positive or negative, depending on the value of W_1. Hence bounces are expected to exist for both positively and negatively curved slices.

Case (b):

$$S_0^2 = \frac{2V_1}{d+1} \ , S_1 = 0, S_2 = \frac{V_0 + 3(d-1)V_2}{(d-1)(d+3)S_0} \tag{E.11}$$

$$W_0 = (d-1)S_0 \ , W_1 = 0 \ , W_2 = -\frac{(d+4)V_0 - (d-1)dV_2}{d(d+3)S_0} \tag{E.12}$$

$$T_0 = \frac{d(d-1)}{4}S_0^2 \ , T_1 = 0 \ , T_2 = \frac{dS_0W_2}{2} + V_0. \tag{E.13}$$

In this case, $\ddot{\varphi} = \frac{1}{2}\frac{d}{dx}S^2 = S_0^2 = \frac{2V_1}{d+1} \neq 0$. Although the flow does not stop here, the space-time ends. Hence this is an IR solution. Again, it seems that there are two possible solutions with $S_0 = \pm\sqrt{\frac{2V_1}{d+1}}$. However, note that $W_0 = (d-1)S_0$. As we have chosen $W > 0$, only the solution with $S_0 = +\sqrt{\frac{2V_1}{d+1}}$ is acceptable. Furthermore, here we have tacitly assumed that $V_1 > 0$. As $T_0 > 0$, this solution only occurs for positive curvature (e.g. a dS slicing).[1]

Case (c): It is worthwhile to highlight another solution, which corresponds to a special case of situation (a) described above. In particular, this is the case with $W = 0$ at $x = 0$, i.e. we have $W_0 = 0 = W_1$. The solution is given by

$$S_0^2 = 2V_1\,, \tag{E.14}$$

$$W_0 = 0\,, \qquad W_1 = 0\,, \qquad W_2 = \frac{4V_0}{dS_0}\,, \tag{E.15}$$

$$T_0 = 0 \qquad T_1 = 0\,, \qquad T_2 = V_0\,. \tag{E.16}$$

As $V_0 < 0$ we find $T < 0$ in this case. Hence this corresponds to the IR solution with negatively curved slices.

[1] If $V_1 < 0$ we can replace V_1 by $|V_1|$ in all expressions. The solution persists and corresponds to a space-time with positively curved d-dimensional slices.

Appendix F

Calculation of the on-shell action

We begin with on-shell action in the case of a field theory on a Lorentzian manifold. The starting point is the action (1.4.2) which we proceed to rewrite as a functional of $A(u)$. As a first step note that for our ansatz the curvature scalar $R^{(g)}$ of the $(d+1)$ space-time can be written as:

$$R^{(g)} = -\left(2d\ddot{A} + d(d+1)\dot{A}^2\right) + e^{-2A}R^{(\zeta)} = \frac{1}{2}\dot{\varphi}^2 + \frac{d+1}{d-1}\,V\,.$$

where in the last step we used the equations of motion (2.1.5)–(2.1.7). Inserting this into (1.4.2) we find

$$S_{\text{on-shell}} = \frac{2}{d-1}M^{d-1}V_d\int_{\text{UV}}^{\text{IR}} du\, e^{dA}V + S_{GHY}\,, \tag{F.1}$$

i.e. we have successfully eliminated the explicit dependence on $R^{(g)}$ and $\dot{\varphi}^2$. Here we also defined

$$V_d \equiv \int d^dx\sqrt{|\zeta|}\,. \tag{F.2}$$

In the next step we use (2.1.5)–(2.1.6) to replace the potential V in (F.1) by

$$V = -(d-1)\ddot{A} - d(d-1)\dot{A}^2 + \frac{d-1}{d}\,e^{-2A}R^{(\zeta)}\,. \tag{F.3}$$

Inserting and after some manipulations we obtain:

$$\begin{aligned} S_{\text{on-shell}} = {} & 2M^{d-1}V_d\left[e^{dA}\dot{A}\right]_{\text{UV}} - 2M^{d-1}V_d\left[e^{dA}\dot{A}\right]_{\text{IR}} \\ & + \frac{2M^{d-1}R^{(\zeta)}}{d}V_d\int_{\text{UV}}^{\text{IR}} du\, e^{(d-2)A} + S_{GHY}\,, \end{aligned} \tag{F.4}$$

where the subscript UV/IR denotes that the expression is to be evaluated at the UV/IR locus. One can check that, given the asymptotic form of $A(u)$ in the IR (2.5.13) the second term in (F.4) vanishes (as long as $d \geq 2$). Last, we turn to the Gibbons-Hawking-York term, This is given by

$$S_{GHY} = 2M^{d-1}\left[\int d^d x \sqrt{|\gamma|}\, K\right]_{\text{UV}} = -2dM^{d-1}V_d \left[e^{dA}\dot{A}\right]_{\text{UV}}, \tag{F.5}$$

where $K = -d\dot{A}$ is the extrinsic curvature of the boundary and the induced metric $\gamma_{\mu\nu}$ was defined in (2.1.3). Putting everything together we obtain

$$S_{\text{on-shell}} = -2(d-1)M^{d-1}V_d \left[e^{dA}\dot{A}\right]_{\text{UV}} + \frac{2M^{d-1}R}{d}V_d \int_{\text{UV}}^{\text{IR}} du\, e^{(d-2)A}. \tag{F.6}$$

Here we also replaced $R^{(\zeta)}$ by R as the two are identical in our conventions. The expression (F.6) is the on-shell action for a holographic RG flow on a Lorentzian manifold. For the corresponding expression in the Euclidean case we simply have to swap the sign, i.e. we have

$$S_{\text{on-shell},E} = -S_{\text{on-shell}}\,. \tag{F.7}$$

Appendix G

Calculation of the entanglement entropy

In this appendix, we review the calculation of the entanglement entropy which will be used for constructing F-functions. Here we work with a field theory on dS_d, which in our holographic setting corresponds to a bulk spacetime with dS_d boundary. To calculate an entanglement entropy, we then need to specify an entangling surface on the boundary. To this end, we first specify the bulk metric. Here we will work with

$$ds^2 = du^2 + e^{2A(u)}\left[-dt^2 + \alpha^2 \cosh^2(t/\alpha)\left(d\theta^2 + \sin^2\theta d\Omega_{d-2}^2\right)\right] \tag{G.1}$$

where $d\Omega_{d-2}^2$ is the metric on a $(d-2)$-dimensional unit sphere. To find the static entanglement entropy we set $t = 0$ so that the bulk metric becomes:

$$ds^2 = du^2 + \alpha^2 e^{2A(u)}\left(d\theta^2 + \sin^2\theta d\Omega_{d-2}^2\right) \tag{G.2}$$

Our choice of entanglement surface is then given by $\theta|_{u\to-\infty} = \frac{\pi}{2}$. This corresponds to calculating the entanglement entropy between two cap-like regions as shown in fig. 3.4.

The entanglement entropy in our holographic setting is then calculated following the prescription of Ryu and Takayanagi [83]. According to this we need to find the minimal surface in the bulk which has the entangling surface as the boundary. The entanglement entropy is then given by

$$S_{\mathrm{EE}} = \frac{\gamma}{4G_{d+1}} \tag{G.3}$$

where γ is the area of the minimal surface. The equation for the surface is $\theta = \theta(u)$. Then the metric on the surface is

$$ds^2 = \left[1 + \alpha^2 e^{2A(u)}\left(\frac{d\theta}{du}\right)^2\right] du^2 + \alpha^2 \sin^2\theta e^{2A(u)} d\Omega_{d-2}^2. \tag{G.4}$$

From this the surface area functional is obtained as:

$$\gamma = \alpha^{d-2}\mathrm{Vol}(S^{d-2}) \int du \left[1 + \alpha^2 e^{2A(u)} \left(\frac{d\theta}{du}\right)^2\right]^{1/2} \sin^{d-2}\theta \; e^{(d-2)A(u)} \quad \text{(G.5)}$$

where $\mathrm{Vol}(S^{d-2})$ is the volume of a unit radius $(d-2)$-dimensional sphere. To minimise the area the surface $\theta(u)$ has to satisfy the following equation:

$$\alpha^2 e^{2A(u)} \Big[\dot{A}(u)\dot{\theta}(u)\sin(\theta(u)) \Big\{\alpha^2(d-1)e^{2A(u)}(\dot{\theta}(u))^2 + d\Big\}$$
$$-(d-2)(\dot{\theta}(u))^2\cos(\theta(u)) + \ddot{\theta}(u)\sin(\theta(u))\Big] - (d-2)\cos(\theta(u)) = 0 \quad \text{(G.6)}$$

subject to the boundary condition

$$\lim_{u\to-\infty} \theta(u) = \frac{\pi}{2}. \quad \text{(G.7)}$$

We also impose regularity on the surface. The solution of the equation (G.6) subject to the boundary condition (G.7) is:

$$\theta(u) = \frac{\pi}{2}. \quad \text{(G.8)}$$

Then the minimal surface area is

$$\gamma = \alpha^{d-2}\Omega_{d-2} \int_{\mathrm{UV}}^{\mathrm{IR}} du\, e^{(d-2)A(u)}\,, \qquad \text{with} \qquad \Omega_n = \frac{2\pi^{\frac{n+1}{2}}}{\Gamma(\frac{n+1}{2})}\,. \quad \text{(G.9)}$$

Using $\Omega_d = \frac{2\pi}{d-1}\alpha^2\Omega_{d-2}$ and $R = \frac{d(d-1)}{\alpha^2}$ the minimal surface area can be written as

$$\gamma = \frac{2R}{d}\frac{1}{4\pi}\mathrm{Vol}(S^d)\int_{\mathrm{UV}}^{\mathrm{IR}} du\, e^{(d-2)A(u)}\,. \quad \text{(G.10)}$$

The holographic entanglement entropy is then

$$S_{EE} = \frac{\gamma}{4G_{d+1}} = M^{d-1}\frac{2R}{d}\mathrm{Vol}(S^d)\int_{\mathrm{UV}}^{\mathrm{IR}} du\, e^{(d-2)A(u)}\,, \quad \text{(G.11)}$$

where we also rewrote Newton's constant as $G_{d+1} = 1/(16\pi M_p^{d-1})$.

Appendix H

Analytical results for large and small boundary curvature

H.1 Large curvature expansion

RG flows with large dimensionless curvature $\mathcal{R}$ are found when the IR end point is very close to the corresponding UV fixed point $\varphi_{\rm UV}$. In particular, when $\varphi_0 \to \varphi_{\rm UV}$ we find $\mathcal{R} \to \infty$. In this regime we can find solutions analytically by solving perturbatively in $\varphi_\star \equiv |\varphi_0 - \varphi_{\rm UV}|$.

UV fixed points are associated with extrema of the potential, so that in the vicinity of $\varphi_{\rm UV}$ we can write the potential as[1]

$$V(\varphi) = -\frac{d(d-1)}{\ell^2} - \frac{\Delta_-(d-\Delta_-)}{2\ell^2}(\varphi-\varphi_{\rm UV})^2 + \mathcal{O}\big((\varphi-\varphi_{\rm UV})^3\big)\,. \quad \text{(H.1.1)}$$

The solutions for $A(u)$ and $\varphi(u)$ can then be organised as an expansion in $\varphi_\star$ about the solution associated with the UV fixed point $\varphi_{\rm UV}$, which we will refer to as $A_0(u)$ and $\varphi_0(u)$. At the fixed point, the scale factor $A(u)$ is that of AdS_{d+1} space-time given in (2.4.11) :

$$S^d/\mathrm{dS}_d\text{:} \qquad A_0(u) = \log\left(-\frac{\ell}{\alpha}\sinh\frac{u+c}{\ell}\right)\,, \quad \text{(H.1.2)}$$

$$\mathrm{AdS}_d\text{:} \qquad A_0(u) = \log\left(\frac{\ell}{\alpha}\cosh\frac{u+c}{\ell}\right)\,, \quad \text{(H.1.3)}$$

[1]The calculation performed here only applies to UV fixed points at maxima of the potential, as these fixed points come with a family of RG flow solutions with φ_0 a continuous parameter over this family. In contrast, UV fixed points at minima only exist as individual solutions with a discrete set of IR end points φ_0. Hence the limit of taking $\varphi_0 \to \varphi_{\rm UV}$ is ill-defined in this case.

and $\varphi_0(u) = \varphi_{UV}$ is constant. We then find that the system of equations (2.1.5)–(2.1.7) can be solved self-consistently by expanding about $(A_0(u), \varphi_0(u))$ as follows:

$$A(u) = A_0(u) + \mathcal{O}(\varphi_\star^2)\,, \tag{H.1.4}$$
$$\varphi(u) = \varphi_0(u) + \varphi_1(u) + \mathcal{O}(\varphi_\star^2)\,, \tag{H.1.5}$$

and where the subscript indicates the order in the expansion in $\varphi_\star$.

In the following, we will solve explicitly for $\varphi_1(u)$. Also, for simplicity, we will set $\varphi_{\rm UV} = 0$ in the following. Inserting the ansatz for $A_0(u)$ into the Klein-Gordon equation (2.1.7) then results in a differential equation for $\varphi_1(u)$, which will allow us to determine the leading order contribution to flows $\varphi(u)$. The resulting equations take the form:

$$S^d/\mathrm{dS}_d: \qquad \ddot{\varphi}_1 + \frac{d}{\ell}\coth\left(\frac{u+c}{\ell}\right)\dot{\varphi}_1 + m^2\varphi = 0\,, \tag{H.1.6}$$

$$\mathrm{AdS}_d: \qquad \ddot{\varphi}_1 + \frac{d}{\ell}\tanh\left(\frac{u+c}{\ell}\right)\dot{\varphi}_1 + m^2\varphi = 0\,. \tag{H.1.7}$$

The leading contributions to RG flows are given by regular solutions to these equations subject to the boundary conditions:

$$\varphi(-c) = \varphi_0\,, \quad \dot{\varphi}(-c) = 0\,, \quad \text{or, equivalently} \quad \varphi_1(-c) = \varphi_\star\,, \quad \dot{\varphi}_1(-c) = 0\,. \tag{H.1.8}$$

These boundary conditions ensure that flows end at $u_{\rm IR} = -c$, the value at which the scale factor $e^{A(u)}$ vanishes.

We can discuss both equations (H.1.6) and (H.1.7) in a unified way if we define a new coordinate U as follows:

$$U \equiv \begin{cases} -\coth\frac{u+c}{\ell}\,, & S^d/\mathrm{dS}_d \\ -\tanh\frac{u+c}{\ell}\,, & \mathrm{AdS}_d \end{cases}\,. \tag{H.1.9}$$

Equations (H.1.6) and (H.1.7) then become

$$(1-U^2)^2\varphi_1'' + (d-2)U(1-U^2)\varphi_1' + \Delta_-(d-\Delta_-)\varphi_1 = 0\,, \tag{H.1.10}$$

where we defined $' \equiv \frac{d}{dU}$. The general solution is given by:

$$\varphi_1(U) = \Bigg[\ \tilde{C}_1\,(U-1)^{\frac{\Delta_-}{2}}(U+1)^{\frac{d-\Delta_-}{2}}\,{}_2F_1\left(\frac{2-d}{2}, \frac{d}{2}, \frac{2-d+2\Delta_-}{2}, \frac{1-U}{2}\right) \tag{H.1.11}$$
$$-\tilde{C}_2\,(U-1)^{\frac{\Delta_+}{2}}(U+1)^{\frac{d-\Delta_+}{2}}\,{}_2F_1\left(\frac{2-d}{2}, \frac{d}{2}, \frac{2-d+2\Delta_+}{2}, \frac{1-U}{2}\right)\Bigg]\,,$$

where $\tilde{C}_{1,2}$ are integration constants. Imposing the boundary conditions results in the following solution for $\varphi(u)$:

$$\varphi(u) = \varphi_\star \frac{2^{\frac{d}{2}-1}\sqrt{\pi}}{\sin\left(\pi\left(\frac{d-2\Delta_-}{2}\right)\right)} \frac{\Gamma\left(\frac{d+1}{2}\right)}{\Gamma(\Delta_-)\Gamma(d-\Delta_-)}$$
$$\left[(U-1)^{\frac{\Delta_-}{2}}(U+1)^{\frac{d-\Delta_-}{2}} \frac{\Gamma(\Delta_-)}{\Gamma\left(\frac{2-d+2\Delta_-}{2}\right)} {}_2F_1\left(\frac{2-d}{2}, \frac{d}{2}; \frac{2-d+2\Delta_-}{2}; \frac{1-U}{2}\right)\right.$$
$$\left. -(U-1)^{\frac{d-\Delta_-}{2}}(U+1)^{\frac{\Delta_-}{2}} \frac{\Gamma(d-\Delta_-)}{\Gamma\left(\frac{2+d-2\Delta_-}{2}\right)} {}_2F_1\left(\frac{2-d}{2}, \frac{d}{2}; \frac{2+d-2\Delta_-}{2}; \frac{1-U}{2}\right)\right]$$
$$+ \mathcal{O}(\varphi_\star^2)\,. \tag{H.1.12}$$

The above result is valid for general d. Now we collect the results $d = 4$ which have been discussed in chapter 2. An additional benefit is that this will make the expressions more manageable. For $d = 4$ we find :

$$S^4/\mathrm{dS}_4\text{:}\quad A(u) = \log\left(-\frac{\ell}{\alpha}\sinh\frac{u+c}{\ell}\right) + \mathcal{O}(\varphi_\star^2)\,, \tag{H.1.13}$$
$$\varphi(u) = \frac{3\varphi_\star}{2\delta(\delta^2-1)} \frac{1}{\sinh^2\frac{u+c}{\ell}} \left[e^{\delta\frac{u+c}{\ell}}\left(\delta - \coth\frac{u+c}{\ell}\right)\right. \tag{H.1.14}$$
$$\left. + e^{-\delta\frac{u+c}{\ell}}\left(\delta + \coth\frac{u+c}{\ell}\right)\right] + \mathcal{O}(\varphi_0^3)\,,$$
$$\mathrm{AdS}_4\text{:}\quad A(u) = \log\left(\frac{\ell}{\alpha}\cosh\frac{u+c}{\ell}\right) + \mathcal{O}(\varphi_\star^2)\,, \tag{H.1.15}$$
$$\varphi(u) = \frac{\varphi_\star}{2\delta} \frac{1}{\cosh^2\frac{u+c}{\ell}} \left[e^{\delta\frac{u+c}{\ell}}\left(\delta - \tanh\frac{u+c}{\ell}\right)\right. \tag{H.1.16}$$
$$\left. + e^{-\delta\frac{u+c}{\ell}}\left(\delta + \tanh\frac{u+c}{\ell}\right)\right] + \mathcal{O}(\varphi_0^3)\,,$$
$$\text{with} \qquad \delta \equiv \sqrt{4 - m^2\ell^2} \qquad \text{and} \qquad \varphi_0 \ll \sqrt{\frac{|V_0|}{m^2}}\,.$$

There is one interesting feature which we wish to point out. One can check that for $S^4/$ dS_4 slicings $\varphi(u)$ grows strictly monotonically along a flow from UV to IR. For the AdS_4 case, this is only true as long as $\Delta_- < 1$. For $\Delta_- > 1$ we find that $\varphi(u)$ changes direction along the flow: The flow leaves the UV point at $\varphi = 0$ in one direction, then turns around, before terminating on the other side of $\varphi = 0$. This is what was referred to as a 'bounce'. Interestingly, we find that in the regime of small φ_0 bounces are generic for $\Delta_- > 1$.

Analytical relations between UV data

Given the analytical solutions for $A(u)$ and $\varphi(u)$, we can then find how the UV data (φ_-, R, B, C) are related to one another and also to the IR quantity φ_0.

For one, note that both φ_- and C appear in the near-boundary expansion of $\varphi(u)$ given in (2.4.10) and which we reproduce here for convenience:

$$\varphi(u) = \varphi_- \ell^{\Delta_-} e^{\Delta_- u/\ell} + \frac{Cd|\varphi_-|^{\Delta_+/\Delta_-}}{\Delta_-(d-2\Delta_-)} \ell^{\Delta_+} e^{\Delta_+ u/\ell} + \dots . \tag{H.1.17}$$

We can hence find relations involving φ_- and C by comparing with the near boundary behaviour of (H.1.12) above. The boundary is reached for $u \to -\infty$. In this limit the expression (H.1.12) becomes:

$$\begin{aligned}\varphi(u) \underset{u\to-\infty}{=} \varphi_\star \frac{2^{d-1}\sqrt{\pi}}{\sin\left(\pi\left(\frac{d-2\Delta_-}{2}\right)\right)} \frac{\Gamma\left(\frac{d+1}{2}\right)}{\Gamma(\Delta_-)\Gamma(d-\Delta_-)} \times \\ \times \left[\frac{\Gamma(\Delta_-)}{\Gamma\left(\frac{2-d+2\Delta_-}{2}\right)} e^{\Delta_- c/\ell} e^{\Delta_- u/\ell} \left(1 + \mathcal{O}(e^{2u/\ell}) + \mathcal{O}(e^{2\Delta_- u/\ell})\right)\right. \\ \left. + \frac{\Gamma(\Delta_+)}{\Gamma\left(\frac{2-d+2\Delta_+}{2}\right)} e^{\Delta_+ c/\ell} e^{\Delta_+ u/\ell} \left(1 + \mathcal{O}(e^{2u/\ell}) + \mathcal{O}(e^{2\Delta_+ u/\ell})\right)\right] \\ + \mathcal{O}(\varphi_\star^2)\,,\end{aligned} \tag{H.1.18}$$

where c is related to the UV curvature as $\ell^2 R = 4d(d-1)e^{2c/\ell}$. By comparing the coefficients of $e^{\Delta_- u/\ell}$ and of $e^{\Delta_+ u/\ell}$ we can then find

$$\varphi_\star \sim \mathcal{R}^{-\frac{\Delta_-}{2}} \left(1 + \mathcal{O}\big(\mathcal{R}^{-\frac{\Delta_-}{2}}\big)\right), \tag{H.1.19}$$

where we neglected extracting the exact numerical prefactor, as this will not be important. This confirms that an expansion in small $\varphi_\star$ is indeed an expansion for large $\mathcal{R}$. Similarly, we find

$$C \sim \mathcal{O}\left(\mathcal{R}^{\frac{d}{2}-\Delta_-}\right), \tag{H.1.20}$$

where again we ignored numerical prefactors.

So far, the discussion is valid for general d. Now we restrict to $d = 3$. For this case, we will extract B by calculating the entanglement entropy S_{EE} explicitly for large $\mathcal{R}$. Recall that the unrenormalized entanglement entropy is given by (see e.g. equation (3.4.12))

$$S_{\text{EE}}(\Lambda_\epsilon, \mathcal{R}_\epsilon) = (M\ell)^2 \tilde{\Omega}_3 \, \mathcal{R}_\epsilon^{-1/2} \Big(\Lambda_\epsilon\text{-dependent part} + B(\mathcal{R}_\epsilon)\Big). \tag{H.1.21}$$

That is the parameter B corresponds to what we will call the 'universal contribution' to the entanglement entropy, i.e. the part of the entanglement entropy that does not depend on the cutoff Λ_ϵ defined in (3.2.19). This observation will allow us to extract B as follows. From (3.4.3) recall that the entanglement entropy (in $d = 3$) can also be written as

$$S_{\rm EE}(\Lambda_\epsilon, \mathcal{R}_\epsilon) = \frac{2}{3} M^2 \tilde{\Omega}_3 \, R^{-1/2} \int_{u_\epsilon}^{-c} du \, e^{A(u)} \,, \tag{H.1.22}$$

with $u_\epsilon = \ell \log \epsilon$. The idea is to insert our analytic solution $A(u) = A_0(u) + \mathcal{O}(\varphi_\star^2)$ into (H.1.22) and evaluate the integral. After isolating the cutoff-independent part we can then read off B. One obtains

$$S_{\rm EE}(\Lambda_\epsilon, \mathcal{R}_\epsilon) = -\frac{2}{3} M^2 \tilde{\Omega}_3 \, R^{-1/2} \int_{u_\epsilon}^{-c} du \, \frac{\ell}{\alpha} \sinh\left(\frac{u+c}{\ell}\right) \big(1 + \mathcal{O}(\varphi_\star^2)\big) \tag{H.1.23}$$

$$= -\frac{2}{3} (M\ell)^2 \tilde{\Omega}_3 \, \alpha^{-1} \, R^{-1/2} \left[\cosh\left(\frac{u+c}{\ell}\right)\right]_{u_\epsilon}^{-c} - \frac{1}{\alpha} \, \mathcal{O}(\varphi_\star^2) \tag{H.1.24}$$

$$= -8\pi^2 (M\ell)^2 \tilde{\Omega}_3 \left[\cosh\left(\frac{u+c}{\ell}\right)\right]_{u_\epsilon}^{-c} - R^{1/2} \, \mathcal{O}(\varphi_\star^2) \,, \tag{H.1.25}$$

where we have used $R = 6/\alpha^2$ and $\tilde{\Omega}_3 = 12\sqrt{6}\pi^2$. Any contribution from the lower integration limit will depend on ϵ and hence Λ_ϵ. The universal contribution purely comes from the upper integration limit $-c$. Then, comparing with (H.1.21) one finds

$$\begin{aligned} B(\mathcal{R}) &= \lim_{\epsilon \to 0} \Big[- 8\pi^2 \tilde{\Omega}_3^{-2} \mathcal{R}_\epsilon^{1/2} \Big(1 + \mathcal{O}\big(\mathcal{R}_\epsilon^{-\Delta_-}\big) \Big) \Big] \\ &= -8\pi^2 \tilde{\Omega}_3^{-2} \mathcal{R}^{1/2} \Big(1 + \mathcal{O}\big(\mathcal{R}^{-\Delta_-}\big) \Big) \,. \end{aligned} \tag{H.1.26}$$

where we also used (H.1.19).

H.2 Small curvature expansion

Here we will derive analytical expressions for RG flow solutions for small values of the dimensionless curvature $\mathcal{R}$. The results will be obtained by expanding about a *flat* flow solution. We will derive two expansions, one valid in the vicinity of the UV fixed point, and one appropriate when close to the IR end point. With the help of these we will then find expressions for $C(\mathcal{R})$ and $B(\mathcal{R})$ valid for small $\mathcal{R}$.

Expansion in the vicinity of the UV fixed point

Consider a potential with a maximum at $\varphi = \varphi_{\rm UV}$ which gives rise to a UV fixed point. In the vicinity of $\varphi_{\rm UV}$ the potential can then be expanded as in (H.1.1). We also choose the UV to be reached for $u \to -\infty$. An RG flow solution with $R = 0$ then has the following well-known expansion in the vicinity of the UV (see e.g. [17, 5]):

$$A_{\rm flat}(u) = \bar{A} - \frac{u}{\ell} - \frac{\varphi_-^2 \ell^{2\Delta_-}}{8(d-1)} e^{2\Delta_- u/\ell} + \dots \,, \tag{H.2.1}$$

$$\varphi_{\rm flat}(u) = \varphi_{\rm UV} + \varphi_- \ell^{\Delta_-} e^{\Delta_- u/\ell} + \varphi_+ \ell^{\Delta_+} e^{\Delta_+ u/\ell} + \dots \,, \tag{H.2.2}$$

with $\bar{A}$, φ_- and φ_+ integration constants.

Once we switch on a small finite value for $\ell^2 R$, we write the solution for $(A(u), \varphi(u))$ as an expansion in powers of $\ell^2 R$ about the flat solution. In particular, one can check that the equations of motion (2.1.5)–(2.1.7) can be solved self-consistently with the ansatz:

$$A(u) = A_{\rm flat}(u) + \ell^2 R\, A_1(u) + \mathcal{O}\big((\ell^2 R)^2\big) \,, \tag{H.2.3}$$

$$\varphi(u) = f_{\rm flat}(u) + \ell^2 R\, \varphi_1(u) + \mathcal{O}\big((\ell^2 R)^2\big) \,. \tag{H.2.4}$$

Instead of solving for $(A(u), \varphi(u))$ we could have equally considered the functions $W(\varphi)$ and $S(\varphi)$. Again, the solution in the vicinity of $\varphi_{\rm UV}$ can be organised as an expansion about the flat solutions $W_{\rm flat}(\varphi)$ and $S_{\rm flat}(\varphi)$, but now expanding in powers of $\mathcal{R}$. Explicit solutions for $(A(u), \varphi(u))$ and $(W(\varphi), S(\varphi))$ in the vicinity of a UV fixed point at a maximum of the potential are given in appendix C.

However, in the vicinity of the IR end point φ_0 of an RG flow the above expansion is not sufficient. As can be seen from the results in section 2.4.1 a power of $\ell^2 R$ in $(A(u), \varphi(u))$ always comes together with $e^{2u/\ell}$, so that the effective expansion parameter is $\ell^2 R\, e^{2u/\ell}$. Note that for small R the IR end point will will be at $u = u_0 \gg 1$ with $u_0 \to +\infty$ for $R \to 0$. As a result, in the vicinity of the IR the combination $\ell^2 R\, e^{2u/\ell}$ ceases to be a good expansion parameter. Hence, in the following, we will find a different expansion for $(A(u), \varphi(u))$ valid in the vicinity of the IR end point.

Expansion in the vicinity of the IR end point

Here, we will again expand about the solution for a flat flow. Recall that a flow with $\mathcal{R} = 0$ has its IR end point $\varphi_{\rm IR}$ at a minimum of the potential. In contrast, a flow with finite $\mathcal{R}$ can never reach the minimum and ends at a generic point φ_0 (see [8] for details). For $\mathcal{R} \to 0$ the IR end point will

approach the minimum, i.e. $\varphi_0 \to \varphi_{\rm IR}$. Here, we will be interested in solutions valid in the vicinity of φ_0, and hence close to $\varphi_{\rm IR}$. As we will confirm later, a good expansion parameter at small $\mathcal{R}$ for obtaining solutions perturbatively is then $\varphi_* \equiv |\varphi_{\rm IR} - \varphi_0|$.

To begin, we record the expressions for the scale factor $A_{\rm flat}(u)$ and the dilaton $\varphi_{\rm flat}(u)$ for a flat RG flow solution. The IR fixed point $\varphi_{\rm IR}$ is reached for $u \to +\infty$ and in its vicinity one finds [5]:

$$A_{\rm flat}(u) = \bar{\bar{A}} - \frac{u}{\ell_{\rm IR}} + \mathcal{O}\big(e^{2\Delta_-^{\rm IR} u/\ell_{\rm IR}}\big)\,, \tag{H.2.5}$$

$$\varphi_{\rm flat}(u) = \varphi_{\rm IR} + \bar{\varphi}_-\, e^{\Delta_-^{\rm IR} u/\ell_{\rm IR}} + \mathcal{O}\big(e^{2\Delta_-^{\rm IR} u/\ell_{\rm IR}}\big)\,, \tag{H.2.6}$$

where $\bar{\bar{A}}$ and $\bar{\varphi}_-$ are integration constants, $\ell_{\rm IR}$ and $\Delta_-^{\rm IR}$ are given in (3.2.46). On the contrary, for finite $\mathcal{R}$ the IR end point φ_0 is reached for $u \to u_0$ with u_0 finite. The scale factor and dilaton in the vicinity of the IR are given by (see [8]):

$$A(u) \underset{u\to u_0}{=} \ln\left(-\frac{\ell_0}{\alpha}\sinh\frac{u-u_0}{\ell_0}\right)\,, \qquad \varphi(u) = \varphi_0 + \mathcal{O}\big((u-u_0)^2\big)\,, \tag{H.2.7}$$

and

$$\ell_0^2 \equiv -\frac{d(d-1)}{V(\varphi_0)}\,. \tag{H.2.8}$$

We are now in a position to set up the small-curvature expansion. The idea is to expand about a solution of the form (H.2.7) but with $\ell_0 \to \ell_{\rm IR}$ and $\varphi_0 \to \varphi_{\rm IR}$. That is, we expand about a curved ansatz in the flat limit. Also, u_0 is taken to be large and positive, i.e. $u_0 \gg 1$. The full solution can then be constructed in a perturbative expansion in $\varphi_* \equiv |\varphi_{\rm IR} - \varphi_0| \ll 1$ about the leading order expressions. In particular, the equations of motion (2.1.5)–(2.1.7) can be solved self-consistently with the following expansion:

$$A(u) = A_{\rm IR}(u) + \mathcal{O}(\varphi_*^2)\,, \quad \text{with} \quad A_{\rm IR}(u) = \ln\left(-\frac{\ell_{\rm IR}}{\alpha}\sinh\frac{u-u_0}{\ell_{\rm IR}}\right)\,, \tag{H.2.9}$$

$$\varphi(u) = \varphi_{\rm IR} + \varphi_1(u) + \mathcal{O}(\varphi_*^2)\,, \tag{H.2.10}$$

subject to the boundary conditions $\dot{A}(u)|_{u\to u_0} \to \frac{1}{(u-u_0)}$, $\varphi(u_0) = \varphi_0$ and $\dot{\varphi}(u_0) = 0$. The subscript on φ_1 indicates that this term is of order $\mathcal{O}(\varphi_*)$. Furthermore, note that in the regime of interest, the potential can be expanded as

$$V = -\frac{d(d-1)}{\ell_{\rm IR}^2} + \frac{1}{2}m_{\rm IR}^2(\varphi-\varphi_{\rm IR})^2 + \mathcal{O}\big((\varphi-\varphi_{\rm IR})^3\big)\,. \tag{H.2.11}$$

We can now make the following observation. Consider a point $u = u_1$ towards the IR end of the flow, but not close to u_0, that is

$$u_1 \gg 1, , \quad \text{with} \quad u_1 < u_0 \,, \quad \text{and} \quad |u_0 - u_1| \gg 1 \,. \tag{H.2.12}$$

We choose u_1 sufficiently large such that our expansion (H.2.9) is expected to hold. At the same time, any flow that reaches $u_1 \gg 1$ must be a small correction to a flat flow and hence the expression (H.2.5) should also be a good approximation at $u = u_1$. We can then write two expressions for $A(u_1)$. From (H.2.9) we find

$$\begin{aligned} A(u_1) &= \ln\left(-\frac{\ell_{\rm IR}}{\alpha}\sinh\frac{u_1-u_0}{\ell_{\rm IR}}\right)\Big|_{\substack{u_0\gg 1\\ u_1\ll u_0}} + \mathcal{O}\big(\varphi_*^2\big) \\ &= \ln\left(\frac{\ell_{\rm IR}}{2\alpha}\right) + \frac{u_0}{\ell_{\rm IR}} - \frac{u_1}{\ell_{\rm IR}} + \mathcal{O}\big(e^{-2(u_0-u_1)/\ell_{\rm IR}}\big) + \mathcal{O}\big(\varphi_*^2\big)\,. \end{aligned} \tag{H.2.13}$$

while from (H.2.5) one obtains:

$$A(u_1) = \bar{\bar{A}} - \frac{u_1}{\ell_{\rm IR}} + \mathcal{O}\big(e^{2\Delta_-^{\rm IR}u_1/\ell_{\rm IR}}\big)\,, \tag{H.2.14}$$

At leading order, the two expressions for $A(u_1)$ for are consistent if we make the following identification:

$$\frac{u_0}{\ell_{\rm IR}} = \ln\left(\frac{2\alpha}{\ell_{\rm IR}}\right) + \bar{\bar{A}} = \frac{1}{2}\ln\left(\frac{4d(d-1)}{\ell_{\rm IR}^2\,R}\right) + \bar{\bar{A}}\,, \tag{H.2.15}$$

i.e. the value of u_0 is related to the UV curvature R. It is this observation which will be useful in the following. Note that, as expected, we find that $u_0 \to +\infty$ for $R \to 0$.

We can then make one more observation. For $u_0 \gg 1$ we also expect that the flat solution for $\varphi(u)$ given in (H.2.6) should be a good approximation to the full result. In particular, at $u = u_0$ the exact result is given by $\varphi(u_0) = \varphi_0$. Comparing this to the flat expression at $u = u_0$ one finds

$$\varphi_0 = \varphi_{\rm IR} + \bar{\varphi}_-\, e^{\Delta_-^{\rm IR}u_0/\ell_{\rm IR}} + \mathcal{O}\big(e^{2\Delta_-^{\rm IR}u_0/\ell_{\rm IR}}\big)\,.$$

Using the relation (H.2.15) between u_0 and R this can be rewritten as

$$\varphi_* \sim (\ell_{\rm IR}^2 R)^{-\frac{\Delta_-^{\rm IR}}{2}} + \mathcal{O}\big((\ell_{\rm IR}^2 R)^{-\Delta_-^{\rm IR}}\big)\,. \tag{H.2.16}$$

This confirms that an expansion in φ_* is indeed an expansion for small UV curvature R (recalling that $\Delta_-^{\rm IR} < 0$).

Expressions for $B(\mathcal{R})$ and $C(\mathcal{R})$ at small $\mathcal{R}$

While above we have been working with general d here we again specialise to $d = 3$. To extract B we use our insight developed in the previous section H.1. There we used the fact that the parameter $B(\mathcal{R})$ is given by the universal (i.e. cutoff-independent) contribution to the following integral:

$$B(\mathcal{R}) = \lim_{\epsilon\to 0}\left[\frac{2}{3}\ell^{-2}|\varphi_-^\epsilon|^{-1/\Delta_-}\int_{u_\epsilon}^{u_0} du\, e^{A(u)} - (\Lambda_\epsilon\text{-dependent terms})\right]. \tag{H.2.17}$$

Here we wish to determine $B(\mathcal{R})$ for small $\mathcal{R}$. In particular, we want to write $B(\mathcal{R})$ in terms of an expansion about $B_0 = B(0)$, which in terms of an integral is given by

$$B_0 = \lim_{\epsilon\to 0}\left[\frac{2}{3}\ell^{-2}|\varphi_-^\epsilon|^{-1/\Delta_-}\int_{u_\epsilon}^{\infty} du\, e^{A_{\text{flat}}(u)} - (\Lambda_\epsilon\text{-dependent terms})\right]. \tag{H.2.18}$$

The main difficulty in determining B is to calculate the integral appearing in (H.2.17). For small R this can be done perturbatively by using the expansions developed above. The main idea is to to split the integration interval $[u_\epsilon, u_0]$ into two and integrate over $[u_\epsilon, u_1]$ and $[u_1, u_0]$ separately. Here u_1 is an auxiliary parameter and can take any value as long as it satisfies (H.2.12). We therefore write the integral in (H.2.17) as:

$$I = \int_{u_\epsilon}^{u_0} du\, e^{A(u)} = \int_{u_\epsilon}^{u_1} du\, e^{A(u)} + \int_{u_1}^{u_0} du\, e^{A(u)}\,. \tag{H.2.19}$$

Then, on the interval $[u_\epsilon, u_1]$ we can use the expansion (H.2.3) for $A(u)$ in powers of R. On the interval $[u_\epsilon, u_1]$ close to the IR we instead use the expansion given in (H.2.9). This is summarised below:

$$A(u) = \begin{cases} A_{\text{flat}}(u) + \mathcal{O}(R)\,, & u < u1\,, \\ A_{\text{IR}}(u) + \mathcal{O}(\varphi_*^2)\,, & u > u_1\,, \end{cases} \tag{H.2.20}$$

with the two solutions matched at $u = u_1$ up to the required order. Inserting this, the integral becomes:

$$\begin{aligned} I &= \int_{u_\epsilon}^{u_1} du\, \exp\left(A_{\text{flat}}(u) + \mathcal{O}(R)\right) + \int_{u_1}^{u_0} du\, \exp\left(A_{\text{IR}}(u) + \mathcal{O}(\varphi_*^2)\right) \\ &= \int_{u_\epsilon}^{u_1} du\, e^{A_{\text{flat}}(u)} + \int_{u_\epsilon}^{u_1} du\, \mathcal{O}(R) + \int_{u_1}^{u_0} du\, e^{A_{\text{IR}}(u)+\mathcal{O}(\varphi_*^2)}\,. \end{aligned} \tag{H.2.21}$$

In the next step, we split the first integral in (H.2.21) into two as follows:

$$I = \int_{\log\epsilon}^{\infty} du\, e^{A_{\rm flat}(u)} - \int_{u_1}^{\infty} du\, e^{A_{\rm flat}(u)} + \int_{\log\epsilon}^{u_1} du\, \mathcal{O}(R) + \int_{u_1}^{u_0} du\, e^{A_{\rm IR}(u)+\mathcal{O}(\varphi_*^2)}\,. \tag{H.2.22}$$

Also, as the two solutions for $u < u_1$ and $u > u_1$ are matched at u_1, the contributions to the integrals in (H.2.22) from the limit u_1 will vanish. Hence we need to evaluate

$$\begin{aligned} I &= \int_{u_\epsilon}^{\infty} du\, e^{A_{\rm flat}(u)} - \int^{\infty} du\, e^{A_{\rm flat}(u)} + \int_{u_\epsilon} du\, \mathcal{O}(R) + \int^{u_0} du\, e^{A_{\rm IR}(u)+\mathcal{O}(\varphi_*^2)} \\ &= I_1 + I_2 + I_3 + I_4\,. \end{aligned} \tag{H.2.23}$$

The first term I_1 in the above is then the same integral that appears in the expression for B_0 given in (H.2.18). Therefore, the first term will indeed contribute a term B_0 to $B(\mathcal{R})$ while the remaining terms will give rise to corrections.

We will then proceed as follows. In the next step we will insert the appropriate expressions for $A_{\rm flat}$ and $A_{\rm IR}$ into the 2nd (I_2) and 4th term (I_4) in (H.2.23) and perform the integrations. In particular, in the 2nd integral we replace $A_{\rm flat}$ by its near IR-expansion given in (H.2.5). In the 4th term we insert expression (H.2.9). To remove clutter we will set $\bar{\bar{A}} = 0$ in the following. Then these two integrals become:

$$\begin{aligned} I_2 + I_4 =& -\int^{\infty} du\, e^{A_{\rm flat}(u)} + \int^{u_0} du\, e^{A_{\rm IR}(u)+\mathcal{O}(\varphi_*^2)} \\ =& -\int^{\infty} du\, e^{-\frac{u}{\ell_{\rm IR}}} \left(1+\mathcal{O}\big(e^{2\Delta_-^{\rm IR}u/\ell_{\rm IR}}\big)\right) - \frac{\ell_{\rm IR}}{\alpha}\int^{u_0} du\, \sinh\left(\tfrac{u-u_0}{\ell_{\rm IR}}\right)\left(1+\mathcal{O}(\varphi_*^2)\right) \\ =& \ell_{\rm IR}\left[e^{-\frac{u}{\ell_{\rm IR}}} + \mathcal{O}\big(e^{(2\Delta_-^{\rm IR}-1)u/\ell_{\rm IR}}\big)\right]^{\infty} - \frac{\ell_{\rm IR}^2}{\alpha}\left[\cosh\left(\frac{u-u_0}{\ell_{\rm IR}}\right)\right]^{u_0} + \frac{\ell_{\rm IR}}{\alpha}\,\mathcal{O}\big(\varphi_*^2\big) \\ =& -\frac{\ell_{\rm IR}^2}{\alpha}\left(1+\mathcal{O}(\varphi_*^2)\right) \\ =& -\frac{\ell_{\rm IR}^2}{\sqrt{6}}\,R^{1/2}\left(1+\mathcal{O}\big(R^{-\Delta_-^{\rm IR}}\big)\right), \end{aligned} \tag{H.2.24}$$

where in the last step we have used $R = 6/\alpha^2$ and (H.2.16). Then, putting everything together, we are left with

$$I = \int_{u_\epsilon}^{\infty} du\, e^{A_{\rm flat}(u)} + \mathcal{O}(R) - \frac{\ell_{\rm IR}^2}{\sqrt{6}}\,R^{1/2}\left(1+\mathcal{O}\big(R^{-\Delta_-^{\rm IR}}\big)\right). \tag{H.2.25}$$

Inserting this back into (H.2.17) we obtain

$$B(\mathcal{R}) = \lim_{\epsilon\to 0}\Bigg[\frac{2}{3}\ell^{-2}|\varphi_-^\epsilon|^{-1/\Delta_-}\int_{u_\epsilon}^{\infty} du\, e^{A_{\text{flat}}(u)} + \mathcal{O}(\mathcal{R}_\epsilon) \qquad \text{(H.2.26)}$$
$$- 8\pi^2\tilde{\Omega}_3^{-2}\frac{\ell_{\text{IR}}^2}{\ell^2}\mathcal{R}_\epsilon^{1/2}\left(1+\mathcal{O}\big(\mathcal{R}_\epsilon^{-\Delta_-^{\text{IR}}}\big)\right) - (\Lambda_\epsilon\text{-dependent terms})\Bigg],$$

As stated before, the first term contributes B_0. Therefore, overall we find

$$B(\mathcal{R}) \underset{\mathcal{R}\to 0}{=} B_0 + \mathcal{O}(\mathcal{R}) - 8\pi^2\tilde{\Omega}_3^{-2}\frac{\ell_{\text{IR}}^2}{\ell^2}\mathcal{R}^{1/2}\left(1+\mathcal{O}\big(\mathcal{R}^{-\Delta_-^{\text{IR}}}\big)\right). \qquad \text{(H.2.27)}$$

We can perform a similar analysis for extracting $C(\mathcal{R})$ for small $\mathcal{R}$. In particular, we can determine $C(\mathcal{R})$ from the first term in (3.2.3). After introducing a cutoff Λ_ϵ as in (3.2.19) this term gives rise to the first line in expression (3.2.23). From this it follows that $C(\mathcal{R})$ can be determined as

$$C(\mathcal{R}) = \lim_{\epsilon\to 0}\Bigg[-4\ell^{-2}|\varphi_-^\epsilon|^{-3/\Delta_-}\, e^{3A(u)}\dot{A}(u)\Big|_{u=u_\epsilon} - (\Lambda_\epsilon\text{-dependent terms})\Bigg]. \qquad \text{(H.2.28)}$$

We define $C_0 = C(0)$ as the value of $C(\mathcal{R})$ for $\mathcal{R} = 0$. This can be calculated as

$$C_0 = \lim_{\epsilon\to 0}\Bigg[-4\ell^{-2}|\varphi_-^\epsilon|^{-3/\Delta_-}\, e^{3A_{\text{flat}}(u)}\dot{A}_{\text{flat}}(u)\Big|_{u=u_\epsilon} - (\Lambda_\epsilon\text{-dependent terms})\Bigg]. \qquad \text{(H.2.29)}$$

In the following, it will be useful to write $C(\mathcal{R})$ in terms of an integral. In particular note that

$$\int_{u_\epsilon}^{u_0} du\, e^{3A}(\ddot{A}+3\dot{A}^2) = \Big[e^{3A}\dot{A}\Big]_{u_\epsilon}^{u_0} = -\,e^{3A}\dot{A}(u)\Big|_{u=u_\epsilon}, \qquad \text{(H.2.30)}$$

where we observe that the integral does not receive any contributions from its IR limit. Hence we can write $C(\mathcal{R})$ as

$$C(\mathcal{R}) = \lim_{\epsilon\to 0}\Bigg[4\ell^{-2}|\varphi_-^\epsilon|^{-3/\Delta_-}\int_{u_\epsilon}^{u_0} du\, e^{3A}(\ddot{A}+3\dot{A}^2) - (\Lambda_\epsilon\text{-dependent terms})\Bigg]. \qquad \text{(H.2.31)}$$

As before, we again split the integration range into the two intervals $[u_\epsilon, u_1]$ and $[u_1, u_0]$ with u_1 satisfying (H.2.12). We then insert for $A(u)$ with the

appropriate expansions as detailed in (H.2.20). Then the integral in (H.2.31) becomes

$$\begin{aligned}\mathcal{I} &= \int_{u_\epsilon}^{u_0} du\, e^{3A}(\ddot{A}+3\dot{A}^2)\\ &= \int_{u_\epsilon}^{u_1} du\, e^{3A_{\text{flat}}}(\ddot{A}_{\text{flat}}+3\dot{A}_{\text{flat}}^2)\\ &\quad + \ell_{\text{IR}}^2 R\int_{u_\epsilon}^{u_1} du\, e^{3A_{\text{flat}}}\Big(\ddot{A}_1+3\dot{A}_1^2+3A_1(\ddot{A}_{\text{flat}}+3\dot{A}_{\text{flat}}^2)\Big)\\ &\quad + \int_{u_\epsilon}^{u_1} du\,\mathcal{O}(R^2)+\int_{u_1}^{u_0} du\, e^{3A_{\text{IR}}}(\ddot{A}_{\text{IR}}+3\dot{A}_{\text{IR}}^2)\Big(1+\mathcal{O}(\varphi_*^2)\Big) \qquad \text{(H.2.32)}\end{aligned}$$

To make contact with the expression for C_0 we rewrite the first integral in (H.2.32) as

$$\begin{aligned}&\int_{u_\epsilon}^{u_1} du\, e^{3A_{\text{flat}}}(\ddot{A}_{\text{flat}}+3\dot{A}_{\text{flat}}^2)\\ &= \int_{u_\epsilon}^{\infty} du\, e^{3A_{\text{flat}}}(\ddot{A}_{\text{flat}}+3\dot{A}_{\text{flat}}^2)-\int_{u_1}^{\infty} du\, e^{3A_{\text{flat}}}(\ddot{A}_{\text{flat}}+3\dot{A}_{\text{flat}}^2)\,. \qquad \text{(H.2.33)}\end{aligned}$$

By ensuring that the solutions for $u<u_1$ and $u>u_1$ match at $u=u_1$ to the appropriate order, we can ensure that u_1 does not appear in the final expression and can therefore be deleted from (H.2.32). We are hence left with

$$\begin{aligned}\mathcal{I} &= \int_{u_\epsilon}^{\infty} du\, e^{3A_{\text{flat}}}(\ddot{A}_{\text{flat}}+3\dot{A}_{\text{flat}}^2)-\int^{\infty} du\, e^{3A_{\text{flat}}}(\ddot{A}_{\text{flat}}+3\dot{A}_{\text{flat}}^2)\\ &\quad + \ell_{\text{IR}}^2 R\int_{u_\epsilon} du\, e^{3A_{\text{flat}}}\Big(\ddot{A}_1+3\dot{A}_1^2+3A_1(\ddot{A}_{\text{flat}}+3\dot{A}_{\text{flat}}^2)\Big)\\ &\quad + \int_{u_\epsilon} du\,\mathcal{O}(R^2)+\int^{u_0} du\, e^{3A_{\text{IR}}}(\ddot{A}_{\text{IR}}+3\dot{A}_{\text{IR}}^2)\Big(1+\mathcal{O}(\varphi_*^2)\Big)\\ &= \Big[e^{3A_{\text{flat}}}\dot{A}_{\text{flat}}\Big]_{u_\epsilon}+\ell_{\text{IR}}^2 R\int_{u_\epsilon} du\, e^{3A_{\text{flat}}}\Big(\ddot{A}_1+3\dot{A}_1^2+3A_1(\ddot{A}_{\text{flat}}+3\dot{A}_{\text{flat}}^2)\Big)\\ &\quad + \mathcal{O}(R^2)+\Big[e^{3A_{\text{IR}}}\dot{A}_{\text{IR}}\Big]^{u_0}-\frac{\ell_{\text{IR}}^3}{\alpha^3}\,\mathcal{O}(\varphi_*^2)\,. \qquad \text{(H.2.34)}\end{aligned}$$

Inserting for A_{IR} from (H.2.9) one finds that

$$\Big[e^{3A_{\text{IR}}}\dot{A}_{\text{IR}}\Big]^{u_0}=0\,. \qquad \text{(H.2.35)}$$

Hence we are left with

$$\mathcal{I} = \left[e^{3A_{\text{flat}}}\dot{A}_{\text{flat}}\right]_{u_\epsilon} + \ell_{\text{IR}}^2 R \int_{u_\epsilon} du\, e^{3A_{\text{flat}}} \left(\ddot{A}_1 + 3\dot{A}_1^2 + 3A_1(\ddot{A}_{\text{flat}} + 3\dot{A}_{\text{flat}}^2)\right) + \mathcal{O}(R^2) + \mathcal{O}\left(R^{\frac{3}{2}-\Delta_-^{\text{IR}}}\right). \tag{H.2.36}$$

where we have also used $R = 6/\alpha^2$ and (H.2.16). Inserting this back into (H.2.28) we then find the following. We identify the first term in (H.2.36) with C_0, while the second term gives a contribution $\sim \mathcal{R}C_1$. Overall we hence find that for small $\mathcal{R}$ we can write

$$C(\mathcal{R}) = \left(C_0 + \mathcal{R}C_1 + \mathcal{O}(\mathcal{R}^2)\right) + \mathcal{O}\left(\mathcal{R}^{\frac{3}{2}-\Delta_-^{\text{IR}}}\right), \tag{H.2.37}$$

where we also used that $C(\mathcal{R})$ depends on R only via $\mathcal{R}$.

Appendix I

Holographic entanglement entropy of a spherical region in flat space

In this appendix, we will calculate the holographic entanglement entropy of a spherical entangling region in flat space. In this regard, we write the $(d+1)$-dimensional bulk in flat slicing as

$$ds^2 = du^2 + e^{2A(u)}\left(-dt^2 + dr^2 + r^2 d\Omega_{d-2}^2\right). \tag{I.1}$$

At constant time slicing we can write the metric in conformal coordinates as

$$ds^2 = \rho^2(z)\left(dz^2 + dr^2 + r^2 d\Omega_{d-2}^2\right) \tag{I.2}$$

where the coordinate z and the scale factor $a(z)$ are defined as

$$e^{-A(u)}du = dz\ , \quad \rho(z) = e^{A(u(z))}\ . \tag{I.3}$$

We are interested in computing the entanglement entropy between a ball of radius α , $r \leq \alpha$, and the rest on the boundary. That means the entangling "surface" is a $(d-2)$-dimensional sphere of radius α on the boundary. To compute the entanglement entropy holographically, we need to find the minimal $(d-1)$-dimensional "surface" in the bulk which coincides with a $(d-2)$-dimensional sphere of radius α on the boundary. To find this, we take the ansatz: $r = r(z)$ while the angular coordinates coincide. The induced metric on this "surface" becomes

$$ds_{ind}^2 = \rho^2(z)\left[\left(1 + r'^2(z)\right)dz^2 + r^2(z)d\Omega_{d-2}^2\right]\ . \tag{I.4}$$

From this induced the metric we can find the area functional

$$\mathcal{S}[r(z)] = \Omega_{d-2}\int dz\ \rho^{d-1}(z)r^{d-2}(z)\sqrt{1 + r'^2(z)}. \tag{I.5}$$

which needs to be minimized subject to the boundary condition that $r(\epsilon) = \alpha$, where $z = \epsilon$ is the boundary. Variation of the area functional leads to the equation

$$\rho(z)\left((d-2)r'(z)^2 + d - 2 - r(z)r''(z)\right) - (d-1)r(z)\rho'(z)r'(z)\left(r'(z)^2+1\right) = 0\,. \tag{I.6}$$

This equation needs two boundary conditions. One is fixed by asking that the surface intersects the (regulated) boundary at $z = \epsilon$ on a circle of radius α; The second condition is that the surface is regular where it closes off: if the minimal surface ends $z = z_0$, we must impose

$$z(0) = z_0\ , \quad z'(0) = 0\ . \tag{I.7}$$

for regularity. Near $r = 0$ we then have

$$z(r) \approx z_0 + \kappa r^2\ , \tag{I.8}$$

where κ can be taken to 1 which is equivalent to a coordinate rescaling. Eq. (I.8) sets the initial condition for $r(z_0)$ and $r'(z_0)$ and then we solve the eq. (I.6) numerically.

Denoting the solution of this equation as $r = r_0(z)$, we find the minimal area is

$$\mathcal{A} = \Omega_{d-2}\int dz\ \rho^{d-1}(z) r_0^{d-2}(z)\sqrt{1 + r_0'^2(z)}\ . \tag{I.9}$$

The entanglement entropy calculated by this way is divergent near the UV boundary $z = \epsilon$ and requires regularisation. The holographic entanglement entropy is then

$$S_{\rm FEE} = \frac{\mathcal{A}}{4G_{d+1}} = 4\pi M^{d-1}\mathcal{A}\ . \tag{I.10}$$

Appendix J

De Sitter entanglement entropy and thermodynamics

In this appendix we show that the entanglement entropy computed in section 3.4 is the same as the bulk gravitational entropy of the space-time which one obtains by writing the slice metric in de Sitter static coordinates. This gives rise to a horizon in the bulk, with an associate temperature and entropy. The internal energy is identified with the ADM mass associated to the timelike killing vector.

Using the thermodynamic relation between free energy, internal energy and entropy, it is possible to derive relation (3.4.10) relating the functions $B(\mathcal{R})$ and $C(\mathcal{R})$ which appear in the F-functions.

J.1 The de Sitter static patch: thermal entropy, and the ADM mass

The metric of dS in the expanding patch is

$$\zeta_{\mu\nu}dx^\mu dx^\nu = -dt^2 + \alpha^2 \cosh^2(t/\alpha)\left(d\theta^2 + \sin^2\theta d\Omega_{d-2}^2\right) \ . \tag{J.1.1}$$

On the other hand the dS metric in the static patch is

$$\zeta_{\mu\nu}dx^\mu dx^\nu = -\left(1-\frac{r^2}{\alpha^2}\right)d\tau^2 + \left(1-\frac{r^2}{\alpha^2}\right)^{-1} dr^2 + r^2 d\Omega_{d-2}^2 \ . \tag{J.1.2}$$

The coordinate transformations from the expanding patch to the static patch is

$$\tau = \alpha \sinh^{-1}\left\{\frac{\sinh(t/\alpha)}{\sqrt{1-\cosh^2(t/\alpha)\sin^2\theta}}\right\}, \tag{J.1.3}$$

$$r = \alpha \cosh(t/\alpha)\sin\theta\ , \tag{J.1.4}$$

and all the other angular coordinates are the same.

The bulk metric in the static patch coordinates is

$$ds^2 = du^2 + e^{2A(u)}\left[-\left(1-\frac{r^2}{\alpha^2}\right)d\tau^2 + \left(1-\frac{r^2}{\alpha^2}\right)^{-1}dr^2 + r^2 d\Omega_{d-2}^2\right]\ . \tag{J.1.5}$$

We can see that there is a horizon at $r=\alpha$, parametrized by the coordinates (u, Ω_{d-2}). The associated temperature is

$$T = \frac{1}{2\pi\alpha}\ . \tag{J.1.6}$$

as can be easily seen by going to Euclidean time and imposing the right periodicity to demand regularity at $r=\alpha$, i.e. $\tau \sim \tau + i2\pi\alpha$.

Entropy

The thermodynamic entropy associated to the horizon is given by

$$S_{\rm th} = \frac{\text{Area}}{4G_{d+1}} = 4\pi M^{d-1}\text{Vol}(S^{d-2})\,, \int_{\rm UV}^{\rm IR} du\, e^{(d-2)A(u)} \tag{J.1.7}$$

where we have also used $G_{d+1} = (16\pi M^{d-1})^{-1}$. Using the fact that $\alpha^2 = d(d-1)/R$ and the geometric relation $\text{Vol}(S^{d-2}) = \frac{d-1}{2\pi\,\alpha^2}\text{Vol}(S^d)$, we obtain

$$S_{\rm th} = 2M^{d-1}\frac{R}{d}V_d \int_{\rm UV}^{\rm IR} du\, e^{(d-2)A(u)} = S_{\rm EE}, \tag{J.1.8}$$

where we have used the explicit expression for $S_{\rm EE}$ established in equation (3.4.3) for the last identification, and the definition $V_d = \text{Vol}(S^d)$.

ADM Mass

For a static metric such as the one in equation (J.1.5) the internal energy is identified with the ADM mass, defined as

$$\begin{aligned} M_{\rm ADM} &= -2M^{d-1}\int_{\rm UV} d^{d-1}x\sqrt{h}NK_{\rm ADM} \\ &= 2(d-1)M^{d-1}\left[e^{dA(u)}\dot{A}(u)\right]_{\rm UV}\Omega_{d-2}\int_0^{\alpha} drr^{d-2}\ . \end{aligned} \tag{J.1.9}$$

On the fixed time slice and on boundary the metric is

$$h_{ab}dx^a dx^b = \left[e^{2A(u)}\right]_{\rm UV}\left[\left(1-\frac{r^2}{\alpha^2}\right)^{-1}dr^2 + r^2 d\Omega_{d-2}^2\right] \tag{J.1.10}$$

where $\left[e^{2A(u)}\right]_{\rm UV}$ means $e^{2A(u)}$ evaluated at the UV boundary. The extrinsic curvature of this hypersurface of codimension 2 is

$$K_{\rm ADM} = -(d-1)[\dot{A}(u)]_{\rm UV}\ . \tag{J.1.11}$$

and the lapse function is

$$N = e^{A(u)}\left(1-\frac{r^2}{\alpha^2}\right)^{1/2}\ . \tag{J.1.12}$$

Using the relation $\Omega_d = \frac{2\pi}{d-1}\Omega_{d-2}$ and evaluating the integral in equation (J.1.9) we find,

$$M_{\rm ADM} = 2(d-1)M^{d-1}\left[e^{dA(u)}\dot{A}(u)\right]_{\rm UV}\Omega_d\frac{\alpha^{d-1}}{2\pi}\ . \tag{J.1.13}$$

Using the relations $\beta = 2\pi\alpha$ and $V_d = \alpha^d\Omega_d$, we arrive at

$$\beta M_{\rm ADM} = 2(d-1)M^{d-1}\left[e^{dA(u)}\dot{A}(u)\right]_{\rm UV}V_d \tag{J.1.14}$$

Identifying the ADM mass with the internal energy, $M_{\rm ADM} = U_{\rm th}$, equation (3.2.3) becomes the (integrated) first law.

$$\beta F_{\rm th} = \beta U_{\rm th} - S_{\rm th} \tag{J.1.15}$$

J.2 Identities from thermodynamic relations

We begin with the renormalized stress-tensor, which is computed holographically by

$$\langle T_{\mu\nu}^{(\text{ren})} \rangle = -\frac{2}{\sqrt{\zeta}} \frac{\delta S_{\text{on-shell}}^{(\text{ren})}}{\delta\, \zeta^{\mu\nu}}\,, \tag{J.2.1}$$

where $\zeta_{\mu\nu}$ denotes the metric on S^3. Expressions for both the cutoff-regulated and the renormalized free energy $F = -S_{\text{on-shell}}$ are collected in (3.2.39) and (3.2.40). Using these expressions we obtain

$$\langle T_{\mu\nu}^{(\text{ren})} \rangle = -\frac{1}{3}\, R^{3/2}\, \mathcal{C}^{(\text{ren})}\, \zeta_{\mu\nu}\,, \tag{J.2.2}$$

with

$$\begin{aligned}\mathcal{C} = -(M\ell)^2 \tilde{\Omega}_3 \Big(& 3\mathcal{R}_\epsilon^{-3/2} \big[4\Lambda_\epsilon^3 (1 + \ldots) + C \big] + \mathcal{R}_\epsilon^{-1/2} \big[\Lambda_\epsilon (1 + \ldots) + B - 2C' \big] \\ & - 2\mathcal{R}_\epsilon^{1/2} B' \Big)\,, \end{aligned} \tag{J.2.3}$$

$$\mathcal{C}^{\text{ren}} = -(M\ell)^2 \tilde{\Omega}_3 \Big(3\mathcal{R}^{-3/2} (C - C_{ct}) + \mathcal{R}^{-1/2} (B - B_{ct}) - 2\mathcal{R}^{-1/2} C' - 2\mathcal{R}^{1/2} B' \Big)\,, \tag{J.2.4}$$

where $(\ldots)$ contain all remaining terms that depend on the cutoff Λ_ϵ explicitly. Furthermore, starting with (3.2.39) and (3.2.40) one can also show that

$$\mathcal{R}_{(\epsilon)} \frac{\partial}{\partial \mathcal{R}_{(\epsilon)}} F^{(\text{ren})} = -\frac{1}{2} \mathcal{C}^{(\text{ren})}\,. \tag{J.2.5}$$

We now use the thermodynamic identifications discussed in the first part of this appendix,

$$\beta F_{\text{th}} = F^{(\text{ren})}\,, \tag{J.2.6}$$

$$S_{\text{th}} = S_{\text{EE}}^{(\text{ren})}\,, \tag{J.2.7}$$

$$\beta U_{\text{th}} = \int d^3x\, \sqrt{\zeta}\, \langle T_0^0 \rangle = \frac{1}{3} \mathcal{C}^{(\text{ren})}\,. \tag{J.2.8}$$

Then the thermodynamic relation (J.1.15) implies:

$$\begin{aligned} S_{\text{EE}}^{(\text{ren})} &= \frac{1}{3} \mathcal{C}^{(\text{ren})} - F^{(\text{ren})} \\ &= -\frac{2}{3} \mathcal{R}_{(\epsilon)} \frac{\partial}{\partial \mathcal{R}_{(\epsilon)}} F^{(\text{ren})} - F^{(\text{ren})} \\ &= -\mathcal{D}_{3/2}\, F^{(\text{ren})} \end{aligned} \tag{J.2.9}$$

where when going from the 1st to the 2nd line we used (J.2.5) and where $\mathcal{D}_{3/2}$ is defined in (3.3.9). Therefore, starting with the thermodynamic relation (J.1.15) we successfully reproduced the relations (3.4.26)–(3.4.27).

In addition, consider once more the thermodynamic relation (now in terms of the cutoff-regulated quantities only)

$$S_{\text{EE}}(\Lambda_\epsilon, \mathcal{R}_\epsilon) = \frac{1}{3}\mathcal{C} - F(\Lambda_\epsilon, \mathcal{R}_\epsilon)\,. \tag{J.2.10}$$

Inserting (3.4.12), (J.2.3) and (3.2.39) and taking the limit $\Lambda_\epsilon \to \infty$ one can show that this reduces to

$$C'(\mathcal{R}) = \frac{1}{2}B(\mathcal{R}) - \mathcal{R}B'(\mathcal{R})\,, \tag{J.2.11}$$

We also confirmed this identity numerically for a wide range of examples.

Note that to arrive at (J.2.9) and (J.2.11) it was crucial that the the entanglement entropy $S_{\text{EE}}^{(\text{ren})}$ is identified with a thermal entropy as in (J.2.7). Our numerical evidence for the validity of (J.2.9) and (J.2.11) can therefore be seen as evidence for the validity of this assertion.

From (J.2.11) we can make another observation. As shown in app. H.2 for small $\mathcal{R}$ the functions $B(\mathcal{R})$ and $C(\mathcal{R})$ can be expanded as

$$\begin{aligned} B(\mathcal{R}) &= B_0 + B_{1/2}\mathcal{R}^{1/2} + \mathcal{O}(\mathcal{R}) + \mathcal{O}(\mathcal{R}^{1/2-\Delta_-^{\text{IR}}}) \\ C(\mathcal{R}) &= C_0 + C_1\mathcal{R} + \mathcal{O}(\mathcal{R}^2) + \mathcal{O}(\mathcal{R}^{3/2-\Delta_-^{\text{IR}}})\,. \end{aligned}$$

Then (J.2.11) implies that

$$B_0 = 2C_1 \qquad \Rightarrow \qquad B(\mathcal{R})\big|_{\mathcal{R}=0} = 2\,\frac{\partial C(\mathcal{R})}{\partial \mathcal{R}}\bigg|_{\mathcal{R}=0}\,. \tag{J.2.12}$$

This in turn gives the following relation between the renormalization scheme parameters $B_{ct,0}$ and $\tilde{B}_{ct,0}$ defined in (3.3.11) and (3.4.21):

$$B_{ct,0} = B_0 + C_1 \overset{(\text{J.2.12})}{=} \frac{3}{2}B_0 = \frac{3}{2}\tilde{B}_{ct,0}\,. \tag{J.2.13}$$

In this section we will give further physical insight into the renormalization scheme employed in section 3.3.2. There we found that for constructing good $\mathcal{F}$-function from the on-shell action for a theory on S^3, we need to choose the two counterterms $C_{ct,0}$ and $B_{ct,0}$ as

$$C_{ct,0} = C(0) = C_0\,, \qquad B_{ct,0} = B(0) + C'(0) = B_0 + C_1\,. \tag{J.2.14}$$

Here we will relate (J.2.14) to a renormalization condition for correlation functions of the stress tensor for the field theory on S^3. The key ingredient will be a set of identities already derived in [80]. Here we we reproduce the relevant equations, rewriting them using our notation.

We start by collecting the relevant expressions. The (expectation value of the) renormalized stress tensor can be written in terms of the renormalized on-shell action as

$$\begin{aligned}\langle T^{\rm ren}_{\mu\nu}(x)\rangle &= -\frac{2}{\sqrt{\zeta(x)}}\frac{\delta\, S^{\rm ren}_{\text{on-shell}}(\mathcal{R}|B_{ct},C_{ct})}{\delta\,\zeta^{\mu\nu}(x)}\\ &= -\frac{1}{3}|\varphi_-|^{3/\Delta_-}\mathcal{R}^{3/2}\,\mathcal{C}^{\rm ren}(\mathcal{R}|B_{ct},C_{ct})\,\zeta_{\mu\nu}(x)\,,\end{aligned}\tag{J.2.15}$$

with $\mathcal{C}^{\rm ren}$ given in (J.2.4). We also have the two-point function

$$\langle T^{\rm ren}_{\mu\nu}(x)T^{\rm ren}_{\rho\sigma}(y)\rangle = \frac{4}{\sqrt{\zeta(x)}\sqrt{\zeta(y)}}\frac{\delta^2\, S^{\rm ren}_{\text{on-shell}}(\mathcal{R}|B_{ct},C_{ct})}{\delta\,\zeta^{\mu\nu}(x)\;\delta\,\zeta^{\rho\sigma}(y)}\,.\tag{J.2.16}$$

If we consider variations with respect to $\zeta_{\mu\nu}$ respecting the spherical symmetry of S^3 (i.e. restricting to homogeneous Weyl rescalings,) the following holds

$$\int d^3y\,\zeta^{\rho\sigma}(y)\,\frac{\delta}{\delta\,\zeta^{\rho\sigma}(y)} = \mathcal{R}\,\frac{\partial}{\partial\mathcal{R}}\,.\tag{J.2.17}$$

By applying the above operator to (J.2.15) one can derive the following identity:

$$\begin{aligned}&\left\langle\Big(\int d^3y\,\sqrt{\zeta(y)}\,T^{\rm ren}(y)\Big)\,T^{\rm ren}_{\mu\nu}(x)\right\rangle - 3\langle T^{\rm ren}_{\mu\nu}(x)\rangle\\ &\qquad= \frac{2}{3}|\varphi_-|^{3/\Delta_-}\mathcal{R}\frac{\partial}{\partial\mathcal{R}}\Big(\mathcal{R}^{3/2}\,\mathcal{C}^{\rm ren}\Big)\,\zeta_{\mu\nu}(x) + \frac{2}{3}|\varphi_-|^{3/\Delta_-}\,\mathcal{R}^{3/2}\,\mathcal{C}^{\rm ren}\,\zeta_{\mu\nu(x)}\,,\end{aligned}\tag{J.2.18}$$

where we have also used (J.2.16) and $T^{\rm ren}\equiv\zeta^{\mu\nu}T^{\rm ren}_{\mu\nu}$.

We are now in a position to rewrite the conditions (J.2.14) as a set of conditions on the 1pt and 2pt-functions of $T^{\rm ren}_{\mu\nu}$. To this end we take expression (J.2.15) and expand $\mathcal{C}^{\rm ren}$ for small $\mathcal{R}$. Using our results from appendix H.2 one finds

$$\begin{aligned}\langle T^{\rm ren}_{\mu\nu}(x)\rangle &= -\frac{1}{3}|\varphi_-|^{3/\Delta_-}\mathcal{R}^{3/2}\,\mathcal{C}^{\rm ren}(\mathcal{R}|B_{ct},C_{ct})\,\zeta_{\mu\nu}(x)\\ &\underset{\mathcal{R}\to0}{=} (M\ell)^2|\varphi_-|^{3/\Delta_-}\Big((C_0-C_{ct})+\mathcal{O}(\mathcal{R})+\mathcal{O}\big(\mathcal{R}^{\frac{3}{2}-\Delta^{\rm IR}_-}\big)\Big)\,\zeta_{\mu\nu}(x)\,.\end{aligned}$$

Rearranging this we find

$$(C_0 - C_{ct})\,\zeta_{\mu\nu}(x) = (M\ell)^{-2}|\varphi_-|^{-3/\Delta_-}\,\langle T^{\text{ren}}_{\mu\nu}(x)\rangle\Big|_{R\to 0}\,. \tag{J.2.19}$$

If we recall the identification of φ_- with the source j and C with the (dimensionless) vev of the deforming operator, equation (J.2.19) is nothing but the trace identity $\langle T\rangle = \beta(j)\langle O\rangle$ in the $R = 0$ theory. Equation (J.2.19) implies that renormalizing with $C_{ct} = C_{ct,0} = C_0$ is equivalent to the renormalization condition, that the renormalized stress tensor $\langle T^{\text{ren}}_{\mu\nu}(x)\rangle$ (or, equivalently, the renormalized operator vev $\langle O\rangle$) of the flat theory ($R = 0$) vanishes.

For the 2nd renormalization condition, we start with expression (J.2.18), adding $2\langle T^{\text{ren}}_{\mu\nu}(x)\rangle$ on both sides:

$$\left\langle \Big(\int d^3y\,\sqrt{\zeta(y)}\,T^{\text{ren}}(y)\Big)\,T^{\text{ren}}_{\mu\nu}(x)\right\rangle - \langle T^{\text{ren}}_{\mu\nu}(x)\rangle = \frac{2}{3}|\varphi_-|^{3/\Delta_-}\mathcal{R}\frac{\partial}{\partial\mathcal{R}}\Big(\mathcal{R}^{3/2}\,\mathcal{C}^{\text{ren}}\Big)\,\zeta_{\mu\nu}(x)\,. \tag{J.2.20}$$

Inserting for $\mathcal{C}^{\text{ren}}$ with (J.2.4) and using our results from appendix H.2 this becomes:

$$\begin{aligned}
&\left\langle \Big(\int d^3y\,\sqrt{\zeta(y)}\,T^{\text{ren}}(y)\Big)\,T^{\text{ren}}_{\mu\nu}(x)\right\rangle - \langle T^{\text{ren}}_{\mu\nu}(x)\rangle \\
&= -\frac{2}{3}(M\ell)^2|\varphi_-|^{3/\Delta_-}\Big(\mathcal{R}(B + C' - B_{ct}) - \mathcal{R}^2B' - 2\mathcal{R}^2C'' - 2\mathcal{R}^3B''\Big)\,\zeta_{\mu\nu}(x) \\
&\underset{\mathcal{R}\to 0}{=} -\frac{2}{3}(M\ell)^2|\varphi_-|^{3/\Delta_-}\Big(\mathcal{R}(B_0 + C_1 - B_{ct}) + \mathcal{O}(\mathcal{R}^2) + \mathcal{O}\big(\mathcal{R}^{\frac{3}{2}-\Delta^{\text{IR}}_-}\big)\Big)\,\zeta_{\mu\nu}(x)\,.
\end{aligned} \tag{J.2.21}$$

This can be rearranged as follows:

$$\begin{aligned}
&(B_0 + C_1 - B_{ct})\,\zeta_{\mu\nu}(x) \\
&= \frac{3}{2}(M\ell)^{-2}|\varphi_-|^{-1/\Delta_-}\left[\frac{1}{R}\left(\left\langle \Big(\int d^3y\,\sqrt{\zeta(y)}\,T^{\text{ren}}(y)\Big)\,T^{\text{ren}}_{\mu\nu}(x)\right\rangle - \langle T^{\text{ren}}_{\mu\nu}(x)\rangle\right)\right]_{R\to 0}\,.
\end{aligned} \tag{J.2.22}$$

Therefore, the choice $B_{ct} = B_{ct,0} = B_0 + C_1$ is again related to a vanishing condition on correlators involving $T^{\text{ren}}_{\mu\nu}$ for $R \to 0$.

Appendix K

Zeta-function renormalization vs. covariant counterterms

Here we calculate the free energy for conformally coupled massive boson on S^3 and renormalize it with the help of covariant counterterms. We then compare with the corresponding expression obtained via zeta-function renormalization.

The action for a conformally coupled massive scalar on S^3 is given by

$$S = \frac{1}{2}\int d^dx\,\sqrt{\zeta}\,\left((\nabla\phi)^2 + \frac{d-2}{4(d-1)}R\phi^2 + m^2\phi^2\right)\,. \tag{K.1}$$

where $\zeta_{\mu\nu}$ is a metric on S^3 of radius α. The free energy is then calculated as

$$F_S = -\log|Z| = \frac{1}{2}\log\det\left(\mu_0^{-2}\mathcal{O}_S\right)\,, \quad \text{with} \quad \mathcal{O}_S = -\nabla^2 + \frac{d-2}{4(d-1)}R + m^2\,, \tag{K.2}$$

and μ_0 is a scale introduced to make the functional determinant well-defined.

The determinant of $\mathcal{O}_S$ can be calculated as the product of its eigenvalues. In $d = 3$ these are given by (see e.g. [66])

$$\lambda_j = \frac{1}{\alpha^2}\left(j+\frac{3}{2}\right)\left(j+\frac{1}{2}\right) + m^2\,, \qquad j \geq 0\,. \tag{K.3}$$

The multiplicity of each level n is

$$m_j = (j+1)^2\,. \tag{K.4}$$

Putting everything together and defining $n = j+1$, we arrive at the following expression for the free energy:

$$F_S = \frac{1}{2}\sum_{n=1}^{\infty} n^2 \, \log\left(\frac{n^2 - \frac{1}{4} + (\alpha m)^2}{(\alpha\mu_0)^2}\right) . \tag{K.5}$$

To regulate this expression, we cut off the sum at a maximum level $n_{\max} = N$. Also, for μ_0 we choose the corresponding eigenvalue at this level, i.e.

$$\mu_0^2 = \lambda_{j_{\max}} = \lambda_{N-1} = \frac{1}{\alpha^2}\left(N^2 - \frac{1}{4} + (\alpha m)^2\right) . \tag{K.6}$$

Thus we arrive at an expression for the regulated free energy which is given by

$$F_S^{\rm reg}(N, \alpha m) = \frac{1}{2}\sum_{n=1}^{N} n^2 \, \log\left(\frac{n^2 - \frac{1}{4} + (\alpha m)^2}{N^2 - \frac{1}{4} + (\alpha m)^2}\right) , \tag{K.7}$$

where we made it manifest that it is a function of the cutoff N and the dimensionless combination αm.

We will be particularly interested in the divergent terms (i.e. terms with positive powers of N) and finite terms ($\sim \mathcal{O}(N^0)$) in F_S for $N \to \infty$. One can extract those explicitly by rewriting the sum in F_S with the help of the Euler-Maclaurin formula:

$$\sum_{n=a}^{b} f(n) = \int_a^b dx\, f(x) + \frac{f(a)+f(b)}{2} + \sum_{k=1}^{\lfloor p/2 \rfloor} \frac{B_{2k}}{(2k)!}\Big(f^{(2k-1)}(b) - f^{(2k-1)}(a)\Big) + R_p \, , \tag{K.8}$$

with

$$R_p = (-1)^{p+1}\int_a^b dx\, \frac{B_p(x - \lfloor x \rfloor)}{p!}\, f^{(p)}(x) \, , \tag{K.9}$$

where $\lfloor x \rfloor$ is the largest integer that is not greater than x. Here B_{2k} denote Bernoulli numbers and $B_p(x)$ is the p-th Bernoulli polynomial.

Then, in the limit $N \to \infty$ one finds that

$$F_S^{\rm reg}(N, \alpha m) = -\frac{1}{9}N^3 + \frac{(\alpha m)^2}{3}N + F_S^{\rm finite}(\alpha m) + \mathcal{O}(N^{-1}) \, , \tag{K.10}$$

where we denoted the $\mathcal{O}(N^0)$-term by $F_S^{\rm finite}(\alpha m)$. It is a function of (αm) and we can only evaluate it numerically.

Having arrived at a regulated expression for F_S, we now renormalize by adding appropriate counterterms to the action (K.1). As a fist step, we define a dimensionful cutoff Λ as

$$\Lambda \equiv \frac{N}{\alpha}\,. \tag{K.11}$$

We then add covariant counterterms of the form

$$S_{ct,1} = \int d^3x\sqrt{\zeta}\,\Lambda^3\, f_1(m/\Lambda)\,, \qquad S_{ct,2} = \int d^3x\sqrt{\zeta}\,R\,\Lambda\, f_2(m/\Lambda)\,, \tag{K.12}$$

where the functions $f_1(m/\Lambda)$ and $f_2(m/\Lambda)$ are to be chosen such that one arrives at a finite expression for the free energy. Given the divergences in (K.10), the appropriate counterterms are

$$S_{ct,1} = \int d^3x\sqrt{\zeta}\,\left(\frac{\Lambda^3}{18\pi^2} - \frac{m^2\Lambda}{6\pi^2} + c_{ct}m^3\right) = \frac{1}{9}N^3 - \frac{(\alpha m)^2}{3}N + 2\pi^2 c_{ct}(\alpha m)^3\,, \tag{K.13}$$

$$S_{ct,2} = \int d^3x\sqrt{\zeta}\,R\,b_{ct}m = 12\pi^2 b_{ct}\,\alpha m\,. \tag{K.14}$$

Here c_{ct} and b_{ct} are two unspecified coefficients that multiply finite counterterms, i.e. UV-cutoff-independent terms. Picking values for c_{ct} and b_{ct} modifies the finite part of F_S and hence a choice of c_{ct} and b_{ct} amounts to choosing a renormalization scheme.

Hence, we arrive at an expression for the (counterterm-)renormalized free energy. This is given by

$$F_S^{\rm ren}(\alpha m\,|\,b_{ct},c_{ct}) = \lim_{N\to\infty}\Big(F^{\rm reg}(N,\alpha m) + S_{ct,1}(\alpha m\,|\,c_{ct}) + S_{ct,2}(\alpha m\,|\,b_{ct})\Big)\,, \tag{K.15}$$

where we also indicated the dependence on the renormalization-scheme parameters b_{ct}, c_{ct}.

We are now in a position to compare the expression (K.15) with the zeta-function-renormalized expression for F_S given in (3.5.22). While we cannot do this analytically, a numerical evaluation shows that

$$F_S^{\rm ren}(\alpha m\,|\,\zeta\text{-function-renormalized}) = F_S^{\rm ren}(\alpha m\,|\,b_{ct}=0,c_{ct}=0)\,. \tag{K.16}$$

Thus, in the case of the free massive scalar on S^3, zeta-function-renormalization is equivalent to adding counterterms with all finite counterterms chosen to vanish ($b_{ct}=0, c_{ct}=0$).

Appendix L

Junction conditions for curved brane embeddings in a flat-sliced bulk

Here we consider a brane describing a curve $u = u_\star(\tau)$, which constitutes the interface between solutions of the form

$$ds^2 = du^2 + e^{2A(u)}\eta_{\mu\nu}dx^\mu dx^\nu, \quad \varphi = \varphi(u) \tag{L.1}$$

in which the scale factor and scalar field profile are, a priori, different on each side of the interface,

$$(A,\varphi) = \begin{cases} (A_-(u),\varphi_-(u)) & u < u_\star(\tau) \\ \\ (A_+(u),\varphi_+(u)) & u > u_\star(\tau) \end{cases} \tag{L.2}$$

The connection across the brane is specified by Israel's junction conditions:

1. The metric and scalar field are continuous:

$$\Big[g_{ab}\Big]_{IR}^{UV} = 0, \qquad \Big[\varphi\Big]_{UV}^{IR} = 0 \tag{L.3}$$

2. The extrinsic curvature and normal derivative of φ are discontinuous:

$$\Big[K_{\mu\nu} - \gamma_{\mu\nu}K\Big]_{UV}^{IR} = \frac{1}{\sqrt{-\gamma}}\frac{\delta S_{brane}}{\delta\gamma^{\mu\nu}}, \qquad \Big[n^a\partial_a\varphi\Big]_{UV}^{IR} = -\frac{1}{\sqrt{-\gamma}}\frac{\delta S_{brane}}{\delta\varphi}, \tag{L.4}$$

where $\gamma_{\mu\nu} = e^{2A(u)}\eta_{\mu\nu}$ is the induced metric, $K_{\mu\nu}$ is the extrinsic curvature of the brane with trace $K = \gamma^{\mu\nu}K_{\mu\nu}$, and n^a a unit vector normal to the brane with orientation towards the IR.

The first of these conditions, the continuity of the metric and scalar field across the interface, implies

$$A_-(u_\star(\tau)) = A_+(u_\star(\tau)), \qquad \varphi_-(u_\star(\tau)) = \varphi_+(u_\star(\tau)). \tag{L.5}$$

If $u_\star(\tau)$ is a non-trivial function, equation (L.5) implies the identity of the functions $A_-(u)$ and $A_+(u)$, and of $\varphi_-(u)$ and $\varphi_+(u)$, over a continuous set of values. Since in the bulk these functions satisfy a system of *ordinary* differential equations, this implies that the solutions on each side must coincide,

$$A_-(u) = A_+(u), \quad \varphi_-(u) = \varphi_+(u), \qquad \forall\, u. \tag{L.6}$$

Therefore, not only A and φ but also their derivatives must be continuous. Then, the second junction conditions require

$$\frac{\delta S_{brane}}{\delta \gamma^{\mu\nu}} = 0, \qquad \frac{\delta S_{brane}}{\delta \varphi} = 0. \tag{L.7}$$

In other words, the induced metric and the scalar on the brane must satisfy their lower-dimensional field equations, as dictated by the brane action alone. Recall however that the induced metric $\gamma_{\mu\nu}$ and the brane scalar field φ are not independent quantities, but they are determined by the bulk metric and scalar field, via the embedding function $u_\star(\tau)$: therefore, generically the solution of equations (L.7) will be incompatible with the bulk solution.

To illustrate this more explicitly, we write the induced metric and scalar field for a general embedding $u_*(\tau)$:

$$ds^2_{ind} = \left[\left(\frac{du_\star}{d\tau}\right)^2 - e^{2A(u_\star(\tau))}\right] d\tau^2 + e^{2A(u_\star(\tau))} dx_i dx^i, \qquad \phi(\tau) = \varphi(u_\star(\tau)) \tag{L.8}$$

where we have used a different notation $\phi(\tau)$ to denote the induced scalar field. We can change coordinates on the brane to proper time η, where the induced metric takes the canonical FRW form

$$ds^2_{ind} = -d\eta^2 + a^2(\eta) dx_i dx^i, \qquad a(\eta) \equiv e^{A(u_\star(\eta))}. \tag{L.9}$$

Because of (L.7), the induced scale factor $a(\eta)$ and scalar field $\phi(\eta)$ must satisfy the brane Einstein-scalar equations, whose solution is determined purely by the brane potentials without reference to the bulk.

Given a solution $(a(\eta), \phi(\eta))$ of the brane Einstein's equations and knowing the bulk geometry $A(u)$ we can determine the embedding $u_\star(\eta)$ by inverting the implicit relation

$$A(u_\star(\eta)) = \log a(\eta) \tag{L.10}$$

Having found $u_\star(\eta)$ we can go back to the bulk time coordinate τ by solving the differential equation

$$\frac{d\eta}{d\tau} = \frac{a(\eta)}{\left[1 + \left(\frac{du_\star}{d\eta}\right)^2\right]^{1/2}}, \tag{L.11}$$

which follows from the change of coordinates between (L.8) and (L.9).

The embedding $u_\star(\eta)$ must be such that, at the same time as (L.10), one must also satisfy the relation

$$\varphi(u_\star(\eta)) = \phi(\eta) \tag{L.12}$$

On the other hand, the functions $A(u)$ and $\varphi(u)$ are determined by the *bulk* Einstein equations, which generically know nothing about the brane potentials. Therefore, if we determine $u_\star(\tau)$ from knowledge of $a(\eta)$ and $A(u)$ as explained above, generically the relation (L.12) will *not* hold, and we are forced to conclude that the ansatz we started from does not lead to a solution of the full system.

The argument above assumes generic (and unrelated) bulk and brane potentials. However, if we abandon genericity, it may be possible to tune the model such that equations (L.10)–(L.12) are indeed compatible, and a solution exists. This leads to the curious case which we call an *evanescent brane*, i.e. an exact solution of the bulk-brane system in which the brane has no backreaction on the bulk.

Evanescent branes

As we have seen in the previous discussion, embedding a non-trivial brane trajectory in a flat-slicing is possible if the induced quantities on the brane satisfy their lower-dimensional field equations governed by the brane potentials. If that is the case, the bulk is smooth across the brane, and the interface is transparent (or invisible), although all bulk equations and junction conditions are exactly satisfied: curiously, we have a fully backreacted system where the backreaction is exactly vanishing.

A simple example of such a situation is given by a bulk solution which is Poincaré-AdS with constant scalar field (realised e.g. at an extremum of $V(\varphi)$, say at $\varphi = 0$),

$$A(u) = -\frac{u}{\ell}, \quad \varphi(u) = 0, \tag{L.13}$$

and a brane action of the form (5.2.2) with constant U and Z and a potential $W_B(\varphi)$ such that it *also* has an extremum at $\varphi = 0$, with $W_B(0) > 0$. In this

case, the brane field equations (L.7) admit a de Sitter solution with constant scalar $\phi = 0$ and Hubble constant $H = \sqrt{W_B(0)}/M_p^2$, where $M_p^2 = M^3 U$,

$$a(\eta) = e^{H\eta}, \quad \phi(\eta) = 0. \tag{L.14}$$

Comparing equations (L.13) and (L.14) we can read-off the trajectory using equation (L.10),

$$u_\star(\eta) = -\ell H \eta. \tag{L.15}$$

Equation (L.11) becomes

$$\frac{d\eta}{d\tau} = \frac{e^{H\eta}}{[1 + H^2\ell^2]^{1/2}}, \tag{L.16}$$

and by integrating it we can find the trajectory in the original bulk coordinates,

$$u_\star(\tau) = \ell \log\left[-\frac{H}{(1 + H^2\ell^2)^{1/2}}\,\tau\right], \qquad -\infty < \tau < 0. \tag{L.17}$$

From the brane point of view, τ is the de Sitter conformal time. Finally, and crucially, $\varphi(u(\tau)) = \phi(\tau)$ since both sides vanish identically, by equations (L.13-L.14). Therefore, we have an exact solution of the full system, including the junction conditions. This was possible because we have tuned the brane theory such that an extremum of the brane potential coincides with an extremum of the bulk potential. It is likely that similar examples can be constructed with a non-trivial bulk scalar field profile, e.g. by appropriate combinations of bulk and brane exponential potentials.

We stress that in these solutions the bulk does not detect at all the presence of the brane: the bulk AdS solution would be the same were the brane absent. What we have here is a non-trivial generalization of the fact that, if the world-volume action has only a potential term, then a tensionless brane produces no backreaction. In our case instead, we have a non-vanishing tension, but induced kinetic terms for gravity and the scalar. The corresponding statement is that a brane satisfying its own world-volume Einstein equation behaves (from the point of view of the bulk) as if it were tensionless.

Bibliography

[1] Leonard Susskind. The World as a hologram. *J. Math. Phys.*, 36:6377–6396, 1995.

[2] Gerard 't Hooft. Dimensional reduction in quantum gravity. *Conf. Proc.*, C930308:284–296, 1993.

[3] Jacob D. Bekenstein. Black Holes and Entropy. *Phys. Rev. D*, 7, 1973.

[4] S. W. Hawking. Particle creation by black holes. *Comm. Math. Phys.*, 43(3):199–220, 1975.

[5] Elias Kiritsis, Francesco Nitti, and Leandro Silva Pimenta. Exotic RG Flows from Holography. *Fortsch. Phys.*, 65(2):1600120, 2017.

[6] Csaba Csaki, Joshua Erlich, Christophe Grojean, and Timothy J. Hollowood. General properties of the selftuning domain wall approach to the cosmological constant problem. *Nucl. Phys.*, B584:359–386, 2000.

[7] Christos Charmousis, Elias Kiritsis, and Francesco Nitti. Holographic self-tuning of the cosmological constant. *JHEP*, 09:031, 2017.

[8] Jewel Kumar Ghosh, Elias Kiritsis, Francesco Nitti, and Lukas T. Witkowski. Holographic RG flows on curved manifolds and quantum phase transitions. *JHEP*, 05:034, 2018.

[9] Jewel Kumar Ghosh, Elias Kiritsis, Francesco Nitti, and Lukas T. Witkowski. Holographic RG flows on curved manifolds and the F-theorem. *JHEP*, 02:055, 2019.

[10] Jewel Kumar Ghosh, Elias Kiritsis, Francesco Nitti, and Lukas T. Witkowski. De Sitter and Anti-de Sitter branes in self-tuning models. *JHEP*, 11:128, 2018.

[11] J. M. Bardeen, B. Carter, and S. W Hawking. The four laws of black hole mechanics. *Comm. Math. Phys.*, 31:161–170, 1973.

[12] Juan Martin Maldacena. The Large N limit of superconformal field theories and supergravity. *Int. J. Theor. Phys.*, 38:1113–1133, 1999. [Adv. Theor. Math. Phys.2,231(1998)].

[13] Ofer Aharony, Steven S. Gubser, Juan Martin Maldacena, Hirosi Ooguri, and Yaron Oz. Large N field theories, string theory and gravity. *Phys. Rept.*, 323:183–386, 2000.

[14] Elias Kiritsis. *String theory in a nutshell*. 2007.

[15] S. S. Gubser, Igor R. Klebanov, and Alexander M. Polyakov. Gauge theory correlators from noncritical string theory. *Phys. Lett.*, B428:105–114, 1998.

[16] Edward Witten. Anti-de Sitter space and holography. *Adv. Theor. Math. Phys.*, 2:253–291, 1998.

[17] Igor R. Klebanov and Edward Witten. AdS / CFT correspondence and symmetry breaking. *Nucl. Phys.*, B556:89–114, 1999.

[18] L. Girardello, M. Petrini, M. Porrati, and A. Zaffaroni. Novel local CFT and exact results on perturbations of N=4 superYang Mills from AdS dynamics. *JHEP*, 12:022, 1998.

[19] Vijay Balasubramanian and Per Kraus. Space-time and the holographic renormalization group. *Phys. Rev. Lett.*, 83:3605–3608, 1999.

[20] D. Z. Freedman, S. S. Gubser, K. Pilch, and N. P. Warner. Renormalization group flows from holography supersymmetry and a c theorem. *Adv. Theor. Math. Phys.*, 3:363–417, 1999.

[21] Jan de Boer, Erik P. Verlinde, and Herman L. Verlinde. On the holographic renormalization group. *JHEP*, 08:003, 2000.

[22] Massimo Bianchi, Daniel Z. Freedman, and Kostas Skenderis. How to go with an RG flow. *JHEP*, 08:041, 2001.

[23] Ioannis Papadimitriou and Kostas Skenderis. AdS / CFT correspondence and geometry. *IRMA Lect. Math. Theor. Phys.*, 8:73–101, 2005.

[24] Anna Ceresole and Gianguido Dall'Agata. Flow Equations for Non-BPS Extremal Black Holes. *JHEP*, 03:110, 2007.

[25] Ioannis Papadimitriou. Multi-Trace Deformations in AdS/CFT: Exploring the Vacuum Structure of the Deformed CFT. *JHEP*, 05:075, 2007.

[26] U. Gursoy and E. Kiritsis. Exploring improved holographic theories for QCD: Part I. *JHEP*, 02:032, 2008.

[27] U. Gursoy, E. Kiritsis, and F. Nitti. Exploring improved holographic theories for QCD: Part II. *JHEP*, 02:019, 2008.

[28] Idse Heemskerk and Joseph Polchinski. Holographic and Wilsonian Renormalization Groups. *JHEP*, 06:031, 2011.

[29] Thomas Faulkner, Hong Liu, and Mukund Rangamani. Integrating out geometry: Holographic Wilsonian RG and the membrane paradigm. *JHEP*, 08:051, 2011.

[30] Ioannis Papadimitriou. Holographic Renormalization of general dilaton-axion gravity. *JHEP*, 08:119, 2011.

[31] Saso Grozdanov. Wilsonian Renormalisation and the Exact Cut-Off Scale from Holographic Duality. *JHEP*, 06:079, 2012.

[32] Elias Kiritsis and Vasilis Niarchos. The holographic quantum effective potential at finite temperature and density. *JHEP*, 08:164, 2012.

[33] Jun Bourdier and Elias Kiritsis. Holographic RG flows and nearly-marginal operators. *Class. Quant. Grav.*, 31:035011, 2014.

[34] Elias Kiritsis, Wenliang Li, and Francesco Nitti. Holographic RG flow and the Quantum Effective Action. *Fortsch. Phys.*, 62:389–454, 2014.

[35] Robert C. Myers and Aninda Sinha. Seeing a c-theorem with holography. *Phys. Rev.*, D82:046006, 2010.

[36] Francesco Nitti, Leandro Silva Pimenta, and DaniÃ¨le A. Steer. On multi-field flows in gravity and holography. *JHEP*, 07:022, 2018.

[37] Christos Charmousis, Blaise Gouteraux, Bom Soo Kim, Elias Kiritsis, and Rene Meyer. Effective Holographic Theories for low-temperature condensed matter systems. *JHEP*, 11:151, 2010.

[38] H. Osborn. Weyl consistency conditions and a local renormalization group equation for general renormalizable field theories. *Nucl. Phys.*, B363:486–526, 1991.

[39] M. Henningson and K. Skenderis. The Holographic Weyl anomaly. *JHEP*, 07:023, 1998.

[40] Sebastian de Haro, Sergey N. Solodukhin, and Kostas Skenderis. Holographic reconstruction of space-time and renormalization in the AdS / CFT correspondence. *Commun. Math. Phys.*, 217:595–622, 2001.

[41] Curtis G. Callan, Jr. and Frank Wilczek. Infrared Behavior At Negative Curvature. *Nucl. Phys.*, B340:366–386, 1990.

[42] Elias Kiritsis and Costas Kounnas. Infrared regularization of superstring theory and the one loop calculation of coupling constants. *Nucl. Phys.*, B442:472–493, 1995.

[43] Daniel L. Jafferis. The Exact Superconformal R-Symmetry Extremizes Z. *JHEP*, 05:159, 2012.

[44] Daniel L. Jafferis, Igor R. Klebanov, Silviu S. Pufu, and Benjamin R. Safdi. Towards the F-Theorem: N=2 Field Theories on the Three-Sphere. *JHEP*, 06:102, 2011.

[45] Robert C. Myers and Aninda Sinha. Holographic c-theorems in arbitrary dimensions. *JHEP*, 01:125, 2011.

[46] Ofer Aharony, Micha Berkooz, David Tong, and Shimon Yankielowicz. Confinement in Anti-de Sitter Space. *JHEP*, 02:076, 2013.

[47] N. C. Tsamis and R. P. Woodard. The Structure of perturbative quantum gravity on a De Sitter background. *Commun. Math. Phys.*, 162:217–248, 1994.

[48] N. C. Tsamis and R. P. Woodard. Strong infrared effects in quantum gravity. *Annals Phys.*, 238:1–82, 1995.

[49] N. C. Tsamis and R. P. Woodard. The Quantum gravitational back reaction on inflation. *Annals Phys.*, 253:1–54, 1997.

[50] S. A. Ramsey and B. L. Hu. O(N) quantum fields in curved space-time. *Phys. Rev.*, D56:661–677, 1997.

[51] C. P. Burgess, L. Leblond, R. Holman, and S. Shandera. Super-Hubble de Sitter Fluctuations and the Dynamical RG. *JCAP*, 1003:033, 2010.

[52] Julien Serreau. Effective potential for quantum scalar fields on a de Sitter geometry. *Phys. Rev. Lett.*, 107:191103, 2011.

[53] Julien Serreau. Renormalization group flow and symmetry restoration in de Sitter space. *Phys. Lett.*, B730:271–274, 2014.

[54] Viatcheslav F. Mukhanov, L. Raul W. Abramo, and Robert H. Brandenberger. On the Back reaction problem for gravitational perturbations. *Phys. Rev. Lett.*, 78:1624–1627, 1997.

[55] Alexei A. Starobinsky and Junichi Yokoyama. Equilibrium state of a selfinteracting scalar field in the De Sitter background. *Phys. Rev.*, D50:6357–6368, 1994.

[56] Kostas Skenderis. Lecture notes on holographic renormalization. *Class. Quant. Grav.*, 19:5849–5876, 2002.

[57] Ioannis Papadimitriou and Kostas Skenderis. Correlation functions in holographic RG flows. *JHEP*, 10:075, 2004.

[58] M. J. Duff. Twenty years of the Weyl anomaly. *Class. Quant. Grav.*, 11:1387–1404, 1994.

[59] Andreas Karch and Lisa Randall. Locally localized gravity. *JHEP*, 05:008, 2001. [,140(2000)].

[60] Juan Martin Maldacena and Liat Maoz. Wormholes in AdS. *JHEP*, 02:053, 2004.

[61] A. B. Zamolodchikov. Irreversibility of the Flux of the Renormalization Group in a 2D Field Theory. *JETP Lett.*, 43:730–732, 1986. [Pisma Zh. Eksp. Teor. Fiz.43,565(1986)].

[62] John L. Cardy. Is There a c Theorem in Four-Dimensions? *Phys. Lett.*, B215:749–752, 1988.

[63] Zohar Komargodski and Adam Schwimmer. On Renormalization Group Flows in Four Dimensions. *JHEP*, 12:099, 2011.

[64] H. Casini and M. Huerta. A Finite entanglement entropy and the c-theorem. *Phys. Lett.*, B600:142–150, 2004.

[65] Tatsuma Nishioka. Entanglement entropy: holography and renormalization group. *Rev. Mod. Phys.*, 90(3):035007, 2018.

[66] Igor R. Klebanov, Silviu S. Pufu, and Benjamin R. Safdi. F-Theorem without Supersymmetry. *JHEP*, 10:038, 2011.

[67] Horacio Casini, Marina Huerta, and Robert C. Myers. Towards a derivation of holographic entanglement entropy. *JHEP*, 05:036, 2011.

[68] Simone Giombi and Igor R. Klebanov. Interpolating between a and F. *JHEP*, 03:117, 2015.

[69] Teruhiko Kawano, Yuki Nakaguchi, and Tatsuma Nishioka. Holographic Interpolation between a and F. *JHEP*, 12:161, 2014.

[70] Christopher P. Herzog, Igor R. Klebanov, Silviu S. Pufu, and Tiberiu Tesileanu. Multi-Matrix Models and Tri-Sasaki Einstein Spaces. *Phys. Rev.*, D83:046001, 2011.

[71] Daniel R. Gulotta, Christopher P. Herzog, and Silviu S. Pufu. From Necklace Quivers to the F-theorem, Operator Counting, and T(U(N)). *JHEP*, 12:077, 2011.

[72] Daniel Z. Freedman and Silviu S. Pufu. The holography of F-maximization. *JHEP*, 03:135, 2014.

[73] C. G. Beneventano, I. Cavero-Peláez, D. D'Ascanio, and E. M. Santangelo. Searching for a C-function on the three-dimensional sphere. *J. Phys.*, A50(45):455401, 2017.

[74] Hong Liu and Mark Mezei. A Refinement of entanglement entropy and the number of degrees of freedom. *JHEP*, 04:162, 2013.

[75] H. Casini and Marina Huerta. On the RG running of the entanglement entropy of a circle. *Phys. Rev.*, D85:125016, 2012.

[76] Horacio Casini, Marina Huerta, Robert C. Myers, and Alexandre Yale. Mutual information and the F-theorem. *JHEP*, 10:003, 2015.

[77] Igor R. Klebanov, Tatsuma Nishioka, Silviu S. Pufu, and Benjamin R. Safdi. Is Renormalized Entanglement Entropy Stationary at RG Fixed Points? *JHEP*, 10:058, 2012.

[78] Nozomu Kobayashi, Tatsuma Nishioka, Yoshiki Sato, and Kento Watanabe. Towards a C-theorem in defect CFT. *JHEP*, 01:039, 2019.

[79] Marika Taylor and William Woodhead. The holographic F theorem. 2016.

[80] Omer Ben-Ami, Dean Carmi, and Michael Smolkin. Renormalization group flow of entanglement entropy on spheres. *JHEP*, 08:048, 2015.

[81] Roberto Emparan, Clifford V. Johnson, and Robert C. Myers. Surface terms as counterterms in the AdS / CFT correspondence. *Phys. Rev.*, D60:104001, 1999.

[82] Per Kraus, Finn Larsen, and Ruud Siebelink. The gravitational action in asymptotically AdS and flat space-times. *Nucl. Phys.*, B563:259–278, 1999.

[83] Shinsei Ryu and Tadashi Takayanagi. Aspects of Holographic Entanglement Entropy. *JHEP*, 08:045, 2006.

[84] Juan Maldacena and Guilherme L. Pimentel. Entanglement entropy in de Sitter space. *JHEP*, 02:038, 2013.

[85] Marika Taylor and William Woodhead. Renormalized entanglement entropy. *JHEP*, 08:165, 2016.

[86] Yago Bea and David Mateos. Heating up Exotic RG Flows with Holography. *JHEP*, 08:034, 2018.

[87] Umut GÃ$\frac{1}{4}$rsoy, Elias Kiritsis, Francesco Nitti, and Leandro Silva Pimenta. Exotic holographic RG flows at finite temperature. *JHEP*, 10:173, 2018.

[88] Ignatios Antoniadis, Nima Arkani-Hamed, Savas Dimopoulos, and G. R. Dvali. New dimensions at a millimeter to a Fermi and superstrings at a TeV. *Phys. Lett.*, B436:257–263, 1998.

[89] Lisa Randall and Raman Sundrum. A Large mass hierarchy from a small extra dimension. *Phys. Rev. Lett.*, 83:3370–3373, 1999.

[90] Lisa Randall and Raman Sundrum. An Alternative to compactification. *Phys. Rev. Lett.*, 83:4690–4693, 1999.

[91] Juan Maldacena. Unpublished.

[92] Steven S. Gubser. AdS / CFT and gravity. *Phys. Rev.*, D63:084017, 2001.

[93] Nima Arkani-Hamed, Massimo Porrati, and Lisa Randall. Holography and phenomenology. *JHEP*, 08:017, 2001.

[94] Pierre Binetruy, Cedric Deffayet, and David Langlois. Nonconventional cosmology from a brane universe. *Nucl. Phys.*, B565:269–287, 2000.

[95] James M. Cline, Christophe Grojean, and Geraldine Servant. Cosmological expansion in the presence of extra dimensions. *Phys. Rev. Lett.*, 83:4245, 1999.

[96] Pierre Binetruy, Cedric Deffayet, Ulrich Ellwanger, and David Langlois. Brane cosmological evolution in a bulk with cosmological constant. *Phys. Lett.*, B477:285–291, 2000.

[97] Cedric Deffayet. Cosmology on a brane in Minkowski bulk. *Phys. Lett.*, B502:199–208, 2001.

[98] Cedric Deffayet, G. R. Dvali, and Gregory Gabadadze. Accelerated universe from gravity leaking to extra dimensions. *Phys. Rev.*, D65:044023, 2002.

[99] V. A. Rubakov and M. E. Shaposhnikov. Do We Live Inside a Domain Wall? *Phys. Lett.*, 125B:136–138, 1983.

[100] V. A. Rubakov and M. E. Shaposhnikov. Extra Space-Time Dimensions: Towards a Solution to the Cosmological Constant Problem. *Phys. Lett.*, 125B:139, 1983.

[101] Nima Arkani-Hamed, Savas Dimopoulos, Nemanja Kaloper, and Raman Sundrum. A Small cosmological constant from a large extra dimension. *Phys. Lett.*, B480:193–199, 2000.

[102] Shamit Kachru, Michael B. Schulz, and Eva Silverstein. Selftuning flat domain walls in 5-D gravity and string theory. *Phys. Rev.*, D62:045021, 2000.

[103] Thomas Faulkner and Joseph Polchinski. Semi-Holographic Fermi Liquids. *JHEP*, 06:012, 2011.

[104] Elias Kiritsis. Gravity and axions from a random UV QFT. *EPJ Web Conf.*, 71:00068, 2014.

[105] G. R. Dvali, G. Gabadadze, and M. Porrati. Metastable gravitons and infinite volume extra dimensions. *Phys. Lett.*, B484:112–118, 2000.

[106] G. R. Dvali, Gregory Gabadadze, and Massimo Porrati. 4-D gravity on a brane in 5-D Minkowski space. *Phys. Lett.*, B485:208–214, 2000.

[107] Steven S. Gubser. Curvature singularities: The Good, the bad, and the naked. *Adv. Theor. Math. Phys.*, 4:679–745, 2000.

[108] Steven S. Gubser and Abhinav Nellore. Mimicking the QCD equation of state with a dual black hole. *Phys. Rev.*, D78:086007, 2008.

[109] B. Gouteraux and E. Kiritsis. Generalized Holographic Quantum Criticality at Finite Density. *JHEP*, 12:036, 2011.

[110] Blaise Gouteraux, Jelena Smolic, Milena Smolic, Kostas Skenderis, and Marika Taylor. Holography for Einstein-Maxwell-dilaton theories from generalized dimensional reduction. *JHEP*, 01:089, 2012.

[111] A. B. Clark, D. Z. Freedman, A. Karch, and M. Schnabl. Dual of the Janus solution: An interface conformal field theory. *Phys. Rev.*, D71:066003, 2005.

[112] A. Kehagias and E. Kiritsis. Mirage cosmology. *JHEP*, 11:022, 1999.

[113] E. Kiritsis. Mirage cosmology and universe-brane stabilization. 1999. [PoStmr99,025(1999)].

[114] Antonio Padilla. Cosmic acceleration from asymmetric branes. *Class. Quant. Grav.*, 22:681–694, 2005.

[115] Antonio Padilla. Infra-red modification of gravity from asymmetric branes. *Class. Quant. Grav.*, 22(6):1087–1104, 2005.

[116] Christos Charmousis, Ruth Gregory, and Antonio Padilla. Stealth Acceleration and Modified Gravity. *JCAP*, 0710:006, 2007.

[117] Chang-hyun Ahn and Jinsub Paeng. Three-dimensional SCFTs, supersymmetric domain wall and renormalization group flow. *Nucl. Phys.*, B595:119–137, 2001.

[118] Chang-hyun Ahn and Kyungsung Woo. Supersymmetric domain wall and RG flow from 4-dimensional gauged N=8 supergravity. *Nucl. Phys.*, B599:83–118, 2001.

[119] Chang-hyun Ahn and Kyung-sung Woo. Domain wall and membrane flow from other gauged d = 4, N=8 supergravity. Part 1. *Nucl. Phys.*, B634:141–191, 2002.

[120] Chang-hyun Ahn and Kyung-sung Woo. Domain wall from gauged d = 4, N=8 supergravity. Part 2. *JHEP*, 11:014, 2003.

[121] Richard Corrado, Krzysztof Pilch, and Nicholas P. Warner. An N=2 supersymmetric membrane flow. *Nucl. Phys.*, B629:74–96, 2002.

[122] Nikolay Bobev, Nick Halmagyi, Krzysztof Pilch, and Nicholas P. Warner. Holographic, N=1 Supersymmetric RG Flows on M2 Branes. *JHEP*, 09:043, 2009.

[123] Stefan Hohenegger and Ingo Kirsch. A Note on the holography of Chern-Simons matter theories with flavour. *JHEP*, 04:129, 2009.

[124] Yasuaki Hikida, Wei Li, and Tadashi Takayanagi. ABJM with Flavors and FQHE. *JHEP*, 07:065, 2009.

[125] Martin Ammon, Johanna Erdmenger, Rene Meyer, Andy O'Bannon, and Timm Wrase. Adding Flavor to AdS(4)/CFT(3). *JHEP*, 11:125, 2009.

[126] Yago Bea, Eduardo Conde, Niko Jokela, and Alfonso V. Ramallo. Unquenched massive flavors and flows in Chern-Simons matter theories. *JHEP*, 12:033, 2013.

[127] Daniel L. Jafferis and Silviu S. Pufu. Exact results for five-dimensional superconformal field theories with gravity duals. *JHEP*, 05:032, 2014.

[128] Lin Fei, Simone Giombi, and Igor R. Klebanov. Critical $O(N)$ models in $6 - \epsilon$ dimensions. *Phys. Rev.*, D90(2):025018, 2014.

[129] Cumrun Vafa. The String landscape and the swampland. 2005.

[130] Hirosi Ooguri and Cumrun Vafa. On the Geometry of the String Landscape and the Swampland. *Nucl. Phys.*, B766:21–33, 2007.

[131] Daniel Klaewer and Eran Palti. Super-Planckian Spatial Field Variations and Quantum Gravity. *JHEP*, 01:088, 2017.

[132] Eran Palti. The Weak Gravity Conjecture and Scalar Fields. *JHEP*, 08:034, 2017.

[133] Arthur Hebecker, Philipp Henkenjohann, and Lukas T. Witkowski. Flat Monodromies and a Moduli Space Size Conjecture. *JHEP*, 12:033, 2017.

[134] Thomas W. Grimm, Eran Palti, and Irene Valenzuela. Infinite Distances in Field Space and Massless Towers of States. *JHEP*, 08:143, 2018.

[135] Georges Obied, Hirosi Ooguri, Lev Spodyneiko, and Cumrun Vafa. De Sitter Space and the Swampland. 2018.